Biological Effects of Radiation Exposure During Endovascular Aortic Aneurysm Repair

El-Sayed, Tamer

Awarding institution:
King's College London

Biological Effects of Radiation Exposure During Endovascular Aortic Aneurysm Repair

Tamer El-Sayed

Thesis submitted for the degree of

Doctor of Medicine

2021

Academic Department of Vascular Surgery

King's College London

Faculty of Life sciences & Medicine

School of Cardiovascular Medicine and Sciences

St Thomas' Hospital

1st Floor North Wing

Westminster Bridge Road

London, SE1 7EH

Statement of originality

The work contained in this thesis is my own original work, except where acknowledged in the text.

Acknowledgements

I would like to thank my supervisors Professor Bijan Modarai, Mr Ashish Patel and Professor Alberto Smith, whom I will always be indebted to for their support and guidance throughout my research.

I would also like to express my gratitude to our team within the Academic Department of Vascular Surgery for their technical assistance and advice, and the clinical team within the Vascular Unit at Guy's & St Thomas' NHS Foundation Trust for their continued support throughout my clinical and academic time.

Finally, I would like to dedicate this thesis to my mother, Kamelia, for her endless love and encouragement despite her illness. I could not have achieved this without her support and prayers.

Abstract

Health risks associated with ionising radiation is a growing concern. Fluoroscopically guided interventions such as endovascular aortic repair (EVAR) is associated with radiation exposure, particularly thoracoabdominal repairs using branched and/or fenestrated stent grafts.

Conventional methods of measuring radiation exposure such as personal dosimeters or dose area product (DAP) do not give a true reflection of the biological effect of radiation exposure. In contrast, bio-dosimetry directly measures the effects of radiation exposure in biological specimens such as circulating lymphocytes, which are sensitive to radiation exposure and exhibit upregulation of DNA damage biomarkers such as γ-H2AX when exposed to ionising radiation (Beels, et. al., 2009)
This study aimed to measure DNA damage/repair biomarkers in patients and operators after radiation exposure associated with EVAR.

The expression of DNA damage/repair markers, γ-H2AX and phosphorylated ataxia telangiectasia mutated (pATM), was quantified in circulating lymphocytes in patients and operators during the peri-operative period of endovascular repair and compared with open aortic repair using flow cytometry. The role of leg shielding in radiation protection was assessed separately measuring these markers in the same operators wearing leg lead shielding and compared with those operating with unprotected legs. Susceptibility to radiation damage was determined by irradiating operators' blood in vitro.

γ-H2AX and pATM levels increased significantly in patients and operators immediately after EVAR and recovered after 24 hrs. There was no change in γ-H2AX or pATM expression after open repair. Leg protection abrogated γ-H2AX and pATM response after branched endovascular aortic repair/fenestrated endovascular aortic repair. The expression of γ-H2AX varied significantly when operators' blood was exposed to the same radiation dose in vitro.

This is the first study to measure the acute DNA damage response in patients and operators after fluoroscopically guided aortic procedures and highlights the protective effect of leg shielding. Defining the relationship between this response and cancer risk may better inform safe levels of chronic low-dose radiation exposure and help to tailor individualised radiation protection strategi

Table of Contents

List of Abbreviations

AAA	Abdominal aortic aneurysm
ANOVA	Analysis of variance
ATM	Ataxia telangiectasia mutated
BEVAR	Branched endovascular aneurysm repair
BER	Base excision repair
BSA	Bovine serum albumin
DAP	Dose area product
DAPI	4',6-diamidino-2-phenylindole
DDR	DNA Damage Response
DNA	Deoxyribonucleic acid
DSBs	Double strand breaks
DSA	Digital subtraction angiography
EDTA	Ethylenediaminetetraacetic acid
ELISA	Enzyme-linked immunosorbent assay
EVAR	Endovascular aneurysm repair
FACS	Fluorescence-activated cell sorting
FEVAR	Fenestrated endovascular aneurysm repair
FMO	Fluorescence minus one
HSCs	Haematopoietic stem cells
IEVAR	Infra-renal endovascular aneurysm repair
IR	Ionising radiation
LET	Low energy transfer
MAG1	3-methyladenine glycosylase
Micro-CT	Micro-computed tomography
miRNA	Micro RNA
MRA	Magnetic resonance angiography
MRI	Magnetic resonance imaging
mRNA	Messenger RNA
MSC	Mesenchymal stem cell
NK	Natural killer
OGG1	8-oxyguanine glycosylase
OSL	Optically Stimulated Luminescence
pATM	Phosphorylated ataxia telangiectasia mutated
PBMCs	Peripheral blood mononuclear cells
PBS	Phosphate buffered saline
PCI	Percutaneous coronary intervention
PMA	Phorbol 12-myristate-acetate
RNA	Ribonucleic acid
RT-PCR	Real time polymerase chain reaction
ROS	Reactive oxygen species
SSBs	Single strand breaks
TAAA	Thoraco-abdominal aortic aneurysm
TLD	Thermo-luminescent Dosimeter
TNFα	Tumour necrosis factor α
XRCC1	X-ray repair cross-complementing protein 1
GG-NER	Global genomic nucleotide excision repair
TC-NER	Transcription-coupled nucleotide excision repair
γ-H2AX	Gamma histone 2AX

Index of Figures

Index of Tables

CHAPTER 1

General Introduction

The health risks associated with medical ionising radiation exposure are increasingly worrisome for both patients and practitioners. Minimally invasive, fluoroscopy-guided interventional procedures have increased treatment options for patients. However, the resulted radiation exposure to both patients and staff has raised concerns about deleterious effects such as an increased incidence of cancers.

Endovascular aortic aneurysm repair (EVAR) is a minimally invasive alternative to open surgical repair of the aortic aneurysm, but a long-term follow up study suggested that patients are more likely to develop cancer after EVAR, compared with open surgical repair.[1] While patients are exposed to a single high radiation dose during the index procedure, operators, performing procedures such as EVAR, are chronically exposed to lower doses over the course of their career. In a similar vein as patients, epidemiological studies of interventionists performing fluoroscopically guided procedures describe a higher incidence of malignancy, including brain and breast cancers.[2 - 4]

1.1 Aortic Aneurysms

1.1.1 Background

Aneurysmal degeneration of the aorta can be a life-threatening condition caused by a dilatation (usually >1.5-fold normal diameter) that can affect any part of the aortic tree and eventually cause rupture with sufficient enlargement. Aortic aneurysms can be classified as infra-renal, juxta-renal, supra-renal and thoracoabdominal depending on their extent (Figure 1.1).

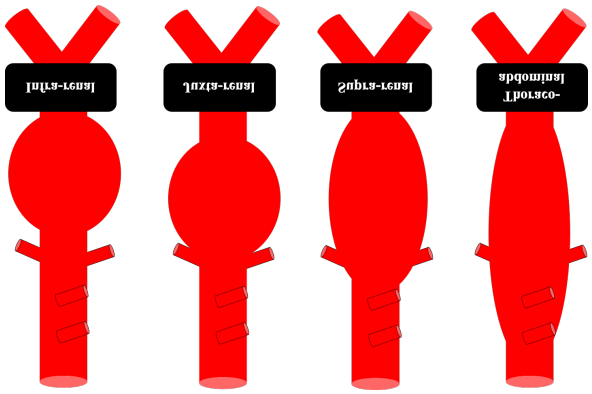

Figure 1.1 Different types of aortic aneurysms
Types of aortic aneurysms are infra-renal, juxta-renal, supra-renal and thoraco-abdominal.

Abdominal aortic aneurysms (AAAs) are mainly below the level of renal arteries (infra-renal), whilst less than 10% are above the renal arteries (supra-renal).[5] Juxtarenal AAAs are aneurysmal adjacent to the renal arteries. AAA is a disease of elderly males (sex ratio 6:1) and infra-renal aneurysms, for example, with a prevalence of up to 1.3% in the UK National Screening Programme, and 5% in the USA.[6–8] When AAA ruptures, it is potentially fatal, with mortality rates up to 90%.[9] Currently, around 7,000 people in England and Wales die each year as a result of ruptured AAA.[10]

Elective aneurysm repair is preferred for the management of large aneurysms as emergency repair of ruptured aneurysms carries a high mortality and morbidity. However, aortic surgery is associated with risks, and therefore, elective AAA repair is not recommended until the risk of rupture exceeds the risks associated with the repair, which is when aneurysm diameter exceeds 5.5 cm.[11,12] Other factors, such as age, rate of aneurysm expansion, and co-morbidities are also important to consider elective AAA repair.

1.1.2 Endovascular aortic repair (EVAR)

Endovascular aortic aneurysm repair (EVAR) was first described by Voldos and colleagues in 1986 and Parodi and colleagues in 1991.[13] EVAR uses an intraluminal stent-graft prosthesis that is inserted via a transfemoral or transiliac approach to exclude the aneurysmal segment of the aorta from the systemic circulation using a stent-graft, which could be placed below the renal vessels (Infra-renal), or more complex stent grafts that have fenestrations or branches to perfuse the visceral vessels (FEVAR and BEVAR) (Figure 1.2), in order to prevent aneurysm rupture. Between 2000 and 2010, the use of EVAR increased from 5% to 74% of all AAA repairs in the USA.[14 - 16] Examples of endovascular abdominal aortic aneurysm repair are infra-renal (IEVAR), fenestrated (FEVAR), and branched (BEVAR).

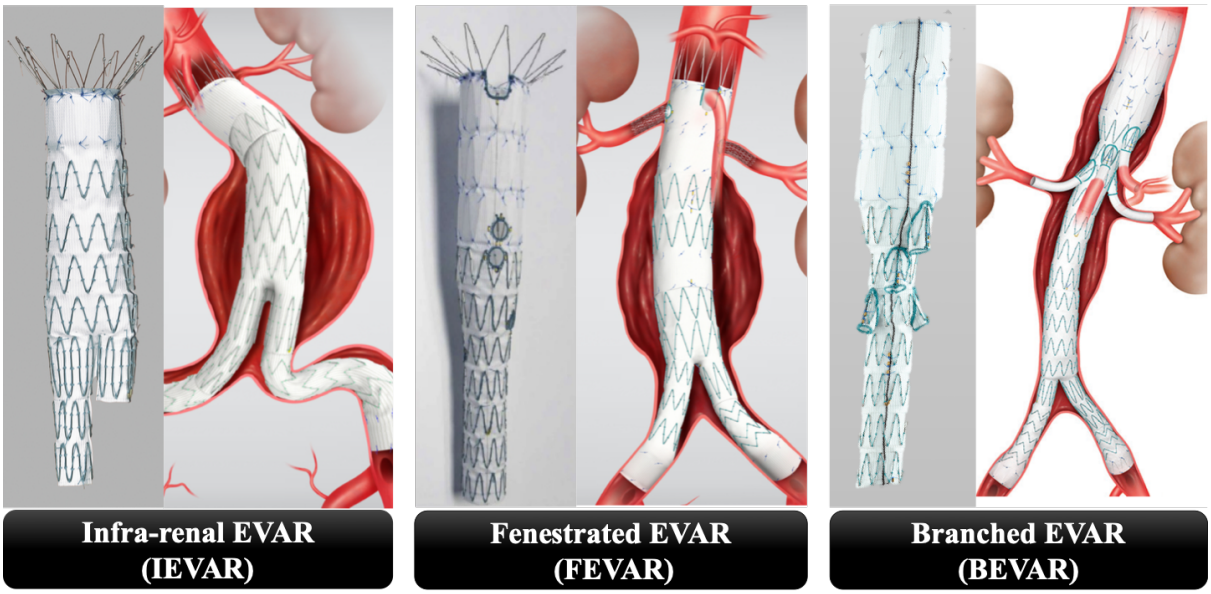

Figure 1.2 Examples of endovascular stent grafts (Adapted from CookMedical.com and Timaran et al, 2017)
Examples of endovascular abdominal aortic aneurysm repair are infra-renal (IEVAR), fenestrated (FEVAR), and branched (BEVAR)

Infrarenal EVAR (IEVAR)

Infrarenal EVAR (IEVAR) is used for aneurysms with an adequate length of the healthy infrarenal aorta (>15mm) before the aneurysm begins. This allows a safe landing zone for the proximal end of the prosthetic stent-graft in a healthy segment of the aorta to provide an intact repair to avoid endoleaks or compromising renal perfusion.

IEVAR procedure involves deployment of covered metallic stent-graft below the renal arteries proximally and either to the aorta, bi-iliac or uni-iliac arteries distally.[17 - 19]

Complex endovascular aortic repair

Juxtarenal and thoracoabdominal aortic aneurysms (TAAAs) involve the visceral branches (e.g. Renal, SMA and Coeliac arteries), and when these complex aneurysms are repaired with open surgery, this is associated with significant morbidity and mortality.[20 – 22] Endovascular repair such as fenestrated and branched endovascular aortic repairs provide a good option for those patients who might not be deemed fit for open surgery

Fenestrated EVAR (FEVAR) is used for cases with <10mm infrarenal neck and juxtarenal aneurysms. They are patient-specific custom-made grafts to incorporate the renal vessels,

coeliac and superior mesenteric arteries. All branches reinforced with covered balloon-expandable stents.

These special stent-grafts allow blood flow to visceral vessels through fenestrations through the graft material. It can be challenging to align the fenestration with the branch vessel during stent deployment, and in maintaining alignment with the vessel during the repair, to ensure long-term branch patency.[23]

Branched EVAR (BEVAR) are stent grafts that are typically used for thoracoabdominal aortic aneurysm repair. A main stem stent-graft is used to exclude the aneurysmal segment. Then visceral vessels, e.g., Coeliac and SMA, are cannulated either antegrade from the arm or retrograde transfemoral/transiliac. Once the branch vessels cannulated, bridging stents are deployed into these visceral branches. FEVAR and BEVAR are advanced techniques to treat challenging anatomy, mainly in high-risk patients.

1.2 Physics of Ionising Radiation (IR)

1.2.1 Definition and background

Ionising radiation (IR) is described as radiation that has adequate energy to dislodge an electron from molecules. Free electrons can cause harm to affected cells. IR can provoke adverse health risks, such as skin injuries, cancer, and cataract. Nuclear bomb survivors also experienced cardiovascular disease and stroke after exposure to high radiation dosages.[24]

In 1895, Nobel Prize winner Wilhelm Conrad Roentgen (1845-1923) was examining the electrical discharge created in a glass tube. The free electrons generated in this tube were a form of radiation and called cathode rays. These electrons made a fluorescent screen glow, which Roentgen named these invisible emissions X-rays.[24]

1.2.2 Types of Radiation

Radiation could be either ionising or non-ionising, depending on its capacity to ionise materials.[25 – 26] Ionising radiation is further divided into two main categories, directly and non-directly ionising radiation.

Directly ionising radiation is caused by charged particles which can ionise atoms directly. Charged particles could be either Alpha (α) or Beta (β) particles. Alpha particles are produced

as a result of alpha decay, and consist of two protons and two neutrons, and they are highly ionising with low penetration (less than 0.1mm).[27] While beta particles are produced from beta decay and are high energy electrons which have less of an ionising effect, but penetrating more compared with alpha particles.[28]

Indirectly ionising (neutral particles), on the other hand, are electrically neutral, and therefore they are unable to interact with the matter directly, and their effect occurs mainly via secondary ionisation. Examples of neutral particles are photons, neutrons, gamma and x-rays.
Photons have the ability to deposit all or part of their energy via interaction with electrons, causing their ejection. The ejected electron becomes a secondary beta particle that is able to ionise other atoms; therefore, photons are called indirect ionising particles.[29] Gamma rays are produced by a nuclear reaction or radioactive decay within the nucleus of an atom. They can carry high energy with high penetration to cause human body tissue damage and can only be stopped by dense materials such as lead or concrete.[30]
X-rays are generated in the electron fields outside the nucleus and have a lower energy than gamma rays, inducing their effect through photoelectric absorption. They are the most common type of ionising radiation used in diagnostic and interventional medical appliances.[31]
Neutrons are also produced by nuclear reactions and have high penetration, resulting in the production of protons and gamma radiation.[32] When neutrons interact with protons in hydrogen atom via linear energy transfer (LET), this causes indirect ionisation of the hydrogen atoms and production of ionising photons.[33]

Alternative classification of radiation

Linear energy transfer (LET) describes the amount of energy released by a radioactive particle or wave over the length of its decay track. There are two types of LET: (i) High LET radiation such as alpha and beta particles, which can deposit high energy within the volume of one cell that results in a higher level of DNA damage in a localised area and (ii) Low LET radiation such as X-rays and gamma rays, which induce ionisation through depositing their energy over a longer course producing diffuse DNA damage. The localised DNA damage caused by intense ionisation from high LET is more challenging to repair compared with the diffuse DNA damage caused by the sparse ionisation induced by low LET radiation.[34] The National Academy of Sciences Committee defines low dose ionising radiation when it is below 100mSv of low LET.[35]

1.2.3 Units used to describe radiation dose

There are many units to define the amount of radiation produced or received, for example, **Radioactivity** is a measure of the amount of ionising radiation released by a matter by counting the number of atoms produced from the material decay in a given time. The units of measurement are the curie (U.S.) and Becquerel (standard international unit, SI).

While **radiation exposure** is the amount of radiation travelling through the air. The units of exposure are the Roentgen (U.S.) and Coulomb/kilogram (SI).

Absorbed dose describes how much radiation absorbed by an exposed object. The units for absorbed dose are the rad (U.S. unit) or the Gray (Gy, SI).

Whereas, the **effective dose** is the amount of radiation absorbed by the person, adjusted to the type of radiation and the effect on exposed organs. The units for the effective dose are rem (U.S. unit) or Sievert (Sv, international unit).

Dose area product (DAP) is the absorbed dose as a product of the area irradiated. The unit of dose area product is Gray/squared centimetre ($Gy.cm^2$). DAP is considered as one of the main conventional methods to assess the absorbed dose of radiation from medical equipment as it is automated and easily measured, with the permanent installation of a DAP meter on the X-ray source. That is why DAP can be used as a tool for comparison of different diagnostic and interventional procedures within the same institution or various institutions.[36]

1.2.4 Methods of measuring radiation

There are many ways to detect radiation and measure it.

The Geiger Counter or Geiger-Muller tube is the most common radiation detection tool used. When the Geiger counter detector identifies ionisation, an output pulse causes meter readings and audio signals.

The Geiger counter is composed of a hollow inert gas-filled chamber fitted with a thin window at one end. There is a constant high voltage between the chamber exterior wall and an internal electrode, and radiation that passes through causes the filling gas to conduct by ionising it. The ionisation is amplified within the tube by a process called the Townsend discharge that results in a signal that is processed and displayed electronically. The main disadvantage of the Geiger-counter is that different ionising sources and exposure results in the same size output pulses. Therefore, the meter does not differentiate between the various types of radiation.[37]

The Film Badge is considered as one of the first devices used to monitor occupational radiation exposure. Film badges consist of a film with an emulsion coating and a special metal filters used in an X-ray film holder. These badges require regular calibration of exposure in order to provide an accurate radiation dose measurement. Emulsions offer recording doses of radiation over long periods of exposure time. In order to identify the radiation dose that is detected by the film badge accumulated over some time, the density of the exposed film is compared with a matching film exposed to a known radiation dose.[38]

The Thermoluminescent Dosimeter (TLD) badge is currently the most commonly used method in measuring and monitoring medical staff occupational radiation exposure. Thermoluminescence occurs when the TLD crystal is exposed to radiation and absorbs the energy produced from the radiation, leading to excitation of the crystal atoms. This atomic excitation results in the production of free electrons and holes in the thermoluminscent crystal. These electrons are trapped by the imperfections of the crystal lattice, which keeps the excitation energy within the crystal. TLD provides a measure of the amount of radiation it is exposed to when the crystal is heated, and the intensity of the resulting luminescence measured with a TLD reader (Figure 1.3).[39] TLDs have many forms and shapes to facilitate usage, for example operators can use them as badges over the lead, wear them as rings or mount them over their protective goggles to measure different parts of the body radiation doses.

Figure 1.3 Examples of Thermo-luminescent Dosimeter (TLD) Badges (Adapted from Public Health England, Body Thermoluminescence Dosimeter, 2018)
Thermo-luminescent Dosimeter components and its different forms that operators can wear as rings and mount over their protective goggles measure different parts of the body radiation doses.

The Optically Stimulated Luminescence (OSL) badge is able to measure doses as low as 0.01mSv, and similar to TLD, after exposure to radiation, the amount of radiation is measured by exposing OSL to laser light, which causes the aluminum oxide to luminescence. The intensity of luminescence is proportionally related to the amount of radiation absorbed. Individualised OSL badges are used by operators to monitor their accumulated radiation doses, and they can be worn over the lead usually in the chest and/or neck area (Figure 1.4).[39]

Figure 1.4 An example of Optically Stimulated Luminescence (OSL) Badge

Pocket Dosimeters provide an immediate reading of the radiation dose. The most commonly used types are:

Direct Reading Dosimeter (DRD) has a charged quartz fibre that can be displaced electroscopically by charging it to a potential of about 200 V. An image of the fibre is focused on a scale and is viewed through a lens. When the dosimeter is exposed to radiation, the fibre discharges and it slides returning to its original position. The amount discharged, and consequently, the change in position of the fibre is proportional to the radiation dose. DRDs provide an immediate measurement of radiation dose, but they are fragile devices that might leak and require regular calibration and leakage checks.[39]

Digital Electronic Dosimeter (DED) measures instant radiation exposure and can provide real-time dosimetry. DED stores dose rates from 1μSv/hr to 10mSv/hr and also displays the cumulative dose. The real-time dosimeter is an excellent example of electronic dosimeters, where the dosimeter measures and records dose and dose rate every second. Data is transferred to the real-time display during procedures so staff can continuously monitor their radiation exposure and modify their behaviours accordingly (Figure 1.5).[39]

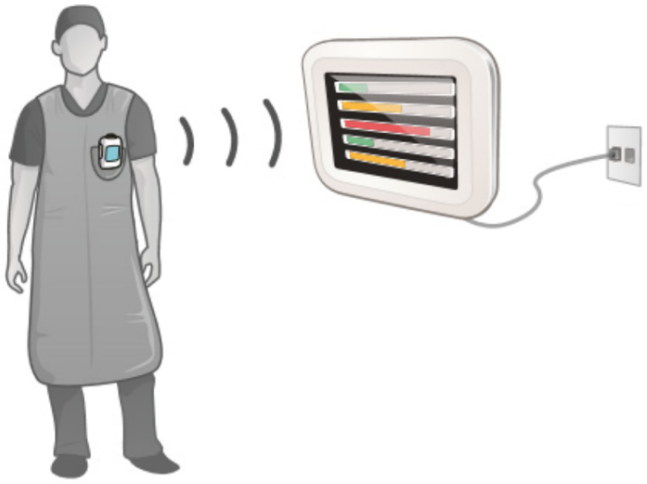

Figure 1.5 An example of real time dosimeter (Adapted from RaySafe Real-time Radiation Dosimeter, https://www.raysafe.com/products/real-time-dosimetry-systems)
An operator is wearing a real time dosimeter and monitoring his received radiation doses on a monitor intra-operatively.

1.2.6 Background exposure to ionising radiation

Humans are continuously exposed to background radiation every day from many natural sources such as the ground, building materials, air, the universe, and elements in human bodies. This is in addition to human-made sources of radiation such as medical diagnostic and therapeutic procedures, nuclear industry (Chernobyl in 1986), and nuclear weapons (atomic bombings of Hiroshima and Nagasaki in 1945 and atomic weapons testing).

That natural background radiation mainly comes from cosmic ray particles and radionuclides that originated from the earth's crust. While human practices such as phosphate fertiliser production, fossil fuel combustion, nuclear power plants and weapons increase levels of radioactive residues, which add to the background radiation. Workers who are exposed to either of these sources, e.g. aircraft cabin crew and nuclear industry workers suffer from higher levels of background radiation with subsequent increased rates of radiation induced health risks among these workers such as cancer in the skin, breast and leukaemia.[24]

In 2010, Public Health England reported that the UK individual dose from all sources of ionising radiation was about 2.7 mSv per year. 84% of this dose was from natural sources of radiation, while 16% is the result of patient exposure during diagnostic and therapeutic medical procedures. Occupational exposure contributed to less than 1%.[40]

1.2.7 Radiation exposure during endovascular aortic aneurysm repair

EVAR is done under fluoroscopy guidance using a mobile C-arm image intensifier or a fixed imaging system in a hybrid suite. IEVAR is associated with relatively short operative time,

with x-ray fluoroscopy time ranging from 2.4-161mins.[41 - 42] Studies have reported absorbed radiation doses during IEVAR with a wide variation of DAP ranging between 12.2-271Gy.cm2.[43 - 46]

Carrying out complex endovascular aortic aneurysm repair (BEVAR/FEVAR) procedures can be challenging and might require prolonged fluoroscopy guidance and, consequently, higher radiation exposure to patients and medical staff. The amount of radiation, measured by DAP and fluoroscopy time, proportionally increased with the procedure's complexity.[47] The absorbed radiation dose measured by DAP was higher during BEVAR/FEVAR procedures than infrarenal and thoracic aneurysm repair (IEVAR and TEVAR).[42 - 43] There is no reported difference in radiation exposure measured by fluoroscopy time, digital subtraction angiography acquisition time, and DAP between FEVAR and BEVAR procedures.[48] Type II and III endovascular TAAA repair result in higher DAP and longer fluoroscopy time compared with type IV TAAA (1006 vs. 642Gy.cm2 and 141 vs. 82mins, respectively).[49] Operators are exposed to significantly higher radiation levels both over and under their lead garments than the assistant and anaesthetist during EVAR procedures.[50] The head dose is also significantly higher in operators than their assistants when they performed complex endovascular repairs. The head dose is dependent on the operator's height, and there is an inverse relationship between height and head dose.[48] In addition to operator height, other independent predictors of head dose include total digital subtraction angiography (DSA) acquisition time and left anterior oblique (LAO) and cranial positions.[51]

1.3 Ionising radiation-induced DNA damaged

1.3.1 Mechanisms of radiation-induced genomic damage

Ionising radiation induces significant biological consequences at the cellular level, including chromosomal aberrations, mutations and apoptosis. Genome instability and damage can be caused through two different mechanisms:

1.3.1.1 Direct DNA damage

This occurs when ionising radiation causes direct deposition of energy in the DNA. This energy disrupts DNA structure by causing breaks in one or both of the sugar-phosphate backbones or break any of the DNA base pairs. The base pairs, adenine - thymine and guanine - cytosine are held together by weak hydrogen bonds. These bonds can be destroyed by ionising radiation.

The production of single or double-strand breaks depends on the total amount of energy in the ionising radiation.[52]

1.3.1.2 Indirect DNA damage

This is thought to be the main mechanism of radiation-induced DNA damage.[53] It occurs when a photon interacts with a water molecule which causes loss of an electron from a water molecule. This interaction results in an ionised water molecule H_2O^+. Trapping of the electron by polarising water molecules produces a hydrated electron (e_{aq}^-). When the ionised water molecule interacts with another water molecule, it produces a highly reactive hydroxyl radical $OH^\bullet$, according to the reaction $H_2O^+ + H_2O \rightarrow OH^\bullet + H_3O^+$.[54] These reactions produce various reactive oxygen species such as e^-_{aq}, $H^\bullet$, and $OH^\bullet$, which cause the DNA damage.

The interaction between e_{aq}^- and $H^\bullet$ and DNA bases results in various types of DNA damage. Hydroxyl radicals are highly unstable reactive molecules, and they react with the DNA causing damage to its bases and/or sugar moiety. If left unrepaired, this DNA damage can result in genetic instability and mutagenesis.[55 - 56]

1.3.2 Types of radiation-induced DNA damage

DNA damage refers to the alteration in the chemical structure of DNA. There are different types of DNA damage caused by either direct energy transfer or indirect damage resulted from the production and interaction with free radicals. DNA damage is counteracted by (i) the ability of cells to scavenge free radicals produced during ionisation before they induce any genomic damage; and (ii) the integrity of DNA repair mechanisms that are able to detect and rectify any DNA damage to prevent any long-term consequences of radiation-induced damage (Figure 1.6).

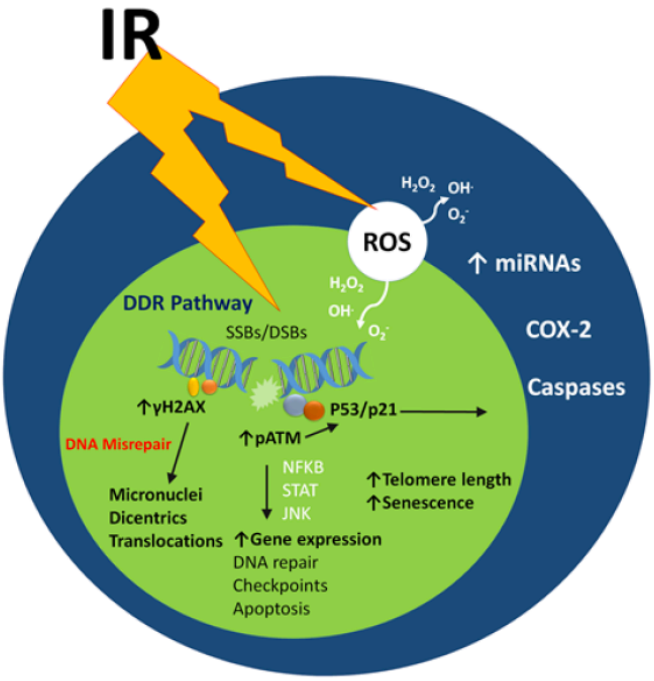

Figure 1.6 Mechanisms of radiation induced DNA damage and its effects (Adapted from Patel et al, Charing Cross Symposium Book, 2017)
Ionising radiation (IR) can cause DNA damage in cells via direct energy transfer and indirectly by production of reactive oxygen species. This activates the DNA Damage Response (DDR) pathway and upregulates a range of genomic and proteomic markers that can be detected within cells, including γ-H2AX and pATM. Misrepair of damaged DNA can produce chromosomal aberrations such as micronuclei, dicentrics and translocations.

Types of DNA damage are as the followings:

1.3.2.1 Base damage

DNA is made of double-helical strands composed of a repeated pattern of nucleotides that is built from a deoxyribose sugar, phosphate groups, and nitrogenous base (adenine, guanine, cytosine, and thiamine).

Ionising radiation induces reactive oxygen species production through indirect reaction with a water molecule. Hydroxyl radicals cause oxidative DNA base damage. This DNA damage is a type of chemical modification to the base of a nucleotide and considered as the most common type of genomic damage, for example, an estimated 120,000 base damage occur in the 6.5 Gbp nuclear genome of human liver cells per day.[57] This DNA base damage could cause DNA malfunction and induction of genomic instability and mutagenesis.[58 - 59] Damage can happen to any DNA base, although guanine is the most sensitive base because of its low reduction potential, making it the best electron donor and therefore more easily oxidised.[60 - 63]

The hydroxyl ($OH^{\bullet}$ radical) group, for example, affects guanine either by the addition of hydroxyl group to the C2-, C4-, C5- and C8- positions or by the abstraction of $H^{\bullet}$ from the NH_2

group attached to C2 (Figure 1.7).[60, 61, 64 - 67] When a hydroxyl group is added to the guanine, this produces OH-adduct radicals, which change the guanine into either reducing or oxidising molecule.[60, 61, 68]

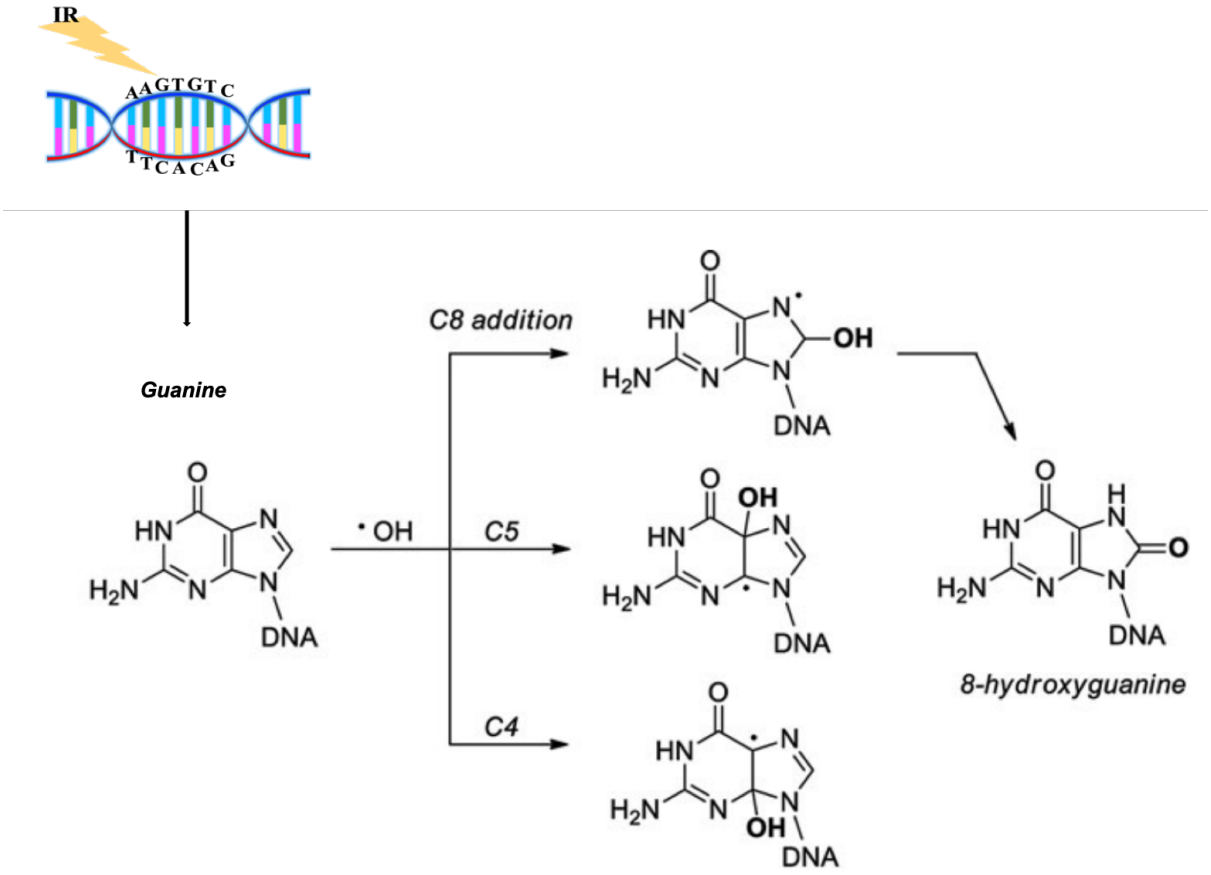

Figure 1.7 Radiation induced guanine base oxidation (Adapted from Reisz et al., Antioxid Redox Signal, 2014)
Once exposed to radiation, Guanine oxidation occurs either by addition of hydroxyl group to or by abstraction of H•.

1.3.2.2 Single-strand breaks (SSBs)

A single-strand break is a disruption in one strand of the DNA double helix and is associated with loss of a single nucleotide and damaged 5′ terminus and/or the 3′ terminus at the site of the break.[78] Fortunately, the other intact DNA strand can be used as a template to guide the repair of the damaged strand. Free radicals are considered as one of the most common sources of single-strand breaks. There are two ways to induced single-strand breaks either by the breakdown of the oxidised sugar moiety or indirectly during the DNA base-excision repair (BER) of damaged bases.

The natural DNA repair process is usually efficient enough to repair radiation-induced single-strand DNA breaks. However, if they are left unrepaired, this might lead to DNA base sequence disturbance, genetic mutations, and instability.[69 - 71]

1.3.2.3 Double-strand breaks (DSBs)

In contrast to single-strand DNA breaks, double-strand breaks are considered to be the most dangerous form of DNA damage, as they can lead to mutagenesis and cell death as they are more challenging to repair.[72]

Double strand breaks can be categorised as: (i) simple double-strand breaks which occur when there are two single-strand breaks (SSBs) within approximately 6-10 base pairs; and (ii) complex double-strand breaks, which are simple double-strand breaks (described earlier) in addition to other DNA damage lesions, e.g., base damage and single-strand breaks. Ionising radiation can produce a wide range of complex double-strand breaks.[73]

High linear energy transfer (LET) is able to cause a wide range of complex double-strand breaks, which are more challenging to repair. This complex damage is different from low linear energy transfer induced complex double-strand breaks, as they are less complicated and relatively easier to repair.[73]

The primary outcomes of any double-strand break are: (i) rejoining with complete repair; (ii) failure to rejoin and remain free, causing deletion mutation; or (iii) rejoining with another break resulting in chromosomal aberration.[74]

1.3.3 Mechanisms of DNA damage repair

Ionising radiation deposits energy into the exposed cell and generates reactive oxygen species, driving oxidative stress and damaging the cellular DNA.[75]

DNA damage is a threat to cell integrity and function and may lead to mutation, cancer, and cell death. Therefore, in the event of DNA damage, a series of cellular responses are initiated to repair the damaged DNA and activate a cell cycle checkpoint response to avoid passing the damaged DNA to daughter cells. Unrepaired DNA damage might eventually lead to development of malignancies. Therefore, genome stability is dependent on intact repair mechanisms and checkpoint pathways.[76] The mechanisms that repair damaged DNA are described below.

1.3.3.1 Base-Excision Repair (BER)

BER is the mechanism that is responsible for repairing DNA base damage in order to protect cells against mutagenesis and genomic instability. It occurs in both nuclei and mitochondria. BER is an enzymatic mechanism to excise and repair the damaged base, and relies mainly on the action of four enzymes (Figure 1.8).[76]

Human cell nuclei usually have 10-12 different ***DNA glycosylases*** to recognise different damaged bases or nucleotides modifications. For example, 8-oxoguanine glycosylase 1 (OGG1) recognises 8-oxoguanine, and 3-methyladenine glycosylase (MAG1) recognises 3-methyladenine base damage. In order to recognise a DNA base lesion, DNA is continuously scanned for lesions to identify any damaged nucleotide to be repaired. Once a base lesion is identified, DNA glycosylase then kinks the DNA strand by compressing the flanking backbone in the affected strand to flip out the abnormal nucleoside residue to place the damaged base in a specific recognition pocket to enable base excision.[78] Base excision results in abasic sites as a result of base loss, e.g., apurinic or apyrimidinic (AP) sites leaving a gap. The repair of AP sites requires further steps to complete base excision repair.

Glycosylases can be monofunctional or bifunctional. Monofunctional enzymes have only glycosylase activity, whereas bifunctional glycosylases also have AP lyase activity. Therefore, bifunctional glycosylases can treat a base lesion and converting it into a single-strand break without requiring any AP endonucleases.[79]

After DNA glycosylase leaves abasic sites behind, AP endonuclease recognises and removes these abasic AP sites. Human cell nuclei have two categories of AP endonucleases, APE1 and APE2. APE1 is the main human apurinic-apyrimidinic endonuclease that is able to recognise and cleaves DNA lesions at the 5′ side of abasic sites.[80]

AP endonucleases produce nicks in DNA on either side of the AP site. Nicking of the sugar-phosphate backbone on either side of an AP site results in a free end. In order to remove these moieties during base excision repair, another type of enzymes called exonucleases is required that are able to repair and degrade DNA with free ends.[88] In base excision repair, the exonuclease enzyme, deoxyribophosphodiesterase, removes the remaining free end of deoxyribose phosphate residue. This excision generates a gap in the DNA duplex of about one to five nucleotides. This gap is filled by DNA polymerase, and the strand is sealed by DNA ligase.[81]

DNA polymerases are the enzymes responsible for the synthesis process of new DNA molecules from deoxyribonucleotides, as they create two identical DNA strands during the DNA replication process. DNA polymerase uses the existing intact DNA strand as a template

in order to replicate this intact DNA strand to create a new strand that matches the existing strand instead of the damaged one.[82 - 87]

Pol β is the main human polymerase that is able to mainly reproduce short patch DNA synthesis as part of the base excision repair. Pol β also has the ability to connect with the noncatalytic X-ray repair cross-complementing protein 1 (XRCC1) subunit of the XRCC1-DNA ligase III complex. This enables XRCC1 to recruit polymerases and ligases to the site of repair.[88 – 90] In the absence of Pol β, Pol λ is able to replace Pol β and do its function in replicating new DNA nucleotide.[91, 92] These enzymes are members of the Pol X group and are able to synthesise a single nucleotide only.

During DNA base excision repair, there are two types of patch repair: (i) short DNA patch repair, which includes inserting one new DNA nucleotide, and (ii) long DNA patch repair, which includes reproducing between 2 and 10 new nucleotides. Long DNA patch repair is carried out by polymerases (pol δ and pol ε) in coordination with proliferating cell nuclear antigen (PCNA), the same polymerases that carry out DNA replication.[79, 93]

DNA ligases facilitate the joining of two DNA strands by formation of a phosphodiester bond to fully repair the DNA, on completion of the synthesis phase. DNA ligases not only take part in base damage but also single and double-strand damage repair.[94]

There are 4 types of ligases. (i) *DNA ligase I* has a primary role in DNA replication is to ligate the nascent DNA of the lagging strand. (ii) *DNA ligase II* is produced through proteolytic action on DNA ligase III, and it has an essential role in DNA repair. (iii) *DNA ligase III*'s main function is to bind to XRCC1 to create the XRCC1-DNA ligase III complex to guarantee a stable binding to the DNA during base excision repair. (iv) *DNA ligase IV* is the only ligase that is able to take part in repairing double-strand breaks through binding to XRCC4 during the final step in the non-homologous end-joining repair pathway.[95]

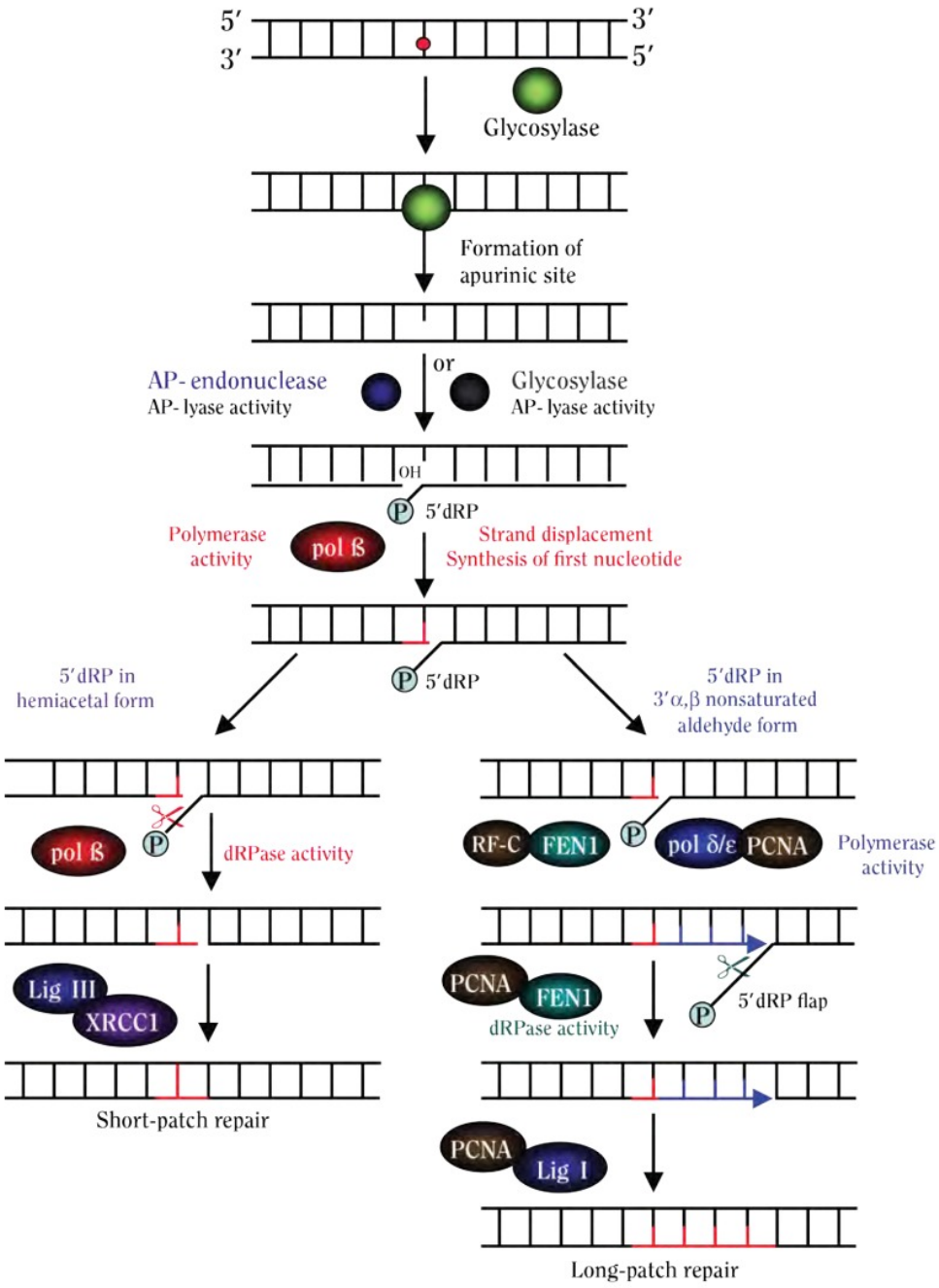

Figure 1.8 Base excision repair pathways. (Adopted from Christmann et al., Toxicology, 2003).

Base excision repair (BER) is an enzymatic dependent process as the DNA damaged base is identified by DNA glycosylase which hydrolyse the N-glycosidic bond to remove the damaged base followed by preparing the damaged site for repair by the AP endonucleases and then synthesis and joining of a new base by DNA polymerases and nucleases.

1.3.3.2 Nucleotide-Excision Repair

This is one of the main DNA repair mechanisms that removes DNA damaged nucleotide induced by ionising radiation.[96, 97] When a damaged nucleotide is identified, the repair

mechanism removes a short segment of single strand DNA that contains the affected nucleotide. Similar to base excision repair, DNA polymerase uses the intact single-strand DNA as a template to replicate a short complementary sequence instead of the resected damaged segment. DNA ligases carry out the final step of nucleotide excision repair by ligating the DNA strands together to form a double-stranded DNA (Figure 1.9).

There are 9 major proteins involved in nucleotide excision repair in mammalian cells. If any of these proteins are absent, this will consequently lead to defected repair mechanisms and accumulation of unrepaired and/or miss-repaired lesions that eventually lead to disease. Therefore, protein names are associated with the resulting disease. For example, Xeroderma Pigmentosum proteins A-G (XPA, XPB, XPC, XPD, XPE, XPF, and XPG) are essential in the processes of DNA damage nucleotide excision repair. Patients with Xeroderma Pigmentosum can carry mutations in any of the transcription genes that produce these proteins.[98]

Nucleotide excision repair has two main pathways: global genomic nucleotide excision repair (GG-NER) and transcription-coupled nucleotide excision repair (TC-NER).[99 - 100] The main difference between these two pathways is in the mechanism of identifying the damaged nucleotide in the DNA strand. However, they share the same process for lesion excision, repair, and ligation.

Global genomic nucleotide excision repair* (GG-*NER) is able to carry out the repair process in damaged transcribed and untranscribed DNA strands in either active or inactive genes. Sensor proteins such as DNA-damage binding (DDB) and Xeroderma Pigmentosa C and UV excision repair protein RAD23 homolog B (XPC-Rad23B) complexes frequently scan the genome to identify any damage. Once the damaged site is identified, repair proteins are recruited to the damaged site, and the same steps as base excision repair continue to excise the damaged segment and replace it with a new segment.[101, 102]

Transcription coupled nucleotide excision repair (TC-NER) is mainly responsible for the repair of damaged nucleotides in the transcribed strand of active genes. Contrasting to global genomic nucleotide excision repair, transcription-coupled nucleotide excision repair does not require sensor proteins such as XPC or DDB to identify damaged sites. When RNA polymerase stalls at the damaged site on the DNA strand, it acts as a sensor protein and activates the transcription-coupled nucleotide excision repair process.[103 - 104]

Transcription factor II H (TFIIH) is the key enzyme involved in dual excision. Xeroderma Pigmentosa protein G (XPG) is the first recruited to the lesion site, which stabilises TFIIH to the damaged segment. The TFIIH subunits of Xeroderma Pigmentosa proteins D and B (XPD and XPB) act as a 5'-3' and 3'-5' helicase, respectively to unwind the DNA.

This allows XPG, which has endonuclease activity to excise the damaged DNA segment on the 3' side. At the same time, the Xeroderma pigmentosa F-Excision repair cross complementation group 1(XPF–ERCC1) complex protein removes the damaged nucleotide on the 5' side. This leads to the removal of a damaged segment with a single strand gap of 25~30 nucleotides, leaving a gap behind for further repair steps.

Replication factor C (RFC) then recruits the Proliferating Cell Nuclear Antigen (PCNA) to the DNA strand. This, in turn, activates DNA polymerases (δ, ε, and/or κ) to use the intact DNA strand as a template to reproduce a new segment. Once a new segment is synthesised, DNA ligases such as DNA ligase I and Flap endonuclease I or DNA Ligase-III-XRCC1 complex fill the gaps to complete nucleotide excision repair.[105]

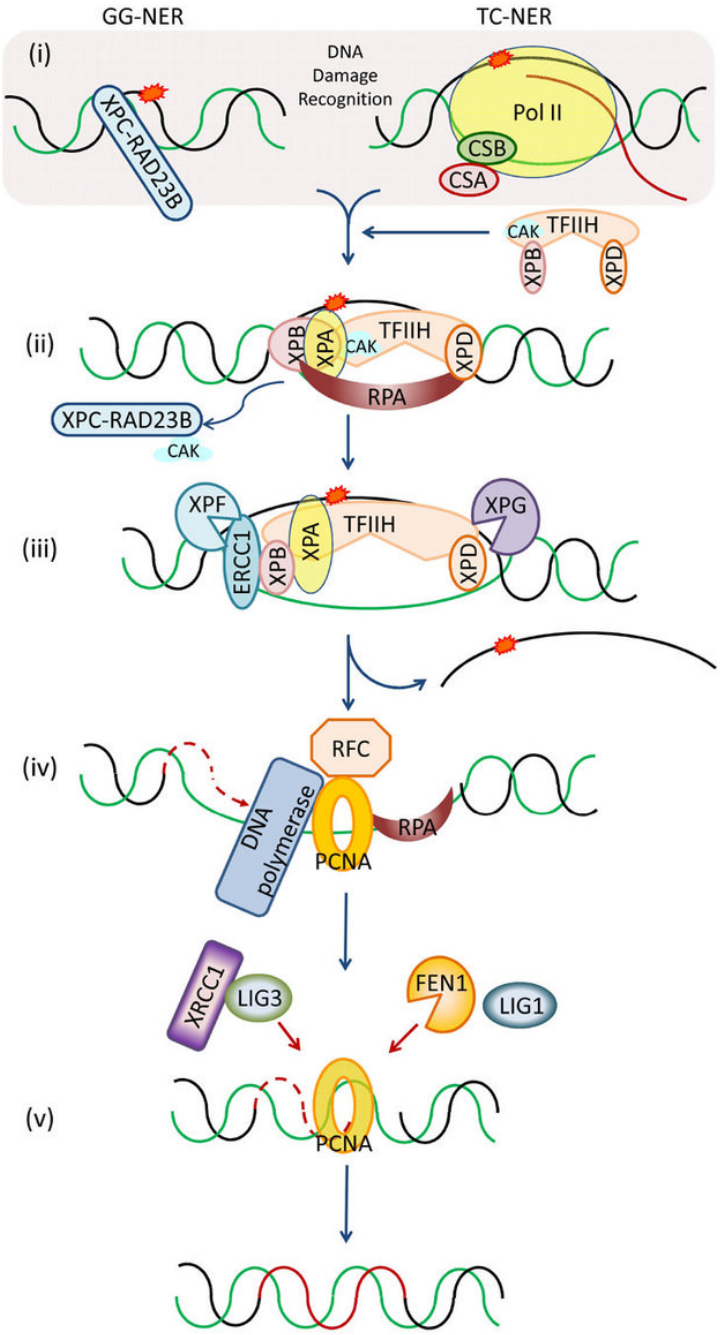

Figure 1.9 Nucleotide excision repair mechanisms (Adapted from Iyama et al., DNA repair (Amst), 2003).

Nucleotide excision repair mechanisms involve two pathways: (i) GG-NER that has XPC-RAD23B which identified DNA damaged nucleotide, while (ii) TC-NER is initiated by stalling of an elongating RNAP at the damage site. Then TFIIH complex is recruited to promotes opening of the DNA duplex around the lesion, facilitating recruitment of endonucleases such as XPF–ERCC1 and XPG, to incise the 5' and 3' ends of the damage site. This followed by new nucleotide synthesis by DNA polymerase prior to sealing the gap site by either XRCC1–LIG3α or a FEN1–LIG1 complex.

1.3.3.3 The DNA mismatch repair (MMR)

During DNA synthesis, DNA polymerases sometimes leave faulty base-base mismatches. In order to avoid leaving these faulty lesions behind, the DNA mismatch repair mechanism is responsible for removing these base–base mismatches.[106 -109] After completing DNA synthesis, the newly produced strand is scanned for errors, which is identified by the mismatch repair mechanism.

Mismatches result from spontaneous deamination of 5- methylcytosine and heteroduplexes formed following genetic recombination. Mismatch repair process dysfunction results in spontaneous mutations and increased microsatellite instability (MSI). For example, mutations in mismatch repair genes cause a predisposition to hereditary nonpolyposis colorectal carcinoma (HNPCC).

Similar to base and nucleotide excision repair mechanisms, in the mismatch repair process, the DNA lesion (base-base mismatch) is identified by the MSH2-MSH6 complex (known as MutS alpha-beta) proteins. Following lesion identification, further recruitment of mismatch repair proteins, such as MLH1-PMS2 (MutL alpha-beta), DNA polymerases, and replication factors, e.g., proliferating cell nuclear antigen (PCNA).[110, 111] DNA mismatch lesion is resected, and a new DNA segment is replicated using an intact template strand is performed by PCNA, *Replication factor C*, and DNA polymerases δ and ε.[112, 113]

1.3.3.4 Repair of single-strand breaks

Reactive oxygen species are considered to be the most common cause of single-strand breaks, which occurs by destroying deoxyribose residues. Intact DNA repair mechanism identifies sites of single-strand breaks to recruit the same proteins as base excision repair for excision of damaged single-strand and replication of newly produced strand using the other intact strand as a template as mentioned earlier.[114]

1.3.3.5 Repair of double-strand breaks

Ionising radiation causes mainly single-strand breaks, with only about 5–7% as many double-strand breaks as single-strand breaks.[115, 1116] Double-strand breaks activate the DNA repair process and cell cycle checkpoints. The majority of double-strand breaks induced by low linear energy transfer (LET) radiation are re-joined within 30-60 min, whereas less than 20% require a longer time to be repaired and may persist more than 24 hrs.[117 - 122]

Immediately after exposure, DNA damage activates the damage sensor Mre11-Rad50-Nbs1 (MRN) complex, which rapidly phosphorylates ataxia telangiectasia mutated (ATM) protein. ATM is considered as the upstream protein that upregulates the activity of many downstream proteins that play a role in cell cycle checkpoints activation, resulting in DNA damage-induced arrest at G1/S, S, and G2/M to provide a chance to the DNA repair process.[123 – 129] There are two main pathways to repair double-strand breaks, (i) non-homologous end-joining (NHEJ) and (ii) homologous recombination (HR)(Figure 1.10).

1.3.3.5.1 Non-homologous End-Joining (NHEJ)

Non-homologous end-joining is the primary pathway to repair double-strand breaks. It is activated by the recruitment of sensor proteins, such as Ku70/80 and DNA-Protein kinases (DNA-PKcs), to the double-strand break site, followed by repairing the double-strand break by the MRN complex.[130, 131] Then gap filling by polymerases m and I, and ligation with Ligase IV, X-ray repair cross-complementing protein 4 (XRCC4), and XRCC4-like Factor (XLF).[132] Non-homologous end-joining operates via (i) a fast process which involves Ku70/80, and DNA-PK, and (ii) a slower process involves MRN, DNA-binding proteins, and exonucleases that repair more complex breaks.[133 - 136]

Fast NHEJ reaction: Double-strand breaks begin to rejoin rapidly after irradiation, with half-time of about 10 mins or less.[137] This rapid rejoining involves the accumulation of sensor proteins Ku70/80, which is recruited to all double-strand breaks, and DNA-PKs that are recruited and take part only in the repair of more complex breaks. End-binding proteins such as DNA ligases are also recruited to the site of the break, and it forms a complex with the cofactor XRCC4, to join the two ends.[118, 138, 139]

Slow NHEJ Reaction*:* After the rapid phase of rejoining is complete, persistent unrepaired double-strand breaks are repaired by a slower non-homologous end-joining pathway, which has a half-time of several hrs. Phosphorylated ATM activates NBS1, which activates MRN complexes at the double-strand breaks. MRN complexes have endonuclease and DNA-binding activity. Therefore, they are involved in the slower repair of persistent double-strand breaks that cannot be repaired by the fast non-homologous end-joining mechanism.[130]

1.3.3.5.2 Homologous Recombination (HR)

It is a genetic recombination process in which nucleotide sequences are exchanged between two similar or identical DNA molecules. It is the most common method for repairing double-

strand breaks. It is a more complicated repair mechanism as it is dependent on matching the damaged DNA with its intact identical sequence in the sister chromatid after DNA replication Homologous recombinant remains a minor pathway for the repair of double-strand breaks caused by ionising radiation in somatic cells due to the low level of sister-chromatid exchange that is induced by X-rays and high-LET radiation.[140]

The hRad51 protein plays an essential role in facilitating homologous pairing, in co-ordination with accessory proteins, such as hRad52, hRad54, XRCC2, and XRCC3.[141] The repair of a double strand break by homologous recombination occurs by matching the broken ends of a damaged DNA strand with identical sequences of intact DNA.

Both of the 5 ends of the double-strand break undergo nucleases degradation to produce 3'-single-stranded DNA (ssDNA) tails. Then, Rad51 helps one of the 3'-ssDNA tails from the broken parental duplex to invade an intact homologous duplex and forms (displacement loop) D-loop structure. The second 3'-ssDNA tail could link to the displaced strand at the joint. 3' ends then prime new DNA synthesis using the intact duplex as a template. The broken and intact molecules are arranged according to their sequences and integrated by hRad51 that co-ordinate the repair by invading the single strands to their homologues in order to produce X-shaped four-armed structure called a Holliday junction. These Holliday junctions are four-stranded branched structures, which is cleaved by a resolvase that cuts the crossed or non-crossed strands, producing two intact double-strand DNA.[142 - 144]

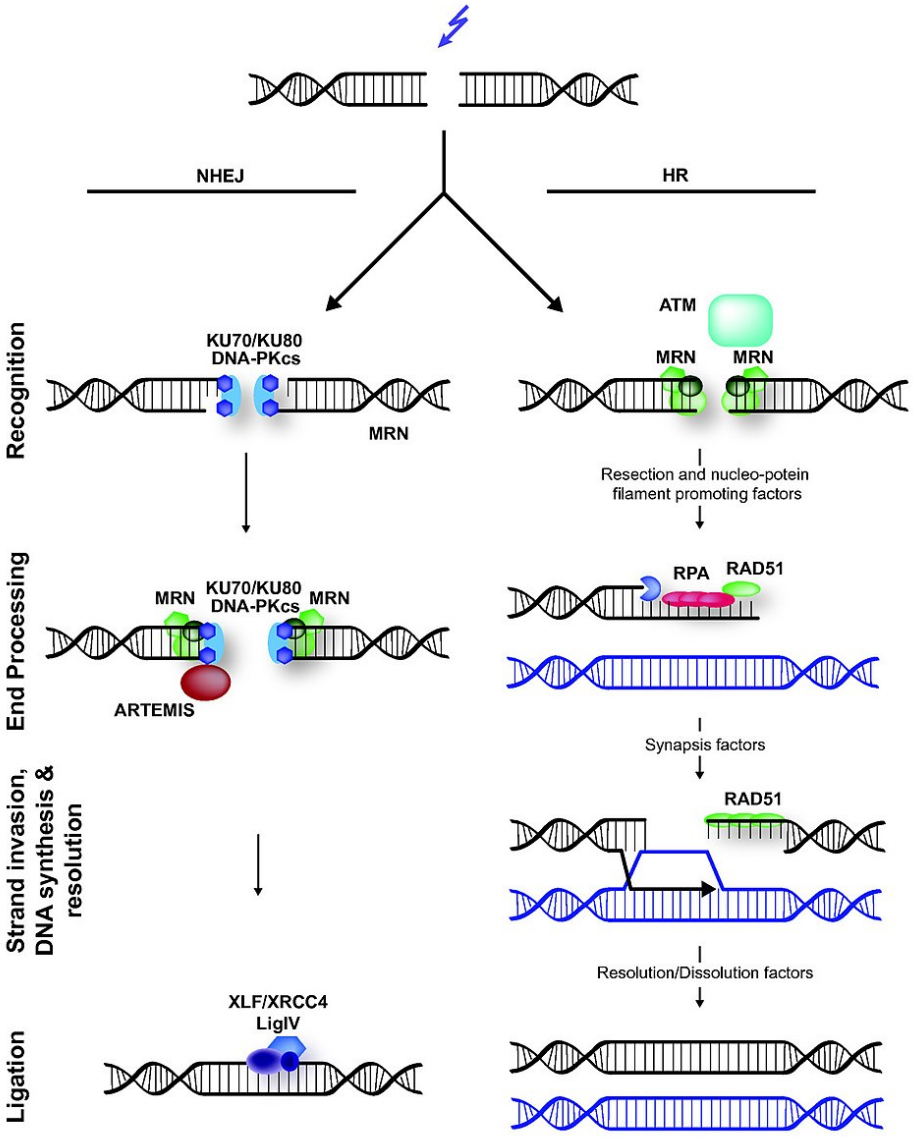

Figure 1.10 Mechanism of double strand DNA breaks repair (Adpated from Hannes Lans, Jurgen A Marteijn and Wim Vermeulen, Biomed Central)
DNA DSBs Repair involves two main pathways which are non-homologous end-joining (NHEJ) or homologous recombination (HR). Four main steps: recognition, end processing, strand invasions and DNA synthesis and ligation.

1.3.4 Cell cycle checkpoints control in cells exposed to ionising radiation

Cell cycle checkpoints are pathways that coordinate the order and timing of the cell cycle transitions to ensure completion of one cellular event prior to the beginning of another. Radiation-induced DNA damage delays the normal progression of the cell cycle and activates checkpoints pathways that inhibit progression of cells through G1 and G2 phases and causes a transient delay in the progression through S phase in order to give cells a chance to repair the damaged genome prior to proceeding to next step in the cycle.[145, 146]

The main function of these checkpoints is to recognise DNA damage and give a chance for its repair.[147, 148] These checkpoints are mainly coordinated by checkpoints proteins such as: (i) Sensor proteins (e.g., Mre11–RAD50–NBS1 [MRN] complex and the BRCA1 protein) which recognise DNA damage and signal the presence of these abnormalities to initiate DNA repair cascade [136, 149, 150] (ii) Transducers are typically protein kinases that amplify the damage signal by phosphorylating downstream target proteins. ATM and ATR are of the phosphoinositide 3-kinase (PI3K)-related family, which are immediately downstream kinases of the damage sensors. The key regulators of the checkpoint pathways in the mammalian DNA damage response are ataxia telangiectasia mutated (ATM) and ataxia telangiectasia and Rad3-related (ATR) protein kinases.[151, 130] ATM is considered to be the main determinant of the early checkpoint response induced by ionising radiation damage, whereas ATR responds later to both ionising radiation and ultraviolet induced lesions.[148] ATM mutation is associated with gross chromosomal abnormalities, radioresistant DNA synthesis, as well as a reduction in G1 and G2 arrest, and (iii) Effector proteins that include the ultimate down-stream targets of the transducer protein kinases e.g. P53, MDM2, BRCA1, CHK2, MDC1 and NBS1.) Once effector proteins get activated/phosphorylated by transducer protein kinases, they induce inhibition of cell cycle progression.[152, 153]

G1 checkpoint

The G1 checkpoint is considered as the restriction point in mammalian cells, where the cell becomes committed to entering the cell cycle. Cells with DNA damage show G1 delay prior to progression to S phase to allow time for repair and prevents replication of a damaged template. Initiation of cell cycle progression depends on the activation of two key regulatory kinases, CDK2 and CDK4, in association with cyclins E and cyclin D, respectively. Phosphorylation of target proteins by CDK4 and CDK2 promotes entry into S phase.[154]

During the acute phase of the ionising radiation induced DNA damage response, activation of ATM leads to phosphorylation and activation of CHK2 which phosphorylates CDC25A leading to its degradation. In the absence of CDC25A, CDK2-cyclin E and CDK4-cyclin D complexes remain inactive, and the cell remains in G1 (Figure 1.11).[155, 156]

A second G1 arrest mechanism also involves ATM and CHK2 through stabilising p53 by phosphorylation. The stable p53 then acts a transcriptional activator of several target genes, including p21, an inhibitor of CDK2-cyclin E complex (Figure 1.11).[157]

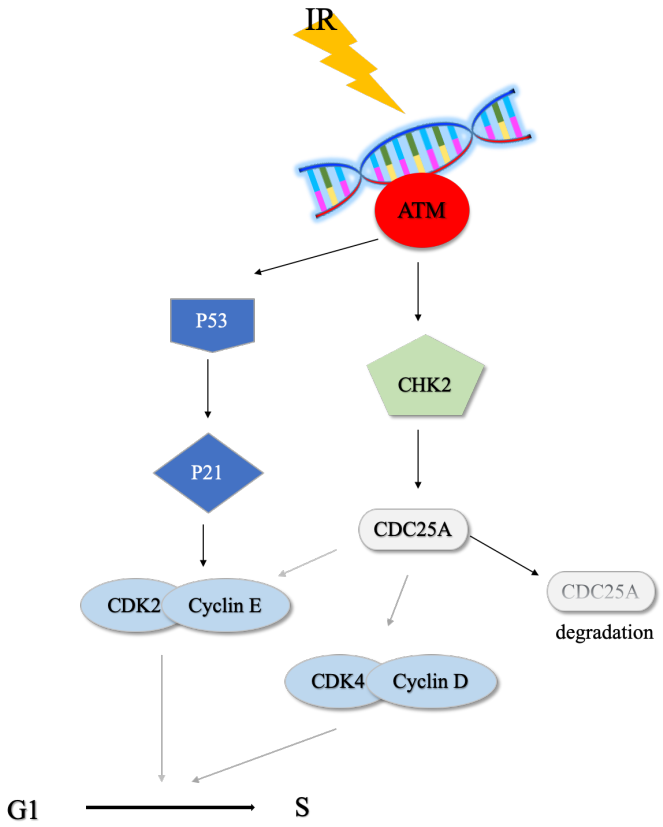

Figure 1.11 Mechanism of G1 checkpoint (Adapted from Nyberg et al., Annu. Rev. Genet., 2002)
The G1 checkpoint stabilises p53 and induces Cdc25A degradation to maintain Cdk2 inhibitory phosphorylation to block Cdk2-cyclin E activity. Faded arrows represent blocked pathways.

S phase checkpoint

Ionising radiation induced DNA damage activates the S-phase checkpoint via at least two parallel pathways, both of which are regulated by ATM.[158-160]

The first pathway is ATM/CHK2/CDC25 pathway, and it happens when radiation induced DNA damage activates ATM which phosphorylates CHK2, which in turn deactivate CDC25A by phosphorylation followed by degradation as mentioned in G1 checkpoint. Degradation of CDC25A maintains inactive phosphorylated CDK2 and stops it from interacting with either cyclin A or cyclin E, and blocks replication process by inhibiting CDC45, leading to delay in S phase progression (Figure 1.12).[161, 162]

The second branch is ATM/NBS1/SMC1 pathway, which is independent of CDC25A, and requires the activities of both ATM and NBS1.[158-160] After radiation exposure, ATM phosphorylates NBS1, and then phosphorylates structural maintenance of chromosome protein 1 (SMC1) in an NBS1-dependent manner.[158-160] Phosphorylated SMC1 may play a role in

removing the signal and participates in the replication elongation process by interrupting the connection between the template and the sister chromatid, thus slowing down the progression of the replication fork (Figure 1.12).[159]

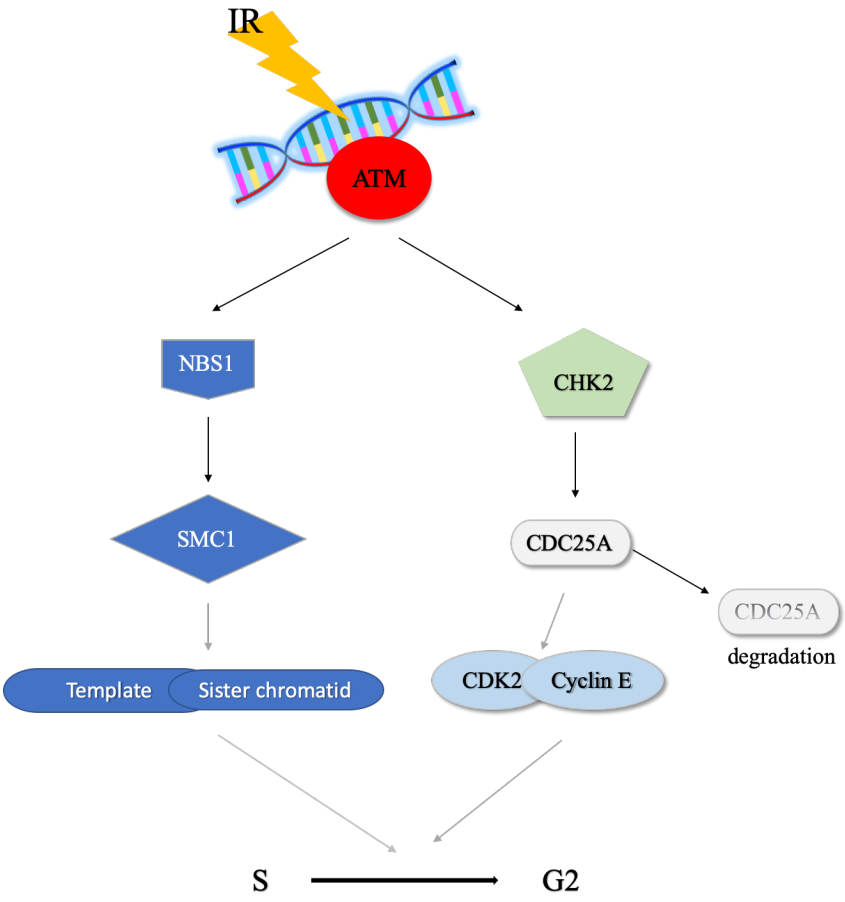

Figure 1.12 Mechanism of S phase checkpoint (Adapted from Nyberg et al., Annu. Rev. Genet., 2002)
S checkpoint involves two main ATM induced pathways, via NBS1 and CHK2 which block cell progression to G2 phase. Faded arrows represent blocked pathways.

G2/M checkpoint

Entry into mitosis is dependent on the activity of the cyclin dependent kinase CDC2, as it is considered a key effector of the G2 checkpoint. When CDC2 binds to cyclin B, it leads to its activation which induces mitosis initiation.[163]

After cell exposure to radiation, ATM recruited to DNA damage sites, and activates CHK2 and p53 to induce cell cycle arrest and stop progression into mitosis.[164] CHK2 phosphorylates CDC25 which, in addition to being inhibited, is also sequestered in the cytoplasm by the 14-3-3 proteins. 14-3-3 are upregulated by p53, which is activated by ATM. p53 activates p21, and both p21 and 14-3-3 in turn inhibit CDC2-cyclin B complexes through the phosphorylation

and cytoplasmic sequestering of CDC2. In addition, the inactivation of CDC25 results in its inability to dephosphorylate and activate CDC2 (Figure 1.13).[165, 166]

ATM activates Polo-like kinase 3 (PIK3) directly and PIK1 through CHK2, which leads to CDC25C inhibition.[167 – 169] Plk1 activation stabilise Wee1 (a tyrosine kinase) which results in phosphorylation of CDC2-cyclin B kinase, and keeping the cell arrested in G2 until the damage is fixed (Figure 1.13).[170]

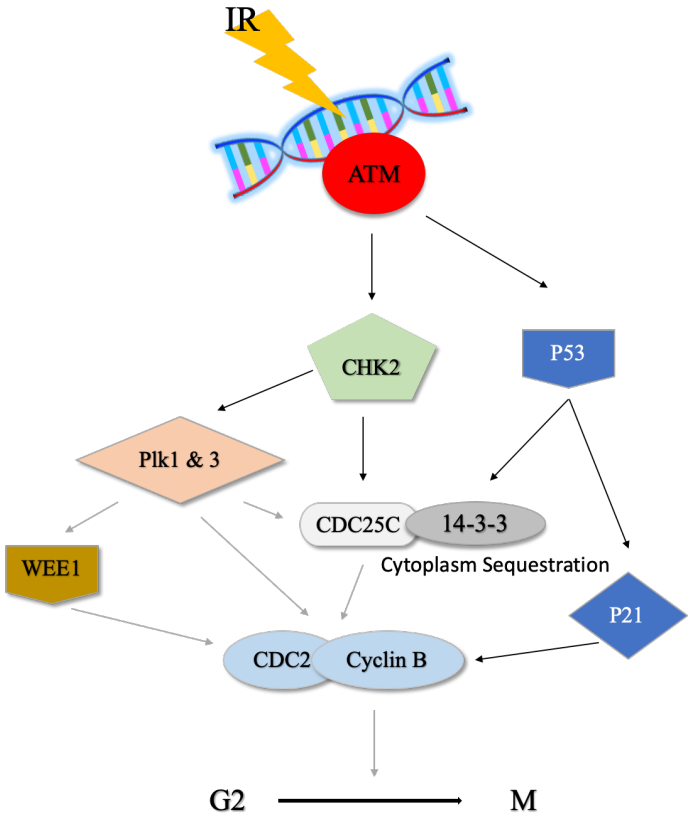

Figure 1.13 Mechanism of G2/M checkpoint (Adapted from Nyberg et al., Annu. Rev. Genet., 2002)
The G2 checkpoint blocks Cdc2- cyclin B activity by blocking Cdc25C phosphatase activity, by stimulating its association with 14-3-3-proteins. Faded arrows represent blocked pathways.

1.3.5 Biomarkers of radiation induced DNA damage/repair

Conventional radiation exposure measuring methods such as dose area product do not take into account operator position or behaviour. Personal dosimeters currently used by operators crudely record cumulative exposure in an isolated body area.

The "safe" exposure limits defined using these tools may not apply universally as they do not take into account individual susceptibility to DNA damage. Recently, biomarkers have

emerged as surrogate sensitive tools for the biological assessment of radiation exposure. These include cytogenetic (e.g., chromosomal aberrations, micronuclei), epigenomic (e.g., miRNA, IncRNA), and proteomic markers (e.g., γ-H2AX and pATM).

1.3.5.1 Protein biomarkers

During the acute phase of exposure, the formation of double strand DNA breaks causes activation of a damage sensor the Mre11-Rad50-Nbs1 (MRN) complex, which triggers rapid phosphorylation of ataxia telangiectasia mutated (ATM) protein and H2AX.[123 - 125, 171]

These markers are sensitive and can be quantified using flow cytometry or immunofluorescence microscopy following low dose radiation exposure < 1mGy.[172]

Gamma-H2AX (γ-H2AX)

In mammalian cells, DNA is wrapped around histone proteins to form chromatin. These histone proteins are H2A, H2B, H3 and H4. H2AX is a variant of the H2A protein, which constitute 2-25% of all nucleosomes.[173]

When double-strand DNA breaks occur, one of the earliest responses is recruiting H2AX to the site of the break, which is rapidly phosphorylated by ATM kinase to γ-H2AX. The repair process of DNA breaks results in γ-H2AX dephosphorylation.[174] Previous studies showed that in human cells, there is a background of 5% intracellular phosphorylated H2AX. When levels of γ-H2AX levels increased to 10% after low doses of X-ray exposure, the majority of affected cells succeeded to recover γ-H2AX by dephosphorylation, except a small percentage remained phosphorylated for longer time.[172] Ionising radiation induces double strand DNA breaks, which leads to phosphorylation of H2AX to form γ-H2AX as one of the acute cellular response to DNA damage. The levels of γ-H2AX that can be detected under the microscope in the cell peaking between 30 to 60 mins after exposure.[72, 172, 175] Studies suggest a strong correlation between measured γ-H2AX foci count under the microscope and numbers of double strand breaks induced, which provides an accurate estimate to DNA damage in circulating cells during the acute phase as an early response to that damage.[176] This enabled investigators to measure γ-H2AX foci which were elevated in mononuclear cells from patients exposed to radiation after computerised tomography (CT) scans,[72] and in paediatrics after cardiac catheterisation procedures.[177]

Phosphorylated ataxia telangiectasia mutated (pATM)

Ataxia telangiectasia mutated kinase (ATM) is a serine/threonine kinase that regulates cell cycle checkpoints and DNA repair.[178]

When patients have ATM mutated gene, they develop ataxia–telangiectasia (AT) genetic disorder, which is caused by a defect in the cellular signaling pathway. These patients suffer from immune deficiency, cerebellar degeneration and also high risk of developing cancer. ATM is involved in the regulation of cell signaling pathways and cell cycle progression due to (1) its C-terminal domain is homologous to phosphatidylinositol-3-kinase (PIK), hence the connection to signaling pathways, and (2) ATM protein also has regions of homology to DNA-dependent protein kinases, which require breaks to bind DNA, ATM protein is therefore involved in the DNA damage/repair process.

During the acute phase as a first response to double strand DNA breaks, stimulation of the damage sensor Mre11-Rad50-Nbs1 complex causes phosphorylation of ATM protein on Ser1981.[132 - 135, 188] ATM phosphorylation leads to activation of downstream targets that act as cell cycle checkpoints, resulting in DNA damage induced arrest at G1/S, S, and G2/M in order to give the opportunity for DNA repair.[127, 148, 180]

ATM deficient cells show higher initial chromosomal damage, and even greater residual chromosomal damage in G1 as well as in G2 after exposure to ionising radiation. These cells are sensitive to ionising radiation induced apoptosis in all cell cycle phases. ATM is therefore believed to have a critical role in cell response after radiation exposure.[181 Expression] of pATM in circulating lymphocytes can be used as a sensitive biomarker of radiation-induced DNA damage. This could facilitate a biological assessment of the acute adverse effects of radiation exposure.[182]

γ-H2AX and pATM are sensitive biological markers and can detect radiosensitive individuals against low dose radiation. These markers can be measured using flow cytometry or immunohistochemistry techniques allowing detection of radiation-induced DNA damage at low doses < 1mGy.[172] Both proteins are, however, only useful for measuring the acute, transient response to radiation induced DNA damage. pATM and γ–H2AX in circulating lymphocytes can, therefore, be used as sensitive biomarkers of measuring the acute phase of radiation-induced DNA damage/repair.

8-oxoguanine DNA glycosylase-1 (OGG1)

Environmental causes such as ionising radiation induce the production of reactive oxygen species (ROS) which, in turn, causes DNA damage. ROS induced oxidative DNA damage

primarily damage guanine because it has the lowest oxidation potential among the DNA bases.[183, 184] Guanine's oxidised product 7,8-dihydro-8-oxoguanine (8-oxoG) is the most predominant DNA oxidative lesion in the genome.[183 – 185] It is estimated that up to 100,000 8-oxoG lesions can be formed daily in DNA per cell.[184, 186] Therefore, 8-oxoG could be used as a biomarker of ionising radiation induced oxidative stress.[184, 187] 8-oxoG is mutagenic protein as it has the ability to pair with adenine instead of cytosine, which result in a G:C to T:A transversion during DNA replication.[184, 187 , 188 – 190] In eukaryotic cells, to prevent 8-oxoG accumulation and its mutagenic effects, 8-oxoG is repaired by 8-oxoG DNA glycosylase 1 (OGG1) through base excision repair (BER) pathway.[184, 185, 188, 191 - 193] OGG1 is a DNA glycosylase with an associated apurinic/apyrimidinic (AP) lyase activity that cleaves DNA at abasic sites via a β-elimination mechanism.[194, 195] The process of recognition and repair of 8-oxoG by OGG1 is well understood, and it represents one of the oldest DNA base excision repair pathways. [193, 194, 205] OGG1 antibody can be used as a validated biomarker of base oxidation using techniques such as flow cytometry and immunocytochemistry.[197, 198]

1.3.5.2 Cytogenetic biomarkers

Ionising radiation induces double strand DNA breaks which are considered the most deleterious forms of DNA damage as they are difficult to repair.[199, 200] If unrepaired, double strand breaks can result in chromosomal instability, deletions and rearrangements such as translocations and inversions that can lead to gene mutations.[126] These can be detected using techniques such as fluorescence *in situ* hybridisation (FISH).[201] These types of chromosomal abnormalities have been detected in lymphocytes of both patients and hospital staff after chronic exposure to low dose radiation.[72, 175, 202]

The frequency of chromosomal aberrations in circulating lymphocytes between children underwent interventional cardiac procedures was higher compared with control group. This was suggested to be used as an endpoint of mutagenesis and a surrogate biomarker of increased the life attributable risk of cancer.[203] Particularly, prospective cohort studies have shown a significant association between high chromosomal change frequency in peripheral human lymphocytes and the risk of cancer.[204]

Chromosomal translocations have been found years after occupational radiation exposure and having been passed on from irradiated stem cells to descendent cells, in radiological technicians.[171] Technological advances using a semi-automated FISH-based micronucleus-centromere assay have shown that, even when interventionists had very low radiation exposure

as reported by their standard dosimetry, they still showed evidence of relatively high levels of chromosomal damage.[205] The frequency of chromosomal abnormalities correlates well with the duration of occupational radiation exposure.[206]

Radiation induced chromosomal abnormalities in dividing cells result in production of micronuclei, which are extranuclear bodies that originate from chromosomal fragments or whole chromosomes that are not included in the daughter nuclei during mitotic division. Micronuclei not only can be used as biological dosimeter for radiation exposure in peripheral lymphocytes, but also as a predictor of increased cancer risk based on reports connecting high micronuclei frequency and cancer development.[207 – 209] Somatic DNA damage was therefore studied after chronic low-dose X-ray radiation exposure among interventional cardiologists working in high-volume cardiac catheterisation services. Interventional cardiologists had higher micronuclei levels (somatic DNA damage) when compared with clinical cardiologists (controls), micronuclei frequency correlated significantly with the number of years of practice/exposure.[206]

Among similar cohort of interventionists, there was an association between higher micronuclei frequency and X-ray repair cross-complementing-3 (XRCC3) Thr241Met genetic polymorphism, which is considered as an indicator of low DNA damaged repair capacity.[210, 211]

Radiation induced cell death and tissue damage was measured in interventionists who exposed to long term low dose radiation by studying their serum cell free-DNA levels and mitochondrial DNA fragments. Exposed operators showed higher levels of cell free DNA and mitochondrial DNA compared with their non-exposed colleagues. This was further analysed to show high-exposure interventionists had significant increased levels of cell free DNA and mitochondrial DNA compared to low-exposure cohort.[212]

Mitochondrial DNA (mtDNA) is vulnerable to oxidative stress, e.g. ionising radiation, as it lacks histone protection with limited DNA repair capacity. The 4977-bp mitochondrial (mtDNA4977) deletion is the most common deletion of mtDNA. Deletions affect mitochondrial function, compromising energy production efficiency, resulting in harmful reactive oxygen species production.[213] Therefore, mtDNA alterations such as the 4977-bp mitochondrial deletions were linked to many diseases, for example, cataract, cardiomyopathy and neuropathy. Hence, it has been suggested that mtDNA could be used as a promising biomarker of oxidative damage such as occupational chronic low dose radiation exposure.[214]

Interventionists have higher levels of mtDNA4977 deletions in their peripheral blood after long term low dose radiation exposure, compared with their unexposed colleagues. The increase in

levels of radiation induced mtDNA4977 deletions indicates that mitochondrial dysfunction could be a common target of ionising radiation, resulting in radiation induced occupational health risks.[215, 216]

This mitochondrial dysfunction is found to have a major role in carcinogenesis, as in a meta-analysis of 1613 cancer cases, mitochondrial DNA mutations and deletions, particularly, the mtDNA 4,977 bp deletion was detected in different types of cancers such as leukaemia, breast, colorectal, gastric, head and neck cancer.[213, 217]

1.3.5.3 Genetic biomarkers

Genome transcription analysis of cells exposed to low doses of radiation has shown an increase in the expression of genes for DNA repair (*DDB2*, *XRCC4*), cell cycle checkpoints (*CDKN1A, GADD45A*) and apoptosis (*PUMA*).[218 - 220] Significant changes in gene expression e.g. *DDB2, XRCC4 and BAX*, have also been reported in patients undergoing CT angiography, and have implications for patients who undergo complex endovascular aortic repair and subsequent regular CT surveillance.[221, 222]

1.3.5.4 Epigenomic Biomarkers

MicroRNAs (miRNAs), are noncoding RNAs that post-transcriptionally regulate gene expression that become dysregulated in many pathologies. Circulating miRNAs have low inter-individual variability and can be measured in samples of serum and plasma.[219, 223, 224]. Brain-specific miR-134 was significantly downregulated in the serum of interventional cardiologists, particularly, among high-exposure group. This brain-specific miRNA is involved in brain synapse development with effect on memory and learning abilities, and is also dysregulated in pathologies such as Alzheimer's, epilepsy, and glioblastomas. Thus, radiation induced brain-specific miR-134 dysregulation advocates that brain damage could be a potential long-term effect of head exposure among interventionists.[225, 226]

1.4 Lymphocytes biology

Two cell lines arise from pluripotent stem cells; these cells are the backbone of the immune system. Two lineages are: (i) the lymphoid lineage which produces lymphocytes, and (ii) the myeloid lineage which produces phagocytes (monocytes, macrophages, and neutrophils) and some other cells such as red blood cells, granulocytes (neutrophils, basophils, and eosinophils), mast cells and dendritic cells (Figure 14).

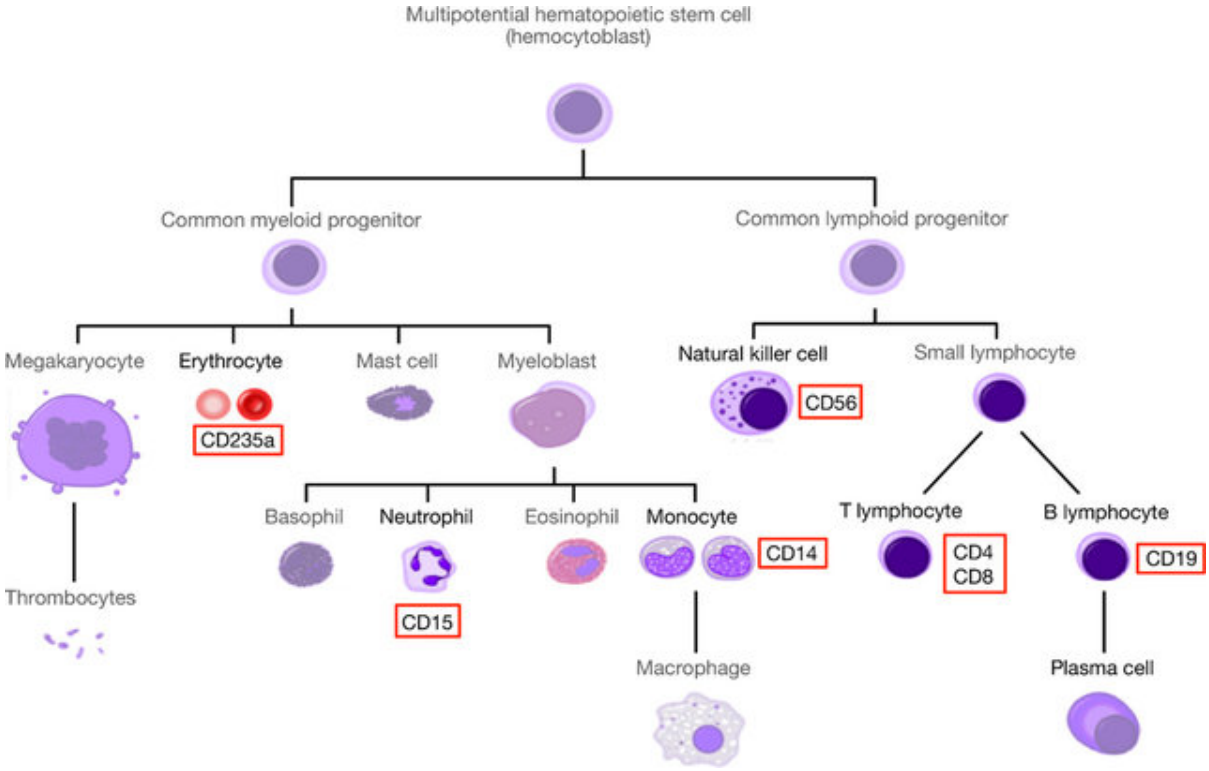

Figure 1.14 Human hematopoietic tree of different cell compounds (Adapted from Juzenas et al., Nucleic Acids Research, 2017)

1.4.1 T-Lymphocytes (T Cells)

In adults, lymphocytes are 20 to 40 % of white blood cells. T Cells are found either in the circulation or concentrated in central lymphoid organs and tissues, such as spleen, tonsils, and lymph nodes. T lymphocytes

Regulatory cells, Memory cells and NKT cells (Figure 1.15)

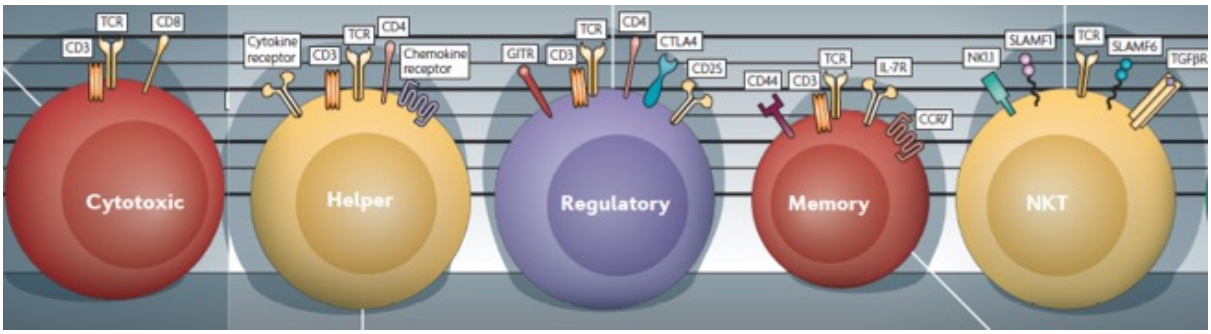

Figure 1.15 Lymphocytes main subpopulations (Adapted from Dong et al., Nature Reviews Immunology, 2010)
Main subpopulations of lymphocytes

Regulatory cells (CD3 and CD25), Memory cells (CD3, CD44, and CCR7), and NKT cells (CD3 and TCR)

Life cycle of T lymphocytes

Lymphoid precursor cells migrate from the bone marrow to the thymus where they divide and differentiate into T cells. T cells acquire antigen receptors and differentiate into helper or cytotoxic T cells. These cell types are similar in appearance, but different in their function and cell surface receptors e.g., CD4 and CD8. Most of T cells die before they leave the thymus, so that those T cells that released into the circulation are the ones capable of identifying foreign antigens. These cells then circulate to blood to the lymphoid tissues, where if suitably stimulated, they further multiply to take part in the immune response. In humans, large numbers of T cells are produced in the neonatal period, but production gradually slows down during adulthood, and is diminished in old age associated thymus atrophy. Cell-mediated immunity however persists throughout life, because of T cells that emerge from the thymus continue to divide and function for life.[227]

1.4.2 B Lymphocytes (B-Cells)

They are lymphocyte subtype, and they mature in the bone marrow. They play an essential role in the humoral immunity element of the adaptive immune system. B lymphocytes are found in blood, lymph nodes, spleen, tonsils and other mucosal tissues. They constitute about 5–25% of all human blood lymphocytes.

1.4.5 Role of lymphocytes in studying the biological effect of radiation

Radiation induced decrease in peripheral blood cells was observed in patients with cancer when they underwent radiotherapy. Further analysis found that circulating lymphocytes were the most radiosensitive cells amongst the erythroid, myeloid and lymphoid lineage cells to ionising

radiation which sometimes required years to recover after the radiotherapy course.[228 – 233] Deeper phenotyping studies showed circulating T lymphocytes were more sensitive and their levels were further reduced compared with B lymphocytes, when patients were exposed to ionising radiation during radiotherapy sessions.[234, 235]

Circulating lymphocytes are not only sensitive to radiation but also accessible, and it requires minimal medical intervention for their sampling and collection from individuals. Therefore, this approach allowed investigators to study the acute biological consequences of low-dose radiation exposure among individuals by collecting their lymphocytes and analysing the effect of radiation using different biomarkers. For example, Löbrich et al., used lymphocytes to measure gamma-H2AX foci from patients underwent computed tomography examination to evaluate radiation induced double strand DNA breaks.[72] Investigators also used peripheral blood T lymphocytes to measure the biological effect of radiation in patients underwent cardiac catheterization procedures, considering T lymphocytes sensitivity to radiation and their easy accessibility.[177]

1.5 The biological effect of radiation exposure

When exposed to ionising radiation, the amount of energy absorbed in the body tissues and organs initiates biochemical changes at the cellular. The harmful effects of ionising radiation can be divided into deterministic and stochastic effects. Deterministic effects (tissue reactions) result from radiation-induced cell death and organ dysfunction. These are characterised by a threshold radiation dose above which the severity of injury increases with increasing delivered dose. These effects only occur with relatively high radiation exposures and are usually evident within hrs or days of a radiation exposure.[236 - 240]

The most common deterministic effects are skin lesions and lens opacities.[241, 242]

Radiation-induced skin injury can be a serious complication of endovascular interventions. Transient erythema occurs at doses of 2 to 5Gy, whereas permanent epilation, ulceration, and desquamation are seen at higher doses. Skin injury usually appears 4 weeks after exposure and can last many weeks, particularly if secondary infection occurs.[35]

The incidence of radiation-induced skin injury is thought to be less than 0.01% of fluoroscopically guided interventions; however, it is likely to be under-reported or misdiagnosed.[243] One recent report evaluated 400 percutaneous coronary interventions and found six patients with mild erythema that was displayed within 4 weeks after the procedure. The minimal skin dose for injury was 6 Gy.[244]

The peak skin dose (PSD) is the highest dose delivered to any individual portion of the skin during a procedure and determines the risk of injury. In a study in Guy's and St Thomas' Hospital, PDS was measured using Gafchromic films that were placed between the operating table and the patient and found that skin doses were 0.8Gy (0.46 - 1.44) for thoracic endovascular aortic repair (TEVAR), 0.71Gy (0.44-13.7) for infra-renal endovascular aortic repair (IEVAR) and 1.3Gy (0.7-8.7) for branched endovascular aortic repair / fenestrated endovascular aortic repair (BEVAR/FEVAR). These data support similar results from other groups.[42, 245] Skin injuries should, therefore, be unlikely in patients undergoing EVAR.[246] Nevertheless, others have found that the threshold for possible radiation-induced skin damage of 2Gy is exceeded in 29% of EVAR procedures.[247]

Skin cancer directly related to radiation from an interventional procedure has not been reported although the risk of basal cell carcinoma was found to be increased in large cohort of US radiology technicians as a result of radiation exposure before the age of 30.[248] A recent survey of 466 interventional cardiologists, electrophysiologist, nurses and technicians revealed higher incidences of skin lesions, cataracts, hypertension, and hypercholesterolemia compared with non-radiation-exposed workers, with increasing incidence in those who had worked for more than 16 years.[249]

Radiation effect on the eyes *such as* posterior subcapsular cataracts are considered as the most frequently sub-type of cataracts associated with ionising radiation exposure. It was believed that radiation-induced cataracts form deterministically, with thresholds of 5 Gy/single exposures and 8 Gy/protracted exposures. However, more recent data suggest that cataracts may form stochastically, without a threshold dose, and potentially in response to the damage of a single cell.[250]

Several studies suggest that lens opacification occurs at exposures lower than 2 Gy and that there may be no dose threshold.[251 - 253]

Studies among Chernobyl clean-up workers, A-bomb survivors, astronauts, residents of contaminated buildings and interventional clinicians have also found that there is an increased incidence of lens opacities at doses below 0.5 Gy.[254] It has also been proposed that cataracts can occur after only 0.1Gy doses, thus supporting a non-threshold model.[255, 256]

Whether deterministic or stochastic in nature, cataracts can be found in up to 50% of interventional cardiologists.[257] The current literature suggests that there is at least a three to six-fold increased risk of posterior subcapsular has been reported in interventional cardiologists compared with unexposed individuals.[258 - 260]

Posterior subcapsular lens changes characteristic of ionising radiation exposure have been found in up to 50% of interventional cardiologists and 41% of nurses and technicians compared with less than 10 % of controls.[261]

The Retrospective Evaluation of Lens Injuries and Dose (RELID) trial also reported the significantly increased risk of cataracts in interventionalists. [258- 260]

Eye exposures are higher for thoracic endovascular aortic repair [TEVAR, (0.57 ± 0.41)], branched endovascular aortic repair [BEVAR, (0.70 ± 0.65)] and fenestrated endovascular aortic repair [FEVAR, (0.69 ± 0.46)] when compared infra-renal endovascular aortic repair [IEVAR, (0.47 ± 0.34)].[262]

Renal and mesenteric vessels embolisation procedures have been shown to be associated with the higher lens doses (60μSv per procedure).[263]

Therefore, in 2011, the International Commission on Radiological Protection (ICRP) reduced the safe dose limit from 150mSv in a year for the lens to 20mSv per year, averaged over 5 years, with no single year exceeding 50 mSv.[257]

Radiation induced carotid artery stenosis can result from the radiation effect causing an increase in carotid intima-media thickness, carotid stenosis and consequently a higher risk of cerebrovascular events, such as transient ischemic attack and stroke. Patients with newly diagnosed nasopharyngeal carcinoma, developed significantly carotid artery stenosis after radiotherapy compared to pre-radiation group (56/71 vs. 11/51, respectively).[264]

Intima-medial thickness severity was found to be proportional to the duration of radiotherapy. As a result, this has led to an increased risk of stroke in patients aged < 60 years irradiated for head and neck tumours.[365]

Similar results were reported with a significantly higher 10-year incidence of cerebrovascular events, in patients with head and neck cancer treated with radiation alone (34%), compared to patients who underwent surgery and radiotherapy (25%) or surgery alone (26%).[266] These cerebrovascular events would indeed have a great impact on the quality of life of survivors of head and neck malignancies.

Stochastic effects may occur by chance without a threshold level of dose. The probability, but not severity, of these effects is related to the dose, the development of a malignancy as a result of radiation exposure is the most common stochastic effect.

Ionising radiation is one of the few established causes of neural tumours.[172, 267] The incidence of nervous system tumours in atomic bomb survivors was dose related with increased risk of

tumour development following exposure to equivalent doses of radiation as low as <100 mSv.[268, 269]

Radiation-induced cancer risk estimates are based mainly on epidemiological studies of exposed human populations, incorporating data from atomic bomb survivor studies, as well as medical and occupational radiation studies. The linear-non-threshold (LNT) model remains the most appropriate risk model for low doses where the risk of cancer proceeds in a linear fashion and that there is no radiation dose, no matter how low, that can be considered completely safe.[24, 35] Although a linear relationship is assumed with between radiation exposure and malignancy studies have found that, when using biomarkers for DNA double-stranded break (DSB) such as ɣ-H2AX foci, the response to low-dose radiation is not linear and instead higher than expected from the extrapolation of high-dose data. Radiation exposure may, therefore, be even more harmful than is currently predicted using estimates from the LNT model. The use of biological markers such as ɣ-H2AX foci has been shown to increase the estimate of lifetime attributable cancer mortality five-fold.[177]

Early epidemiological studies of occupational radiation exposure in medicine prior to 1950 identified an excess risk of death from cancer, with increased rates of leukaemia, skin and breast malignancies.[4] A review of epidemiological studies of radiologists and technicians reported an increase in mortality from leukaemia among workers employed before 1950 and this was associated with duration of work involving radiation exposure in the early years.[270] Radiologists who worked for more than 40 years are reported to have a cancer-related mortality risk of 40%.[271, 272]

In cardiologists, the BRAIN study reported a significantly higher radiation exposure to the left and centre of the cranium compared with the right.[2] It has, therefore, been suggested that chronic low dose exposure has resulted in the development of left sided brain and neck tumours in interventionists, with glioblastoma multiforme the most common type of brain tumour.[2, 3]

However, more robust evidence is still needed due to the lack of large cohort studies with long term follow up.[273] There have been several studies reporting the risk of occupational radiation exposure. Medical x-ray workers have a 20% increased risk of cancer when compared with other medical specialists.[249, 274]

To my knowledge, there are no longitudinal studies that monitor the long-term health effects of radiation on cardiovascular interventionists using biomarkers that might explain the association between protracted exposure to low doses of ionising radiation and increased risk of cancer.

1.6 Variation in inter-individual sensitivity to radiation exposure

Current radiation protection strategies assume that all team members have the same sensitivity to radiation exposure and require the same level of protection. Although, there is an accumulating evidence from various studies suggesting variation in individuals' susceptibility to ionising radiation due to different genetic and lifestyle factors. Radiosensitivity means the sensitivity of cells, tissues or organs to the effect of ionising radiation. Epidemiological studies among atomic bomb survivors showed there was a variation in incidence of radiation induced malignancies based on factors such as age, gender and smoking.[275]

When patients underwent radiotherapy, individuals responded differently to radiation, and radiotherapy specialists noticed a variability in their patients' susceptibility to radiotherapy doses with acute and late tissue toxic reactions.[276] This variable response to standard radiotherapy courses and risk of developing radiation induced second cancer was explained due to factors such as patients' age, gender, lifestyle factors, primary cancer type, other treatments including chemotherapy, radiotherapy modalities and genetic predisposition.[277, 278] This finding raised the question about identifying patients who could be hypersensitive and are at risk of developing acute or late radiation toxicity.

One way to identify patients at higher risk of radiosensitivity, is by clinical phenotyping of individuals with rare syndromes secondary to mutations in genes crucial to the process of identifying DNA damage and/or its repair.

A strong example of the defected repair mechanism is a mutated ataxia telangiectasia gene, that leads to the Ataxia Telangiectasia syndrome. Patients with this syndrome show severe side effects such as skin injuries and even death during or after ionising radiation exposure e.g. radiotherapy.[279] Nijmegen breakage syndrome (NBS) is another example due to mutation in the gene producing NBS1 protein which plays an important role in DNA damage repair and cell cycle checkpoints. Patients with this syndrome display radiation hypersensitivity associated with higher risk of developing non-Hodgkin's lymphoma and brain cancer.[280]

Patients with AT and NBS syndromes showed a higher level of chromosomal aberrations in their lymphocytes when they were exposed to radiation and compared to healthy individuals.[281] These studies of individuals with known genetic mutations displaying clinical phenotypes helped us to establish a connection between genetics and high radiosensitivity. However, it remained challenging to identify subtle variation in inter-individual sensitivity, therefore

scientists studied levels of cell death when exposed to radiation among a relatively homogeneous population. This showed a significant variation in cells apoptotic response when their blood exposed to the same amount of ionising radiation.[282] Also, the ability of individuals to repair their radiation induced DNA damage after exposure during computed tomography examinations varied as measured by the number of gamma-H2AX foci.[72]

Consequently, scientists concluded that the variability in radiosensitivity could be due to generic factors only such as age, gender and lifestyle or due to both generic and genetic factors, thus a genetic profiling of suspected hypersensitive patients was encouraged using surrogate biomarkers to identify risk of developing acute or late radiation toxicity. Nevertheless, the connection between the radiosensitivity and risk of developing cancer has not been strongly established due to lack of long-term longitudinal studies.[276]

1.7 Rational of the present study

Minimally invasive endovascular aortic intervention holds great promise of the treatment of aortic aneurysms particularly in patients with multiple comorbidities and challenging anatomy. This is associated with great modifications and increasing the complexity of these procedures to enable inserting endografts in challenging aneurysm anatomy.

These fluoroscopy guided procedures are associated with inevitable ionising radiation exposure that might put patients and operators at risk of biological changes secondary to this exposure. This is particularly important to operators who are at risk of long term cumulative low dose exposure that might put them at risk of hazardous radiation effects such as malignancies.

Epidemiological studies reported on the risk of radiation induced health effects on individuals mainly originated from major incidents associated with high dose exposure such as Hiroshima and Nagasaki. Recently, reports on adverse effects among interventionists, suggested increase risk of cataract, blood and brain tumours. These hazards were thought to be related to radiation exposure throughout their career time. This has caused a major concern in the interventional community considering the expanding in the use of fluoroscopy guided interventions.

The advent of DNA damage biomarkers such as phosphorylated H2AX and ATM showed a promise to measure the biological effect of radiation exposure during the acute phase, that effect never used to be measurable in the past. This encouraged recent studies to use these DNA damage biomarkers to evaluate the acute response of patients up on radiation exposure during

diagnostic and therapeutic interventions. Strong evidence of radiation induced DNA damage was detected among these patients by an upregulation of their DNA damage biomarkers.
Nevertheless, operators' response to radiation, has not been studied up to date. Similar to patients, operators might respond to radiation exposure by DNA damage biomarkers upregulation. Operators' response might vary among themselves, an indicator of required individualised radiation protection strategies. Therefore, it is important to determine whether there is variation between operators' sensitivity to radiation exposure. It is also essential to identify the extent of protection achieved by conventional protection equipment, and role of extra protection such as leg guards.

1.8 Hypothesis

The radiation exposure to both patient and operator during endovascular aortic repair impacts peripheral blood cells, including the induction of DNA damage/repair in circulating lymphocytes.

1.9 Aims

1. To carry out a retrospective analysis of peri-operative changes in peripheral blood cell numbers after aortic repair.
2. To measure markers of acute DNA damage/repair in circulating lymphocytes isolated from patients and operators after open and endovascular aortic repair.
3. To determine if operators show any differential sensitivity to DNA damage induced by ionising radiation

CHAPTER 2

Analysis of peri-operative changes in circulating numbers of peripheral blood cells after aortic aneurysm repair

2.1 Introduction

Changes in the numbers of peripheral blood cells have been observed in patients after surgery, which may affect the innate and adaptive immune responses and, in turn, increase patient susceptibility to post-operative infection and/or sepsis.[283 - 287] After surgery, the number of peripheral leukocytes, such as neutrophils and monocytes, has been observed to increase, whilst the number of lymphocytes typically decreases.[288]

Anaesthesia and surgical trauma from major abdominal surgery, such as laparotomy and oesophagectomy, are associated with activation of inflammatory responses, including increased programmed lymphocyte death.[285, 286, 289] This apoptosis of lymphocytes is not observed in less traumatic procedures such as cholecystectomy.[290, 291]

After major cardiac surgery requiring cardiopulmonary bypass, a drop in the number of circulating lymphocytes is thought to occur as part of the systemic inflammatory surgical stress response.[292] Cardiopulmonary bypass induces hyperoxygenation, which produces free oxygen radicals, causing oxidative injury and inducing peripheral lymphocyte cells apoptosis.[293, 294]

Anaesthetic agents, particularly Sevoflurane and Isoflurane, can also cause post-operative lymphocytopenia, and induce apoptosis of lymphocytes in a dose-dependent manner.[295]

2.2 Aims

The aim of this part of the study was to carry out a retrospective analysis of changes in peripheral blood leukocytes, monocytes and lymphocytes count after endovascular and open aortic repair.

2.3 Study design and methods

2.3.1 Changes in peripheral blood cell count after aortic aneurysm repair

All patients who underwent endovascular or open aortic aneurysm repair between June 2010 and January 2015 in Guys' and St Thomas' Hospital were included in the study. As part of the routine management protocol, patients undergoing aortic repair would have a pre-operative and daily post-operative full blood count. The pre- and post-operative full blood counts were collated from the hospital electronic patient records. Peripheral leukocytes, monocytes and lymphocytes counts were compared in patients after open aneurysm repair, infra-renal (IEVAR), and branched and fenestrated endovascular aneurysm repair (BEVAR/FEVAR).

2.3.2 Statistical analysis

For comparison of paired groups, the paired t-test was used. For comparison of two groups, Mann-Whitney test was used for non-parametric data. Two-way analysis of variance (ANOVA) was used for comparison of data with more than two groups and Bonferroni post-hoc analysis was used to measure differences between groups. Continuous data is expressed as mean ± standard error of the mean (SEM). P values <0.05 were considered as statistically significant. Analysis was carried out using GraphPad Prism v7.0 (GraphPad Inc., USA) and SPSS v22 (IBM Inc., USA).

2.4 Results

2.4.1 Patient demographics

Peripheral blood cell counts were included for 96 patients who underwent endovascular aortic aneurysm repair (EVAR), out of which 57 patients underwent IEVAR and 39 patients who underwent branched/fenestrated BEVAR/FEVAR. Data were also collected for 35 patients who underwent conventional open aortic aneurysm repair, between June 2010 and January 2015. Open aneurysm repair group was younger than IEVAR and BEVAR/FEVAR cohorts (P=0.004, for both by Mann-Whitney test, Table 2.1). Other co-morbidities such as hyperlipidaemia, coronary artery disease, renal and chronic obstructive diseases were more common among IEVAR and BEVAR/FEVAR compared to open repair patients (P=0.005, 0.0001, 0.02, 0.008, respectively, for both by Mann-Whitney test, Table 2.1). Invasive open aneurysm repair was

associated with more extended hospital stay than minimally invasive endovascular IEVAR and BEVAR/FEVAR; however, that was not significant but had an effect on the number of data points available at each day post-operatively in each group for seven days following intervention.

Changes in the peri-operative peripheral blood cells numbers were not adjusted for the above factors e.g., age, length of stay, coronary and renal diseases that might have affected outcomes. Complex BEVAR/FEVAR were associated with longer fluoroscopy time, and higher radiation exposure measured by dose area product (DAP) compared to standard IEVAR (P<0.0001, for both by Mann-Whitney test, Figure 2.1).

Table 2.1 Subject demographics for analysis of peripheral blood cells during aortic repair

	EVAR (n=96)		**Open AAA Repair (n=35)**	***P* value**
	IEVAR (n=57)	BEVAR/FEVAR (n=39)		
Median age (range)	79 (56-89)	76 (58-89)	71 (57-83)	***0.004***
Male (%)	45 (78.94%)	31 (79.48%)	30 (85.71%)	
Smoking	34	20	13	
Co-morbidities				
Hypertension	37	22	19	
Hyperlipidemia	36	18	10	***0.005***
Coronary artery disease	14	8	29	***0.0001***
Stroke	2	1	0	
Diabetes Miletus	3	2	5	
Renal disease	12	7	0	***0.02***
COPD	3	3	9	***0.008***
Cancer	5	5	0	
Length of hospital stay (range)	4 (2-9)	4 (2-9)	7 (4-20)	

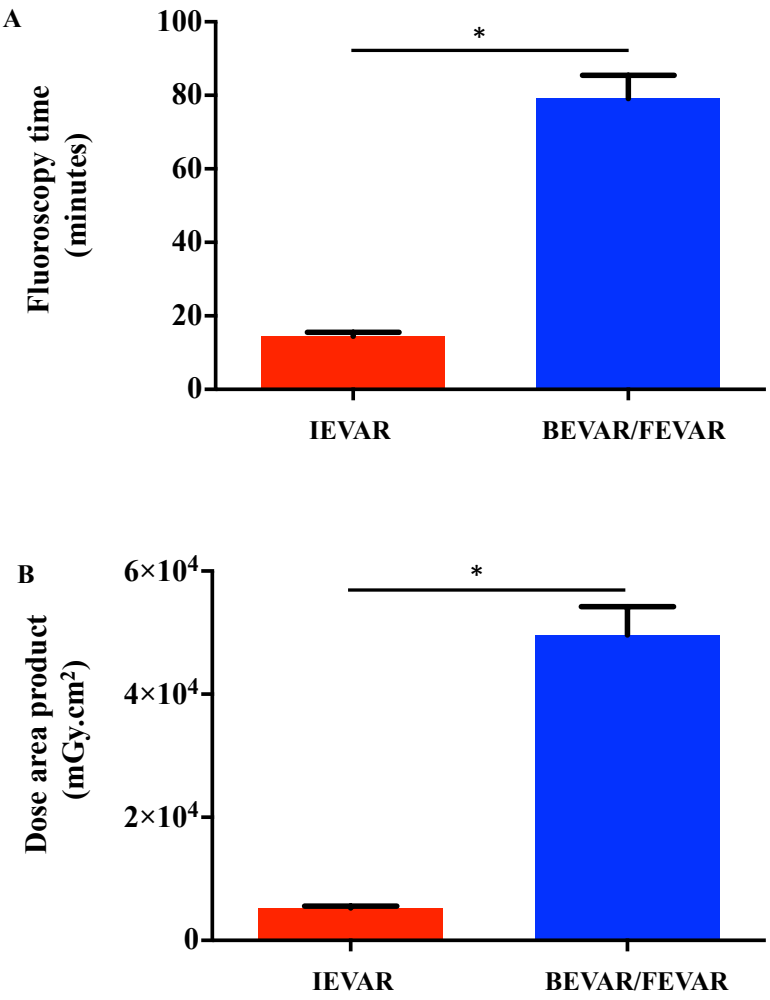

Figure 2.1 Radiation exposure during endovascular aortic aneurysm repair

*(A) Fluoroscopy time in minutes was longer during BEVAR/FEVAR than IEVAR, (B) Similarly, Dose Area Product (DAP) in mGy.cm² was higher in complex EVAR procedures (BEVAR/FEVAR) compared to IEVAR (*P<0.0001, for both by Mann-Whitney test).*

2.4.2 Changes in leukocytes count

White blood cell count was retrospectively studied in patients when they underwent open (n=35, Table 2.2) and endovascular aortic repair (IEVAR, n=57, Table 2.3, BEVAR/FEVAR, n=39, Table 2.4). There was a significant increase in leukocytes count in day one after intervention (P<0.0001, for all groups by Wilcoxon matched pairs signed rank, Figure 2.2). The increase in leukocyte numbers peaked on day 2 and returned towards pre-operative levels by day 3 (Figure 2.3). There was no significant variation in these changes among open repair, IEVAR and BEVAR/FEVAR approaches (Figure 2.3).

Table 2.2 Changes of leukocytes count in the open AAA repair group

Pre	Day 1	%	Day 2	%	Day 3	%	Day 4	%	Day 5	%	Day 6	%	Day 7	%
5.7	8.6	150.8772	14.6	256.1404	13.1	229.8246	13.4	235.0877	8.9	156.1404	8	140.3509	9.3	163.1579
5.2	9.5	182.6923	8.9	171.1538	10.1	194.2308	9.7	186.5385			7.2	138.4615	10.3	198.0769
8.4	12.1	144.0476	14.7	175	9	107.1429	7.8	92.85714						
9.2	10.5	114.1304	9	97.82609	10.1	109.7826	9.5	103.2609	13.6	147.8261	16.7	181.5217		
6.5	8	123.0769	7.4	113.8462	7.8	120	5.8	89.23077	5.3	81.53846				
5	6.5	130	8.2	164	10.9	218	11.8	236	14.5	290	14.1	282	20	400
6.5	8.3	127.6923	9.4	144.6154	10.2	156.9231	9.1	140	9.2	141.5385				
9.7	12.9	132.9897	14.2	146.3918	12.7	130.9278			8.7	89.69072	10.6	109.2784	12.6	129.8969
9.1	14.2	156.044	10.2	112.0879	9.2	101.0989	11.6	127.4725	10.4	114.2857	11.3	124.1758	10.9	119.7802
9.8	8.7	88.77551	11.1	113.2653	10.4	106.1224	8.5	86.73469	7.5	76.53061	6.6	67.34694		
9.7	14	144.3299	15.7	161.8557	13.2	136.0825	10.1	104.1237	9	92.78351				
9.5	14.6	153.6842	15.9	167.3684			12.6	132.6316	14.4	151.5789	16.3	171.5789	13.7	144.2105
8.3	8.6	103.6145	10.6	127.7108	11.7	140.9639	10.1	121.6867	8.7	104.8193	6.3	75.90361	7.7	92.77108
6.5	12.8	196.9231	11.1	170.7692	9	138.4615	6.8	104.6154	8.6	132.3077	8.6	132.3077	10.5	161.5385
9.1	17.2	189.011	12.7	139.5604	16.6	182.4176	14.4	158.2418	9.9	108.7912				
6.9	8.8	127.5362	9	130.4348	7	101.4493	6	86.95652	5.6	81.15942	7.3	105.7971	7.8	113.0435
9.4	15.1	160.6383	15.1	160.6383	13.6	144.6809	13.2	140.4255	10.4	110.6383	7.5	79.78723	7	74.46809
8	9.5	118.75	12.2	152.5	10.5	131.25	9.8	122.5	9.8	122.5	10.7	133.75	11	137.5
9.9	15.2	153.5354	14.6	147.4747	18	181.8182	19.1	192.9293	19.9	201.0101	14.6	147.4747	15.7	158.5859
6.2	11.3	182.2581	13	209.6774	6.2	100	7.6	122.5806	6.3	101.6129	8.6	138.7097	10.9	175.8065
6.7	10	149.2537	10.8	161.194	9.7	144.7761	7.1	105.9701	6.9	102.9851	9	134.3284		
8.7	14.3	164.3678	14	160.9195	13.1	150.5747	10.6	121.8391	11.4	131.0345	9.7	111.4943		
8.8	11.3	128.4091	11.1	126.1364	12.4	140.9091	13.5	153.4091	9.5	107.9545				
8.7	8.3	95.4023	13	149.4253	11	126.4368	12.8	147.1264	12.2	140.2299	13.4	154.023	11.1	127.5862
9.5	10.3	108.4211	11.4	120	9.6	101.0526	9.2	96.84211			8	84.21053		
6.6	9.1	137.8788	10.1	153.0303	8.9	134.8485	6.1	92.42424	7.3	110.6061	8	121.2121	6.7	101.5152
8.9	14.4	161.7978	10.4	116.8539	10.3	115.7303	10.1	113.4831	8.8	98.8764			7.5	84.26966
8.7	15.6	179.3103	12.8	147.1264	14.3	164.3678	13.4	154.023	10.6	121.8391	10.1	116.092		
7.5	9.4	125.3333	7.7	102.6667	8.1	108	7	93.33333	9	120	9.4	125.3333		
9.8	17.1	174.4898	11.5	117.3469	9.1	92.85714	13	132.6531	10.6	108.1633	16.8	171.4286		
10.9	12.3	112.844	15.3	140.367	17.2	157.7982	16.5	151.3761	18.7	171.5596	17	155.9633	17.4	159.633
9.4	17.9	190.4255	15.5	164.8936	14.2	151.0638	12.1	128.7234						
9.7	11.9	122.6804	16.6	171.134	10.4	107.2165			6.4	65.97938	7.1	73.19588		
6.2	13.5	217.7419	16.5	266.129	12.3	198.3871	8.3	133.871	6.2	100	10.1	162.9032	6.8	109.6774
6.1	8.3	136.0656	8.9	145.9016	6.8	111.4754	7.5	122.9508			7.6	124.5902		

Table 2.3 Changes of leukocytes count in the IEVAR group

Pre	Day 1	%	Day 2	%	Day 3	%	Day 4	%	Day 5	%	Day 6	%	Day 7	%
8.1	12.6	155.5556	9.6	118.5185										
6.1	9.2	150.8197					10.1	165.5738	7	114.7541				
6.5	7.5	115.3846	6.3	96.92308	10.2	156.9231	6	92.30769	6.4	98.46154	5	76.92308	5.8	89.23077
8.2			12.9	157.3171	11.9	145.122			7.7	93.90244				
9	12	133.3333	19.8	220	21.5	238.8889	22.2	246.6667	15.8	175.5556	10.8	120	13.7	152.2222
7.6	10.6	139.4737	14.7	193.4211	12.9	169.7368	11.8	155.2632						
6.4	13.3	207.8125	20.9	326.5625	17.5	273.4375	14.8	231.25			16.6	259.375	19.4	303.125
9.7	12.1	124.7423	14.9	153.6082	11.3	116.4948					8.2	84.53608		
10.9	12.1	111.0092	16.8	154.1284	11.9	109.1743								
7.8	16	205.1282	14.7	188.4615										
11.5	17.1	148.6957	19.8	172.1739	17.7	153.913	13.1	113.913						
15.7	17	108.2803	22.1	140.7643	21.6	137.5796	18.1	115.2866	15.4	98.08917	15.8	100.6369	16.3	103.8217
6.1	7.8	127.8689												
8.3	8.5	102.4096	10.4	125.3012	14.2	171.0843	11.3	136.1446	9.3	112.0482	9.2	110.8434	8.3	100
7.7	13.9	180.5195												
4.7	8.7	185.1064	11.1	236.1702	8.4	178.7234	6.7	142.5532						
8.3	10.5	126.506	11.7	140.9639										
16.2	12.5	77.16049	15	92.59259	12.6	77.77778								
10.5	16.9	160.9524	19	180.9524										
5.6	12	214.2857	11.1	198.2143			5.5	98.21429						
7	10	142.8571			9.5	135.7143	8.1	115.7143	6.3	90				
10.8	11.2	103.7037												
6.6	9.3	140.9091	9.8	148.4848										
6.8	13.4	197.0588	19.3	283.8235	15.4	226.4706	8.7	127.9412			5.3	77.94118		
10.2	6	58.82353			5.4	52.94118								
12.4	10.5	84.67742	10.3	83.06452			7.7	62.09677						
8.3	13.8	166.2651	17.3	208.4337										
7.7	12.1	157.1429												
6.9	23.2	336.2319	24.9	360.8696	17.8	257.971	9.7	140.5797						
5.4	7.1	131.4815	8.7	161.1111										
8.5	12.8	150.5882	13.8	162.3529										
9.6	10.4	108.3333			11.7	121.875								
8.6	7	81.39535	8.1	94.18605			5.8	67.44186	19.9	231.3953	15.6	181.3953	11.4	132.5581
5.4	12.2	225.9259												
8.4	11.1	132.1429	12.9	153.5714	11	130.9524								
9.3	10.6	113.9785	16.7	179.5699			11.5	123.6559	9.1	97.84946	8.4	90.32258	9.1	97.84946
7.7	10.4	135.0649	10.8	140.2597	10.1	131.1688			7.4	96.1039	5.8	75.32468		
4.9	5.6	114.2857	5.7	116.3265	5.9	120.4082	7.2	146.9388	6.8	138.7755				
5.3	10.6	200												
7.7	13.9	180.5195	10.1	131.1688	8.9	115.5844								
8.7	11.9	136.7816	15.5	178.1609										
4.9	20.4	416.3265	22.5	459.1837	19.3	393.8776	17.2	351.0204	14	285.7143	9.1	185.7143		
6.9	12.2	176.8116												
6.2	9.8	158.0645	4.6	74.19355	5.2	83.87097	4.9	79.03226	5	80.64516	5.5	88.70968		
8.6	10.3	119.7674												
7.4	11.6	156.7568	14.5	195.9459	11.9	160.8108								
9.2	12	130.4348	14.8	160.8696										
5.7	8.8	154.386	10.4	182.4561										
6.4	12	187.5	12.6	196.875										
11.2	15.8	141.0714	15.9	141.9643	14.2	126.7857	11.2	100	11.2	100	10	89.28571		
11.6	9.1	78.44828												
6	8.7	145	10.7	178.3333										
5.5	6	109.0909	7.5	136.3636	6.2	112.7273	5.6	101.8182	5.2	94.54545	5.2	94.54545	4.3	78.18182
12.2	27.8	227.8689	13.1	107.377	13.9	113.9344	13.4	109.8361						
10.9	13.7	125.6881	13.9	127.5229										
33.9	18.3	53.9823	25.6	75.51622	27.8	82.0059	25.5	75.22124	12.9	38.0531	11.6	34.21829	15.9	46.90265
7.3	16.2	221.9178	12.9	176.7123										

Table 2.4 Changes of leukocytes count in the BEVAR/FEVAR group

Pre	Day 1	%	Day 2	%	Day 3	%	Day 4	%	Day 5	%	Day 6	%	Day 7	%
5.2	9.1	175	7.1	136.5385	6.9	132.6923	6.4	123.0769			8.6	165.3846		
6.9	12.1	175.3623	10.8	156.5217					7	101.4493				
5.3	8.1	152.8302	6.7	126.4151	7	132.0755					5.7	107.5472		
9	15.8	175.5556	14.8	164.4444	12.6	140	9.8	108.8889	9.8	108.8889	10.2	113.3333	11.4	126.6667
6.2	8.9	143.5484	13.6	219.3548										
8	9.8	122.5	10.3	128.75										
11.6	17.6	151.7241	10.2	87.93103	13.9	119.8276	5.1	43.96552						
6.1	9.4	154.0984	11.2	183.6066	9.9	162.2951	8.3	136.0656						
8.1	17	209.8765												
7.5	10.5	140	13.4	178.6667			8.7	116	9.4	125.3333			9.4	125.3333
6.7	11.8	176.1194	8.6	128.3582			9.3	138.806						
6.2	9.9	159.6774	13.7	220.9677										
6.3	14.7	233.3333	19.3	306.3492	16.2	257.1429	10.7	169.8413			9	142.8571	8.9	141.2698
8.1	17.4	214.8148	13.8	170.3704	11	135.8025	11.5	141.9753	9.5	117.284	10.4	128.3951	11.1	137.037
4.1	7.9	192.6829	10.1	246.3415	7.7	187.8049	6.5	158.5366						
10.5	12	114.2857	10.1	96.19048	10	95.2381	10.5	100						
6.6	6.1	92.42424	6.1	92.42424	5.3	80.30303	6.4	96.9697	7.2	109.0909	8.4	127.2727	8	121.2121
8.6	9.3	108.1395												
8	13.6	170												
7.9	31.3	396.2025	34.4	435.443	22.4	283.5443	15.9	201.2658	11.3	143.038	11.9	150.6329	13.5	170.8861
9	10.5	116.6667	12.5	138.8889	15.1	167.7778								
10.8	14.5	134.2593	17.3	160.1852	15.1	139.8148								
8.6	16.3	189.5349			10	116.2791								
11.4	14.4	126.3158												
7.3	11.5	157.5342	14	191.7808	16.4	224.6575	10.9	149.3151	8.1	110.9589				
7.7	15.4	200	17.2	223.3766	17	220.7792	14.7	190.9091	12.7	164.9351	13.3	172.7273		
8.4	23.8	283.3333	18.4	219.0476	14.4	171.4286	11.6	138.0952	9	107.1429	8.8	104.7619		
8.1	9.4	116.0494	10.6	130.8642	13.3	164.1975	11.2	138.2716	10.4	128.3951	7.6	93.82716	11.6	143.2099
7.2	8.5	118.0556	10.3	143.0556	9.8	136.1111								
8.7	9.3	106.8966	11.6	133.3333	10.5	120.6897								
9.5	11.1	116.8421	11.1	116.8421	12.9	135.7895	11	115.7895						
12.6	17.2	136.5079												
12.4	13.6	109.6774	14.5	116.9355	16	129.0323								
5.8	7.7	132.7586	10.3	177.5862	10.9	187.931	10.2	175.8621	6.8	117.2414	6.6	113.7931	6.4	110.3448
6.3	11.7	185.7143	9.7	153.9683										
8.2	19	231.7073	17.1	208.5366										
6.2	10.4	167.7419	10.8	174.1935	11.9	191.9355	7.2	116.129	10.1	162.9032	11	177.4194	13.6	219.3548
12.2	20	163.9344	23.6	193.4426	17.6	144.2623	13.3	109.0164	11.5	94.2623			12.3	100.8197
9.2	11.2	121.7391	22.4	243.4783	21.3	231.5217	16.9	183.6957	12.4	134.7826	13.6	147.8261		

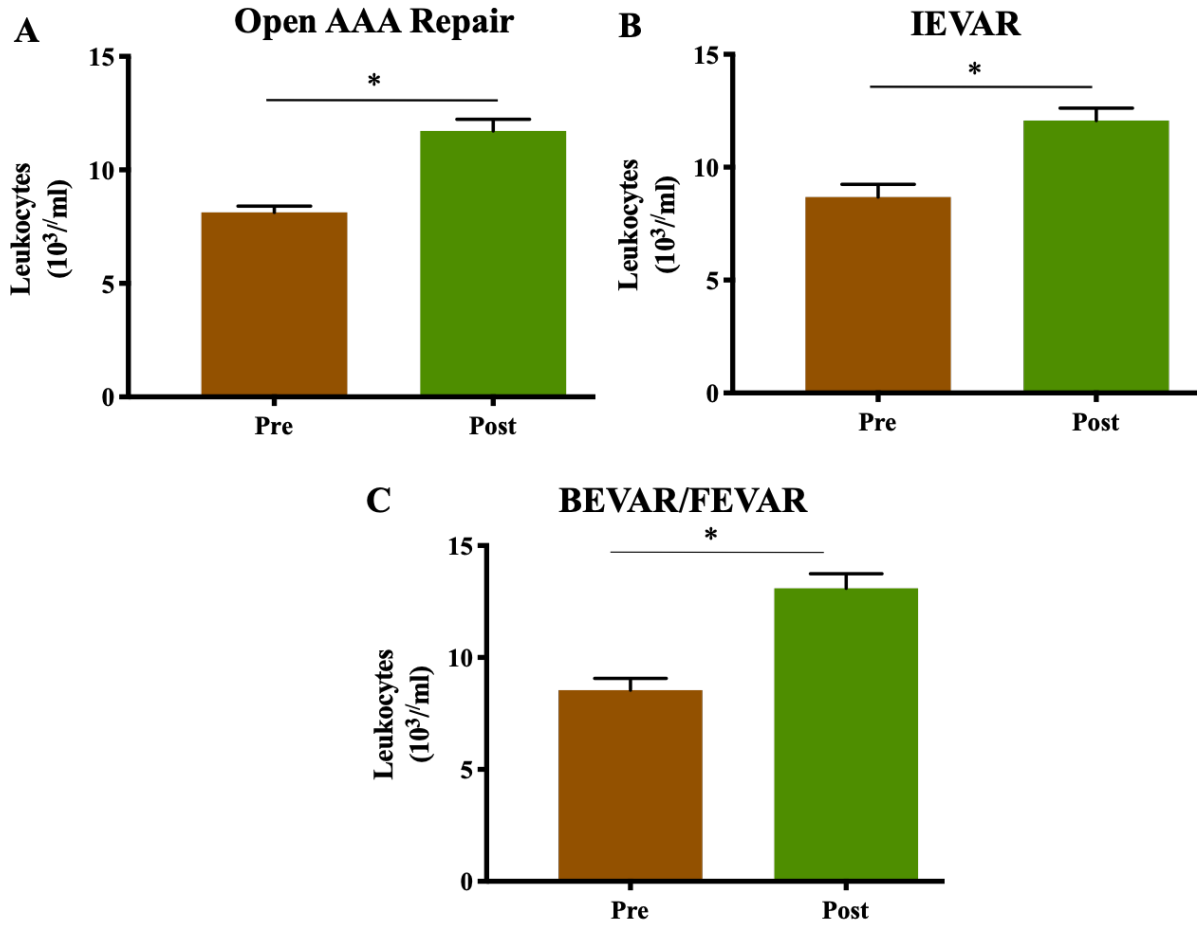

Figure 2.2 Changes of leukocyte count after aortic aneurysm repair

*(A) Leukocytes count increased on day one after open aneurysm repair, (B) Leukocytes count increased on day one after IEVAR, (C) Leukocytes count increased on day one after BEVAR/FEVAR (*P<0.0001, for all by Wilcoxon matched pairs signed rank test).*

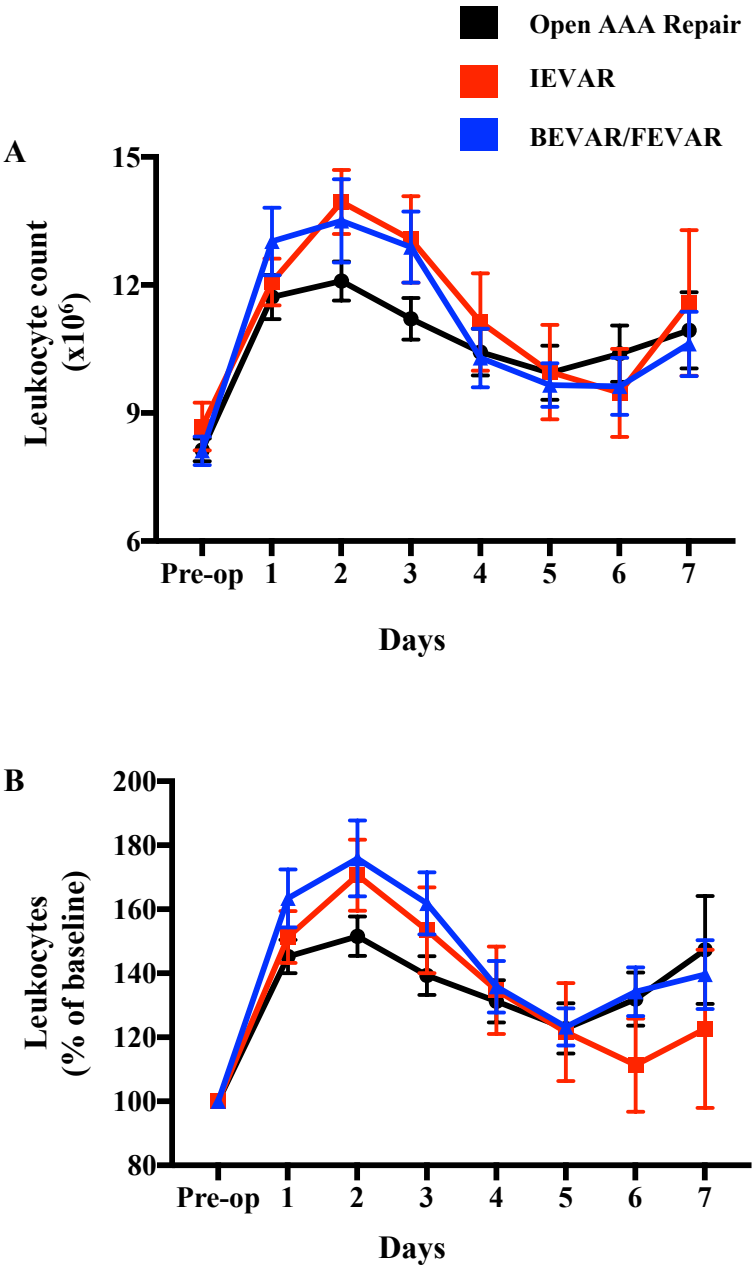

Figure 2.3 Leukocytes count changes during the perioperative aneurysm repair period

(A) Leukocytes count increased after day one from open repair, IEVAR and BEVAR/FEVAR, to reach the peak on day then dropped gradually afterwards. (B) Leukocytes percentage of change from the baseline showed similar trend of an increase on day one after open repair, IEVAR and BEVAR/FEVAR, reached the peak on day two then recovered over 7 days post-intervention. No significant difference in leukocytes count changes between open and endovascular procedures.

2.4.3 Changes in lymphocytes count

Peripheral lymphocytes counts were retrospectively studied in patients after open (n=35, Table 2.5) and endovascular aortic repair (IEVAR, n=57, Table 2.6, BEVAR/FEVAR, n=39, Table 2.7). Lymphocytes count dropped in day one after open repair, IEVAR and BEVAR/FEVAR ($P<0.0001$, for all groups by Wilcoxon matched pairs signed rank, Figure 2.3). Lymphocyte numbers started then to recover over 7 days following interventions. These changes in the absolute lymphocytes numbers after open repair, IEVAR, and BEVAR/FEVAR varied significantly ($P=0.002$ and 0.0001, respectively by Two-way analysis of variance test, Figure 2.4). There was no significant difference between IEVAR and BEVAR/FEVAR groups.

Lymphocytes percentage of change from the baseline showed similar trend and, however only varied significantly between the open repair and BEVAR/FEVAR group ($P=0.0006$ by Two-way analysis of variance test). No statistically significant difference was observed between open and IEVAR lymphocytes percentage of change from the baseline.

Post-operative lymphocytes drop was significantly greater on day one after BEVAR/FEVAR compared with IEVAR and open repair ($P=0.01$, for both by Mann-Whitney test, Figure 2.5A). We also noted a slower recovery rate of lymphocyte count a week after BEVAR/FEVAR compared with open AAA repair ($P=0.04$ by Mann-Whitney test, Figure 2.5B). There was a minimal difference between open aneurysm repair and IEVAR groups on day one and after a week from intervention, but this difference was not great enough to be statistically significant.

Table 2.5 Changes of lymphocytes count in the open AAA repair group

Pre	Day 1	%	Day 2	%	Day 3	%	Day 4	%	Day 5	%	Day 6	%	Day 7	%
1.2	0.6	50	0.6	50	0.8	66.66667	0.7	58.33333	0.9	75	0.8	66.66667	0.9	75
0.8	0.5	62.5	0.7	87.5	1	125	0.3	37.5			0.5	62.5	0.6	75
1.1	0.8	72.72727	1.2	109.0909	0.3	27.27273	0.5	45.45455						
2.5	0.9	36	1.1	44	1.3	52	1.7	68	2.4	96	2.2	88		
1.5	0.5	33.33333	0.7	46.66667	0.7	46.66667	0.6	40	0.6	40				
1.2	0.3	25	0.3	25	0.3	25	0.5	41.66667	0.6	50	0.7	58.33333	0.8	66.66667
1.4	0.6	42.85714	1.1	78.57143	1.1	78.57143	0.8	57.14286	1.4	100				
2.9	2.3	79.31034	1.8	62.06897	1.7	58.62069			2.2	75.86207	2.3	79.31034	2.3	79.31034
2	1.6	80	1.5	75	1.5	75	0.7	35	1.4	70	1.5	75	1.9	95
2	1	50	1.1	55	0.9	45	1.3	65	0.9	45	1	50		
3.1	1.7	54.83871	1.1	35.48387	1.2	38.70968	1.3	41.93548	1.4	45.16129				
1.6	1	62.5	1.3	81.25			1.6	100	1.7	106.25	1.3	81.25	1.1	68.75
2.9	0.8	27.58621	1.7	58.62069	1.9	65.51724	1.1	37.93103	1.8	62.06897	1.3	44.82759	1.4	48.27586
1.5	1.3	86.66667	2.2	146.6667	1.5	100	1.4	93.33333	1	66.66667	0.9	60	1.2	80
2.2	1	45.45455	0.9	40.90909	1.5	68.18182	1.4	63.63636	1.3	59.09091				
1.9	0.5	26.31579	0.8	42.10526	1.8	94.73684	1.1	57.89474	1	52.63158	0.9	47.36842	1.2	63.15789
0.7	0.8	114.2857	3.6	514.2857	0.7	100	4.4	628.5714	4.3	614.2857	2.3	328.5714	2.3	328.5714
1.7	1	58.82353	1.5	88.23529	1.4	82.35294	1.7	100	1.7	100	1.6	94.11765	2	117.6471
2	1.7	85	1.8	90	1.3	65	0.8	40	2	100	1.8	90	1.6	80
1.4	0.6	42.85714	1	71.42857	0.6	42.85714	0.6	42.85714	0.6	42.85714	0.7	50	1	71.42857
0.7	0.6	85.71429	0.4	57.14286	0.3	42.85714	0.5	71.42857	0.6	85.71429	0.6	85.71429		
2.7	1.1	40.74074	1.4	51.85185	1	37.03704	1.1	40.74074	1.5	55.55556	1.5	55.55556		
3.3	1.1	33.33333	0.9	27.27273	1.2	36.36364	1.2	36.36364	1.7	51.51515				
2.3	1.4	60.86957	2.2	95.65217	2	86.95652	2.3	100	3.1	134.7826	2.8	121.7391	2.8	121.7391
1.4	0.9	64.28571	0.8	57.14286	1.2	85.71429	1.3	92.85714			1.2	85.71429		
1.8	0.4	22.22222	0.5	27.77778	0.7	38.88889	0.5	27.77778	0.8	44.44444	0.8	44.44444	0.5	27.77778
1.9	1.2	63.15789	1.1	57.89474	0.9	47.36842	1.2	63.15789	1.1	57.89474			1.7	89.47368
3.3	1.6	48.48485	1.7	51.51515	2.1	63.63636	1.2	36.36364	1.6	48.48485	1.4	42.42424		
2	0.8	40	1.6	80	1.5	75	1.7	85	1.3	65	1.4	70		
2.2	1.5	68.18182	1.2	54.54545	1.3	59.09091	1.4	63.63636	1.6	72.72727	2.4	109.0909		
2	0.7	35	0.6	30	0.7	35	0.7	35	0.9	45	1.2	60	1	50
2.2	1.8	81.81818	1.2	54.54545	1	45.45455	0.7	31.81818						
2.7	1.1	40.74074	1.3	48.14815	1.4	51.85185			1.3	48.14815	1.5	55.55556		
1.6	1.9	118.75	1.2	75	0.9	56.25	0.9	56.25	0.7	43.75	0.5	31.25	0.9	56.25
0.7	0.5	71.42857	0.5	71.42857	0.3	42.85714	0.7	100			0.9	128.5714		

Table 2.6 Changes of lymphocytes count in the IEVAR group

Pre	Day 1	%	Day 2	%	Day 3	%	Day 4	%	Day 5	%	Day 6	%	Day 7	%
1.8	0.5	27.77778					0.9	50	0.8	44.44444				
1.6	1.6	100	1.5	93.75	1.1	68.75					1.3	76.47059		
1.7	0.5	29.41176	0.9	52.94118										
1.7	0.9	52.94118												
2.5	0.8	32	1.1	44										
0.7	0.4	57.14286												
2	0.8	40	1.1	55										
0.3	0.8	266.6667	0.9	300	1.3	433.3333								
2.1			0.9	42.85714	2	95.2381			1.5	71.42857				
0.7	0.5	71.42857	0.3	42.85714			0.2	28.57143						
3.1	0.3	9.677419	0.8	25.80645	1.2	38.70968	1.3	41.93548					1	58.82353
1.7	1.1	64.70588	1	58.82353	0.9	52.94118	1.1	64.70588	0.6	35.29412	1.2	85.71429	2.1	150
1.4	1.9	135.7143	1.5	107.1429	1.5	107.1429	1.6	114.2857	1.2	85.71429	1.9	146.1538		
1.3	0.8	61.53846	1.2	92.30769	0.9	69.23077	1	76.92308	0.8	61.53846	1	76.92308		
1.3	0.3	23.07692			0.9	69.23077	0.8	61.53846	1	76.92308				
1.5	1.7	113.3333												
2.3	1.7	73.91304	3.1	134.7826									0.8	57.14286
1.4	1.1	78.57143	0.5	35.71429	2.4	171.4286	0.8	57.14286	0.7	50	1	52.63158		
1.9	0.5	26.31579	0.9	47.36842									1.4	70
2	1.1	55	0.8	40	1.1	55	0.9	45			1.2	80		
1.5	0.4	26.66667	0.9	60										
1.3	0.7	53.84615	0.7	53.84615										
2.3	1.6	69.56522	1.2	52.17391	1.1	47.82609							1.2	63.15789
1.9	1.2	63.15789	0.8	42.10526	1	52.63158	1.1	57.89474	0.9	47.36842	1.4	73.68421		
1.9	1.5	78.94737	1.3	68.42105	1.4	73.68421								
1.6	1	62.5	1.5	93.75										
1.2	0.5	41.66667	0.8	66.66667	0.9	75	1	83.33333			0.8	53.33333		
1.5	0.6	40											1	90.90909
1.1	0.2	18.18182	0.9	81.81818	0.7	63.63636	0.6	54.54545	0.9	81.81818				
1.4	0.7	50	1	71.42857	0.7	50	0.9	64.28571						
1	0.7	70			0.6	60								
1.4	0.7	50	0.8	57.14286			1	71.42857						
1.2	0.9	75	0.7	58.33333	0.5	41.66667	0.7	58.33333						
2.2	1.3	59.09091	0.8	36.36364										
2.1	0.6	28.57143	1.8	85.71429										
2.1	1.5	71.42857			1.1	52.38095							0.6	31.57895
1.9	1.2	63.15789	1.7	89.47368			0.9	47.36842	0.4	21.05263	0.6	35.29412		
1.7	1.2	70.58824												
1.8	1.2	66.66667	1.3	72.22222	1	55.55556							2.2	66.66667
3.3	1.3	39.39394	1.7	51.51515			1.5	45.45455	1.5	45.45455	1.8	150		
1.2	0.3	25	0.2	16.66667	0.6	50			1	83.33333	0.8	72.72727		
1.3	1.3	100												
2.5	1.5	60	1.2	48	1.3	52								
3.4	2.6	76.47059	2.6	76.47059									1.1	68.75
1.6	0.8	50	1.1	68.75	1	62.5			1.7	106.25	0.8	42.10526		
1.9	0.5	26.31579												
1.1	0.6	54.54545	0.6	54.54545	0.5	45.45455	0.5	45.45455	0.9	81.81818	0.7	43.75		
1.6	1	62.5												
2.2	0.8	36.36364	1.2	54.54545	1.1	50								
2	1.6	80	1	50										
1.9	1.4	73.68421												
1.7	0.9	52.94118	0.6	35.29412									0.9	56.25
1.6	0.7	43.75	1.2	75	0.8	50	1	62.5	0.9	56.25	1.2	54.54545		
2.2	0.6	27.27273	0.8	36.36364	0.8	36.36364	0.7	31.81818						
3.2	1.5	46.875	1.9	59.375									1	31.25
1	0.7	70	1	100	0.8	80	0.8	80	1.2	120	1.2	80	1.7	170
1.9	0.6	31.57895	1	52.63158										

Table 2.7 Changes of lymphocytes count in the BEVAR/FEVAR group

Pre	Day 1	%	Day 2	%	Day 3	%	Day 4	%	Day 5	%	Day 6	%	Day 7	%
1.3	0.2	15.38462	0.4	30.76923	0.6	46.15385					0.6	46.15385		
2.4	0.4	16.66667	1.1	45.83333			1.2	50	1.1	45.83333			1.3	54.16667
1.6	0.5	31.25	0.8	50										
2.3	0.6	26.08696	1.1	47.82609										
2.5	1.4	56												
1.1	0.6	54.54545	0.6	54.54545	0.8	72.72727	0.4	36.36364			0.7	63.63636	0.5	45.45455
2	1.1	55	1.2	60	1.4	70	1.2	60						
1.9	1.4	73.68421												
2.8	1	35.71429	1.1	39.28571	0.5	17.85714	1.2	42.85714						
1.4	0.2	14.28571	0.1	7.142857	0.3	21.42857	0.5	35.71429	1	71.42857	1.2	85.71429	1.3	92.85714
2	0.7	35	1	50										
1.2	0.5	41.66667												
1.3	0.4	30.76923	0.6	46.15385			0.7	53.84615						
2.4	0.5	20.83333	0.7	29.16667	0.6	25	0.9	37.5	1	41.66667	1	41.66667	1.2	50
2.1	0.5	23.80952	0.5	23.80952	0.3	14.28571	0.2	9.52381						
0.8	0.3	37.5	0.5	62.5	0.6	75	0.8	100						
1.4	0.8	57.14286	0.9	64.28571	1	71.42857	0.8	57.14286			1	71.42857		
2.3	1.2	52.17391	1.8	78.26087	1.1	47.82609	0.7	30.43478	0.7	30.43478	0.7	30.43478	1.8	78.26087
1.8	0.8	44.44444	1.2	66.66667					1.1	61.11111				
2.1	0.3	14.28571	0.7	33.33333	0.4	19.04762	1	47.61905	0.9	42.85714	1	47.61905	0.7	33.33333
1.1	0.9	81.81818	0.9	81.81818	1.2	109.0909								
2.5	0.9	36	1.2	48	1.2	48								
2	0.7	35			1	50								
3.3	2	60.60606												
2.2	0.9	40.90909	0.8	36.36364	1	45.45455	0.9	40.90909	1.2	54.54545				
1.3	0.5	38.46154	0.5	38.46154	0.5	38.46154	0.4	30.76923	0.9	69.23077	1.2	92.30769		
2.4	1	41.66667	1.5	62.5	1.3	54.16667	1.5	62.5	1.4	58.33333	1.6	66.66667		
2	2.2	110	1	50	1.5	75	0.7	35	0.7	35	0.8	40	0.7	35
1.6	0.8	50	1	62.5	1.1	68.75								
1.3	0.8	61.53846	0.8	61.53846	0.9	69.23077								
2.1	0.8	38.09524	1	47.61905	1.3	61.90476	0.8	38.09524						
2.4	1.2	50												
1.7	0.5	29.41176	0.7	41.17647	1	58.82353								
1.7	0.4	23.52941	0.6	35.29412	0.7	41.17647	0.7	41.17647	0.6	35.29412	0.7	41.17647	0.8	47.05882
1.3	0.6	46.15385	0.6	46.15385										
2.2	0.6	27.27273	1.5	68.18182										
1.9	0.9	47.36842	1.2	63.15789	1.1	57.89474	1.1	57.89474	1.1	57.89474	0.9	47.36842	1.4	73.68421
2.3	1.8	78.26087	1.9	82.6087	1.9	82.6087	1.3	56.52174	1.4	60.86957			1.6	69.56522
0.8	0.8	100	0.7	87.5	0.9	112.5	0.8	100	0.9	112.5	1	125		

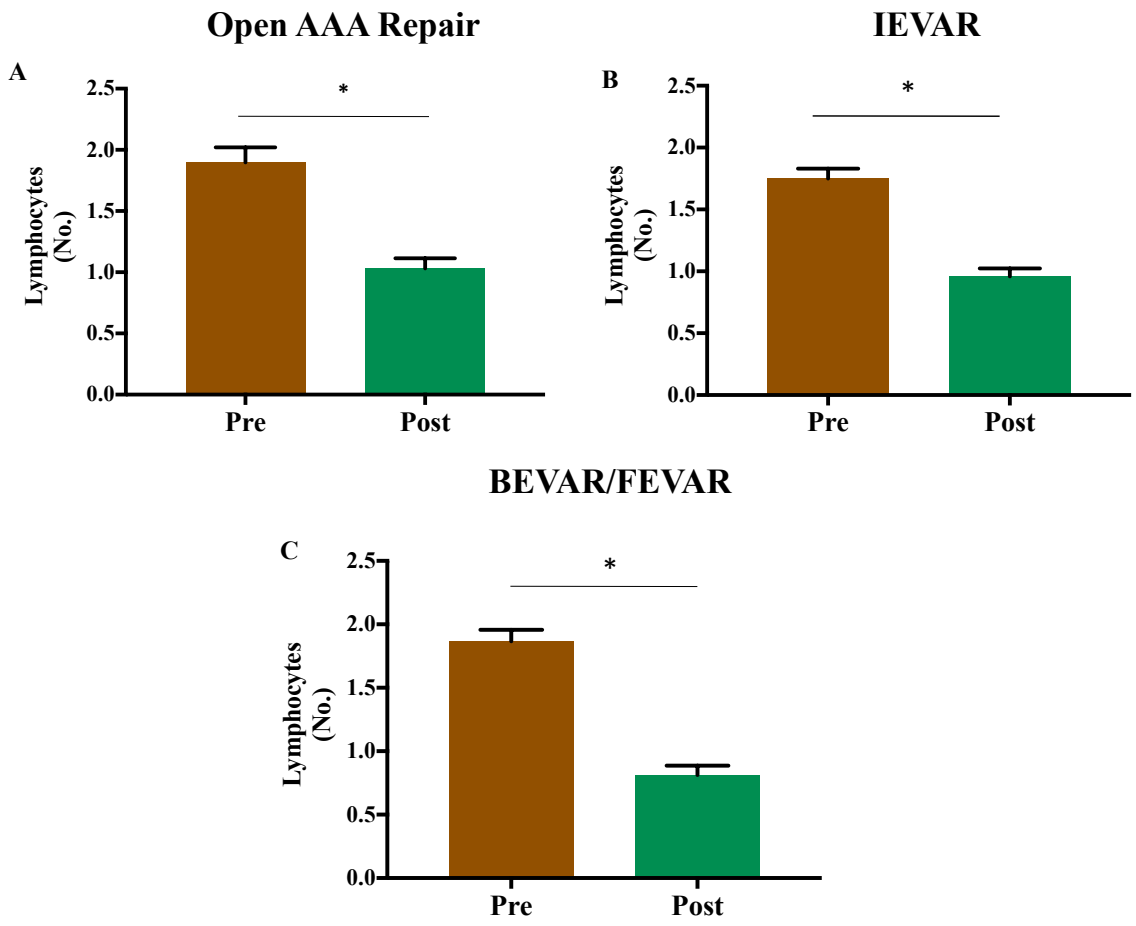

Figure 2.3 Changes of lymphocytes count after aortic aneurysm repair

*(A) Lymphocytes count decreased on day one after open aneurysm repair, (B) Lymphocytes count decreased on day one after IEVAR, (C) Lymphocytes count decreased on day one after BEVAR/FEVAR (*P<0.0001, for all by Wilcoxon matched pairs signed rank test).*

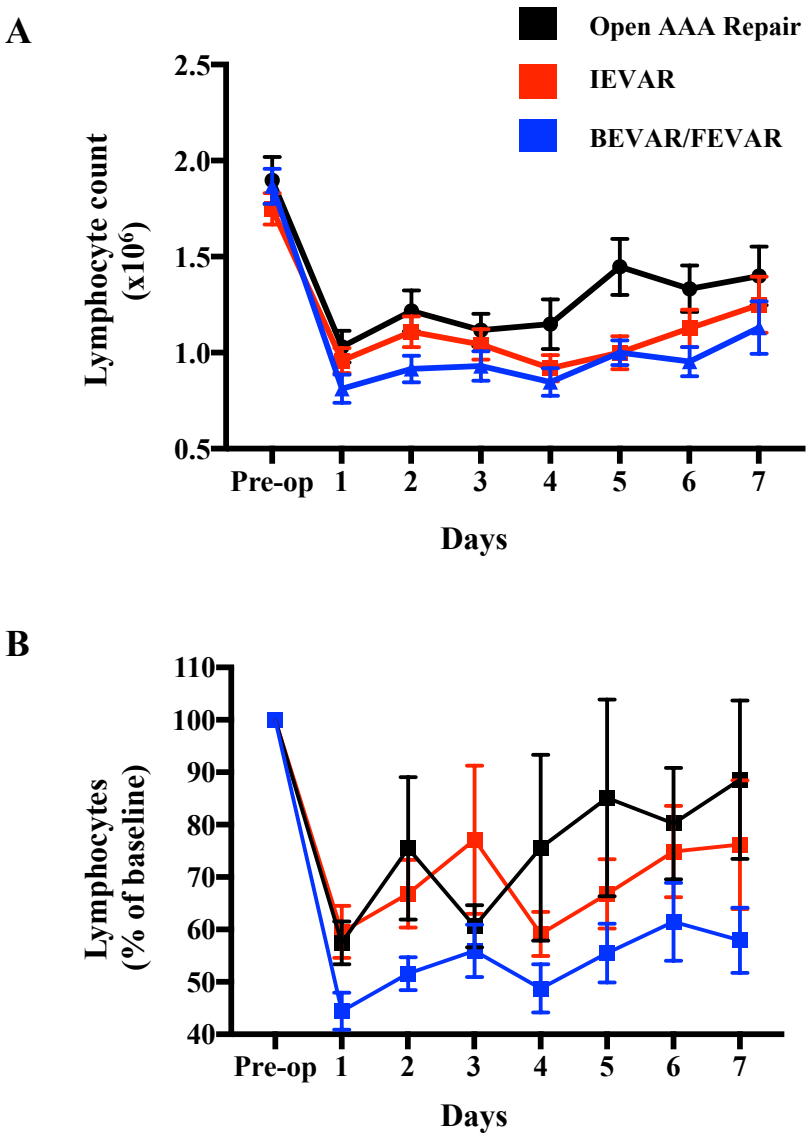

Figure 2.4 Perioperative changes of lymphocytes count after aortic aneurysm repair

(A) Lymphocytes count decreased after day one from open repair, IEVAR and BEVAR/FEVAR, and then recovered gradually over 7 days post-intervention. The changes in lymphocytes count varied significantly between the open group and IEVAR and BEVAR/FEVAR groups (P=0.002 and 0.0001, respectively by Two-way analysis of variance test). No significant difference between the two endovascular groups. (B) Lymphocytes percentage of change from the baseline showed similar trend of a drop on day one after open repair, IEVAR and BEVAR/FEVAR, then recovered over 7 days post-intervention. The percentage of changes in lymphocytes count varied significantly between the open group and BEVAR/FEVAR group (P=0.0006 by Two-way analysis of variance test). No significant difference between open repair and IEVAR groups.

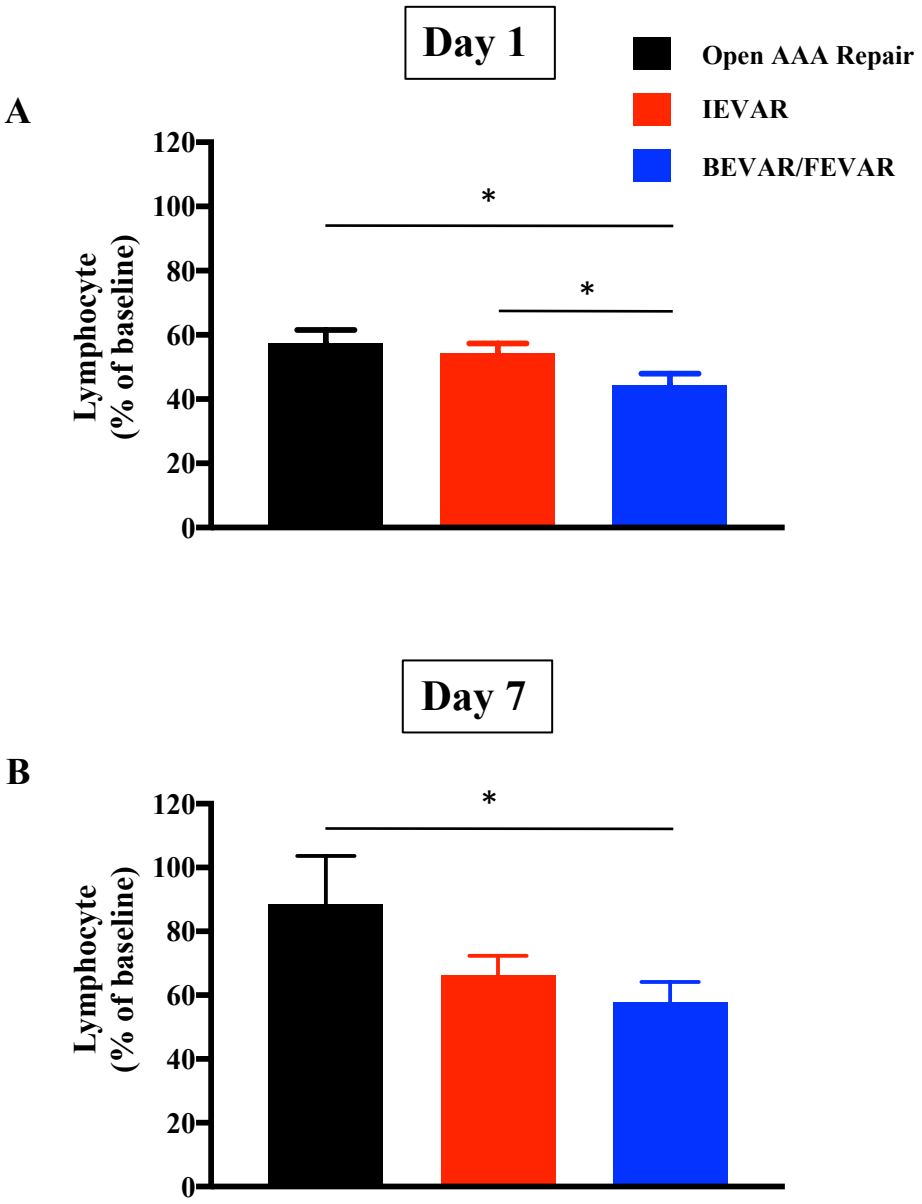

Figure 2.5 Changes of lymphocyte count in Day 1 and Day 7 after aortic aneurysm repair

*(A) On day one after aneurysm repair, the percentage of drop of lymphocytes count after BEVAR/FEVAR greater than IEVAR and Open AAA repair (*P=0.01, for both by Mann-Whitney test, Figure A). (B) A week later, lymphocytes count recovered in open AAA repair quicker than BEVAR/FEVAR group (*P=0.04 by Mann-Whitney test, Figure B).*

2.4.4 Changes in Monocytes count

Monocytes cell numbers were retrospectively studied in patients when they underwent open (n=35, Table 2.5), IEVAR (n=57, Table 2.6), and BEVAR/FEVAR (n=39, Table 2.7). There was a significant increase in monocytes numbers on the first post-operative day after open (P=0.003, Figure 2.5A), IEVAR (P<0.0001, Figure 2.5B) and BEVAR/FEVAR (P=0.01, by Wilcoxon matched pairs signed rank test, Figure 2.5C).

In all groups, monocytes count increased after day one to reach the peak on day two then recovered gradually afterwards. The changes in monocytes absolute numbers varied significantly between the open group and the IEVAR and BEVAR/FEVAR groups (P=0.002 and 0.003, respectively by Two-way analysis of variance test, Figure 2.7). No significant difference between the two endovascular groups. Monocytes percentage of change from the baseline showed similar trend over 7 days post-intervention, however there was no significant difference observed among all groups.

Table 2.8 Changes of monocytes count in the open AAA repair group

Pre	Day 1	%	Day 2	%	Day 3	%	Day 4	%	Day 5	%	Day 6	%	Day 7	%
0.6	0.9	150	1.2	200	0.9	150	1.1	183.33	0.9	150	0.9	150	1	166.66
0.4	1	250	1	250	0.8	200	0.6	150			0.6	150	0.9	225
0.8	1.3	162.5	1.8	225	0.7	87.5	1.1	137.5						
0.6	0.8	133.33	0.6	100	0.7	116.66	0.9	150	1.1	183.33	0.8	133.33		
0.5	0.7	140	0.9	180	1	200	0.8	160	1	200				
0.5	0.6	120	0.4	80	0.4	80	0.7	140	1.2	240	1.3	260	1.6	320
0.6	0.9	150	1.1	183.33	0.9	150	1	166.66	1.1	183.33				
0.7	1.5	214.28	1.6	228.57	1.4	200			1.2	171.42	1.5	214.28	1.8	257.14
0.8	1.4	175	1.1	137.5	0.8	100	0.7	87.5	0.7	87.5	0.9	112.5	0.9	112.5
1	1	100	1.3	130	0.9	90	1	100	0.9	90	0.9	90		
1.3	2	153.84	1.9	146.15	1.6	123.07	1.5	115.38	1.4	107.69				
0.9	1.2	133.33	1.3	144.44			1.1	122.22	1.3	144.44	0.8	88.88	1	111.11
0.7	0.4	57.14	0.7	100	0.8	114.28	0.7	100	0.6	85.71	0.7	100	0.8	114.28
0.5	1.3	260	1.6	320	1.3	260	1	200	1.3	260	1.2	240	1.1	220
0.7	0.3	42.85	0.8	114.28	1.3	185.71	1.2	171.42	1	142.85				
1	0.1	10	0.5	50	0.4	40	0.5	50	0.7	70	0.5	50	0.4	40
1.8	1.4	77.77	0.9	50	1.1	61.11	0.8	44.44	0.7	38.88	0.2	11.11	1	55.55
0.6	0.7	116.66	1.2	200	0.9	150	1.1	183.33	1.1	183.33	1.2	200	1.2	200
0.9	1.8	200	1.8	200	1.8	200	2.3	255.55	3	333.33	2	222.22	1.6	177.77
0.7	0.9	128.57	1.3	185.71	0.6	85.71	0.8	114.28	0.7	100	0.9	128.57	1.2	171.42
0.5	0.8	160	0.6	120	0.6	120	0.6	120	0.6	120	0.6	120		
0.8	0.9	112.5	1.3	162.5	1	125	1	125	1.1	137.5	1.1	137.5		
0.7	0.8	114.28	0.9	128.57	1.1	157.14	0.9	128.57	0.9	128.57				
0.7	0.4	57.14	1.3	185.71	0.9	128.57	1	142.85	1.2	171.42	1.2	171.42	1.2	171.42
0.6	0.9	150	1.1	183.33	1	166.66	0.8	133.33			0.8	133.33		
0.7	0.6	85.71	0.8	114.28	0.7	100	0.6	85.71	0.9	128.57	0.9	128.57	0.7	100
0.8	1.2	150	1.2	150	1.1	137.5	1	125	0.9	112.5			0.8	100
0.6	1.1	183.33	1.2	200	1.1	183.33	0.9	150	1	166.66	0.8	133.33		
0.8	0.8	100	0.8	100	0.8	100	0.7	87.5	0.8	100	0.8	100		
0.7	1.4	200	1.2	171.42	0.7	100	1.2	171.42	1.1	157.14	1.5	214.28		
1.1	1	90.90	1.2	109.09	1.2	109.09	0.8	72.72	1.1	100	1	90.90	1	90.90
0.7	1.6	228.57	1.4	200	1.1	157.14	0.8	114.28						
1.1	1.1	100	1.5	136.36	1	90.90			0.8	72.72	1.1	100		
0.6	0.9	150	1.2	200	1	166.66	0.7	116.66	0.6	100	1	166.66	0.5	83.33
0.5	0.6	120	0.7	140	0.4	80	0.7	140			1	200		

Table 2.9 Changes of monocytes count in the IEVAR group

Pre	Day 1	%	Day 2	%	Day 3	%	Day 4	%	Day 5	%	Day 6	%	Day 7	%
0.7	0.9	128.57					0.7	100	0.5	71.42				
1	1.1	110	1	100	0.8	80					0.7	70		
0.4	0.9	225	0.7	175										
1	1.1	110												
0.8	1.4	175	1.9	237.5										
0.4	0.6	150												
0.6	0.9	150	1.1	183.33										
0.6	1.1	183.33	1.1	183.33	1	166.66								
0.9			1.2	133.33	1.1	122.22			1.3	144.44				
0.6	1.2	200	1	166.66			0.6	100						
0.9	0.9	100	1.2	133.33	1.2	133.33	0.9	100						
0.6	1.2	200	1.6	266.66	1.5	250	1.1	183.33	1.1	183.33	1.2	200	1.4	233.33
0.8	1.5	187.5	1.8	225	1.3	162.5	1.3	162.5	0.9	112.5	0.9	112.5	1.1	137.5
1	1.4	140	1.9	190	1.1	110	1.1	110	1.2	120	1.3	130		
0.4	0.5	125			0.8	200	0.6	150	0.7	175				
0.5	1.1	220												
0.8	1.2	150	1.4	175										
0.6	0.6	100	0.4	66.66	1.2	200	0.6	100	0.6	100	0.5	83.33	0.5	83.33
0.6	1	166.66	0.7	116.66										
0.6	1.3	216.66	1.7	283.33	1.2	200	1.2	200			2	333.33	1.7	283.33
0.9	1	111.11	1.6	177.77										
0.5	0.8	160	1	200										
0.8	1	125	1.5	187.5	1	125								
0.7	1	142.85	1	142.85	0.9	128.57	0.7	100	0.5	71.4	0.6	85.71	0.7	100
0.5	1.3	260	1.3	260	0.8	160								
0.5	0.8	160	1.1	220										
0.5	1.1	220	0.8	160	0.9	180	0.9	180			0.8	160		
0.5	0.8	160												
0.7	1.1	157.14	1.6	228.57	1	142.85	1	142.85	1.1	157.14			1.6	228.57
0.4	0.6	150	0.6	150	0.7	175	0.5	125						
0.8	0.5	62.5			0.6	75								
0.5	0.5	100	0.6	120			0.6	120						
0.3	1.2	400	1	333.33	0.7	233.33	0.6	200						
0.4	0.9	225	0.9	225										
0.9	0.9	100	1.4	155.55										
0.8	0.8	100			1.2	150								
0.5	0.6	120	0.7	140			0.6	120	0.4	80	0.3	60	0.3	60
0.4	1	250												
0.5	0.7	140	0.9	180	0.4	80								
0.7	0.8	114.28	1	142.85			0.8	114.28	0.6	85.71	0.8	114.28	1	142.85
0.6	0.2	33.33	0.3	50	0.6	100			0.8	133.33	0.6	100		
0.5	0.8	160												
0.6	1.3	216.66	0.3	50	0.8	133.33								
0.5	0.8	160	1.2	240										
0.7	1.1	157.14	1	142.85	0.7	100			1.1	157.14	0.9	128.57	0.9	128.57
0.8	1.1	137.5												
0.4	0.8	200	0.3	75	0.4	100	0.3	75	0.4	100	0.4	100		
0.5	0.6	120												
1	1	100	1.7	170	1.3	130								
0.6	0.6	100	0.9	150										
0.5														
0.4	0.7	175	0.6	150										
0.6	0.5	83.33	0.8	133.33	0.5	83.33	0.4	66.66	0.4	66.66	0.5	83.33	0.5	83.33
1.5	2.2	146.66	1.4	93.33	1.4	93.33	1.3	86.66						
0.5	0.5	100	0.8	160										
1	0.5	50	1	100	0.6	60	0.8	80	0.8	80	0.8	80	1	100

Table 2.10 Changes of monocytes count in the BEVAR/FEVAR group

Pre	Day 1	%	Day 2	%	Day 3	%	Day 4	%	Day 5	%	Day 6	%	Day 7	%
0.6	0.7	116.66	0.7	116.66	0.8	133.33	0.7	116.66			0.9	150		
0.5	0.8	160	0.9	180					0.8	160		0		
0.5	0.6	120	0.5	100	0.6	120					0.5	100		
0.5	0.5	100	0.3	60	0.1	20	0.3	60	0.4	80	0.5	100	0.2	40
0.4	0.6	150	1.2	300										
0.8	0.7	87.5	1	125										
0.9	0.5	55.55	0.4	44.44	0.08	8.88	0.2	22.22						
0.4	0.7	175	1	250	0.9	225	0.6	150						
0.7	2.2	314.28												
0.8	0.7	87.5	1.2	150			0.8	100	0.8	100			1.1	137.5
0.9	0.9	100	1.1	122.22			1.1	122.22						
0.4	0.7	175	1	250										
0.4	1	250	1.4	350	1.1	275	0.9	225			0.8	200	0.8	200
0.5	0.7	140	1	200	0.7	140	0.9	180	0.2	40	0.3	60	0.8	160
0.3	0.4	133.33	0.7	233.33	0.5	166.66	0.5	166.66						
0.5	0.7	140	0.8	160	0.7	140	0.3	60						
0.7	0.2	28.57	0.2	28.57	0.3	42.85	0.4	57.14	0.8	114.28	0.7	100	0.9	128.57
0.9	0.7	77.77												
0.8	0.7	87.5												
1.3	2.5	192.30	1.7	130.76	1.1	84.61	1.4	107.69	1.5	115.38	1.5	115.38	1.8	138.46
0.6	0.8	133.33	1	166.66	1.4	233.33								
0.9	0.9	100	1	111.11	0.8	88.88								
1.6	0.7	43.75			0.5	31.25								
0.9	1.3	144.44												
0.7	0.9	128.57	1.1	157.14	1.3	185.71	0.7	100	1	142.85				
0.5	0.9	180	1	200	1	200	0.6	120	1	200	1.3	260		
0.6	1.4	233.33	1.7	283.33	1.4	233.33	1.3	216.66	1.1	183.33	1.1	183.33		
0.6	0.5	83.33	0.4	66.66	0.9	150	0.6	100	0.5	83.33	0.4	66.66	0.6	100
0.9	0.9	100	1.4	155.55	0.4	44.44								
0.4	0.7	175	1	250	0.7	175								
1	0.9	90	1.7	170	1.5	150	0.9	90						
0.9	0.5	55.55												
1.1	1	90.90	1.3	118.18	1.1	100								
0.4	0.6	150	1	250	0.8	200	0.7	175	0.6	150	0.6	150	0.8	200
0.6	0.7	116.66	0.5	83.33										
0.8	1.9	237.5	1	125										
0.5	0.9	180	1	200	0.6	120	0.3	60	0.7	140	1.2	240	1.9	380
1.1	2	181.81	2.8	254.54	1.6	145.45	1.2	109.09	1.2	109.09			1.5	136.36
0.5	0.6	120	0.7	140	0.9	180	0.7	140	0.7	140	0.8	160		

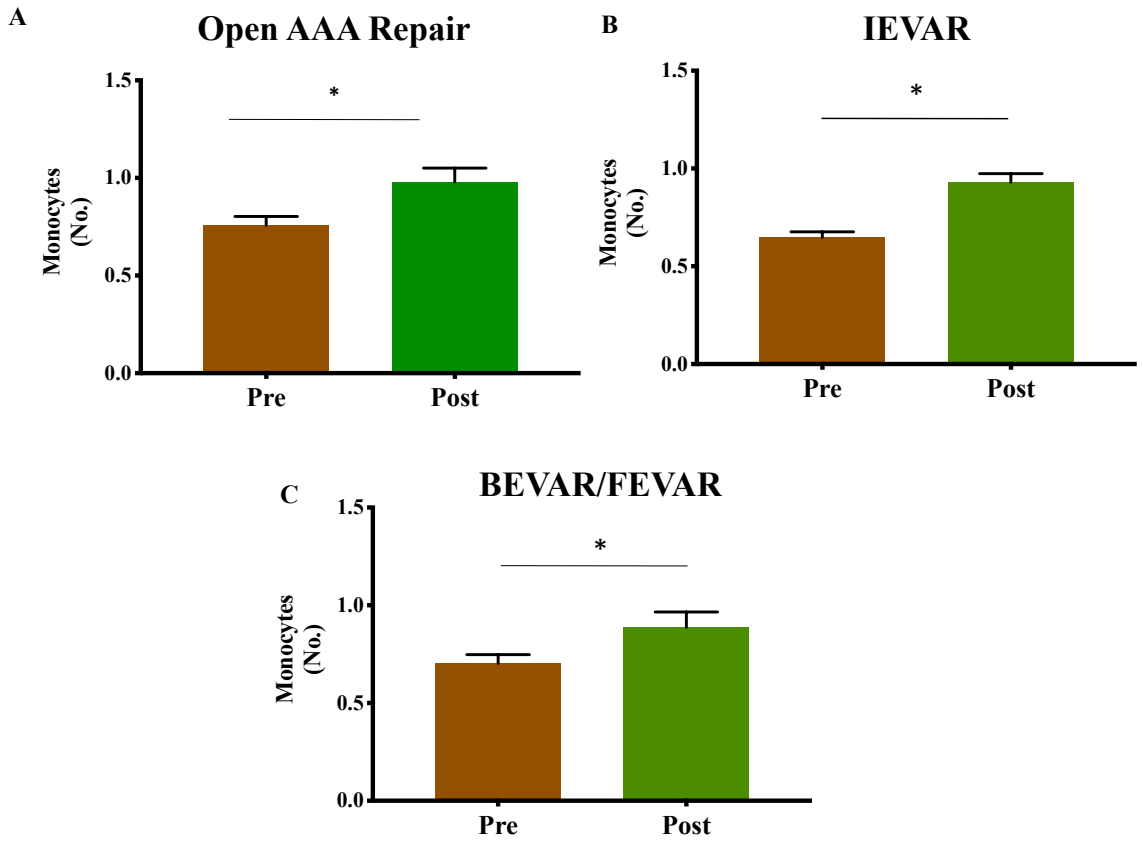

Figure 2.6: Perioperative changes of monocytes count on day one post aortic aneurysm repair

*(A) Monocytes count increased on day one after open aneurysm repair (*P=0.003), (B) Monocytes count increased on day one after IEVAR (*P<0.0001), (C) Monocytes count increased on day one after BEVAR/FEVAR (*P=0.01), by Wilcoxon matched pairs signed rank test.*

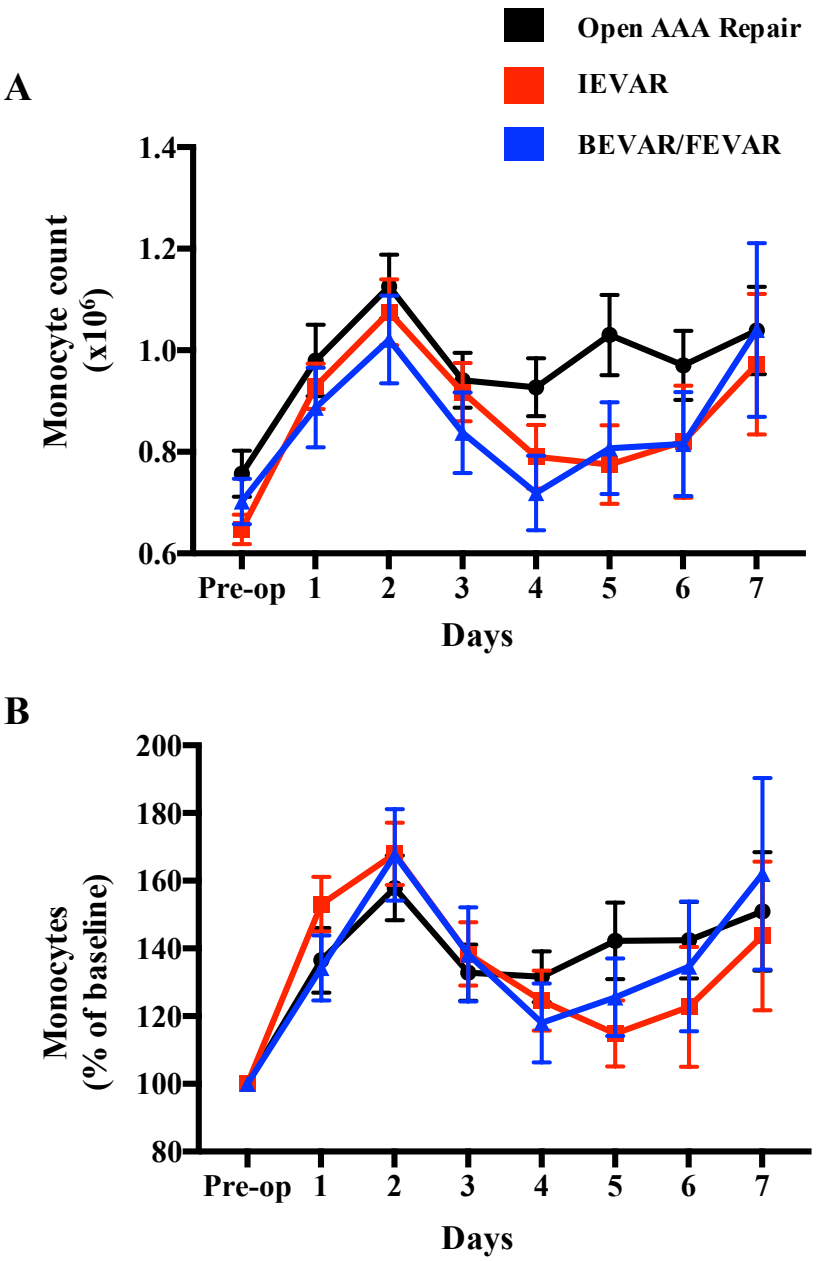

Figure 2.7: Perioperative changes of monocytes count during aortic aneurysm repair

(A) Monocytes count increased after day one from open and endovascular infra-renal (IEVAR) and complex (BEVAR/FEVAR) aortic aneurysm repair, to reach the peak on day two then dropped gradually afterwards. The changes in monocytes count varied significantly between the open group and the endovascular (IEVAR and BEVAR/FEVAR) groups (P=0.002 and 0.003, respectively by Two-way analysis of variance test). No significant difference between the two endovascular groups. (B) Monocytes percentage of change from the baseline showed similar trend of an increase on day one after open and endovascular aortic repair, reached the peak on day two then recovered over 7 days post-intervention. No significant difference in the percentage of changes of monocytes between all groups.

2.5 Discussion

Previous studies reported on the effect of surgical stress on patients during the peri-operative period. The systemic response to surgical injury, infection, ischaemia and reperfusion injury is regulated by both neuroendocrine and immune system. Surgical stress involves activation of hypothalamo–pituitary–adrenal (HPA) axis and release of inflammatory cytokines e.g., tumour necrosis factor (TNF)-a, interleukin (IL)-1b, IL-6 and IL-8.[296, 297]

There is an initial post-operative pro-inflammatory response which leads to not only immune activation at the site of injury, but also induces a systemic anti-inflammatory response that in turn causes suppression of cellular immunity. This anti-inflammatory response is thought to be adaptive in restricting inflammation to the site of injury, preventing inflammatory damage to tissue and organs and limiting undesirable systemic immune reactions toward newly exposed host determinants.[298, 299]

In this part of the study, a retrospective analysis of changes in peripheral blood leukocytes, monocytes, and lymphocytes count was carried out after open repair, IEVAR, and BEVAR/FEVAR. One of the study limitations is that retrospective study risks not capturing all data for more robust conclusions. In particular, more invasive open aneurysm repair, more complex patients, and/or patients with post-operative complications would have a longer hospital stay than straightforward minimally invasive endovascular IEVAR. This could have affected the number of data points available at each day post-operatively in each group for seven days following intervention. Additionally, the reported changes in the peri-operative peripheral blood cells numbers were not adjusted for the other factors, e.g., age, gender, smoking, that might have affected outcomes. Nevertheless, the reported outcomes could help on shedding some lights on the variations of peripheral blood cells during different approaches of aortic aneurysm repair and differences among open, infra-renal (IEVAR) and complex (BEVAR/FEVAR) endovascular aortic aneurysm groups.

2.5.1 Leukocytes

Patients after total hip and knee replacement showed an increase in their white blood cell count to approximately $3x10^6$ cells/ml over the first two post-operative days. This leukocytosis could be explained as part of the normal systemic inflammatory response to surgery.[300] These

changes possibly occur after aortic surgery due to various factors such as tissue injury, aortic clamping, reperfusion injury and/or wound repair.[301]

After aortic aneurysm repair, studies found that leukocytosis was associated with cytokine cascade activation that triggers the systematic inflammatory response and possibly multiorgan failure.[301 - 304]

This response was more pronounced in open aneurysm repair, particularly ruptured aneurysms, compared to endovascular intervention.[302, 305] This observed leukocytosis was even higher in patient who developed sepsis after abdominal aortic aneurysm repair.[306] Patients with leukocytosis after open aneurysm repair had higher risk of early mortality and inferior long-term survival.[307] From our study, on day one after interventions, leukocytes numbers increased in open and endovascular (IEVAR and BEVAR/FEVAR) groups, reaching the peak on day two then recovering afterward. However, there was no difference in postoperative leukocyte numbers between all cohorts, suggesting radiation exposure during endovascular repair did not affect leukocyte number changes after IEVAR and BEVAR/FEVAR compared to open repair.

2.5.2 Lymphocytes

During the peri-operative period of major surgery, significant changes were observed in circulating leukocytes including drop in lymphocyte numbers.[299, 308, 309]

In a study, lymphocyte count dropped significantly on day five in patients underwent surgery e.g., laparotomy, open and laparoscopic nephrectomy, and hernia repair. After major surgery, this count drop was more evident in T lymphocytes rather than B lymphocytes.[299]

Other reports suggested that the mitogenic response of circulating lymphocytes to the T-cell mitogen phytohemagglutinin and/or concanavalin A is potentially altered by major surgery. In these reports, the degree of lymphocyte suppression correlates with the complexity of surgery or severity of injury. In addition, the degree of lymphocyte suppression correlates with the subsequent development of infectious complications and mortality.[310 – 313] These reports suggest that major surgical injury can lead to depression of the mitogenic response of lymphocytes, resulting in subsequent development of infectious complications.[314]

A study of peri-operative Fas mediated apoptosis showed that circulating lymphocytes in the early perioperative period are susceptible to Fas-mediated apoptosis, which may cause depletion of circulating lymphocytes after surgery. These numbers were significantly decreased on days 1 and 4 after surgery ($P<0.02$, $P<0.05$, respectively) and returned to preoperative levels 7 days after surgery.[285] Similar results were observed in patients who

underwent oesophagectomy, as lymphocytes apoptosis was evident by DNA fragmentation and PCR products for the T-cell receptor gamma (TCR-gamma) variable region gene that were found in the serum DNA of these patients until day 5.
These results suggest that transient T-cell apoptosis occurs in the early post-operative period after oesophagectomy.[290] This post-operative T-cell apoptosis is also believed to be mediated through cytokines such as TNF-alpha and IL-6.[296, 297] Lymphocytes apoptosis was found to be associated with greater post-operative infectious complications.[315]

Our data for open surgery group showed similar trends as we observed a drop in lymphocytes count in patient after open AAA repair. However, the reduction in circulating lymphocytes was more pronounced after complex endovascular procedures (BEVAR/FEVAR) compared with open AAA repair (P=0.0001) over 7 days following interventions, particularly with greater drop in lymphocytes after BEVAR/FEVAR on day one (P=0.01) compared to open repair, which might reflect the effect of radiation exposure during complex BEVAR/FEVAR and may be further supported by the slower recovery of lymphocyte count we observed after BEVAR/FEVAR compared with open AAA repair (P=0.04). Complex branched and fenestrated repair necessitates a higher radiation exposure for the patient (Figure 2.1) and this may account for the fact that the drop-in lymphocyte count was more prominent for this group compared with standard EVAR. These changes in lymphocyte numbers reflect the sensitivity of lymphocyte cells to radiation exposure. There was a minimal difference between open aneurysm repair and IEVAR groups on day one and after a week from intervention, but this difference was not great enough to be statistically significant.

Radiation induced decrease in peripheral blood cells was observed in patients with cancer when they underwent radiotherapy. Further analysis found that circulating lymphocytes were the most radiosensitive cells amongst the erythroid, myeloid, and lymphoid lineage cells to ionising radiation which sometimes required years to recover after the radiotherapy course.[228 - 233]

Deeper phenotyping studies showed circulating T lymphocytes were more sensitive and their levels were further reduced compared with B lymphocytes, when patients were exposed to ionising radiation during radiotherapy sessions.[234, 235]
Radiation induced lymphocytopenia could be a sign of acute radiation syndrome (ARS), which occurs when individuals are exposed to at doses greater than 1 Gy and associated with damage to blood cells, particularly circulating lymphocytes that show drop in their numbers 12 to 48

hrs after exposure. The decrease and rapidity of decrease in lymphocyte count could be an indicator of exposed radiation dose, as the higher the exposed dose, the more rapid and severe the decrease in lymphocytes. The kinetics of radiation induced lymphocytopenia is previously described and demonstrated in Andrew's curves (Figure 2.6). Radiation exposure to 1-2 Gy results in drop of 60% of the circulating lymphocytes, while higher dose exposure > 8 Gy diminishes lymphocyte count by 94%.[316]

Lymphocyte depletion kinetics can be used to predict radiation induced drop in the absolute neutrophil count and predicts haematopoietic precursor cells damage results in progressive neutropenia, thrombocytopenia, and anaemia.[316, 317]

Studies explained that radiation-induced lymphocytopenia is the result of direct toxicity to circulating lymphocytes as radiation traverses the irradiated field. The flow rate of circulating oxygenated blood in capillaries is slow (0.3 mm/sec). Therefore, when ionising radiation passes through networks of blood vessels to reach the deep targets, radiation induced reactive oxygen radicals are generated by water and oxygen radiolysis in the blood vessels and directly destroy circulating lymphocytes.[318 - 321]

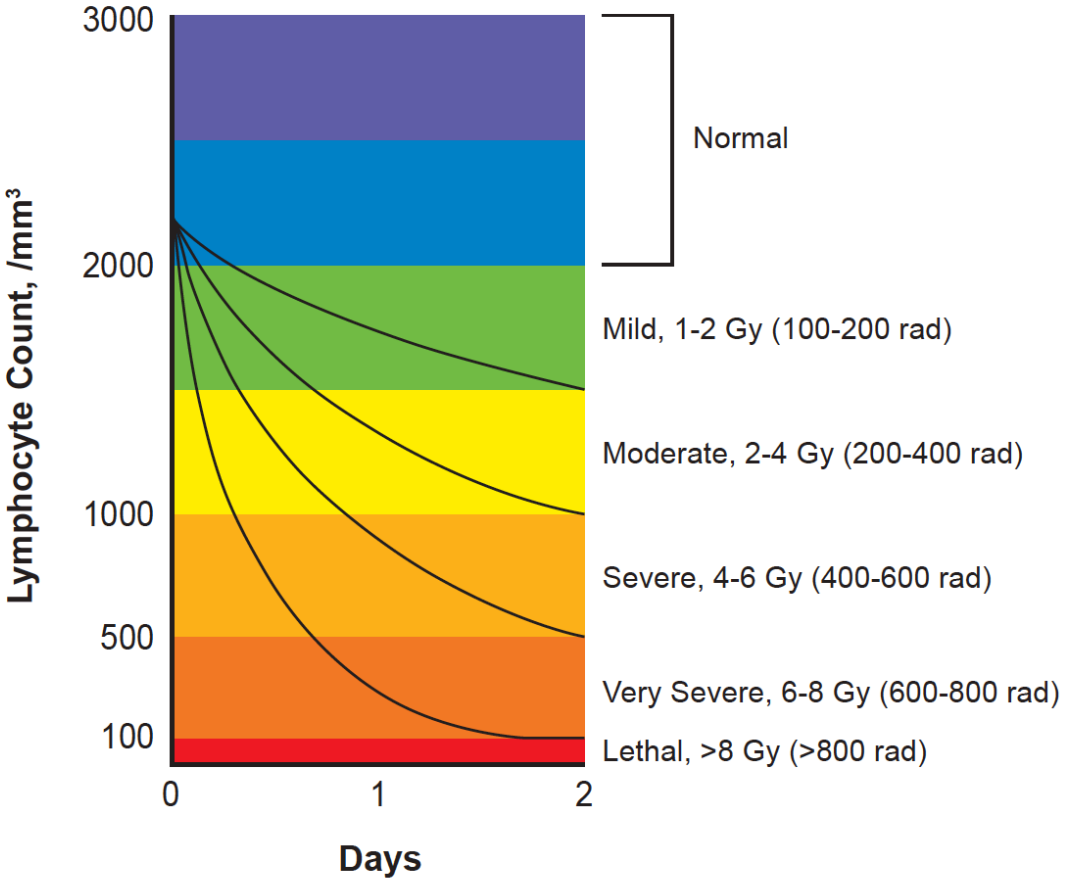

Figure 2.6 Andrews' curves show radiation induced lymphocytopenia kinetics (Adapted from Andrews GA, et al., 1965.)
Andrew's curves (lymphocyte depletion curves) demonstrate radiation induced lymphocyte depletion kinetics.

2.5.3 Monocytes

Monocyte numbers increased but not significantly after laparotomy, open and laparoscopic nephrectomy, and hernia repair. [299] Similar trends were observed in orthopaedics patients after total hip and total knee replacement.[300]

Our study also showed that monocytes numbers increased on day one after open and endovascular aortic repair (Figure 2.6). This could be explained as a response to the surgical stress that induces not only systemic endocrine-metabolic response but also influences the function of the monocytes and leukocytes leading to various systemic responses. When the postoperative clinical course was evaluated between patients undergoing an oesophagectomy. The development of systemic inflammatory response (SIRS) was significant immediately after

oesophagectomy. This was associated with high CD11b expression on monocytes and the TNF-alpha production of monocytes are considered as a response to surgical stress and related to the amount of tissue damage and surgical injury.[300]

This could explain the finding of significant variation in monocytes count between open AAA repair and IEVAR (P=0.002), and BEVAR/FEVAR (P=0.003), as monocyte numbers returned to the baseline after minimally invasive endovascular repair while open AAA repair patient maintained higher monocyte levels in their blood (Figure 2.7).

2.6 Summary

After open and endovascular aortic aneurysm repair, there are changes in the circulating blood cells. Surgical trauma initiates a systemic inflammatory response that causes an increase in the number of leukocytes and monocytes. Ionising radiation during EVAR might have resulted in a more pronounced drop in circulating lymphocytes than open surgery. These cells are the most sensitive subpopulation of peripheral blood leukocytes to ionising radiation. Therefore, the radiation exposure during EVAR, particularly complex BEVAR/FEVAR, may account for the temporal changes in circulating lymphocytes we have observed in the present retrospective analysis.

CHAPTER 3

Optimisation of analysis of DNA damage/repair biomarkers

3.1 Introduction

Ionising radiation deposits direct energy to the cellular nucleic acid and generates reactive oxygen/nitrogen species. This interaction damages the cellular DNA structure by causing base-pair alterations, nucleotide modifications, and single and/or double-strand DNA breaks.[75] As a response to this DNA damage, cell cycle checkpoint response is activated to promote DNA repair. These repair mechanisms trigger the activation of DNA repair proteins and the induction of transcription factors.

Expression of DNA damage/repair biomarkers, such as γ-H2AX and pATM in circulating cells (e.g., lymphocytes), can be a sensitive biomarker of radiation-induced DNA damage. The number of γ-H2AX foci in lymphocytes, for example, correlates with the amount of radiation-induced double-strand DNA breaks.[322]

ATM is believed to play an essential role in all cell cycle checkpoints after ionising radiation exposure, with ATM-deficient cells more susceptible to radiation-induced chromosomal damage and apoptosis.[127] This part of the study aimed to optimise a flow cytometry-based method for measuring γ-H2AX and pATM in lymphocytes from patients and operators after EVAR.

3.2 Aims

To optimise a method to measure radiation induced DNA damage/repair biomarkers γ-H2AX and pATM in circulating lymphocytes and haematopoietic cells from whole blood.

3.3 Methods of optimisation of analysis of DNA damage/repair biomarkers

3.3.1 Patient with AAA and controls

Patients with AAA undergoing endovascular and open repair as well as young healthy controls were recruited into this study. Controls were matched for age, sex, clinical confounding factors (including co-morbidities and medication) and environmental factors, such as smoking. Exclusion criteria included patients with leukemia or lymphoma, patients currently on chemotherapy or radiotherapy, patients who had received radiotherapy in the last 6 months and those exposed to scintigraphy within the last 7 days. This study was approved by the London–City & East Research Ethics Committee (16/LO/1111) following the principles of the Declaration of Helsinki, and written informed consent was obtained from each participant. Blood was taken before, immediately after, and 24hrs following open/endovascular procedures.

3.3.2 Chemically induced γ-H2AX

Lymphocyte DNA double-strand breaks can be induced using DNA topoisomerase II (topo2) inhibitor, Etoposide, which is widely used in treatment of cancer as chemotherapy. DNA topoisomerase II (topo2) inhibitors stabilise cleavable complexes between topo2 and DNA; collisions of DNA replication forks with these complexes convert them into DNA double-strand breaks.[323]

3.3.2.1 Flow cytometric analysis of chemically induced γ-H2AX in lymphocytes

Intracellular γ-H2AX expression on circulating lymphocytes was examined by fluorescence-activated cell sorting (FACS) using the following procedures,

- Peripheral venous blood was collected from the antecubital vein into ethylenediaminetetraacetic acid (EDTA) anti-coagulated tubes (BD Vacutainer, UK).
- Blood samples (2ml) were incubated with 100μM and 200μM of Etoposide (Merck Millipore, Germany) for 24hrs in 37˚C.
- Negative control blood tubes were incubated without Etoposide stimulation for same duration at the same temperature.

- Red blood cells were lysed, and cells were fixed using 10ml of BD Phosflow Lyse/Fix Buffer (BD Bioscience, USA) for 10mins 37˚ C.
- A wash buffer solution containing phosphate buffered saline (PBS)/0.5% bovine serum albumin (BSA) was added (5x dilution) to halt lysis and fixation, the sample centrifuged for 5mins at 400g, washed in FACS buffer and centrifuged again.

For lymphocyte fluorescein isothiocyanate conjugated mouse anti-human CD3 (FITC- anti CD3, Miltenyi Biotec, Appendix 6.2) staining, blood tubes were divided into 2 groups (Figure 3.1):
Group A: tubes with anti-CD3 antibodies before the permeabilisation step
Group B: tubes stained with anti-CD3 antibody after the permeabilisation step

- Group A: Samples were incubated with 10µL human Fc receptors (FcR) blocking reagent (Miltenyi Biotec, UK) for 10mins on ice, followed by incubation with 20µL (concentration 0.5µg/mL) of FITC-CD3 antibody (Miltenyi Biotec) for 30mins on ice in the dark.
- Both groups were washed and permeabilised with 3ml of ice-cold Perm Buffer III added dropwise (BD Phosflow, BD Bioscience, USA) on ice for 30mins.
- Cells were washed twice and stained for γ-H2AX using 5µL (concentration of 0.3µg/mL) of antihuman allophycocyanin (APC) γ-H2AX antibodies (BD Bioscience, USA, Appendix 6.2) to all the tubes (100 µL blood) on ice for a further 60mins in the dark.
- FITC anti-CD3 antibodies (20µL, concentration 0.5µg/mL) were also added to Group B samples.
- Cells were then resuspended in 1mL PBS/0.5% BSA buffer.
- To exclude dead cells, 10uL Hoechst was added 5mins prior to analysis.
- Samples were then analysed using a MACSQuant flow cytometer (Miltenyi Biotec).

A MACSQuant flow cytometer (Miltenyi Biotec) is equipped with red and blue lasers with excitation wavelengths of 633nm and 388nm respectively. Controls included unstained (for voltage settings) for appropriate gating of γ-H2AX. Allophycocyanin-conjugated IgG isotype control antibodies (BD Biosciences and BioLegenad) were used in fluorescence minus one sample for appropriate gating of γ-H2AX. Compensation was carried out using labelled beads (CompBeads Plus, BD Biosciences). Lymphocytes were identified according to forward scatter (size) and side scatter (granularity) properties after gating out doublets, and gating on cells staining positive for CD3. The percentage of lymphocytes expressing γ-H2AX was quantified.

Data for all flow cytometric acquisitions in this study were analysed using FlowJo v10 software (Flow Jo, USA).

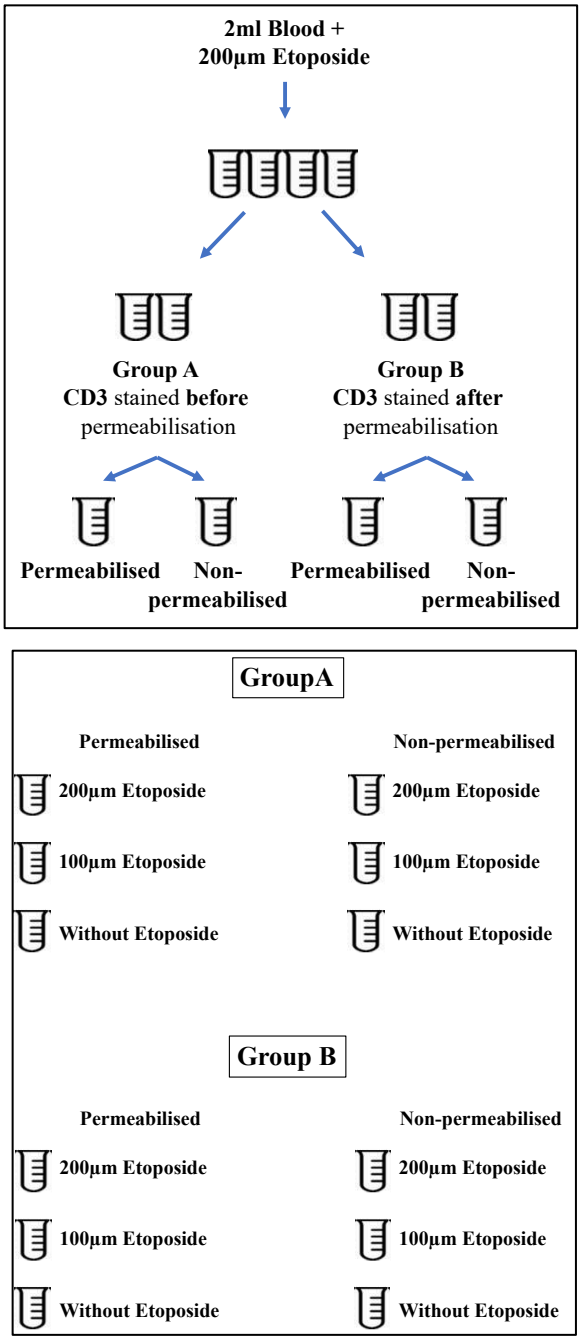

Figure 3.1 Flow chart of measuring Etoposide induced DNA damage in CD3+ T lymphocytes

Collected blood samples were divided into two groups; Group A: CD3 staining before permeabilisation, and Group B: CD3 staining after permeabilisation. Each group was then subdivided to permeabilised and non-permeabilised samples (control). Each subgroup was incubated with 200uM, 100uM Etoposide and control).

3.3.2.2 Stimulation and intracellular staining of PBMCs

Peripheral blood mononuclear cells (PBMCs) were isolated from whole blood to reduce the number of cells being stimulated. 100mls of blood were collected from from the antecubital vein into EDTA tubes and was diluted 1:1 with Dulbecco's Modified Eagle Medium (Sigma, UK) containing 4.5g/L glucose and L-glutamine (Lonza, UK), layered on Ficoll-Paque Plus (GE Healthcare, UK) and centrifuged for 30 mins at 400g. PBMCs were removed and washed in wash buffer. Any remaining red cells were lysed with 5mls of red blood cell lysis solution (PharmLyse, BD Biosciences) for 5 mins. 5 × volume of buffer was then added to halt lysis and the cells centrifuged at 400g. Following red cells lysis, PBMCs were incubated with 100μM Etoposide for 30 mins in 37˚C. Cells were then fixed, permeabilised and stained as previously mentioned in section 3.3.2.1.

3.3.2.3 Phorbol 12-myristate 13-acetate (PMA) stimulation of whole blood and PBMCs

For further optimisation of cell permeabilisation, lymphocytes intracellular signaling was measured using intracellular flow cytometric techniques. I took the opportunity of in-house optimised protocol to measure Mitogen-activated protein kinase (MAPk) and Signal transducer and activator of transcription 1 (Stat1) in order to validate my cell permeabilisation method. Phorbol 12-myristate 13-acetate (PMA) stimulation of whole blood and PBMCs separately was carried out to measure phosphorylated forms of the downstream signaling molecules Stat1 and MAPk.

200mls blood were collected in EDTA tube and divided in to 100ml for PBMCs isolation and 100ml for whole blood sample. PBMCs were isolated as mentioned in Section 3.3.2.2), both groups were then lysed with red blood cell lysis solution (PharmLyse, BD Biosciences) for 5 minutes. 5xvolume of buffer was then added to halt lysis and the cells centrifuged at 400g. Following red cells lysis, cells were then stimulated with 10ng/mL phorbol 12-myristate-acetate (PMA, 400nM for whole blood and 40nM for PBMCS), for 15 mins at 37^{o}C. The cells were then fixed in 4% PFA, T lymphocytes were stained with FITC anti-CD3 antibodies as previously explained. This followed by cell permeabilision in Perm buffer III for 10 mins prior to staining for anti-phosphorylated MAPk and Stat1 for 30mins in ice. Cells were then washed with wash buffer and then analysed with FACS machine as previously mentioned in section 3.3.2.1. Intracellular phosphorylation was compared between stimulated lymphocytes and unstimulated lymphocytes.

3.3.2.4 Etoposide induced γ-H2AX in whole blood using CytoFix/CytoPerm

As chemically induced phosphorylated H2AX could not be detected with previous Lyse/Fix buffer and Perm Buffer III. γ-H2AX upregulation was examined in Etoposide-induced whole blood using BD Cytofix/Cytoperm fixation/Permeabilization Kit (BD Bioscience, USA) as the following:

1. Blood collected as mentioned earlier in section 3.3.2.1. and incubated with Etoposide (75uM) in 37˚for 4 hrs.
2. Red cells were lysed with BD Pharmlyse buffer then washed with wash buffer.
3. Cells were fixed and permeabilised using 500µL of BD Cytofix/Cytoperm Fixation/ Permeabilization solution in the dark in room temperature for 20mins.
4. Cell were then washed and incubated for 10mins in 10µL BD Perm/Wash™ Buffer (Fetal Bovine Serum and saponin).
5. 2 mL BD Perm/Wash™ buffer was added to cells prior to further wash and then were incubated for 10 minutes at RT in the dark.
6. Following sampling centrifugation for 5 minutes at 400g, cell pellets were blocked with FcR Blocking reagent (Miltenyi Biotec).
7. Cells were then stained with APC- Mouse anti-H2AX (BD Bioscience, USA) in the dark for 45mins, and washed with wash buffer prior to running flow cytometric analysis.

3.3.2.5 Etoposide induced γ-H2AX in PBMCs using Cell Signaling Buffer Set A

Another cell fixation and permeabilisation kit was used in order to detect and quantify amount of phosphorylated H2AX in CD3+ T lymphocyte cells. The advantage of Cell Signaling Buffer Set A (Miltenyi Biotec, UK) is that it provides separate agents for each cell fixation and permeabilisation which gives the opportunity for anti-CD3 staining after fixation and before permeabilisation step as the following:

1. PBMCs were isolated from whole blood using Ficoll-Paque Plus (GE Healthcare, UK) as previously mentioned in section 3.3.2.2.
2. Remaining red cells were lysed with red blood cell lysis solution (Pharmlyse, BD Biosciences) for 5 mins, and then washed using wash buffer and spun for 5mins in 400g.
3. Cells were then incubated with 75µM Etoposide for 18hrs in 37˚C.
4. After further washout, cells were fixed with 250uL of Cell Signaling Set A Inside Fix.
5.This was followed by cell washout and then permeabilisation slowly with 3ml of chilled Cell Signaling Buffer Set A Perm Buffer III on ice for 30 mins.

6. After further washout, samples (500µL) were incubated with 10µL human FcR blocking reagent (Miltenyi Biotec, UK) for 10 mins on ice.
7. Cells were stained in the dark with APC-Mouse anti-γ-H2AX antibodies (BD Bioscience, USA) in ice for 60 mins.
8. Stained cells were washed once and then resuspended in wash buffer before proceeding with FACS analysis as previously explained.

3.3.2.6 Comparison between Cytofix/Cytoperm and Cell Signaling Set A buffers

In order to achieve an optimum detection of γ-H2AX from stimulated bloods cells, a comparison between cell fixation and permeabilisation (BD Cytofix/Cytoperm and Miltenyi Cell Signaling Set A) buffers was carried out as the following:
1. Blood samples were collected as previously mentioned and aliquoted into 2ml in Eppendorf tubes and incubated with Etoposide (450uM) in 37˚ for 24 hrs.
2. Red cells were lysed using BD Pharmlyse for 5 mins, and then washed using wash buffer and spun for 5mins in 400g.
3. Samples were split into two groups: Cytofix/Cytoperm protocol group, and Cell Signalling Set A protocol group.
Both protocols were carried out as mentioned earlier simultaneously under same conditions.

Cytofix/Cytoperm protocol:
1. Cell fixation and permeabilisation with Cytofix/Cytoperm, as mentioned in section 3.3.2.4.
2. Cell were then washed and incubated in Perm/wash buffer for 10 mins.
3. After further washout, cell pellet was incubated with human FcR blocking reagent.
4. Cell staining with APC-Mouse anti-γ-H2AX antibodies (BD Bioscience).
5. Stained cells were washed, and then resuspended in wash buffer before FACS analysis.

Cell Signalling Set A protocol:
1. Samples were then fixed with 250uL Inside Fix from Cell Signalling Buffer Set A.
2. After washout, cells were permeabilised with 3ml of Cell Signaling Perm Buffer III.
3. Cell pellet was washed then incubated with human FcR blocking reagent.
4. Cell staining with APC-Mouse anti-γ-H2AX antibodies (BD Bioscience).
5. Stained cells were washed and then resuspended in wash buffer before FACS analysis.

3.3.2.7 Etoposide induced γ-H2AX using Cell Signaling Set A buffers

1. Blood samples were collected as previously mentioned and aliquoted into 2mls.
2. Samples were then stimulated with Etoposide (150 uM) in 37˚for 4 hrs.
3. Red cells were then lysed with BD Pharm Lyse for 5 mins. 5 × volume of buffer was then added to halt lysis and the cells centrifuged at 400g.
4. After washout, cells were fixed with Inside Fix (250ul) in room temperature for 10 mins, then washed out with wash buffer and centrifuged for 5mins in 400g.
5. Cells were incubated with FITC- anti-CD3 antibodies in the dark in 4° C for 10 mins.
6. This followed by cell permeabilisation with Perm Buffer A in ICE for 30 mins.
7.Cells were then stained with APC- Anti- **γ**-H2AX in room temperature in the dark for 30 mins.
8. Cell pellets were washed and resuspended in wash buffer prior to running flow cytometry analysis using the following settings.

3.3.3 Radiation induced γ-H2AX

3.3.3.1 X-ray machine radiation induced γ-H2AX

In parallel with using chemically induced DNA damage, we also used irradiated blood samples to optimise a flow cytometric method for detecting γ-H2AX levels in CD3+ T lymphocytes.
Blood samples were collected from volunteers in EDTA containing tubes, then divided into 3 groups: irradiated, positive control (Etoposide), and negative control (Figure 3.2) 2ml in each tube. Samples were then kept in a water bath at 37˚C and transferred to the X-ray machine (Philips Healthcare, the Netherlands).
Blood tubes were exposed to different radiation doses (Table 3.1); negative and positive controls were kept in a water bath. For positive Control: Etoposide (200μM) was added to 2 ml blood and incubated for 24 hrs at 37˚C.
RBCs were lysed, fixed, and then incubated with anti-human CD3 antibodies followed by cell permeabilisation and staining with γ-H2AX antibodies as described above. Flow cytometry machine settings and acquisitions were set as previously mentioned.

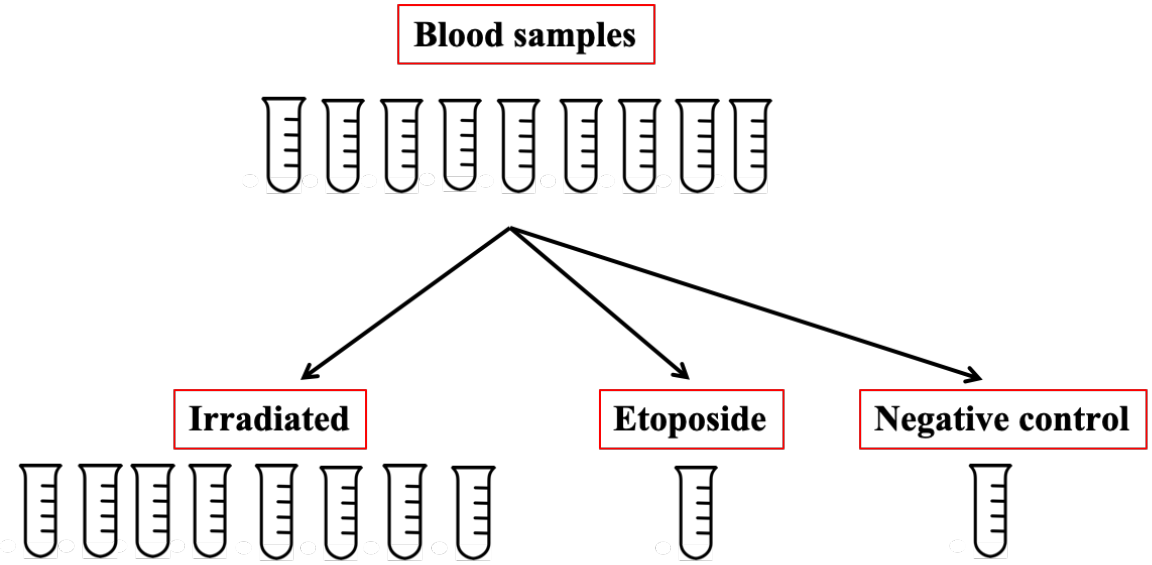

Figure 3.2 Flow chart for the x-ray irradiated blood samples
Collected blood samples were divided into 3 groups; Irradiated (samples were exposed to an increasing radiation exposure doses), positive control (Etoposide) and negative control.

Table 3.1 Radiation exposure measurements from x-ray machine

Sample	mAs	Dose in air (mGy)	Dose in scatter (mGy)
1	10	6	8
2	110	70	88
3	310	196	248
4	610	387	487
5	50	32	40
6	200	127	160
7	450	285	359

3.3.3.2 Micro-CT radiation induced γ-H2AX

Blood samples were collected and transferred to micro-CT scanner in 37˚C in water bath. Samples (0.5ml whole blood in Polypropylene Eppendorf Safe-Lock tubes, Eppendorf UK) were irradiated for 10 and 20 mins (Table 3.2). Radiation doses could not be measured using micro-CT scanner as its only designed for obtaining imaged. Negative control (non-irradiated) and positive control (Etoposide stimulated) were kept in water bath at 37˚C.

Red cells were lysed, and cells were fixed, stained CD3 antibodies, and permeabilised before staining with anti γ-H2AX antibodies as described above.

Table 3.2 Radiation exposure measurements from micro-CT scanner

Sample	Sample Volume	Duration	Tube energy	Projections
First Sample	0.5ml	10mins	65KvP x 123 uA	360˚
Second Sample	0.5ml	20mins	65 KvP x 123uA	360˚

3.3.3.3 Radiotherapy machine radiation induced γ-H2AX

Blood samples from healthy volunteers were collected and exposed in Polypropylene Eppendorf Safe-Lock tubes (1ml each) to radiation doses between 100 and 1000 mGy using a Darpac 2000 (Gulmay Medical) x-ray unit (energy: 80 kVp [half-value layer, 2.0mmAL], 6.9 mA, applicator: 8 cm diameter) positioned ≈25 cm from the x-ray source (Figure 3.3). Irradiated blood samples were taken back to the lab, RBCs lysed, cells were fixed, stained CD3 antibodies, and permeabilised before staining with anti γ-H2AX antibodies as described above.

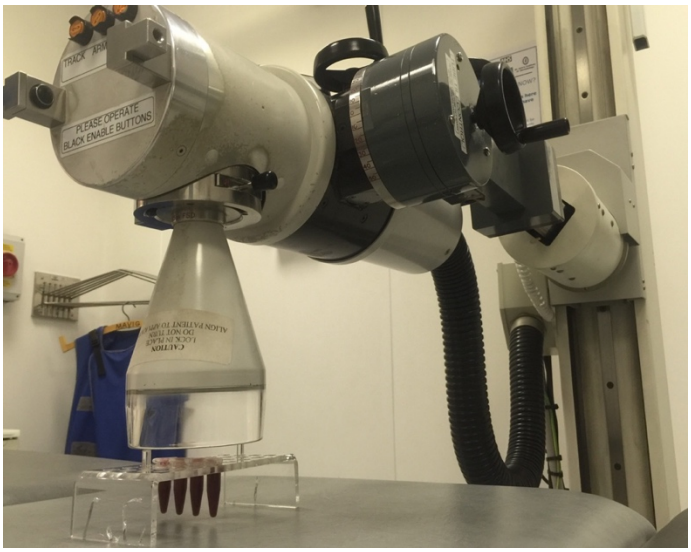

Figure 3.3 In vitro irradiation of blood samples using Darpac 2000 (Gulmay Medical) x-ray unit
Blood containing Polypropylene Eppendorf Safe-Lock tubes (1ml each) were placed in a rack under Darpac 2000 (Gulmay Medical) x-ray unit and exposed to known radiation doses.

3.3.3.4 Reliability of radiation induced γ-H2AX measurement protocol

Further to successful detection of radiation induced γ-H2AX using aforementioned technique and radiotherapy machine as source of radiation. Methodology reliability was tested using blood samples from the same healthy volunteer and exposed to a range of radiation doses (10mGy to 500mGy) at multiple occasions. Exposed samples were lysed, cells were fixed, stained with CD3 antibodies, then permeabilised before γ-H2AX staining and flow cytometric analysis as explained in detail above.

3.3.4 Chemically induced pATM

3.3.4.1 Etoposide induced pATM in PBMCs using Cytofix/Cytoperm

PBMCs were isolated from whole blood as previously mentioned in 3.3.2.2 and stimulated with Etoposide (50uM) for 4 hrs at 37˚. After further washout, samples were blocked with FcR blocking reagent for 10 mins on ice. T lymphocytes were then stained with 10μL of FITC conjugated mouse antihuman CD3 antibody for 30 mins on ice in the dark.

Cells were washed and then fixed and permeabilised using Cytofix/Cytoperm buffer (250uL) and incubated in the dark in 4˚C for 20 mins. After a further washout, cells were incubated with phycoerythrin-conjugated (PE) antihuman pATM antibodies (Biolegend, UK, Appendix 6.2) in ice for 60 mins. Stained cells were washed once and then resuspended in 500μL wash buffer before proceeding with FACS analysis as previously explained.

3.3.4.2 Etoposide induced pATM in PBMCs using Cell Signalling Buffer Set

PBMCs were isolated from whole blood as previously mentioned in 3.3.2.2 and stimulated with Etoposide (50uM) for 4 hrs at 37˚. Cells were fixed using Inside Fix buffer in the dark in Room Temperature for 10 mins. Cells then washed and permeabilised with 1 ml of ice-cold Perm Buffer III for 30 mins. After further washout, samples were blocked with FcR blocking reagent for 10 mins on ice. Cells were then stained with PE antihuman pATM antibodies in ice for 60mins. Stained cells were washed once and then resuspended in 500μL wash buffer before proceeding with FACS analysis as previously explained.

3.3.4.3 Etoposide induced pATM in whole blood using Cell Signalling Buffer Set

Blood samples were collected and incubated with Etoposide (50uM) for 4hrs at 37˚. Red cells were then lysed, followed by cell membrane fixation using Inside Fix buffer. T lymphocytes

were then stained with 10μL of FITC mouse antihuman CD3 antibody for 30 mins on ice in the dark. Samples were tested with Flow cytometry to check efficacy of the CD3+ T lymphocytes staining.

Cells then washed and permeabilised with 1 ml of ice-cold Perm Buffer III for 30 mins. After further washout, samples were blocked with FcR blocking reagent for 10 mins on ice. Samples were stained with PE antihuman pATM antibodies (1 and 5uL) in ice for 60 mins. Control samples were stained with PE conjugated IgG Isotope (1 & 5uL) for appropriate gating of pATM. Stained cells were washed once again and then resuspended in 500μL wash buffer before proceeding with FACS analysis as previously explained.

3.3.4.4 Etoposide induced pATM in T lymphocytes

Blood samples were collected and incubated with Etoposide at 3 different concentrations (50, 100 and 200uM) for 4hrs at 37˚. Red cells were then lysed, this followed by cell membrane fixation using Inside Fix buffer. T lymphocytes were then stained with 10μL of FITC mouse antihuman CD3 antibody for 30 mins on ice in the dark. Samples were tested with Flow cytometry to check efficacy of the CD3+ T lymphocytes staining.

Cells then washed and permeabilised with 1 ml of ice-cold Perm Buffer III for 30 mins. After further washout, samples were blocked with FcR blocking reagent for 10 mins on ice. Samples were stained with PE antihuman pATM antibodies (1 and 5uL) in ice for 60 mins. Control samples were stained with PE conjugated IgG Isotope (1 & 5uL) for appropriate gating of pATM. Stained cells were washed once again and then resuspended in 500μL wash buffer before proceeding with FACS analysis as previously explained.

3.3.5 Peri-operative changes of DNA damage/repair biomarkers

Patients are exposed to ionising radiation throughout EVAR procedures, therefore in this part of the study we aimed to study the acute biological effect of radiation in patients when they undergo EVAR. To study this biological effect of radiation during the acute phase, changes in levels of DNA damage biomarkers γ-H2AX & pATM were measured in patients' lymphocytes during the perioperative period of EVAR. DNA damage biomarkers upregulation after EVAR is compared to similar cohort of patients who underwent open aortic aneurysm surgical repair.

Blood samples were collected from patients in ethylenediaminetetraacetic acid tubes prior to, immediately and 24hrs after endovascular aortic repair procedure. Red blood cells were lysed using Pharmlyse for 10mins and then washed in 0.5% BSA/PBS for 5 mins at 4°C. Cells were then fixed using Inside Fix 10mins at room temperature, followed by staining with FITC-mouse anti-human CD3 antibody for 30mins on ice in the dark. Cell membranes were then permeabilized on ice using Perm Buffer III and washed before staining for APC- mouse anti-human γ-H2AX and PE- mouse anti-human pATM. This followed by samples analysis on a MACSQuant flow cytometer using the previously mentioned settings.

3.3.6 γ-H2AX and pATM expression in T lymphocyte subsets

After identifying γ-H2AX and pATM activation in CD3+ T lymphocytes in operators after endovascular aortic repair procedures. A further assessment is carried out to measure peri-operative changes of γ-H2AX and pATM in T lymphocytes subpopulations CD4+ T Helper and CD8+ Cytotoxic T cells in operators after performing endovascular aortic interventions. We then studied a deeper phenotyping of CD4+ T Helper and CD8+ Cytotoxic T cells, to identify γ-H2AX and pATM in their naïve (CD45RO-/CCR7+), central memory (CD45RO+/CCR7+) and effector memory (CD45RO+/CCR7-) subpopulations

3.3.6.1 Flow cytometric analysis of T lymphocytes subpopulations

In order to identify T lymphocytes subsets, we optimised a flow cytometric method to detect signals from multiple cellular surface markers simultaneously. This could be challenging due to the possibility of interference of signals on excitation from one immunofluorescent marker to another. If this happens, false readings of cellular markers excitations can occur, which result in inaccurate detection of certain cell types in order to measure their radiation induced DNA damage.

Therefore, various steps of optimisation were carried out to ensure accurate detection of each cell type and its associated radiation induced DNA damage. First step of this optimisation process was to detect each cellular surface marker individually on live cells, fixed cells, and fixed and then permeabilised cells (Figure 3.4)

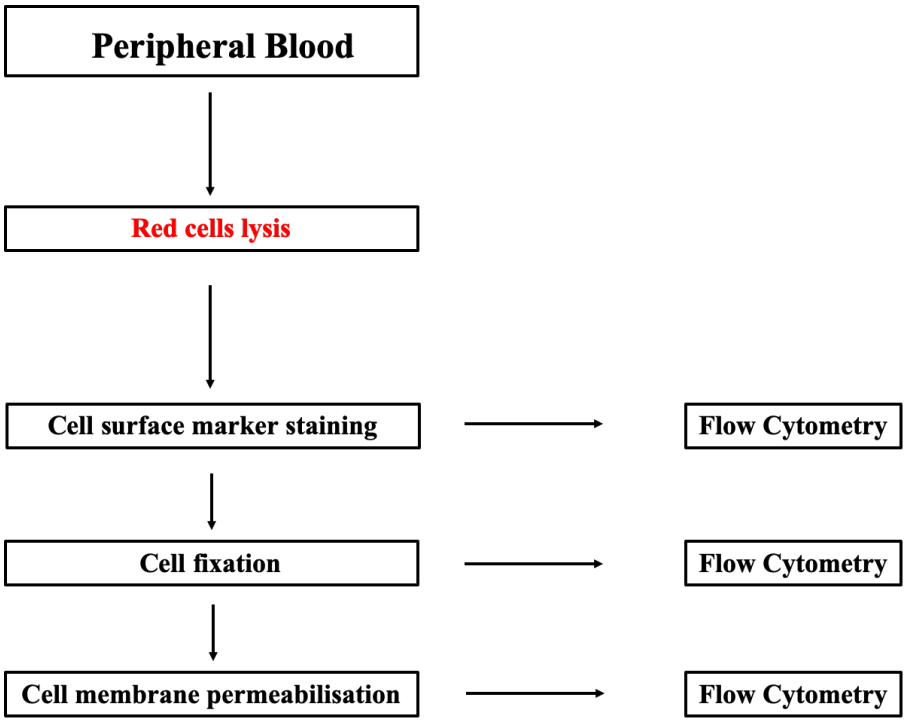

Figure 3.4 Flow chart of optimisation of FACS assessment of T lymphocytes subpopulations
Steps of the optimisation process to detect T lymphocytes subpopulation surface marker individually on live cells, fixed cells, and fixed and then permeabilised cells

Staining on live cells:

Blood samples collected from a healthy volunteer; red cells were lysed as previously mentioned. After washing the cells twice, cells were blocked using FcR block on ice for 15 mins. Cell pellets were resuspended in wash buffer and then aliquoted out into multiple samples. This allowed to stain for individual cell surface markers CD3, CD4, CD8, CCR7 (CD197), and CD45RO (Appendix 6.1). Stained samples were then processed using a MACSQuant flow cytometer and adjusting machine settings accordingly.

Staining on fixed only cells:

After collecting blood samples and red cell lysis, samples were divided into 2 groups (unstained/control and stained). After washing cells twice, they were blocked using FcR block on ice for 15 mins. Cell pellets were resuspended in wash buffer and then aliquoted out into multiple samples. Cells were stained with CD3, CD4, CD8, CCR7 (CD197), CD45RO separately. All samples were then fixed with Inside Fix for 10 mins. After cell wash, cell pellets resuspended in wash buffer and analysed using a MACSQuant flow cytometer.

Staining on fixed and permeabilised cells:

After collecting blood samples and red cell lysis, samples were divided into 2 groups (control and stained). After washing the cells twice, cells were blocked using FcR block on ice for 15 mins. Cell pellets were resuspended in wash buffer and then aliquoted out into multiple samples. Samples were stained with CD3, CD4, CD8, CCR7 (CD197), CD45RO separately. All samples were then fixed with Inside Fix and after wash, cells were permeabilised with Perm buffer III for 30 mins in ice. Cells were then washed prior to analysis with a MACSQuant flow cytometer.

3.3.6.2 Flow cytometric analysis of T lymphocytes subpopulations in fixed cells

After previous results, in order to ensure the accuracy of the signal received from cell surface marker excitation, another flow cytometric analysis was carried out. As demonstrated in the flow chart below (Figure 3.5), samples were collected, and red cells were lysed. After cell pellet wash, cells were fixed as mentioned above. Fixed cells were stained individually with cell surface markers CD3, CD4, CD8, CD45RO and CCR7. A sample from each stained tube was processed for flow cytometric analysis. The rest of stained fixed cells were permeabilised with Perm Buffer III. After a further cell wash, samples were processed using a MACSQuant flow cytometer.

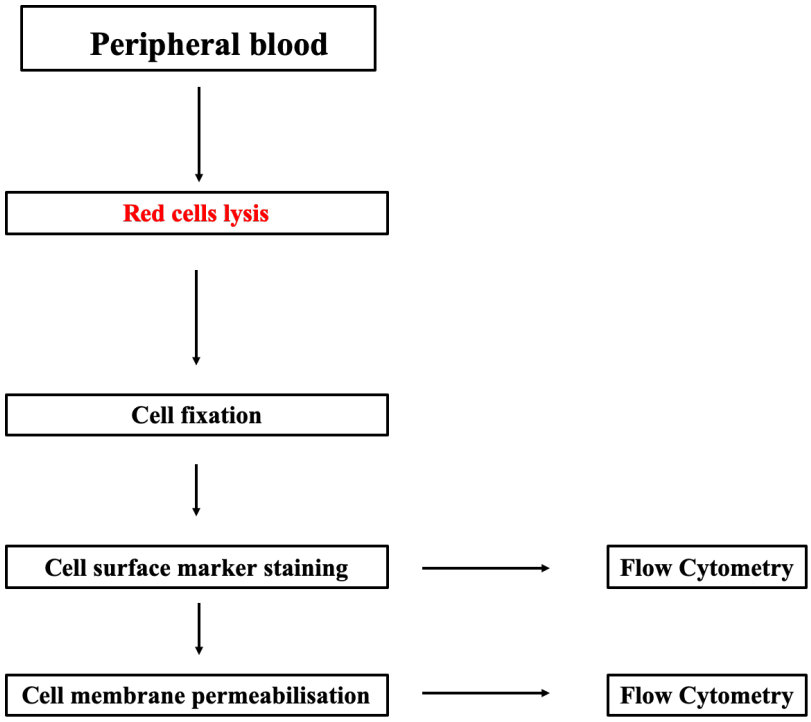

Figure 3.5 Flow chart of optimisation of FACS assessment of T lymphocytes subpopulations
Flow chart of optimisation method of flow cytometric analysis of individual staining of T lymphocytes subpopulations surface markers on fixed only cells and fixed, then stained and permeabilised cells.

3.3.6.3 γ-H2AX & pATM changes in T lymphocytes subpopulations

After identifying CD3+ T lymphocytes subpopulation using the flow cytometric technique, a further assessment is carried out to measure peri-operative changes of γ-H2AX and pATM in T lymphocytes subpopulations CD4+ T Helper and CD8+ Cytotoxic T cells in operators after performing endovascular aortic interventions.

Samples were collected, and red cells were lysed. After cell pellet wash, cells were fixed as mentioned above. Fixed cells were stained individually with cell surface markers CD3, CD4, CD8, CD45RO and CCR7. This was followed with cell membrane permeabilisation with Perm Buffer III. After a further cell wash, cells were incubated with γ-H2AX & pATM prior to final wash and analysis with MACSQuant flow cytometer.

3.3.7 γ-H2AX and pATM expression in haematopoietic stem/progenitor cells

After identifying γ-H2AX and pATM activation in CD3+ T lymphocytes in operators after endovascular aortic repair procedures. A further assessment is carried out to measure peri-operative changes of γ-H2AX and pATM in haematopoietic stem cells (HSCs, CD45- CD38- CD34+ CD90+) and haematopoietic stem/progenitor cells (HSPCs, CD45- CD38+ CD34+ CD90-).

3.3.7.1 Flow cytometric analysis of haematopoietic stem/progenitor cells

A flow cytometric method was optimised to detect signals from multiple cellular surface markers simultaneously specific to these cell types. Therefore, various steps of optimisation were carried out to ensure accurate detection of each cell type and its associated radiation induced DNA damage. First step of this optimisation process was to detect each cellular surface marker individually on live cells, fixed cells, and fixed and then permeabilised cells from blood samples collected from healthy individuals (Figure 3.6).

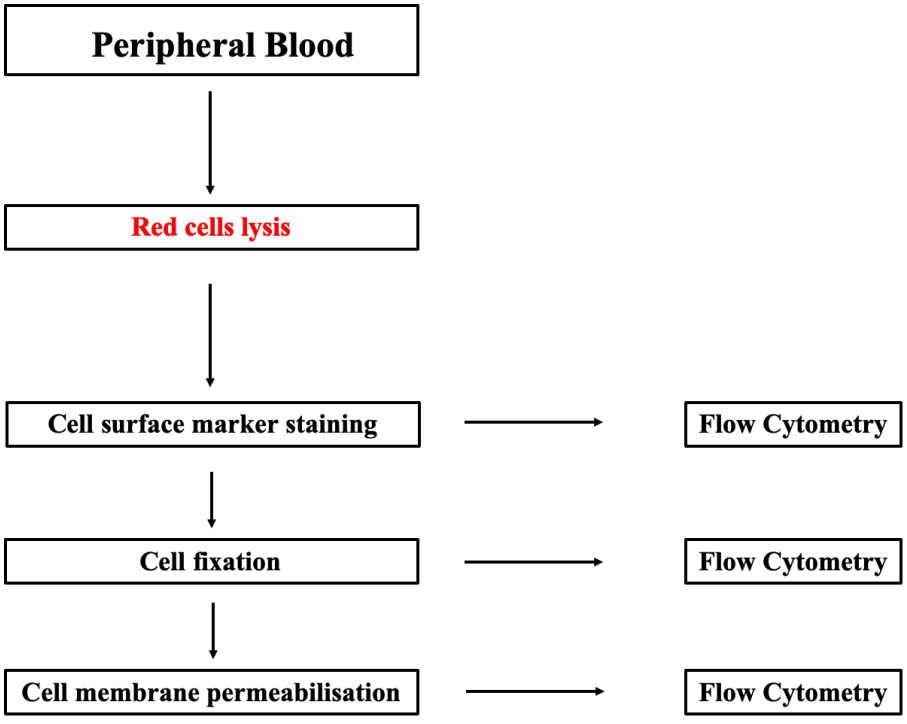

Figure 3.6 Flow chart of optimisation of FACS assessment of HSCs/ HSCPs
Steps of optimisation process to detect cellular surface markers on live cells, fixed cells, and fixed and then permeabilised cells from blood samples.

Staining on live cells:

Blood samples collected from a healthy volunteer; red cells were lysed as previously mentioned. After washing the cells twice, cells were blocked using FcR block on ice for 15 mins. Cell pellets were resuspended in wash buffer and then aliquoted out into multiple samples. This allowed to stain for individual cell surface markers CD45, CD14, CD56, CD34, CD38, and CD90 (Appendix 6.1). Both CD14 and CD56 were on the same dump laser channel to be excluded. Stained samples were then split in to two tubes each, one processed using a MACSQuant flow cytometer and adjusting machine settings accordingly, other samples used in the next steps of optimisation.

Staining on fixed only cells:

Further to previous steps, cells were stained with CD45, CD14, CD56, CD34, CD38, and CD90, were fixed with Inside Fix for 10 mins. After cell wash, cell pellets resuspended in wash buffer and then split in to two tubes each, one processed using a MACSQuant flow cytometer and adjusting machine settings accordingly, other samples used in the next steps of optimisation.

Staining on fixed and permeabilised cells:

Further to previous steps, cells were permeabilised with Perm buffer III for 30 mins in ice. Cells were then washed prior to analysis with a MACSQuant flow cytometer.

3.3.7.2 Analysis of haematopoietic stem/progenitor cells in fixed cells

After previous results, cell surface markers CD38, CD90, CD14/56 and CD45 were successfully detected, nevertheless CD34 was not detected. Consequently, cell surface staining was carried out on fixed cells as demonstrated in the flow chart below (Figure 3.7). Samples were collected, and red cells were lysed. After cell pellet wash, cells were fixed as mentioned above. Fixed cells were stained individually with cell surface markers C34, CD38, CD90, CD14/56 and CD45. A sample from each stained tube was processed for flow cytometric analysis. The rest of stained fixed cells were permeabilised with Perm Buffer III. After a further cell wash, samples were processed using a MACSQuant flow cytometer.

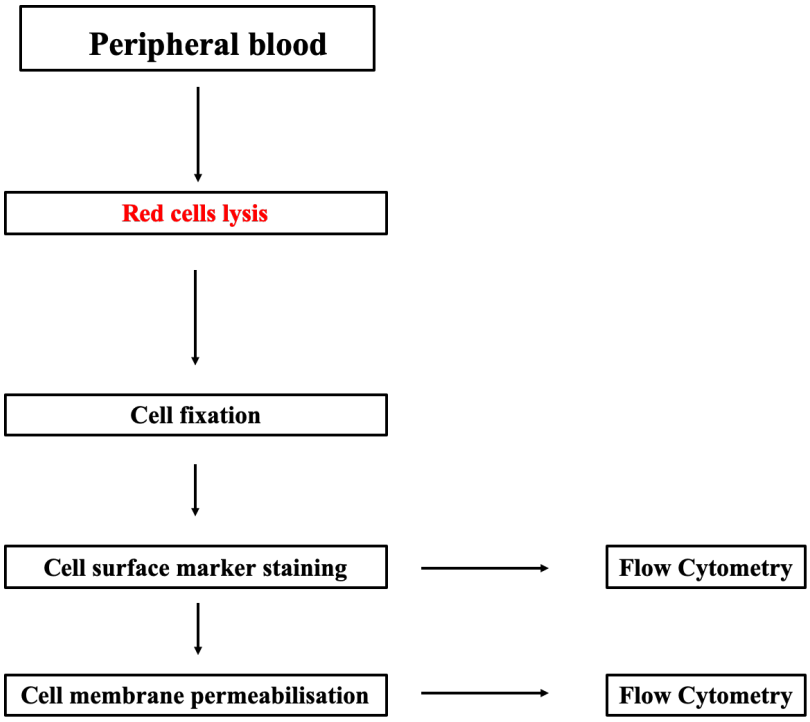

Figure 3.7 Flow chart of optimisation of FACS assessment of fixed HSCs/HSCPs
Steps of optimisation to identify cell surface marker staining on fixed and fixed then permeabilised haematopoietic stem/progenitor cells

3.3.7.3 Analysis to identify haematopoietic stem/progenitor cells from PBMCs

To maximise chances of identifying CD34 and CD90 positive cells, peripheral blood mononuclear cells (PBMCs) were isolated from whole blood to reduce the number of cells being stimulated.

A hundred millilitres of blood were diluted 1:1 with Dulbecco's Modified Eagle Medium (Sigma, UK) containing 4.5g/L glucose and L-glutamine (Lonza, UK), layered on Ficoll-Paque Plus (GE Healthcare, UK) and centrifuged for 30 mins at 400g. PBMCs were removed and washed in wash buffer. Any remaining red cells were lysed with 5 mls of red blood cell lysis solution for 5 mins. Wash buffer was then added to halt lysis and the cells centrifuged at 400g. Following red cells lysis, PBMCs were blocked with FcR block and then stained with individual cell surface markers CD434, CD38, CD90, and CD45. Stained samples were then split in to two tubes each, one processed using a MACSQuant flow cytometer and adjusting machine settings accordingly, other samples used in the next steps of optimisation (Figure 3.8).

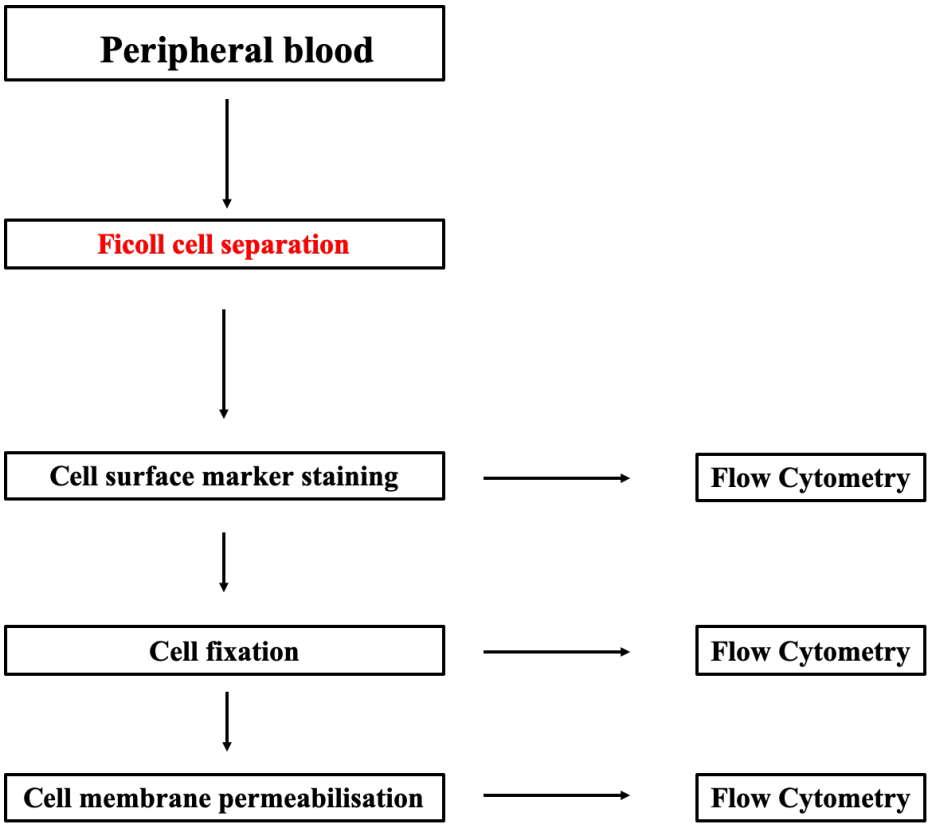

Figure 3.8 Flow chart of optimisation of FACS assessment of HSCs/HSCPs isolated from PBMCs
Step of optimisation process to detect cellular surface markers on live cells, fixed cells, and fixed and then permeabilised cells from blood samples.

Staining on fixed only cells:

Further to previous steps, cells were stained with CD45, CD34, CD38, and CD90, were fixed with Inside Fix for 10 mins. After cell wash, cell pellets resuspended in wash buffer and then split in to two tubes each, one processed using a MACSQuant flow cytometer and adjusting machine settings accordingly, other samples used in the next steps of optimisation.

Staining on fixed and permeabilised cells:

Further to previous steps, cells were permeabilised with Perm buffer III for 30 mins in ice. Cells were then washed prior to analysis with a MACSQuant flow cytometer.

3.3.7.4 γ-H2AX & pATM changes in haematopoietic stem/progenitor cells

Further to previous steps, bloods were collected from operators to measure levels of γ-H2AX and pATM in their circulating hematopoietic stem cells (HSCs, $CD45^{-}$ $CD34^{+}$ $CD38^{-}$ $CD90^{+}$) and haematopoietic stem/progenitor cells (HSPCs, $CD45^{-}$ $CD34^{+}$ $CD38^{+}$ $CD90^{-}$).

Blood samples (100 mls) were collected from operators before and immediately after complex EVAR. Ficoll cell separation was carried out as previously described, and red cell lysis was carried out. PBMCs were blocked with FcR block and then stained with individual cell surface markers CD434, CD38, CD90, and CD45.

Samples were then fixed with Inside Fix for 10 mins. After cell wash, cell pellets were permeabilised with Perm buffer III for 30 mins in ice. Cells were then washed prior to staining with γ-H2AX & pATM for 30 mins in the dark prior to analysis with the flow cytometer.

3.3.8 Radiation induced DNA base damage

Ionising radiation causes DNA damage indirectly by production of reactive oxygen species. ROS mainly damage DNA guanine base due to its low oxidation potential among all DNA bases.[192, 193]

When guanine is oxidised, 7,8-dihydro-8-oxoguanine (8-oxoG) is produced. 8-oxoG has mutagenic effects, and therefore its rapidly repaired by 8-oxoG DNA glycosylase 1 (OGG1) through base excision repair (BER) pathway. OGG1, therefore, could be used as a validated biomarker of radiation induced base oxidation.

3.3.8.1 Reactive oxygen species measurement in lymphocytes

In order to detect radiation induced DNA base damage, it was essential to first be able to identify the production of reactive oxygen species. Consequently, H_2O_2 induced oxidative stress was used to optimise a flow cytometric protocol to measure ROS in lymphocytes.

H_2O_2 causes the oxidation of 2'-7' dichlorofluorescin (H2DCF) to 2'-7'dichlorofluorescein (DCF) which is highly fluorescent and enables measurement levels of ROS using flow cytometry.[324 - 327]

In order to optimise a flow cytometric protocol to measure radiation induced reactive oxygen species (ROS) in lymphocytes, blood samples were stimulated with H_2O_2 (100uM) for 15 and 30 mins then samples incubated in ice to halt further stimulation. RBCs lysed with lysis buffer and samples washed. ROS dye (CM-H2DCFDA, Life Technologies, UK) was added, and

samples incubated in water bath for 30 mins then proceeded to flow cytometry analysis with gating on lymphocytes using forward and side scatter.

3.3.8.2 Hydrogen peroxide induced OGG1 in CD3+ T lymphocytes

Blood samples collected from a heathy volunteer and stimulated with Hydrogen peroxide (500 and 1000uM) and then cells were fixed using Cell Signaling Set A and stained with FITC anti CD3 antihuman antibodies as described earlier. Cells were also stimulated with Etoposide as mentioned earlier. Cells were then permeabilised with Perm buffer III and stained with PerCP antihuman 0.5ug/ml OGG1 (Novus Biologicals, UK), 0.3ug/ml APC- γ-H2AX and 0.1ug/ml PE-pATM antibodies (Appendix 6.2). All samples were then analysed with flow cytometry using previously mentioned settings.

3.3.8.3 Radiation induced OGG1 in CD3+ T lymphocytes

When operators carried out IEVAR procedures, their blood samples were analysed for both base oxidation and DNA DSBs using OGG1, and γ-H2AX and pATM biomarkers. As previously mentioned, using our optimised flow cytometric analysis to measure these biomarkers.

3.3.9 Immunocytochemistry analysis of γ-H2AX in CD3+ T lymphocytes

3.3.9.1 Immunofluorescence staining of T lymphocytes

Blood samples were collected from healthy volunteers and RBCs were lysed as 3.3.2.5. Cells were then fixed by incubation in 4% Paraformaldehyde for 10 mins at room temperature. Cells were washed and incubated with mouse anti-human FITC-CD3 (Miltenyi Biotec, UK) for 30 mins in room temperature in the dark. Cells were washed and mounted on slides using Vectashield anti-fade mounting media with DAPI (4,6-diamidino-2-phenylindole, Sigma-Aldrich, UK). Slides were sealed onto a coverslip and images were taken using a Nikon microscope with an Olympus 40x and 20x magnification and analysed using ImageJ (NIH, USA) software.

3.3.9.2 Immunohistochemistry of chemically induced γ-H2AX in T lymphocytes

Whole blood samples were stimulated with Etoposide in order to induce γ-H2AX upregulation as per section 3.3.2.5. After stimulation with Etoposide, RBCs were lysed, and cells fixed. Following CD3 staining as per section 3.3.2.5 mouse anti-human antibodies for 30 mins in room temperature in the dark.

Cells were then washed and permeabilised with 0.5% Triton X-100 (Sigma-Aldrich) for 30 mins in ice. After washing, cells were incubated with a purified gamma H2AX (5ug/ml; Bio-Legend) primary antibody followed by secondary staining with donkey-antimouse cy3 (5ug/ml; Jackson ImmunoResearch Laboratories) antibody. Cells were washed and mounted on slides using Vectashield anti-fade mounting media with DAPI. Images were taken using a Nikon microscope with an Olympus 40x and 20x magnification and analysed using ImageJ (NIH) software.

3.3.9.3 Immunohistochemistry of radiation induced γ-H2AX in T lymphocytes

Blood samples were collected, lysed and fixed. Cells were then stained with CD3 antibodies, then permeabilised and stained with γH2AX antibodies as described above.

3.3.9.4 Immunocytochemistry analysis of γ-H2AX in isolated T lymphocytes

Blood samples were collected from an operator before and immediately after radiation exposure, when he carried out a complex EVAR procedure.

Red cells were lysed and washed. Rest of cells were fixed as described above. Samples were then incubated with anti-CD3 immunomagnetic microbeads for 30 mins following by positive selection of labelled lymphocytes using LS Columns (Miltenyi Biotec, UK). Isolated CD3+ve cells were permeabilised using Triton X-100 for 30 mins in ice. Cell were then washed and stained with mouse anti-human gamma γH2AX (5ug/ml; Bio-Legend, UK), followed by secondary staining with donkey anti-mouse Cy3 (5ug/ml; Jackson ImmunoResearch Laboratories). After final washout, stained cells were mounted on slides using DAPI gel mount (Sigma-Aldrich, UK). Images were taken using a Nikon Confocal fluorescence microscope with an Olympus 100/1.30 oil lens.

3.4 Results of optimisation of analysis of DNA damage/repair biomarkers

3.4.1 Chemically induced γ-H2AX

3.4.1.1 Flow cytometric analysis of chemically induced γ-H2AX in lymphocytes

When blood samples were stimulated with different concentration of Etoposide, I concluded the followings (Figure 3.9):

1- Successful red cell lysis and cell fixation (Figure 3.9A)

2- There was no difference in CD3 staining either before or after permeabilisation (Figure 3.9B & C)

3- There was concern regarding permeabilisation due to lack of γ-H2AX signaling (Figure 3.9B & C)

4- No γ-H2AX signals were detected which could be either due to fault stimulation with etoposide or inadequate cell permeabilisation (Figure 3.9B & C)

To optimise etoposide stimulation and cell permeabilisation steps, stimulation, and intracellular staining of PBMCs was carried out.

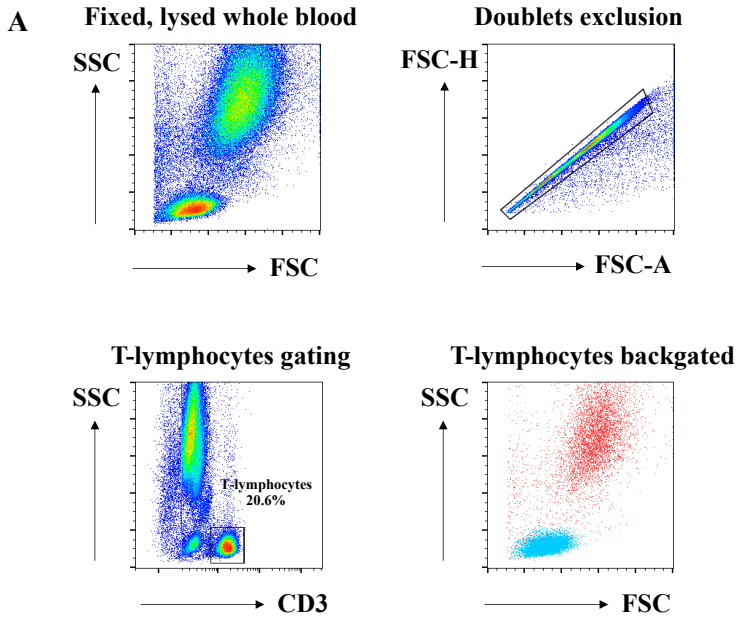

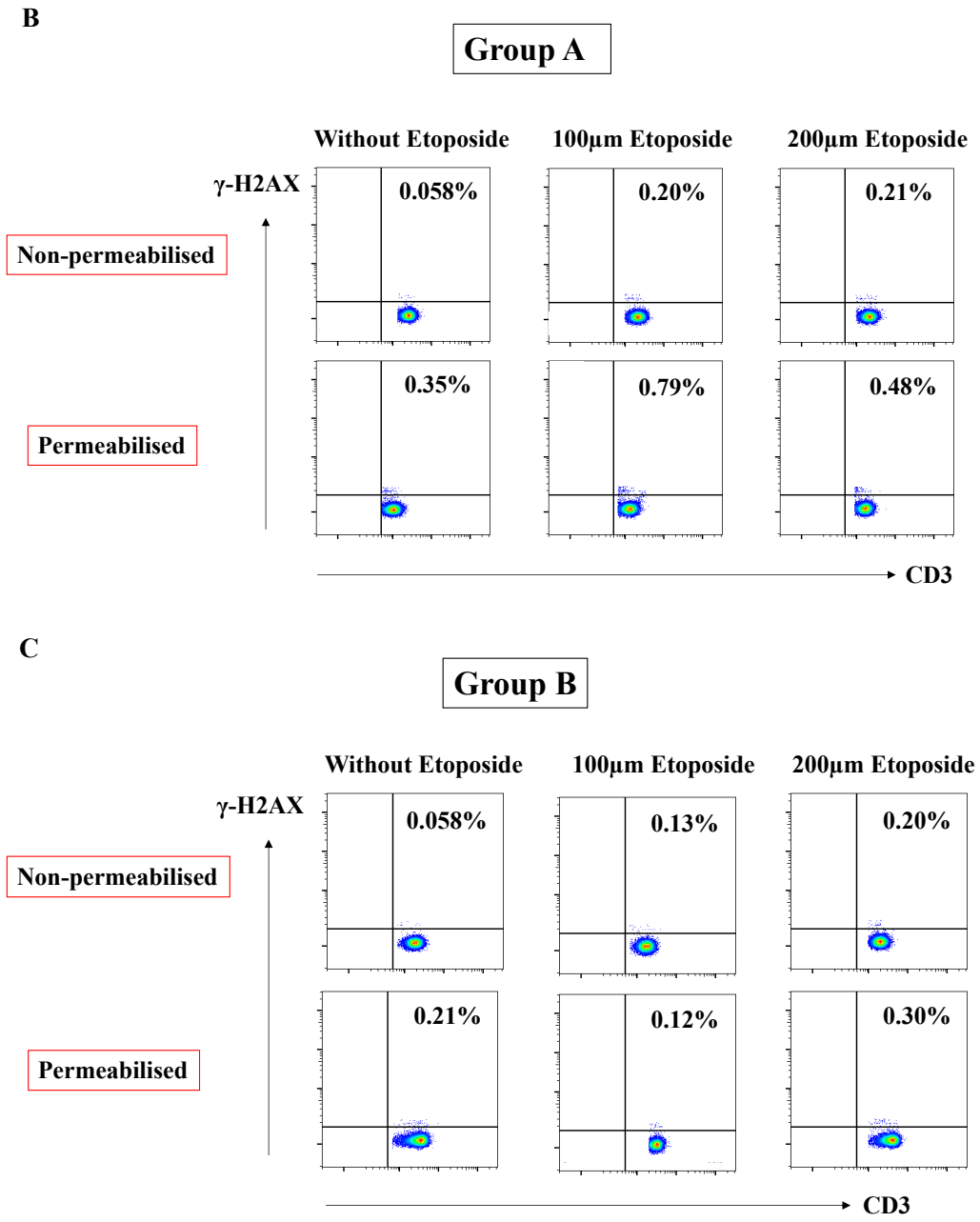

Figure 3.9 Gating strategy to identify Etoposide induced γ-H2AX in CD3+ T-lymphocytes
(A) Flow cytometric dot blots showing fixed, lysed whole blood cells were blotted according to side (SSC) and forward (FSC) scatter. Doublets were excluded when cells were blotted according to their forward scatter heights (FSC-H) and forward scatter surface area (FSC-A). Gating strategy to identify CD3+ T-lymphocytes is demonstrated when cells blotted according to their SSC and CD3. T-lymphocytes CD3+ positive cells were then backgated to identify them among whole lymphocytes population according to cells SSC and FSC. (B) Group A, Flow cytometric dot blots showing expression of CD3+ T lymphocytes when cells were stimulated with Etoposide and permeabilised after staining with CD3 antibodies. (C) Group B, Flow cytometric dot blots showing expression of CD3+ T lymphocytes when cells were stimulated with Etoposide and permeabilised before staining with CD3 antibodies. CD3+ staining was not affected by the order of permeabilisation step, however no significant changes in percentage of γ-H2AX expressing CD3+ cells were identified particularly between permeabilised stimulated and unstimulated cells.

3.4.1.2 Stimulation and intracellular staining of PBMCs

Etoposide induced γ-H2AX signalling was successfully detected in CD3+ T lymphocytes when stimulated PBMCs cells were isolated and permeabilised (Figure 3.10). However, anti-CD3 staining was not as strong as previously illustrated in Figure 3.9.

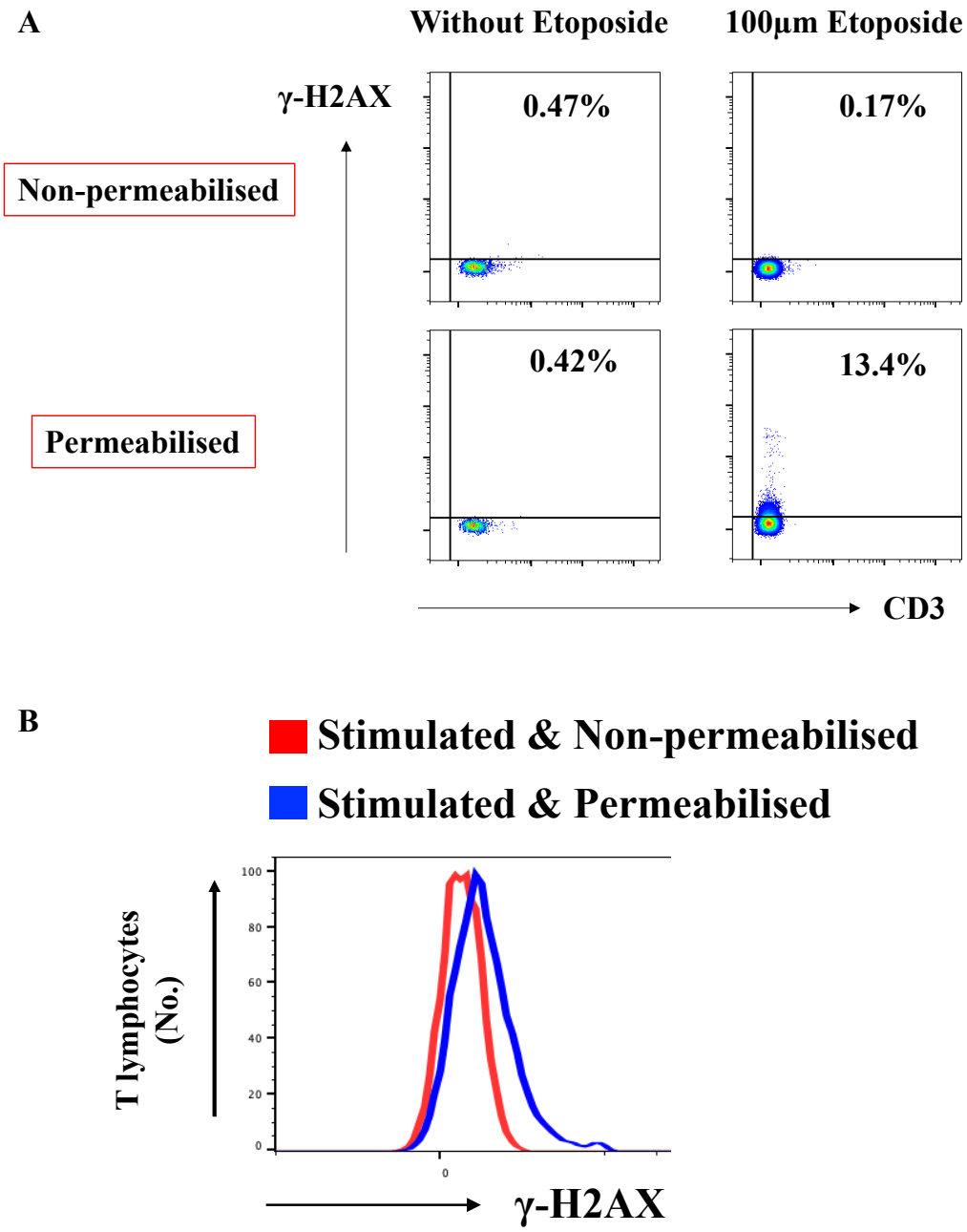

Figure 3.10 γ-H2AX in CD3+ T-lymphocytes when Etoposide stimulated PBMCs
(A) Flow cytometric dot blots showing PBMCs stimulated with Etoposide, permeabilised and stained with γ-H2AX and CD3 antibodies. Higher percentage of CD3+ cells expressed γ-H2AX when they were Etoposide Stimulated and Permeabilised. (B) Histograms showing higher expression of γ-H2AX in Etoposide Stimulated and Permeabilised T lymphocytes compared to Etoposide Stimulated and Non-permeabilised cells.

3.4.1.3 Phorbol 12-myristate 13-acetate stimulation of whole blood and PBMCs

Even though, there was an increase in the MAPk signals in T-lymphocytes when PMA stimulated PBCMs, phosphorylation of MAPk and Stat1 was not detected in whole blood samples. Again, there was issue in anti-CD3 staining which could be secondary to fixation/ permabilising agents (Figure 3.11).

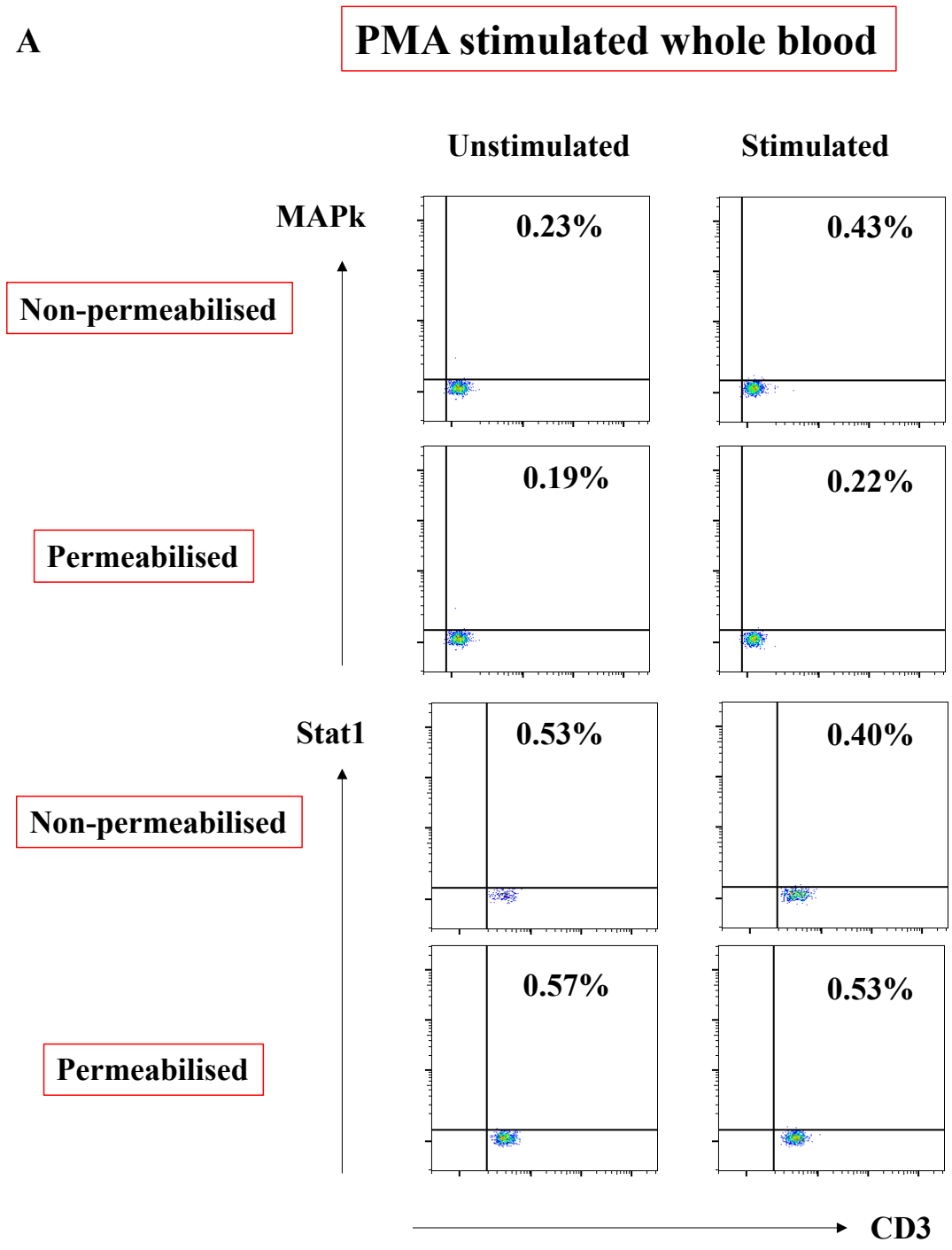

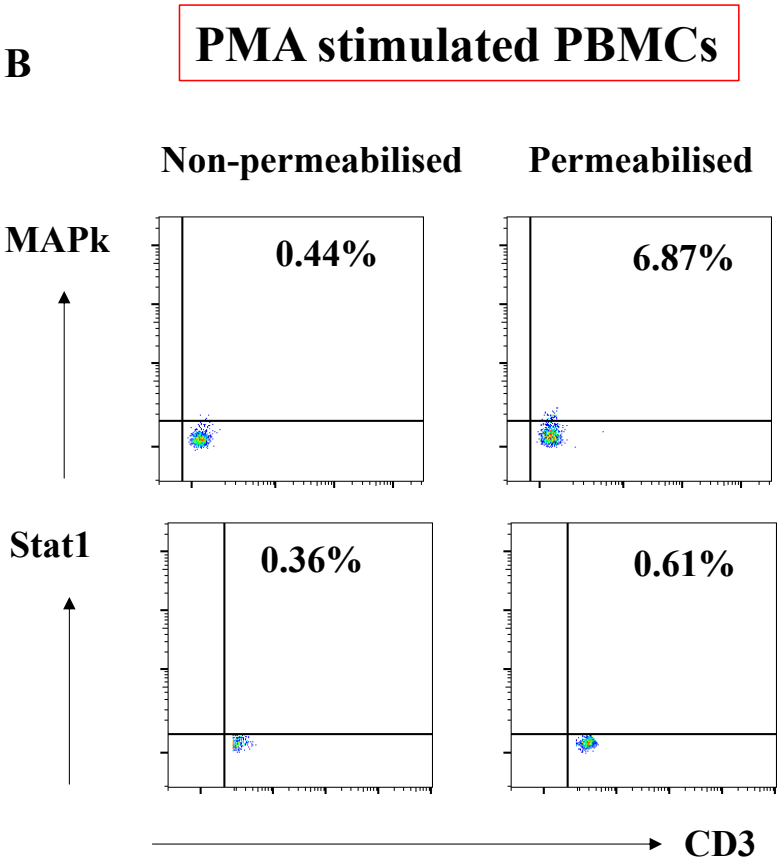

Figure 3.11 MAPk & Stat1 phosphorylation after PMA stimulation of whole blood and PBMCs

(A) Flow cytometric dot blots showing expression of MAPk and Stat1 in permeabilised and non-permeabilised CD3+ T lymphocytes from PMA stimulated whole blood sample. (B) Flow cytometric dot blots showing expression of MAPk and Stat1 in permeabilised and non-permeabilised CD3+ T lymphocytes from PMA stimulated PBMCs. The percentage of MAPk expressing CD3+ T lymphocytes increased only in PMA stimulated PBCMs, no changes of MAPk and Stat1 signals were identified in stimulated whole blood samples.

3.4.1.4 Etoposide induced γ-H2AX in whole blood using CytoFix/CytoPerm

There was an increase in intracellular signalling of γ-H2AX in Etoposide stimulated cells (Figure 3.12). However, there was no ability to identify CD3+ T lymphocytes as staining with anti-CD3 antibodies was not ideal before cell fixation as that might minimise the chances of missing detecting γ-H2AX considering its peak of 30-60 mins after exposure.

Also, it is not possible to stain with anti-CD3 antibodies after cell membrane permeabilisation. Lymphocytes were identified using forward and side scattered during the flow cytometer data analysis. Also, comparison between permeabilised and non-permeabilised cells were not possible as for cell permeabilisation occurred immediately after cell fixation as per the manufacturer guidance.

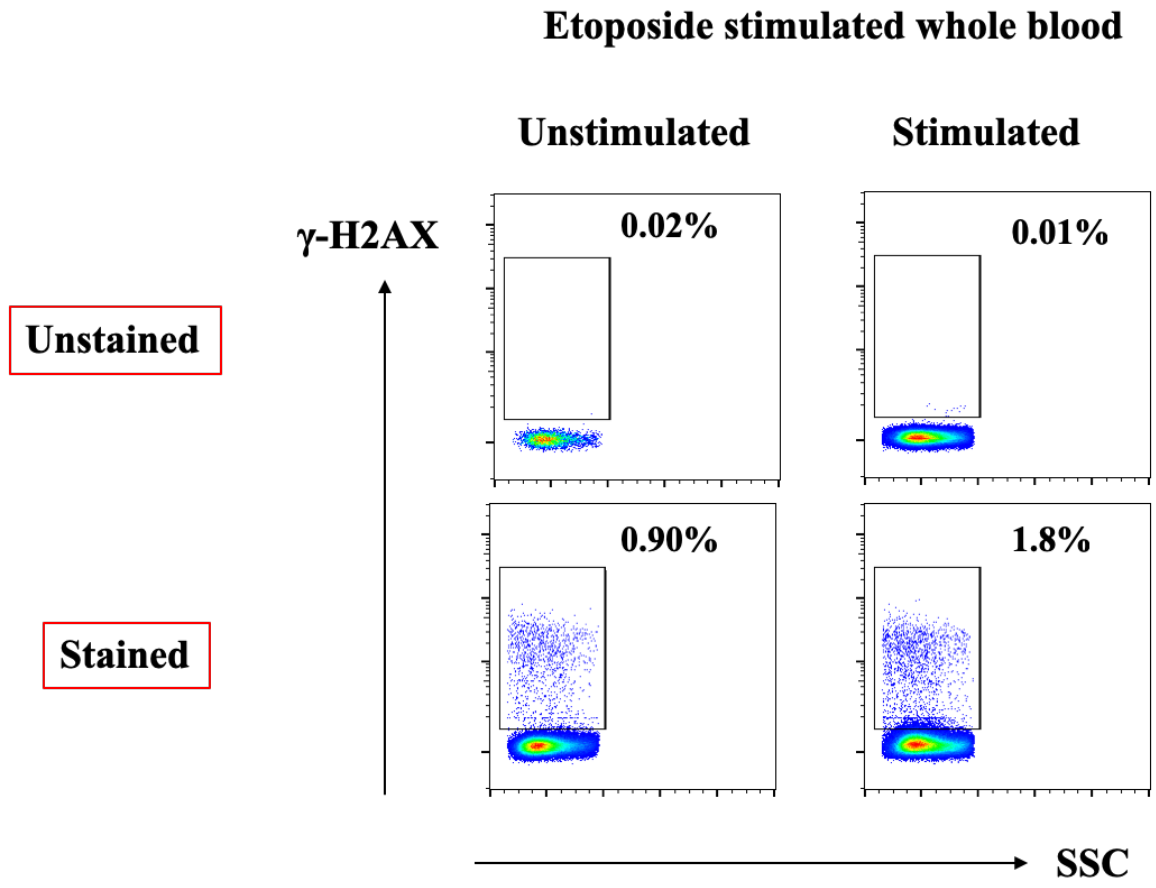

Figure 3.12 γ-H2AX in Etoposide induced whole blood using CytoFix/Cytoperm
Flow cytometric dot blots showing an increase in γ-H2AX expressing lymphocytes percentage when they were Etoposide stimulated and stained from whole blood sample.

3.4.1.5 Etoposide induced γ-H2AX in PBMCs using Cell Signaling Buffer Set A

When cell fixation and permeabilisation were carried out using Cell Signalling Buffer Set A. There was an increase in the percentage of cells expressing γ-H2AX (Figure 3.13) when PBMCs were stimulated with Etoposide, compared to negative controls. This reflected successful cell fixation and permeabilisation.

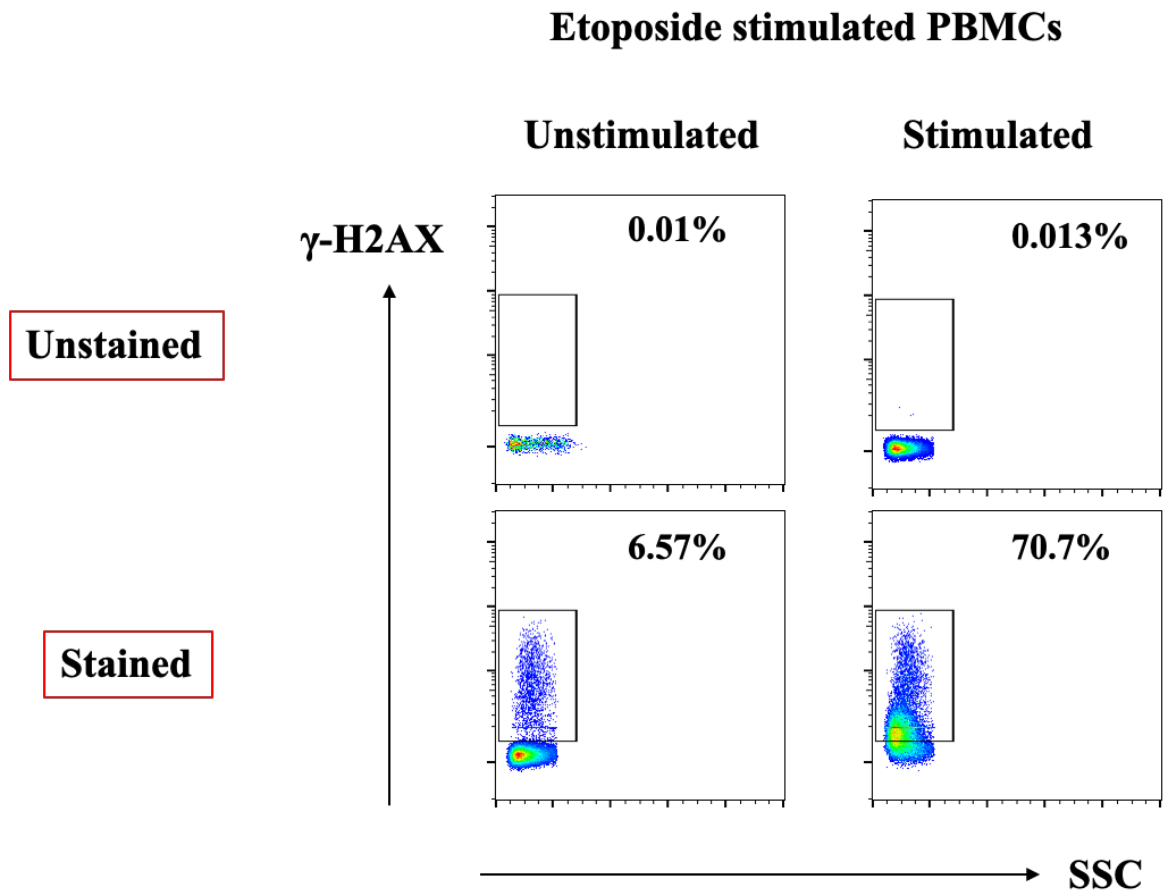

Figure 3.13 γ-H2AX in Etoposide induced PBMCs Cell Signalling Buffer Set A
Flow cytometric dot blots showing an increase in percentage of PBMCs expressing γ-H2AX when they are stimulated with Etoposide stimulated and then fixed and permeabilised using Cell Signalling Buffer Set A.

3.4.1.6 Comparison between Cytofix/Cytoperm and Cell Signaling Set A buffers

From whole blood sample, γ-H2AX was detected using both kits however higher γ-H2AX was detected using Cell Signaling Set A buffer (Figure 3.14). Additionally, unstained-stimulated samples showed more false positive results in Cytofix/Cytoperm reagents (Figure 3.14A). Also, due to the difficulty in identifying CD3+ T lymphocyte using Cytofix/Cytoperm kit, optimised Cell Signaling Buffer Set A protocol was preferred over Cytofix/Cytoperm set.

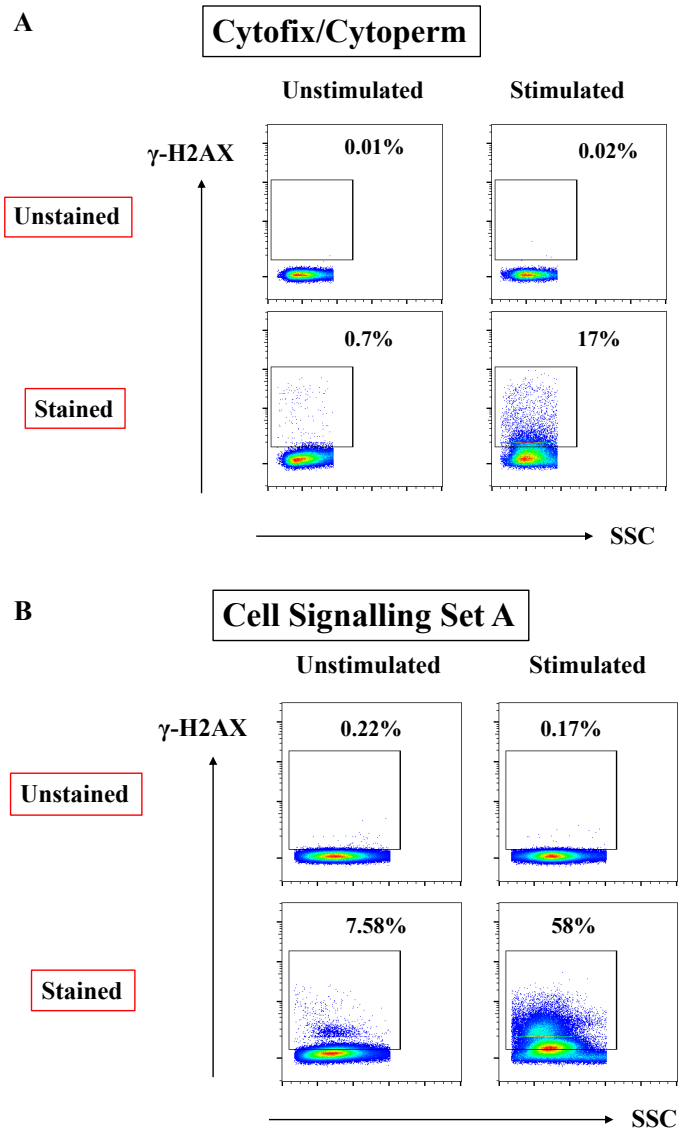

Figure 3.14 Etoposide induced γ-H2AX using Cytofix/Cytoperm and Cell Signaling Set A buffers in whole blood sample

(A) Flow cytometric dot blots showing an increase in percentage of Etoposide induced γ-H2AX lymphocytes compared to unstimulated stained and unstained cells in whole blood sample using Cytofix/Cytoperm buffer, (B) Flow cytometric dot blots showing an increase in percentage of Etoposide induced γ-H2AX lymphocytes compared to unstimulated stained and unstained cells in whole blood sample using Cell Signaling Set A buffer

3.4.1.7 Etoposide induced γ-H2AX using Cell Signaling Set A buffers

γ-H2AX was detected in Etoposide stimulated CD3+ T lymphocytes using Cell Signaling Set A buffers over shorter period of stimulation time of whole blood sample with identifying the upregulation of γ-H2AX in stained CD3+ T lymphocytes. From Figure 3.15, both unstimulated permeabilised and stimulated non-permeabilised samples could be good candidates for negative controls. However, a further analysis and a change of the gating strategy was required to minimise false positive findings. Therefore, further analysis comparing these to simulated permeabilised samples as shown in Figure 3.16.

γ-H2AX was detected in Etoposide stimulated CD3+ T lymphocytes using Cell Signaling Set A buffers from whole blood sample. From Figure 3.16, gating strategy is illustrated to identify, either unstimulated permeabilised or stimulated non-permeabilised samples could be used as a more suitable as negative control. γ-H2AX levels in stimulated non-permeabilised were higher than γ-H2AX levels in unstimulated permeabilised CD3+ T lymphocytes. This suggests stimulated non-permeabilised samples could stand as more potential negative controls to minimise chances of detecting false positive signals, however unstimulated permeabilised remains as a good candidate for negative controls as it also showed low γ-H2AX levels.

From previous optimisation of flow cytometric analysis of chemically induced γ-H2AX, we can identify subtle upregulation of γ-H2AX levels in CD3+ T lymphocytes from whole blood sample using Cell Signaling Set A buffers. Therefore, we proceeded to testing our optimised method in detecting radiation induced γ-H2AX levels in CD3+ T lymphocytes from in vitro-irradiated whole blood sample.

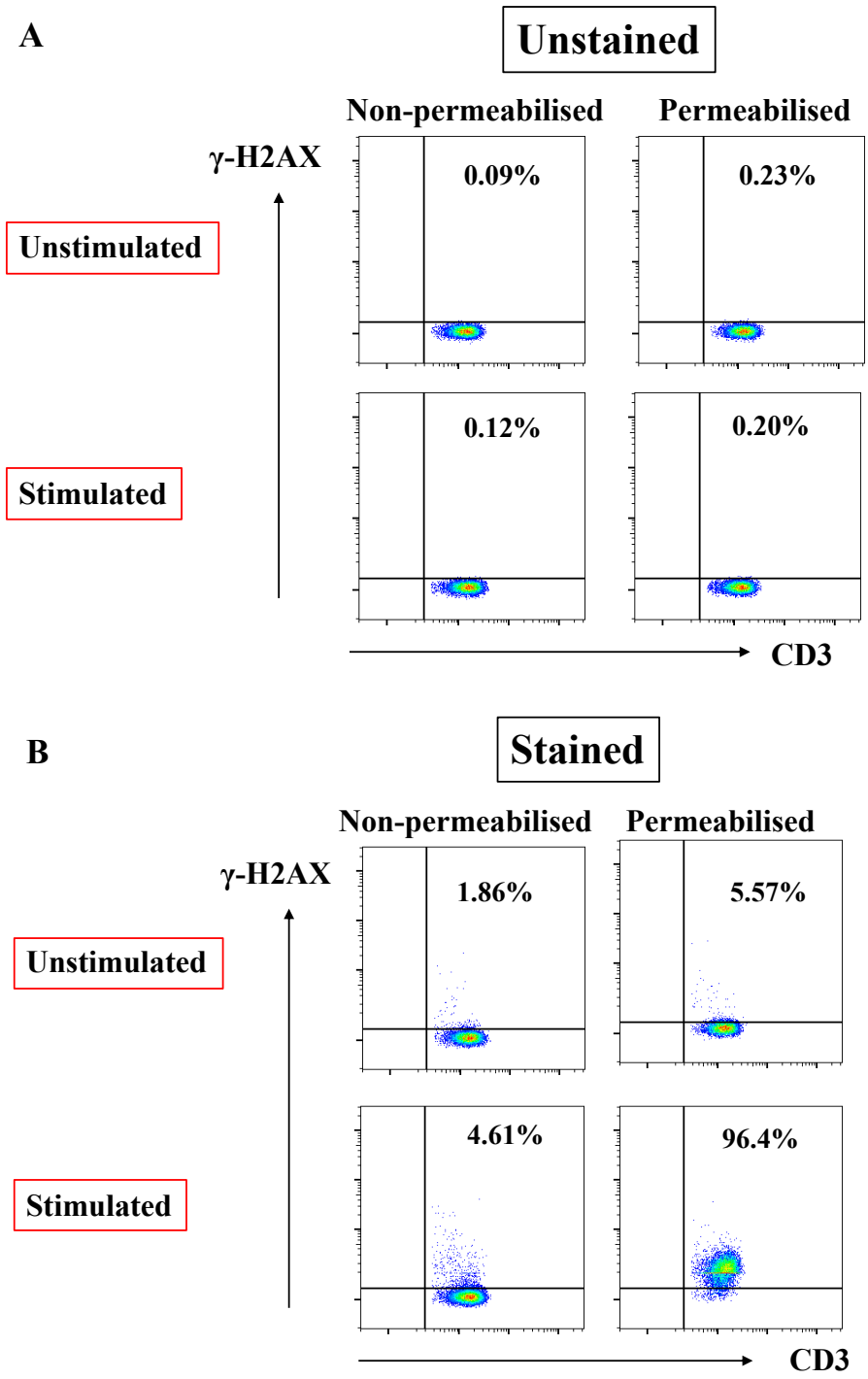

Figure 3.15 Etoposide induced γ-H2AX in CD3+ T lymphocytes using Cell Signaling Set A buffers

(A) Flow cytometric dot blots comparing Etoposide stimulation and cell permeabilisation in unstained γ-H2AX CD3+ T Lymphocytes, (B) Flow cytometric dot blots comparing Etoposide stimulation and cell permeabilisation in stained γ-H2AX CD3+ T lymphocytes. γ-H2AX stained and unstained CD3+ve T Lymphocytes when they were stimulated with Etoposide and permeabilised to identify suitable negative control. Both stimulated stained non-permeabilised and unstimulated stained permeabilised resemble good candidates for negative controls to stimulated permeabilised stained samples.

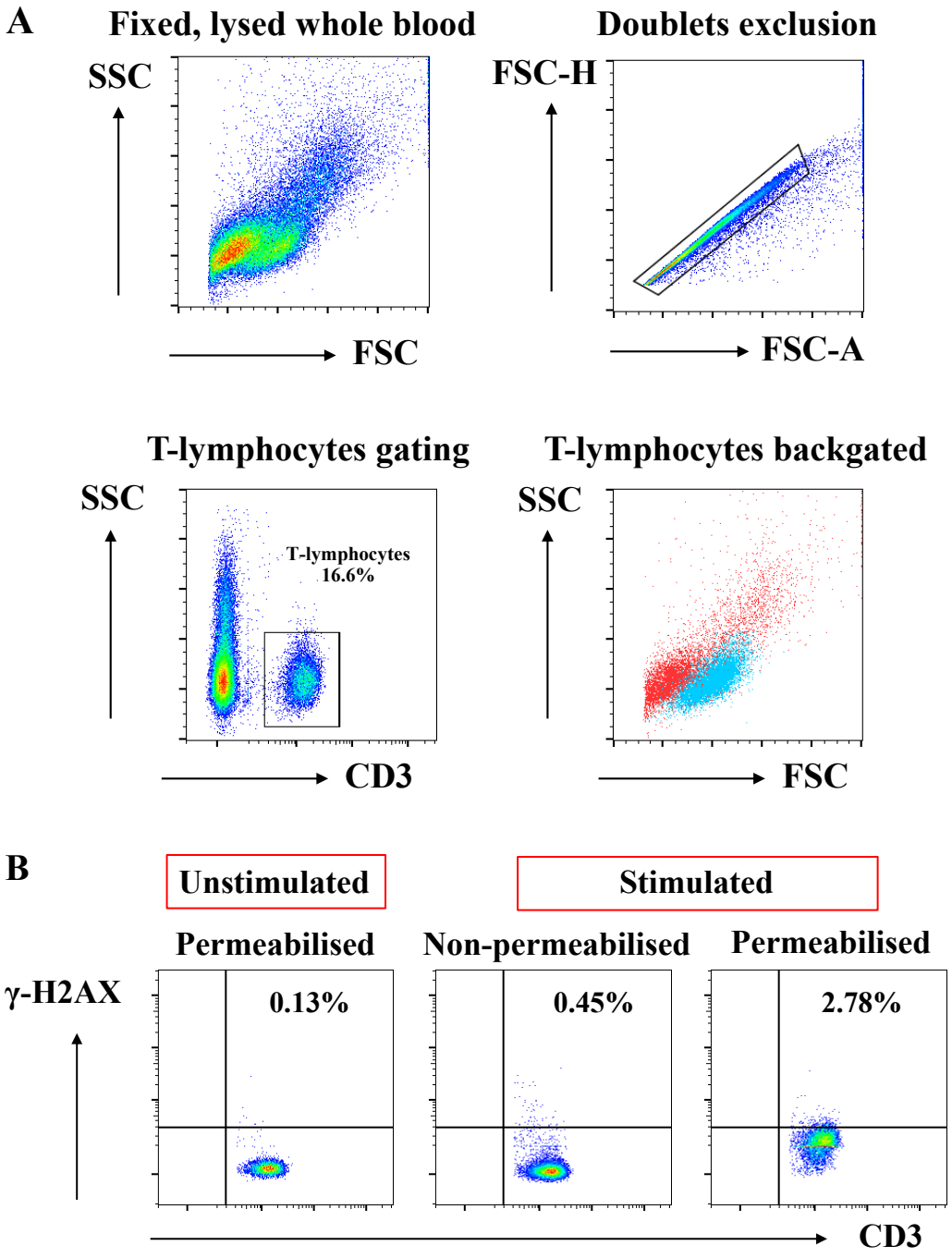

Figure 3.16 Gating strategy to detect Etoposide induced γ-H2AX in CD3+ T lymphocytes
(A) Flow cytometric dot blots showing gating strategy to identify CD3+ T lymphocytes from whole blood samples, (B) Flow cytometric dot blots showing Stimulated non-permeabilised samples could stand as more potential negative controls due to higher γ-H2AX levels in stimulated non-permeabilised compared to unstimulated permeabilised CD3+ T lymphocytes.

3.4.2 Radiation induced γ-H2AX

3.4.2.1 X-ray machine radiation induced γ-H2AX

When blood samples were exposed to radiation and chemical stimulants (Figure 3.17), there was a successful detection of both radiation and chemical induced γ-H2AX signalling in CD3+ T lymphocytes. Additionally, the FACS technique detected a gradual increase in γ-H2AX signalling in CD3+ T lymphocytes in association with the increase in radiation doses.

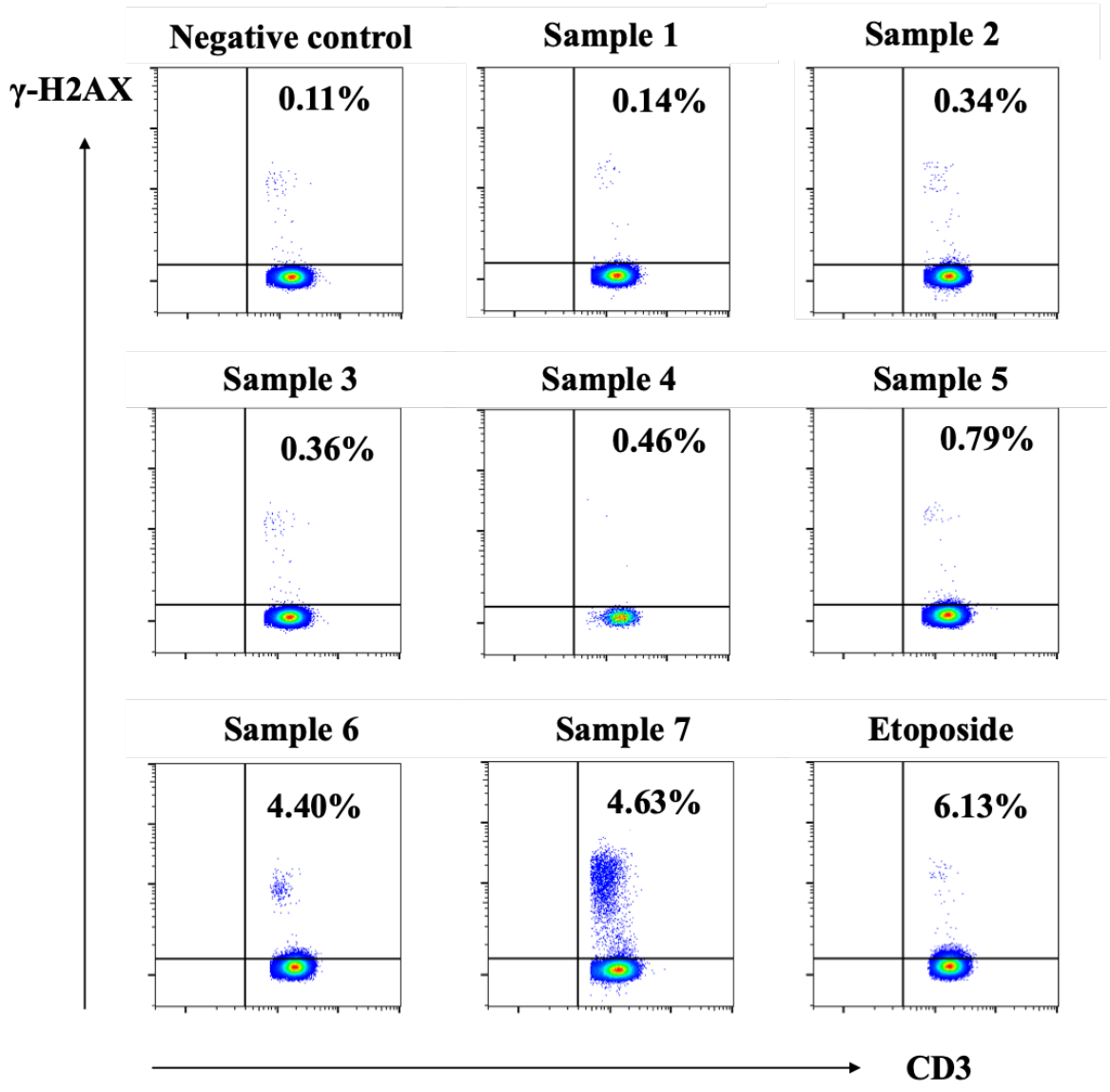

Figure 3.17 X-ray induced γ-H2AX in CD3+ T lymphocytes
Flow cytometric dot blot showing a gradual increase in radiation indued in CD3+ T lymphocytes percentage that are expressing γ-H2AX in association with the increase in radiation doses.

3.4.2.2 Micro-CT radiation induced γ-H2AX

Blood samples were collected and irradiated using Micro CT scanner and compared with chemically induced (Etoposide, positive control) samples. Radiation induced γ-H2AX was upregulated and successfully detected in CD3+ T lymphocytes as per Figure 3.18, however there was a difficulty in assessing radiation dose that was used to irradiate blood samples using micro-CT scanner.

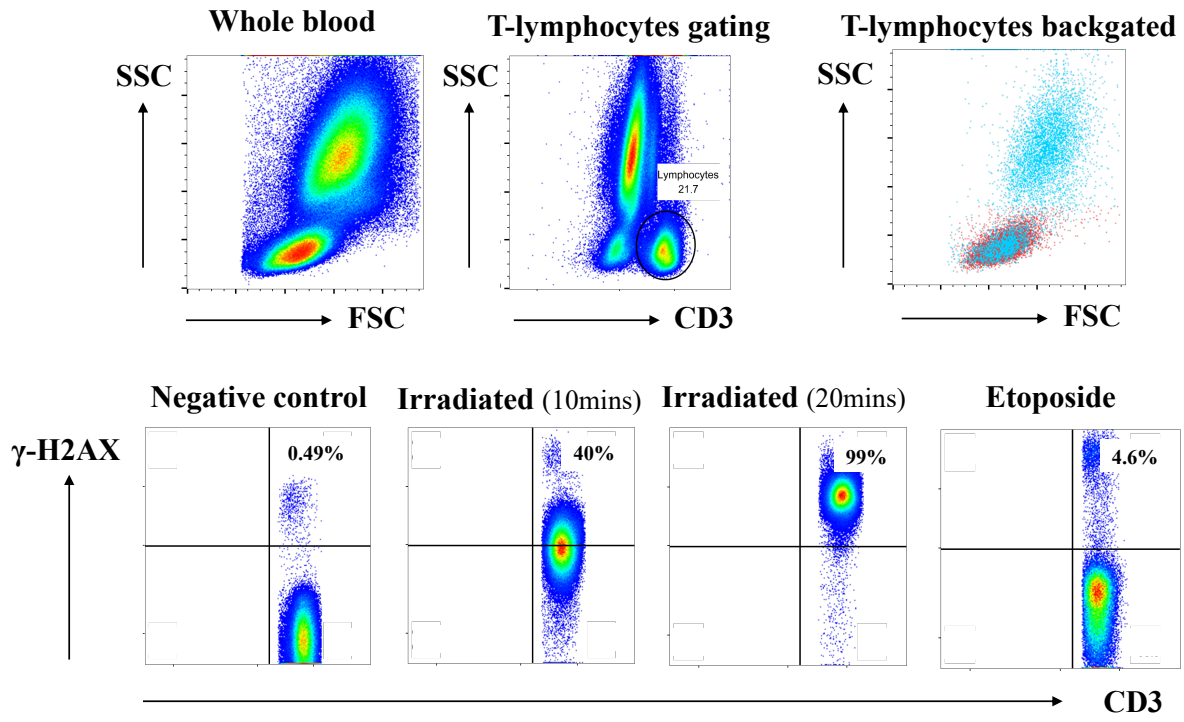

Figure 3.18 FACS analysis of CT radiation-induced γ-H2AX in T lymphocytes
Flow cytometric dot blots showing gating strategy on CD+3 T lymphocytes expression γ-H2AX from whole blood samples that were irradiated in-vitro by Micro CT scanner and compared to chemically (Etoposide) induced samples (Positive control). There was an increase in percentage of CD3+ T lymphocytes expressing γ-H2AX when irradiated for 10 and 20 minutes, however there was a difficulty in assessing radiation dose used to irradiate blood samples.

3.4.2.3 Radiotherapy machine radiation induced γ-H2AX

Using another source of irradiation, radiotherapy DARPAC 2000 machine was used to irradiate blood samples with known radiation doses in-vitro. γ-H2AX was upregulated associated with the gradual increase in radiation doses (Figure 3.19).

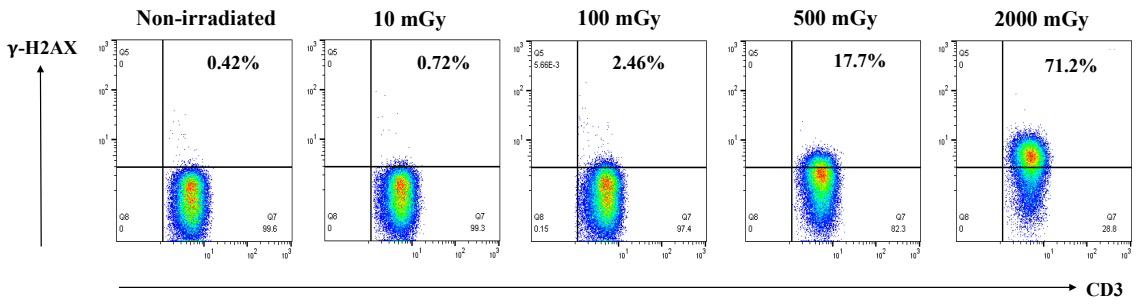

Figure 3.19 An example of radiation-induced γ-H2AX in T lymphocytes using radiotherapy machine

Flow cytometric dot blots radiation induced γ-H2AX upregulation increased in CD3+ T lymphocytes when exposed to gradually increasing radiation doses.

3.4.2.4 Reliability of radiation induced γ-H2AX measurement protocol

When our flow cytometric methodology reliability was tested using blood samples and exposed to a range of radiation doses (10mGy to 500mGy) at multiple occasions. There was a correlation between the percentage of γ-H2AX expression T lymphocytes and the radiation doses they are exposed to ($P<0.001$, $r^2=0.8$, by Spearman nonparametric correlation test, Figure 3.20). This strong correlation supported the flow cytometric technique reliability of measuring radiation induced γ-H2AX in CD3+ T lymphocytes.

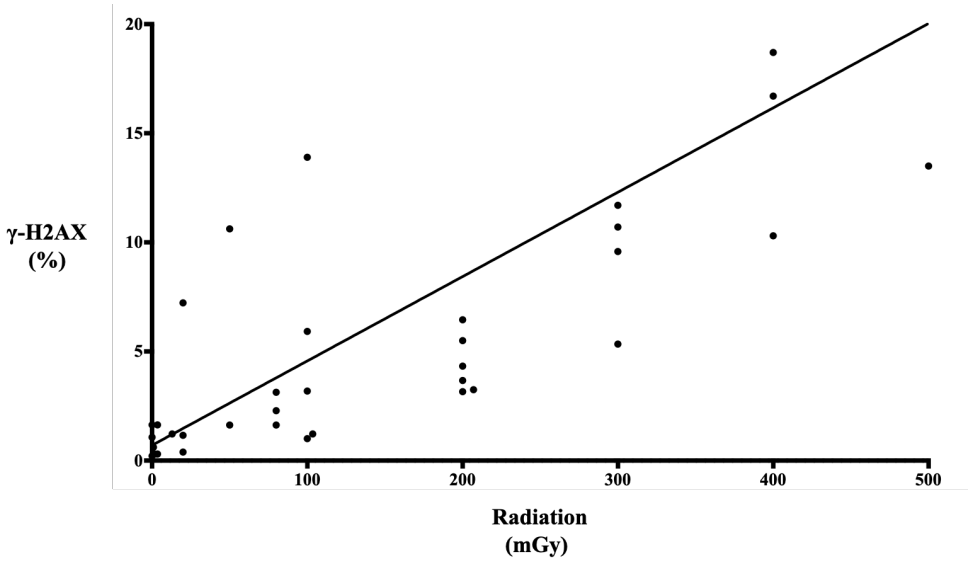

Figure 3.20 Correlation between γ-H2AX expression in CD3+ T lymphocytes and blood radiation dose

Levels of γ-H2AX in CD3+ T lymphocytes correlated with blood radiation doses using Darpac 2000 (Gulmay Medical) x-ray unit ($P<0.001$, $r^2=0.8$, by Spearman nonparametric correlation test).

3.4.3 Chemically induced pATM

3.4.3.1 Etoposide induced pATM in PBMCs using Cytofix/Cytoperm

When PBMCs were isolated from whole blood and stimulated with Etoposide, pATM upregulation was not detected in PBMCs. In addition, CD3 staining was also unsuccessful, therefore Lymphocytes were gated on using forward and side scatter. T lymphocytes were not detected using flow cytometric analysis with Cytofix/Cytoperm reagents (Figure 3.21).

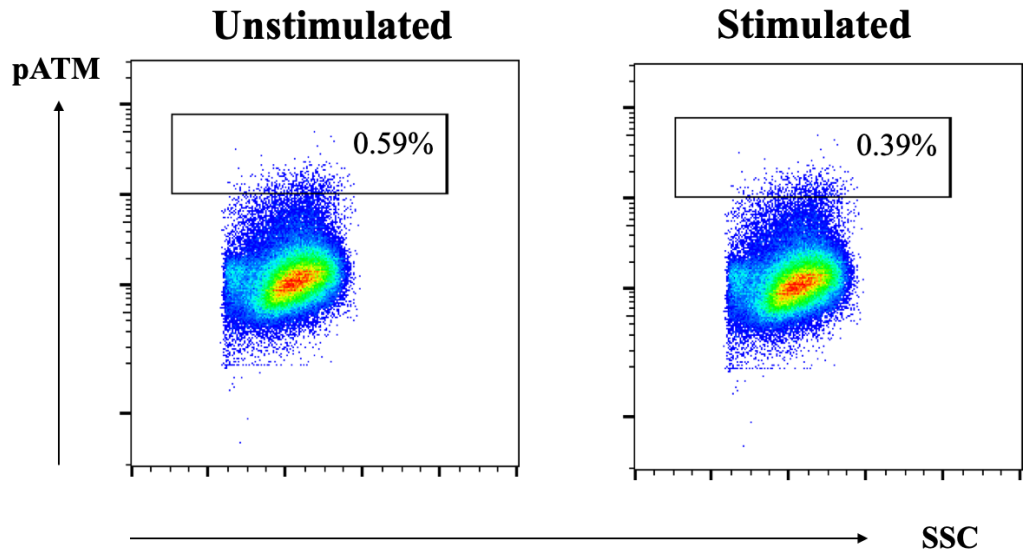

Figure 3.21 FACS analysis of Etoposide induced pATM in PBMCs using Cytofix/Cytoperm
Flow cytometric dot blots showing lymphocytes that were gated on from PBMCs using forward and side scatter. Neither Etoposide induced pATM upregulation nor CD3+ was T lymphocytes were detected using flow cytometric analysis with Cytofix/Cytoperm kit.

3.4.3.2 Etoposide induced pATM in PBMCs using Cell Signalling Buffer Set

When PBMCs were isolated from whole blood and stimulated with Etoposide, pATM upregulation was successfully detected in lymphocytes (gated on using forward and side scatter) (Figure 3.22). This showed a promising result in using Cell Signalling Buffer Set for further optimisation to detect pATM expressing lymphocytes.

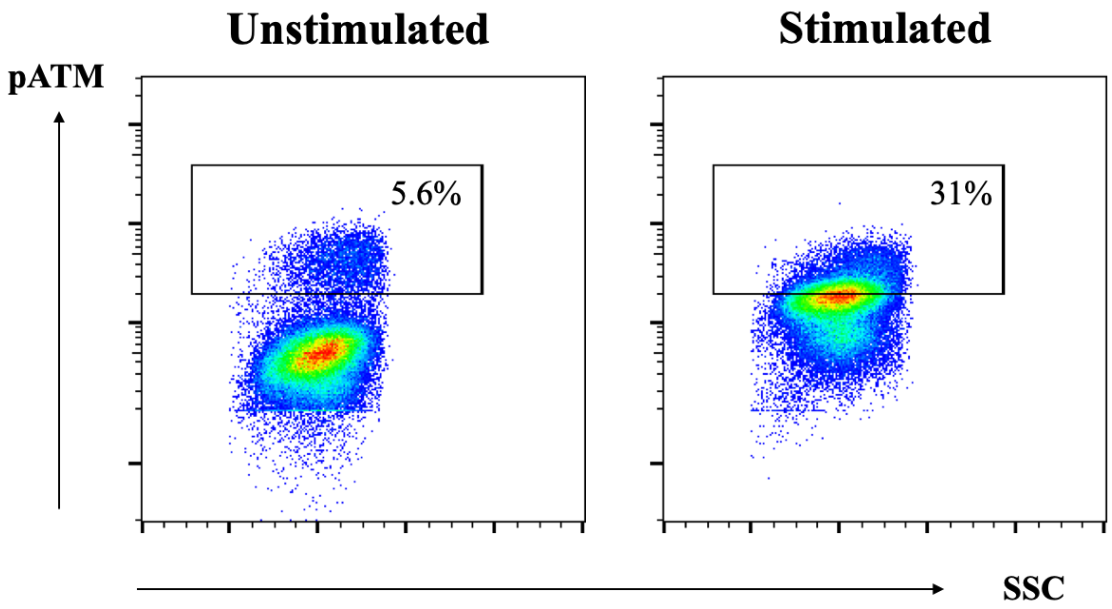

Figure 3.22 FACS analysis of Etoposide induced pATM in PBMCs using Cell Signaling Buffer

Flow cytometric dot blots showing an increase in the percentage of lymphocytes that are expressing Etoposide induced pATM using Cell Signaling Buffer Set A compared to the unstimulated cells.

3.4.3.3 Etoposide induced pATM in whole blood using Cell Signalling Buffer Set

T lymphocytes were successfully identified using CD3+ antibodies, and when stimulated with Etoposide, pATM was upregulated and detected using Cell Signalling Buffer Set A. Low volume pATM conjugated antibodies provided a satisfactory result and preferred over larger volume to avoid any false positive results from overstaining (Figure 3.23).

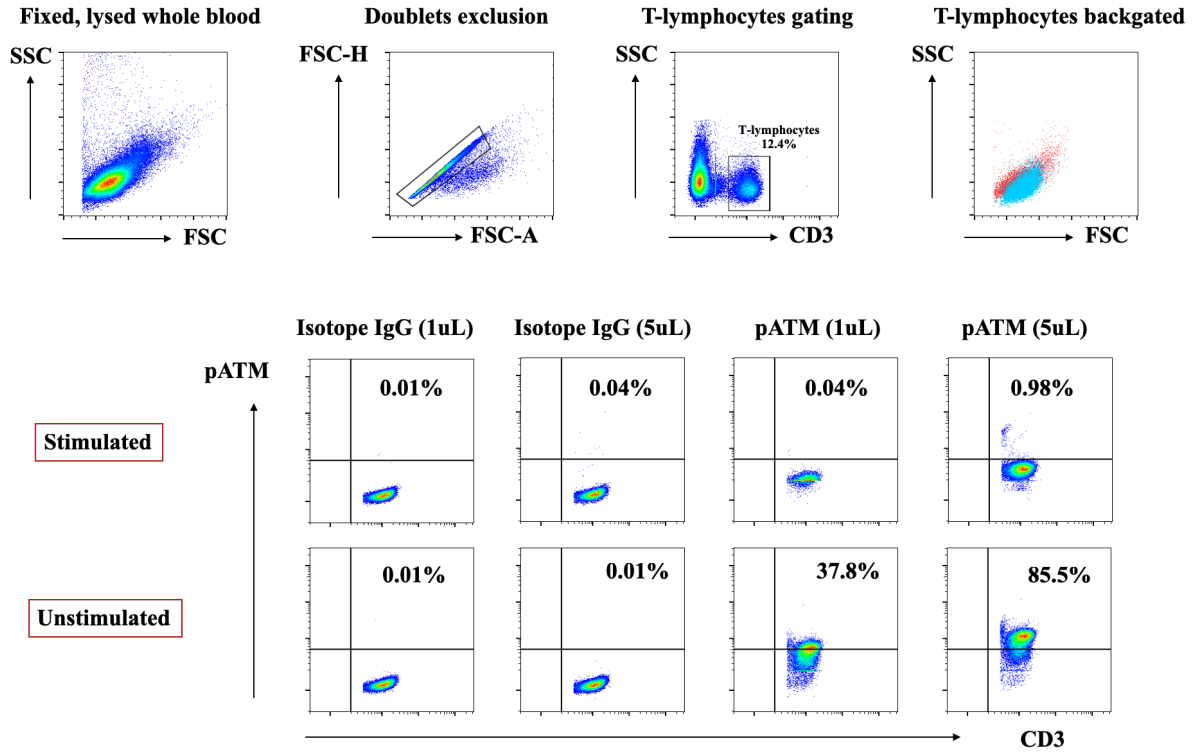

Figure 3.23 FACS analysis of Etoposide induced pATM in T lymphocytes using Cell Signaling Buffer

Flow cytometric dot blots showing antibody titration was carried out to optimise detection of Etoposide induced pATM expressing CD3+ T lymphocytes using Cell Signalling Buffer Set A.

3.4.3.4 Etoposide induced pATM in T lymphocytes

When whole bloods samples were chemically stimulated by different concentrations of Etoposide, using our flow cytometric methodology, CD3+ lymphocytes were successfully identified and pATM upregulation was associated with the increase in Etoposide doses (Figure 3.24).

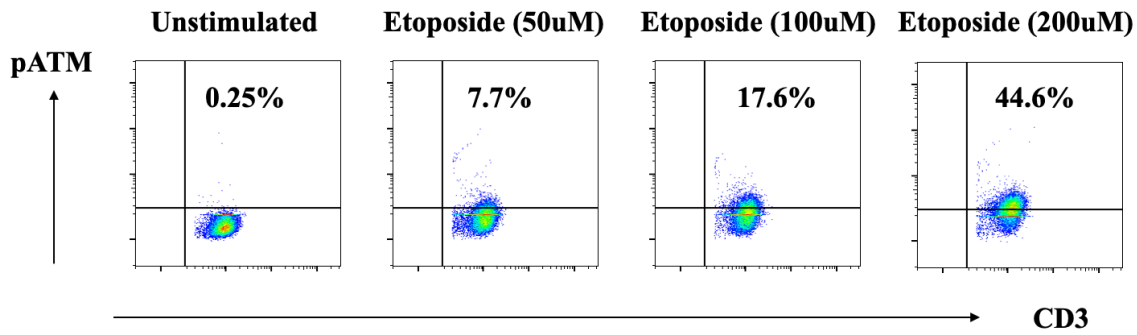

Figure 3.24 FACS analysis of Etoposide induced pATM in T lymphocytes
Flow cytometric dot blots showing an increase in CD3+lympchoytes expressing pATM in association with the increase in Etoposide doses.

3.4.4 Peri-operative changes of DNA damage/repair biomarkers

An example of measuring changes in levels of DNA damage biomarkers γ-H2AX & pATM in patients' CD3+ T lymphocytes during the perioperative period of EVAR. DNA damage. γ-H2AX & pATM were upregulated immediately after radiation exposure and recovered after 24 hrs (Figure 3.25).

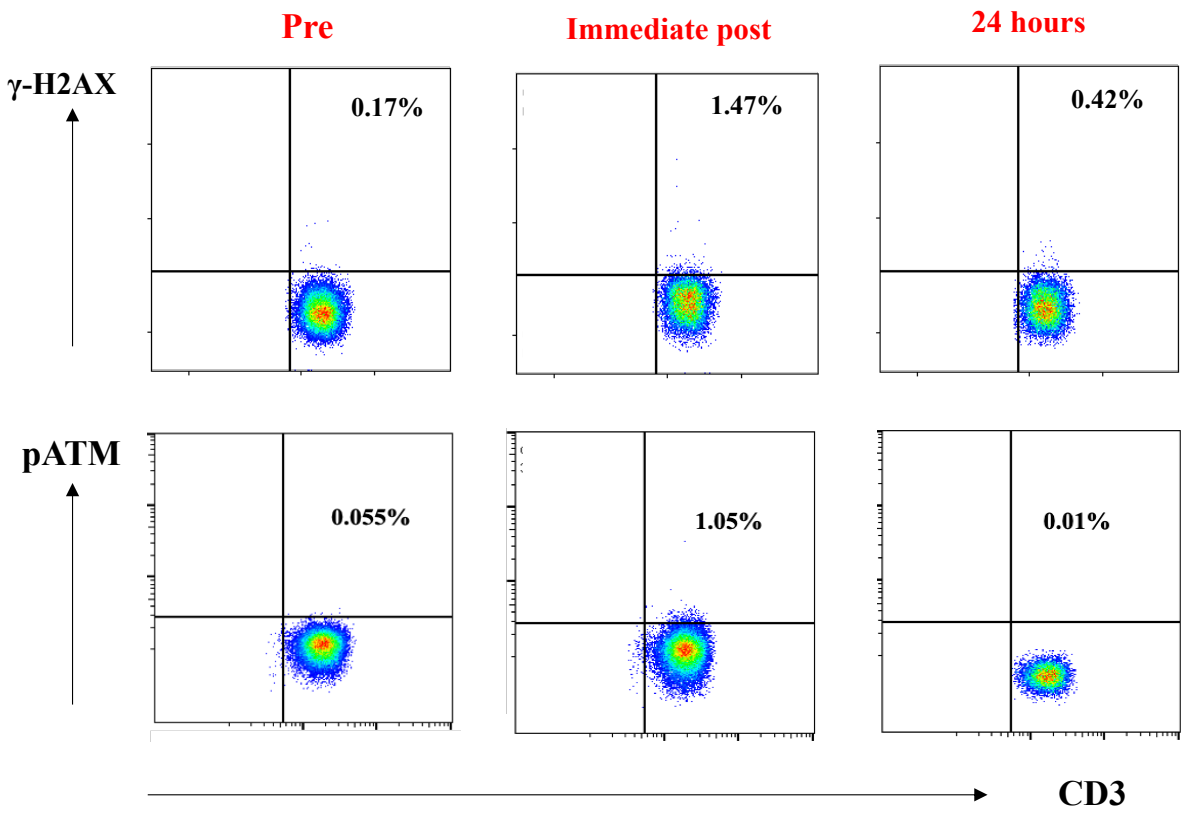

Figure 3.25 FACS analysis of peri-operative γ-H2AX & pATM in patient's T lymphocytes
Flow cytometric dot blots showing radiation induced γ-H2AX & pATM levels in CD3+ T lymphocytes increased immediately after radiation exposure and normalised in 24 hrs.

3.4.5 γ-H2AX and pATM expression in T lymphocyte subsets

3.4.5.1 Flow cytometric analysis of T lymphocytes subpopulations

On further assessment of γ-H2AX and pATM expression in CD3+ T lymphocyte subsets, there was a successful detection of surface markers CD3, CD4, CD8, CCR7 (CD197), CD45RO when cells stained with them separately. Cell fixation and permeabilisation did not compromise flow cytometric detection of individual cell markers (Figure 3.26).

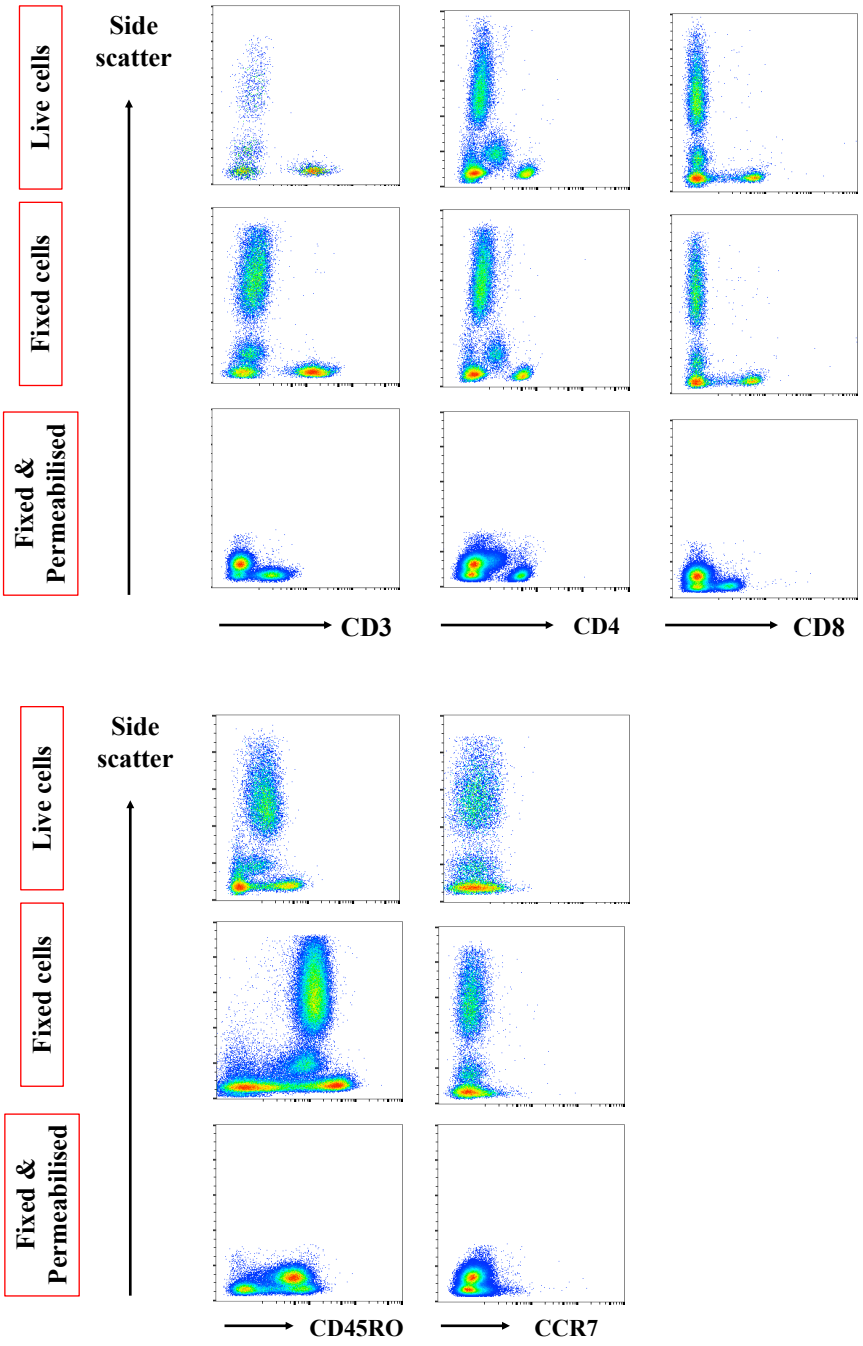

Figure 3.26 FACS dot blots of T lymphocytes surface markers
Flow cytometric dot blots showing successful detection of all surface markers CD3, CD4, CD8, CD45RO and CCR7 on live, fixed, and fixed and then permeabilised cells.

3.4.5.2 Flow cytometric analysis of T lymphocytes subpopulations in fixed cells

There was a successful detection of all surface markers CD3, CD4, CD8, CCR7 (CD197), CD45RO when cells stained with them separately. Cell fixation before staining for these surface markers followed by cell membrane permeabilisation did not compromise flow cytometric detection of individual cell markers (Figure 3.27). This encouraged us to proceed with further optimisation steps of carrying out multiple staining of all these surface markers on the same sample in order to identify targeted T lymphocytes subtypes.

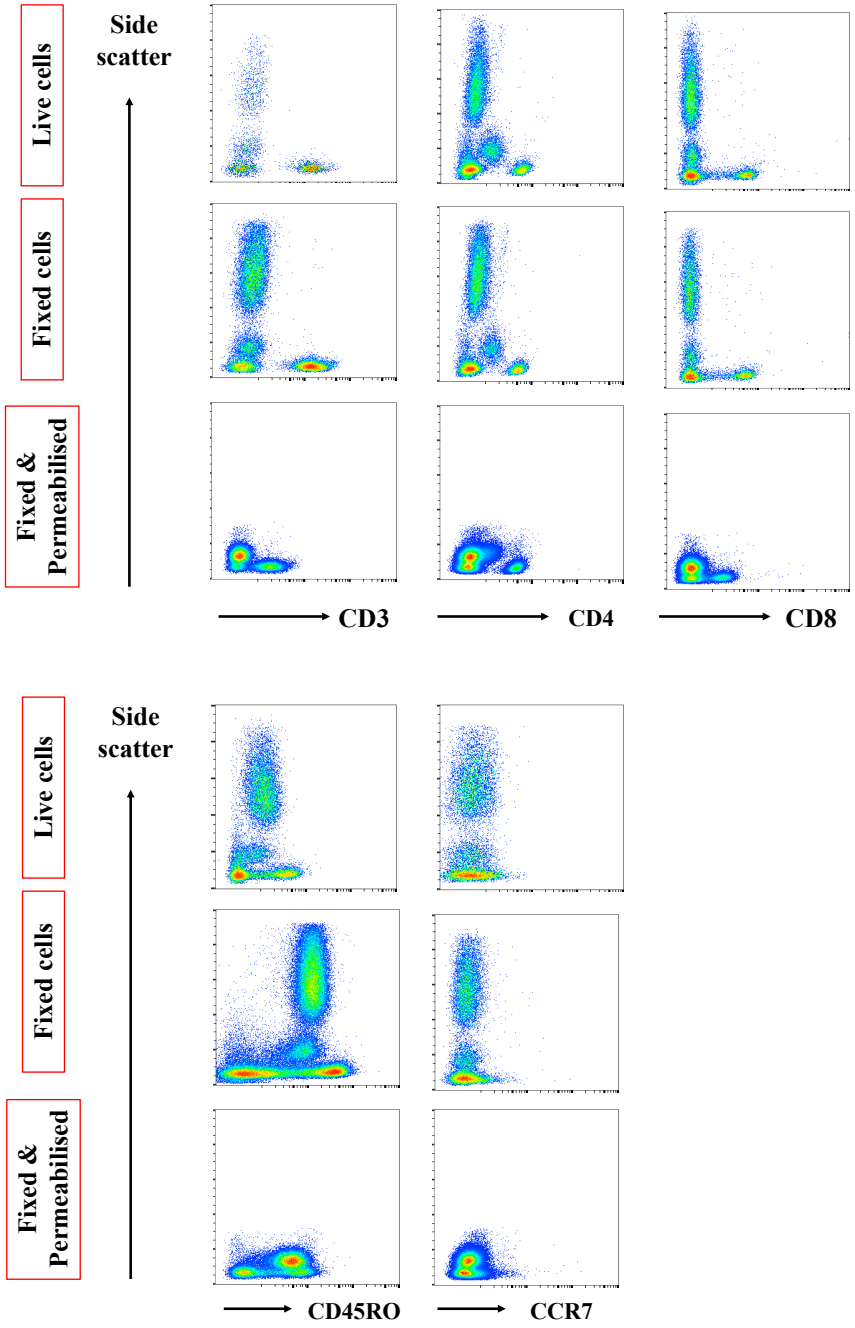

Figure 3.27 FACS analysis of T lymphocytes subpopulations on fixed cells
Flow cytometric dot blots showing successful detection of CD3, CD4, CD8, CCR7 (CD197), CD45RO on fixed and permeabilised cells.

3.3.5.3 γ-H2AX & pATM changes in T lymphocytes subpopulations

γ-H2AX & pATM levels were identified in CD4+ T Helper and CD8+ Cytotoxic T cells, and their subsets naïve (CD45RO-/CCR7+, $T_{(N)}$), central memory (CD45RO+/CCR7+, $T_{(CM)}$) and effector memory (CD45RO+/CCR7-, $T_{(EM)}$) (Figure 3.28, 29, 30).

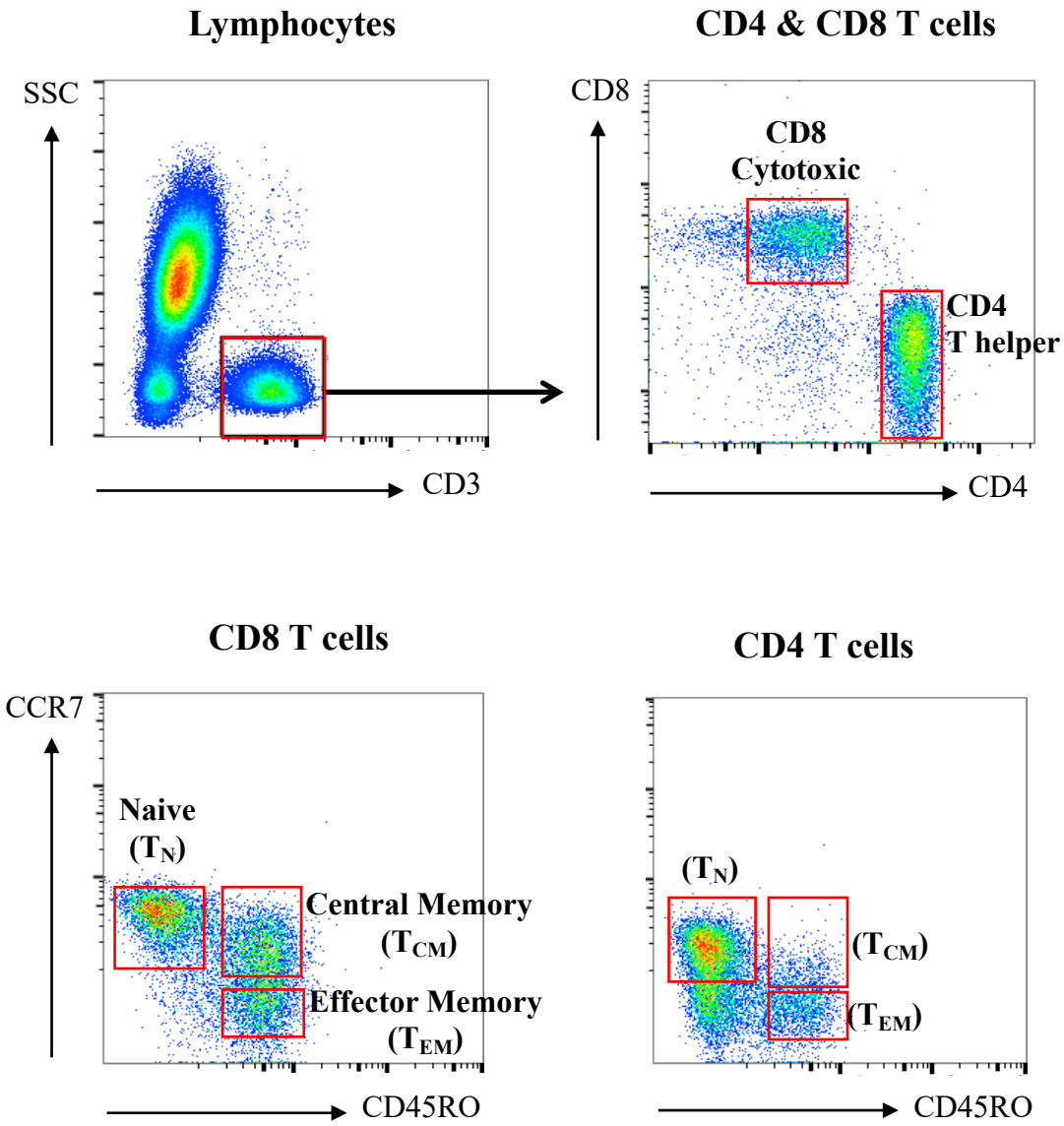

Figure 3.28 Gating strategy to identify T lymphocytes subpopulations
An example of flow cytometric dot blots showing gating strategy to identify CD4+ T Helper and CD8+ Cytotoxic T cells, and their subsets naïve (CD45RO-/CCR7+, $T_{(N)}$), central memory (CD45RO+/CCR7+, $T_{(CM)}$) and effector memory (CD45RO+/CCR7-, $T_{(EM)}$) from a blood sample.

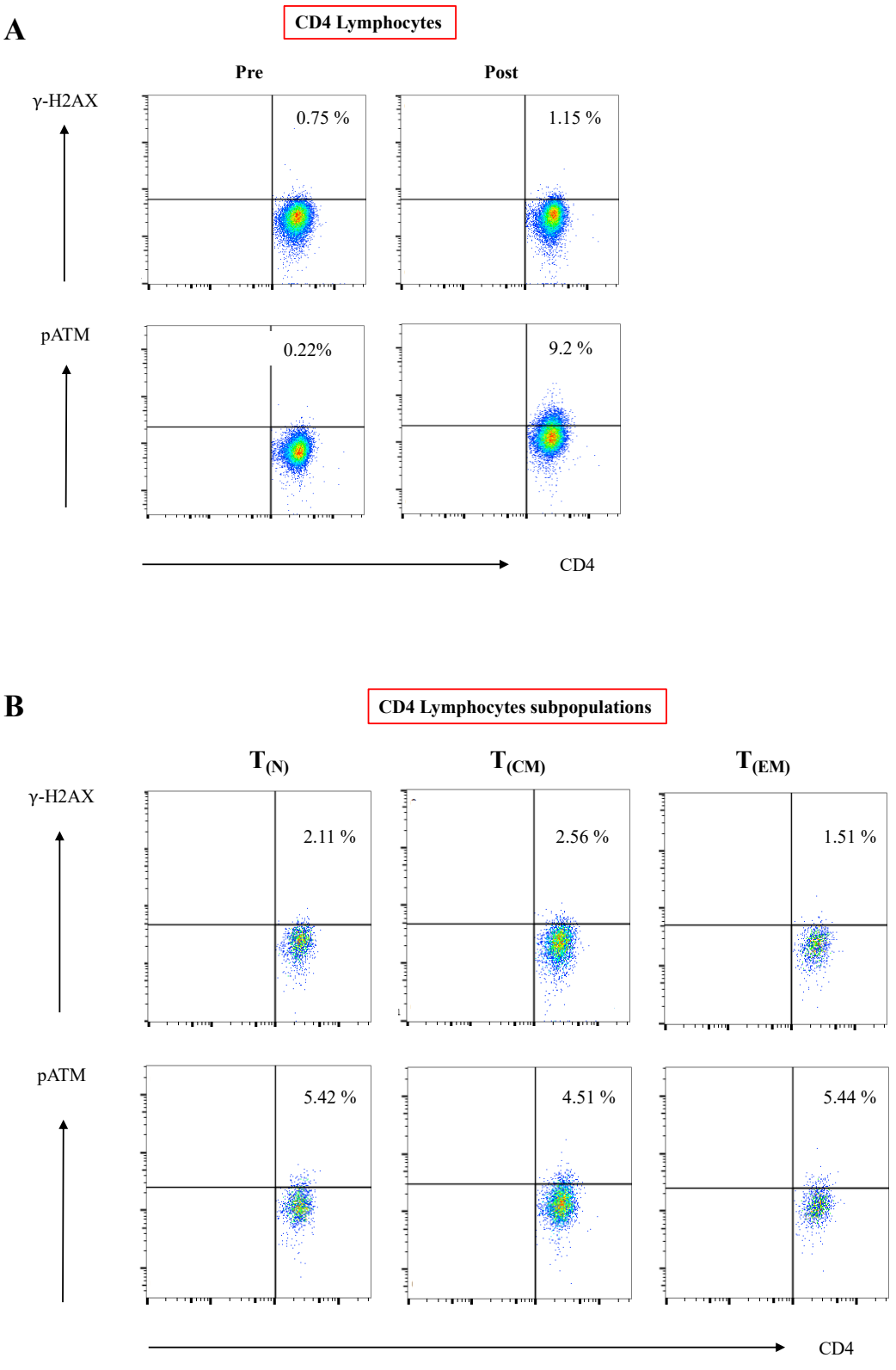

Figure 3.29 γ-H2AX and pATM expression in CD4+ T lymphocytes after EVAR
(A) Flow cytometric dot blots showing radiation induced γ-H2AX & pATM levels that were identified in CD4+ T Helper in an operator before and after exposure to radiation during EVAR, (B) Flow cytometric dot blots showing post-operative γ-H2AX & pATM levels that were identified in CD4+ T Helper subsets naïve (CD45RO-/CCR7+, $T_{(N)}$), central memory (CD45RO+/CCR7+, $T_{(CM)}$) and effector memory (CD45RO+/CCR7-, $T_{(EM)}$).

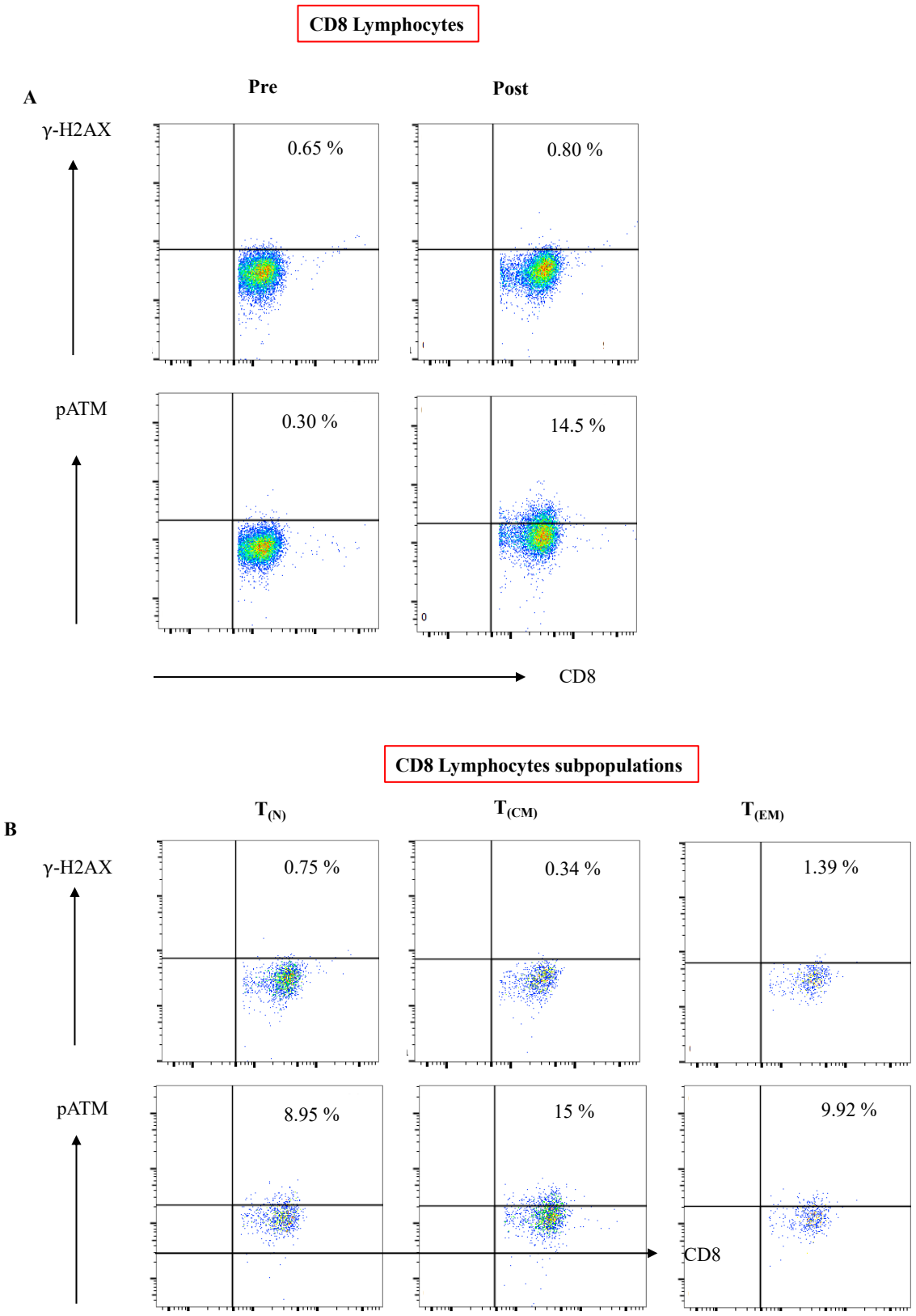

Figure 3.30 γ-H2AX and pATM expression in CD8+ T lymphocytes after EVAR.
(A) Flow cytometric dot blots showing radiation induced γ-H2AX & pATM levels that were identified in CD8+ Cytotoxic T cells *in an operator before and after exposure to radiation during EVAR, (B) Flow cytometric dot blots showing post-operative γ-H2AX & pATM levels that were identified in* CD8+ Cytotoxic T subsets naïve (CD45RO-/CCR7+, $T_{(N)}$), central memory (CD45RO+/CCR7+, $T_{(CM)}$) and effector memory (CD45RO+/CCR7-, $T_{(EM)}$).

3.4.6 γ-H2AX and pATM expression in haematopoietic stem/progenitor cells

As a first step on studying the effect of radiation on DNA damage/repair biomarkers γ-H2AX & pATM in haematopoietic stem/progenitor cells, cell surface markers CD38, CD90, CD14/56 and CD45 were successfully detected as illustrated in Figure 3.31. Although, CD34 was not detected using this technique, and therefore another method of staining fixed cells rather than live cells was used as detailed below.

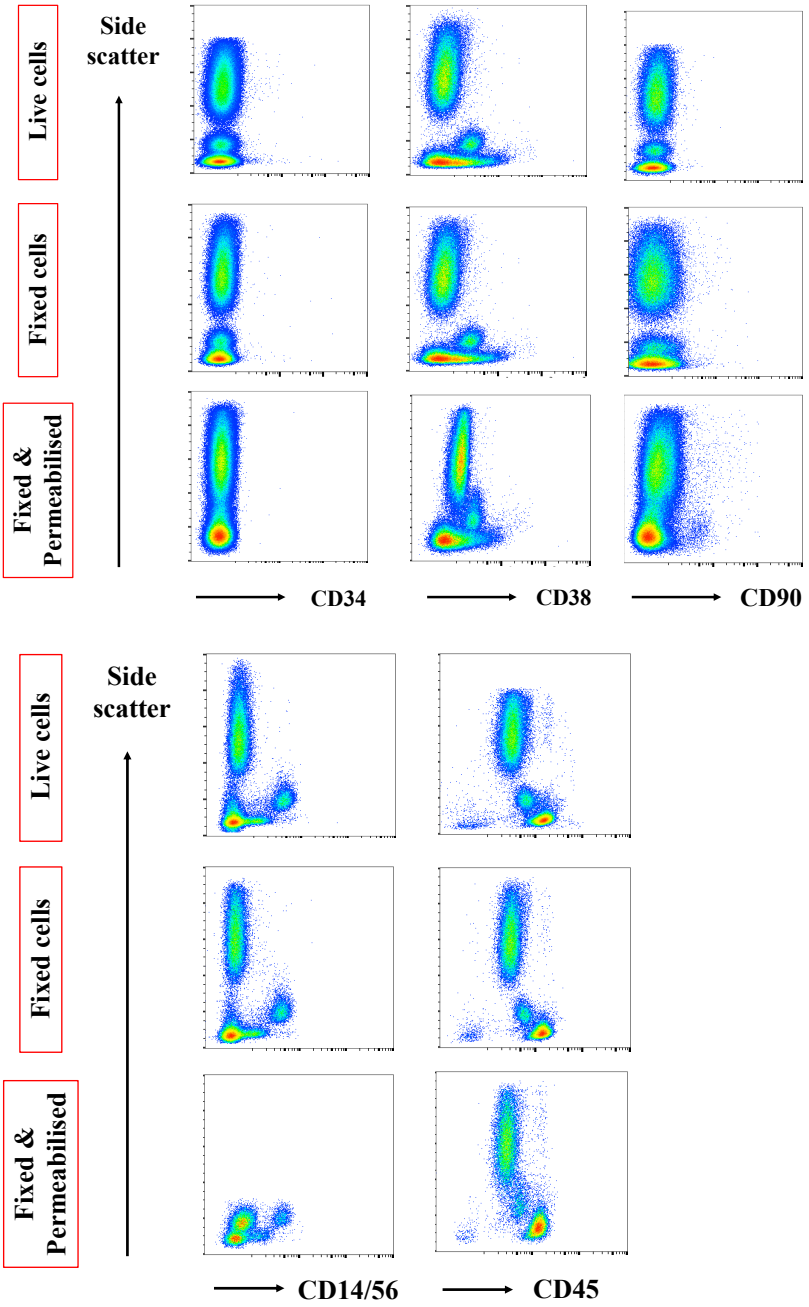

Figure 3.31 FACS analysis of HSCs/HSCPs
Flow cytometric dot blots showing that CD38, CD90, CD14/56 and CD45 were successfully detected but not CD34 in live, fixed, fixed and permeabilised cells.

3.4.6.2 Analysis of haematopoietic stem/progenitor cells in fixed cells

There was a successful detection of surface markers CD38, CD14/56, and CD45 when cells stained with them separately. Although, CD34 and CD90 were not clearly detected using this protocol (Figure 3.32). Therefore, another technique was adopted using Ficoll cell separation protocol.

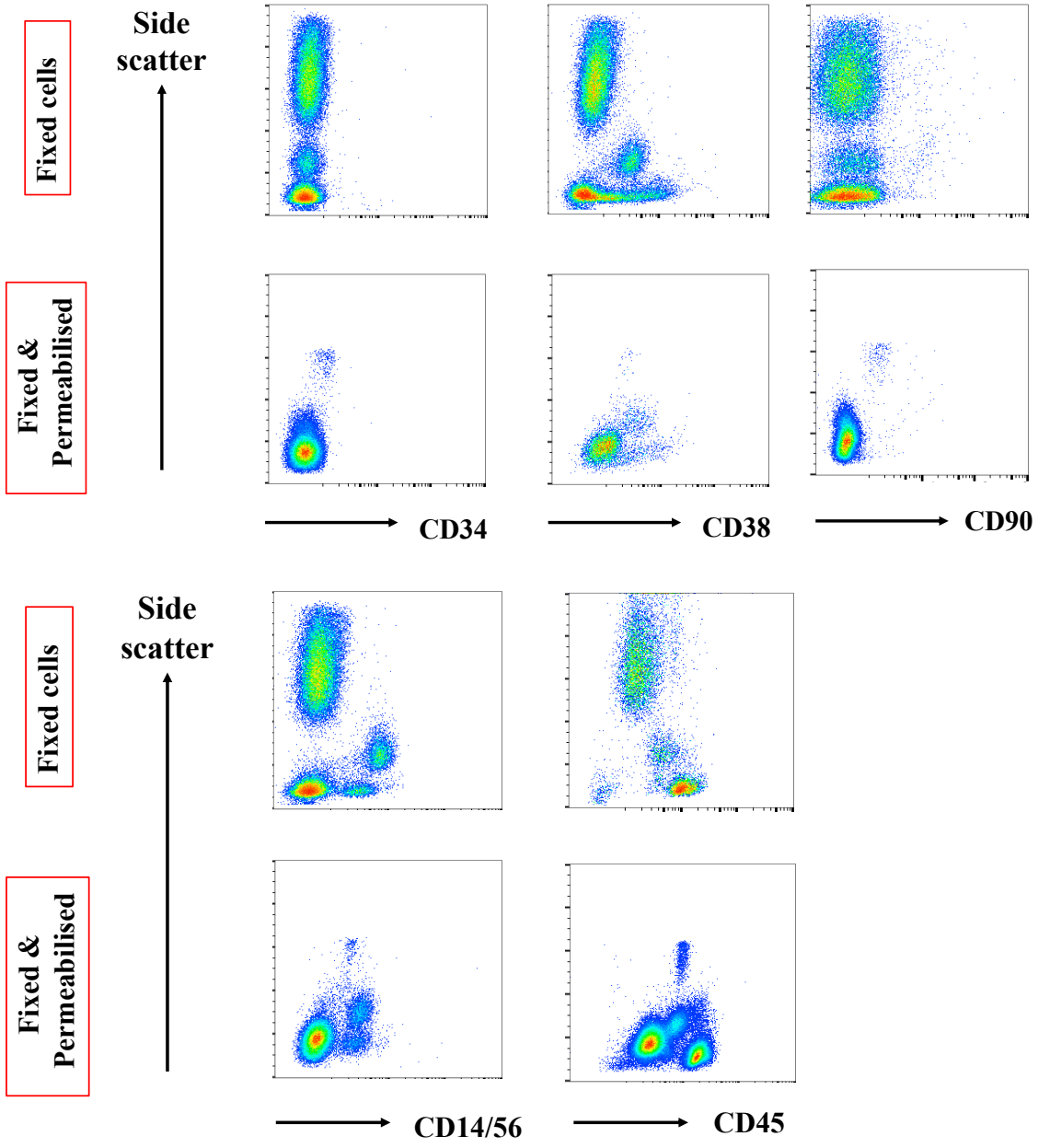

Figure 3.32 FACS analysis of fixed HSCs/HSCPs
Flow cytometric dot blots showing that CD38, CD14/56, and CD45 were detected when cells stained with them separately but not CD34 and CD90 in fixed and fixed and permeabilised cells.

3.4.6.3 Analysis to identify haematopoietic stem/progenitor cells from PBMCs

To identify haematopoietic stem/progenitor cells from PBMCs, cell surface markers CD38, CD90, and CD45 were successfully detected in live, fixed only and fixed and permeabilises cells, as illustrated in Figure 3.33. Although, CD34 signals were detected in stained live cells, signals were reduced in fixed cells, and was further reduced in fixed and permeabilised cells. This could be challenging in measuring levels of γ-H2AX and pATM in fixed and permeabilised haematopoietic stem/progenitor cells.

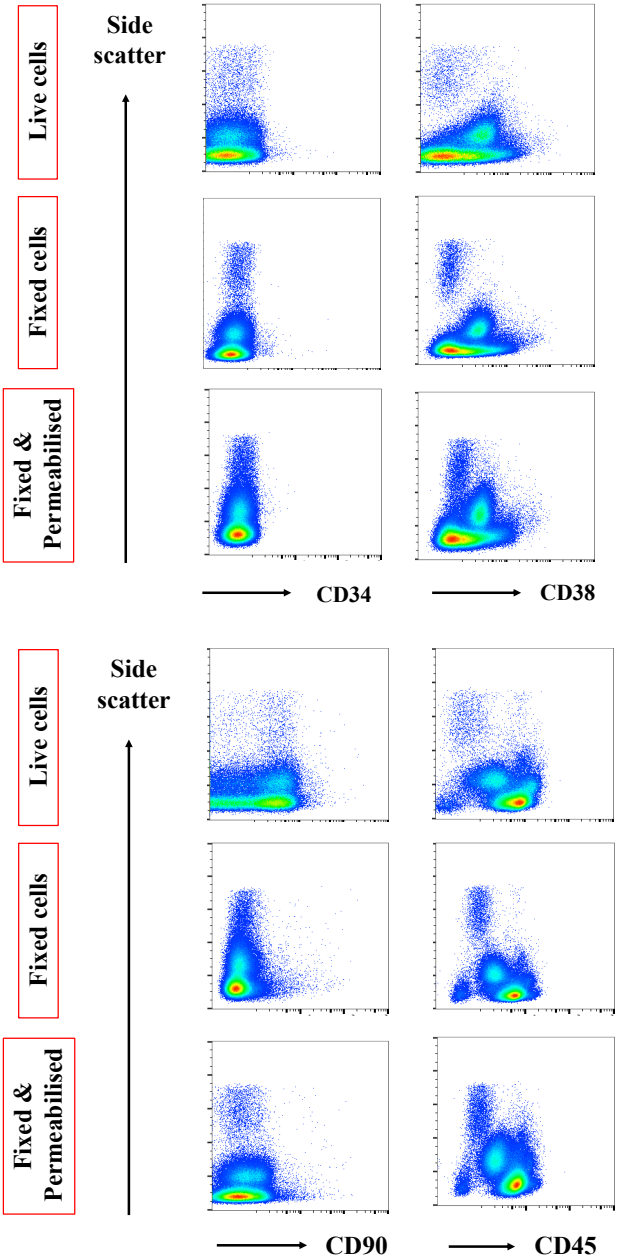

Figure 3.33 FACS analysis of HSCs/HSCPs isolated from PBMCs
Flow cytometric dot blots showing that CD38, CD90, and CD45 were successfully detected in live, fixed only and fixed and permeabilises PBMCs. CD34 signals were detected in stained live cells only.

3.4.6.4 γ-H2AX & pATM changes in haematopoietic stem/progenitor cells

When we studied γ-H2AX and pATM in haematopoietic stem/progenitor cells, we found a small number of HSCs or HSPCs were detected. This made it very challenging to identify any significant changes in γ-H2AX and pATM (Figure 3.34, 35 & 36).

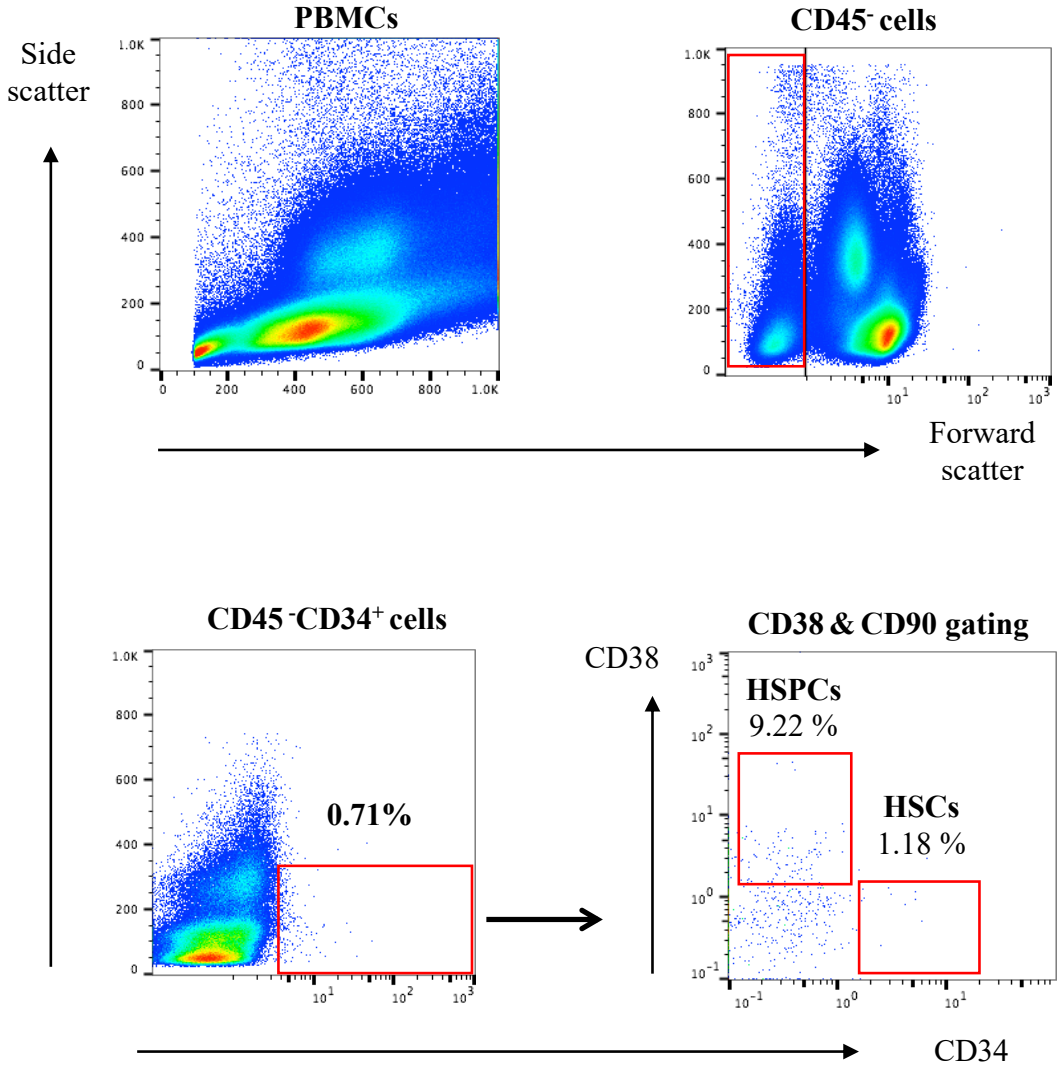

Figure 3.34 FACS gating strategy to identify HSCs/HSCPs isolated from PBMCs
Flow cytometric dot blots showing a gating strategy to detect HSCs/HSPs, however a small number of HSCs or HSPCs were detected from 100ml blood sample.

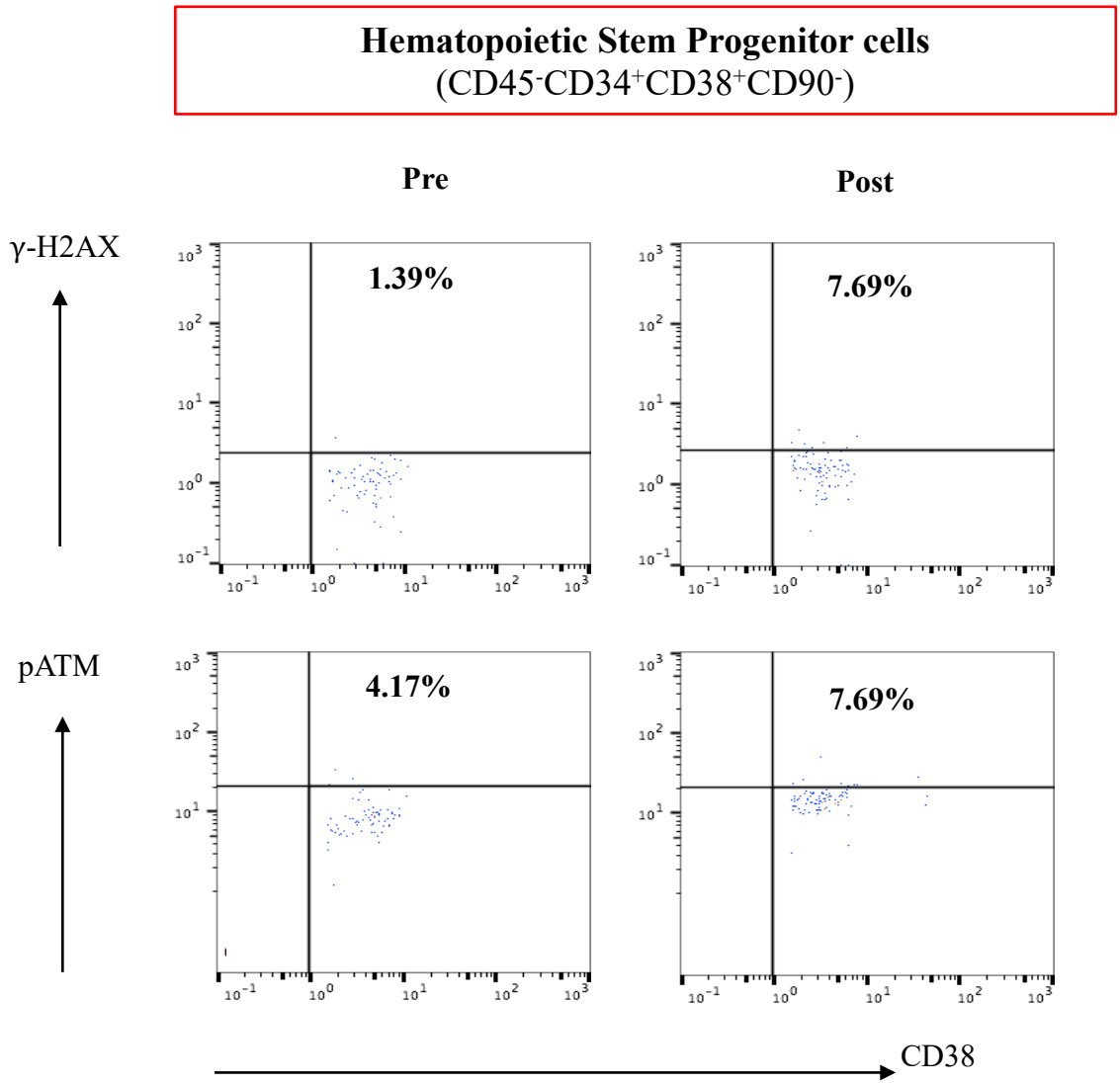

Figure 3.35 FACS analysis of γ-H2AX and pATM expression in HSPCs after EVAR
Flow cytometric dot blots showing γ-H2AX and pATM upregulation in HSPCs, however due to small number of HSPCs, γ-H2AX and pATM upregulation detection was difficult to assess.

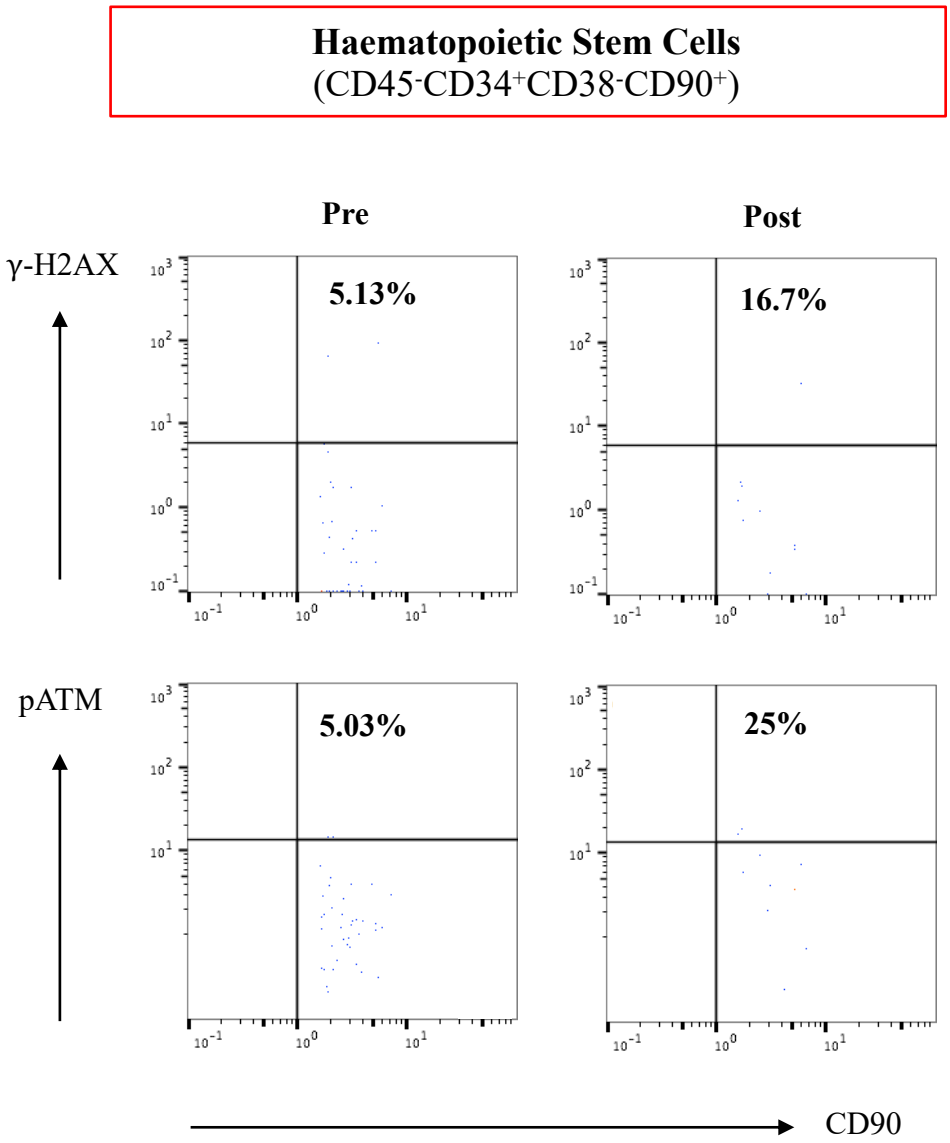

Figure 3.36 FACS analysis of γ-H2AX and pATM expression in HSCs after
Flow cytometric dot blots showing γ-H2AX and pATM upregulation in HSCs, however due to small number of HSCs, γ-H2AX and pATM upregulation detection was difficult to assess.

3.4.7 Radiation induced DNA base damage

3.4.7.1 Reactive oxygen species measurement in lymphocytes

Blood stimulated with H_2O_2 at two different time points, and ROS levels are detected using flow cytometric analysis of highly fluorescent ROS dye (CM-H2DCFDA). This demonstrates a successful stimulation of oxidative stress and optimised methodology to detect this oxidative stress (Figure 3.37).

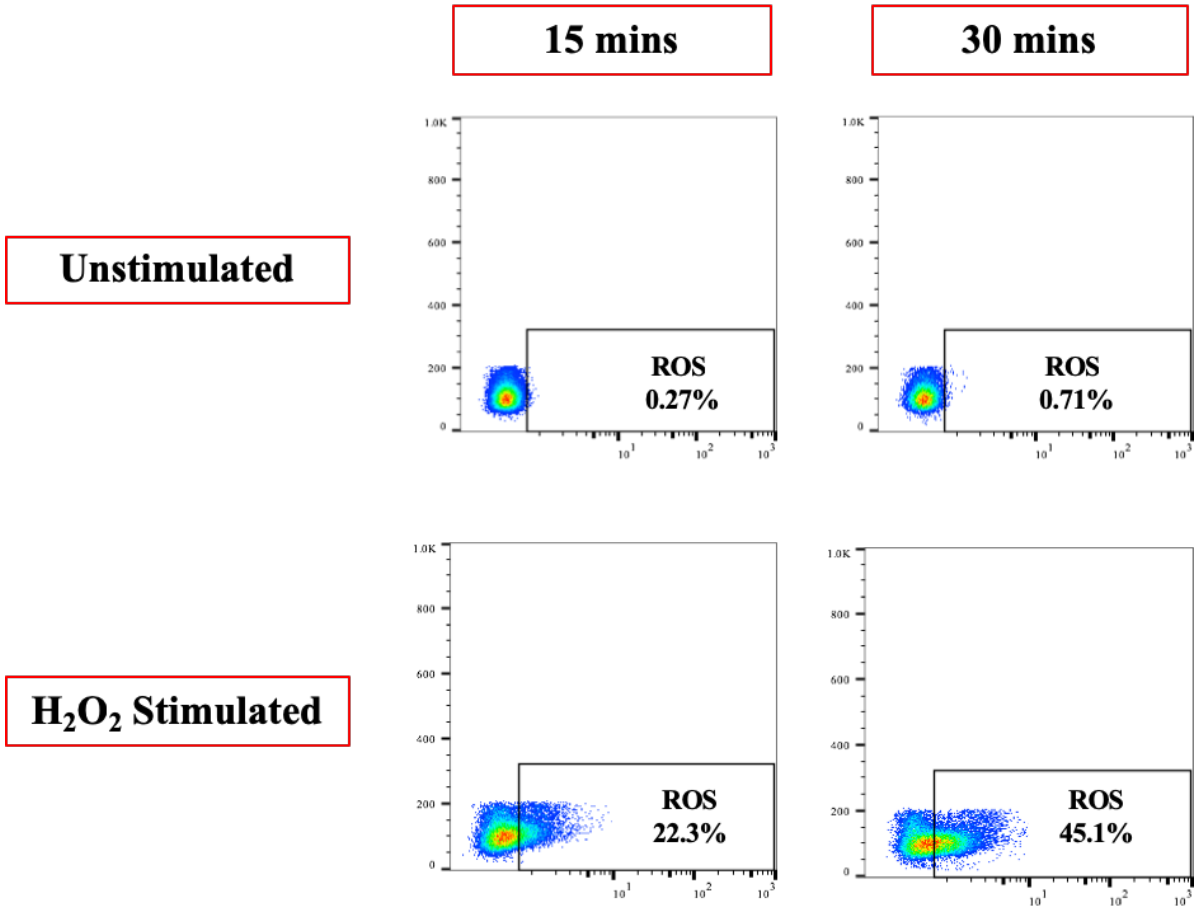

Figure 3.37 FACS analysis of H_2O_2 induced oxidative stress in lymphocytes
Flow cytometric dot blots showing ROS levels are detected using flow cytometric analysis of highly fluorescent ROS dye (CM-H2DCFDA) after 15 and 30 mins.

3.4.7.2 Hydrogen peroxide induced OGG1 in CD3+ T lymphocytes

Blood stimulated with H_2O_2 at two different concentrations. DNA base oxidation was measured using OGG1, and γ-H2AX and pATM were measured to identify DNA DSBs through flow cytometric analysis. High doses of H_2O_2 induced both base oxidation and double stranded breaks which was reflected in the upregulation of OGG1, γ-H2AX and pATM biomarkers. This also demonstrates the high sensitivity of the methodology of measuring base (Figure 3.38).

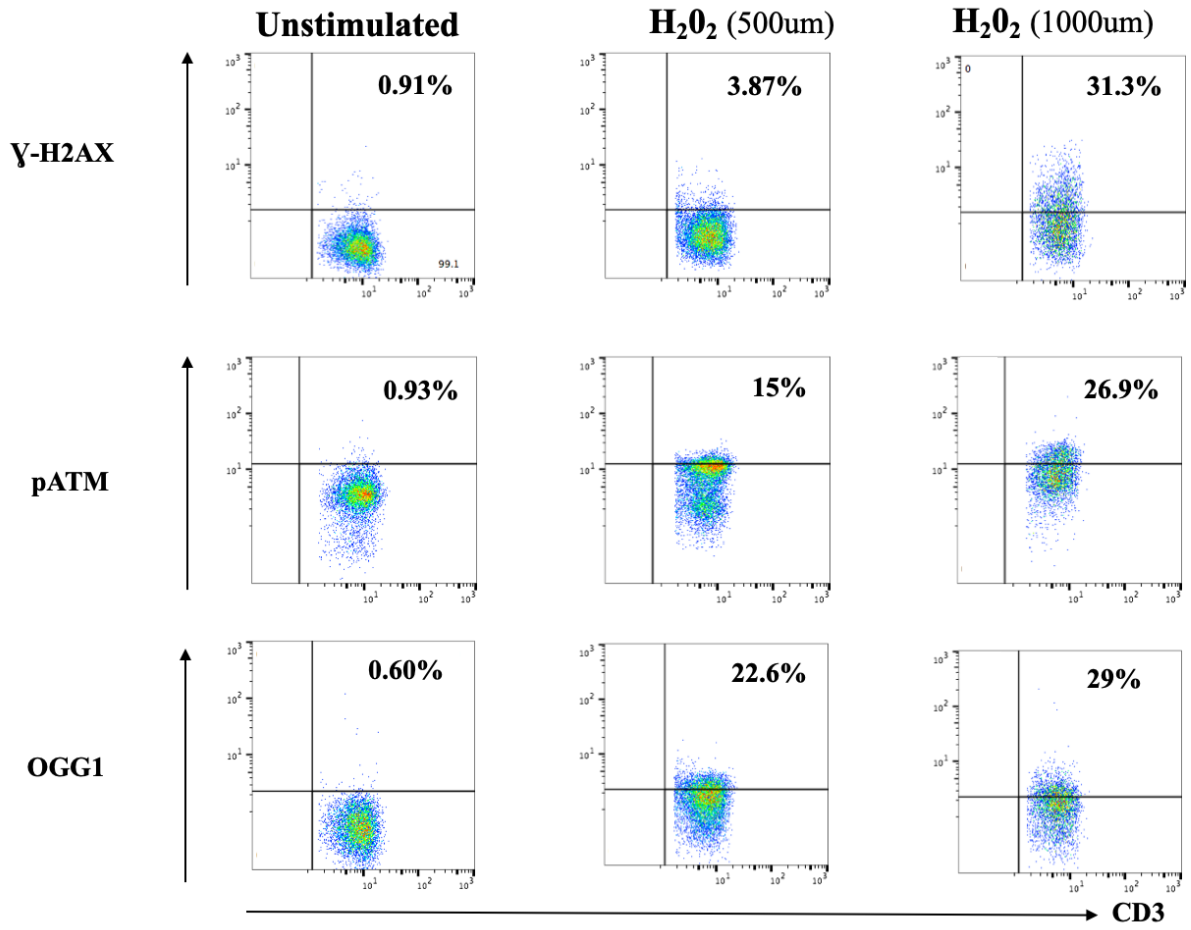

Figure 3.38 FACS analysis of H_2O_2 induced lymphocytes
Flow cytometric dot blots showing high doses of H_2O_2 induced the upregulation of OGG1, γ-H2AX and pATM biomarkers in CD3+ T lymphocytes.

3.4.7.2 Radiation induced OGG1 in CD3+ T lymphocytes

We observed an increase in both OGG1 and pATM explaining this observed upregulation in the operators CD3+ T lymphocytes is secondary to DNA base oxidation rather than DNA DSBs, confirmed by absence of γ-H2AX upregulation (Figure 3.39). Moreover, on further analysis of pATM expressing cells, they also expressed high levels of OGG1 compared to γ-H2AX expressing cells.

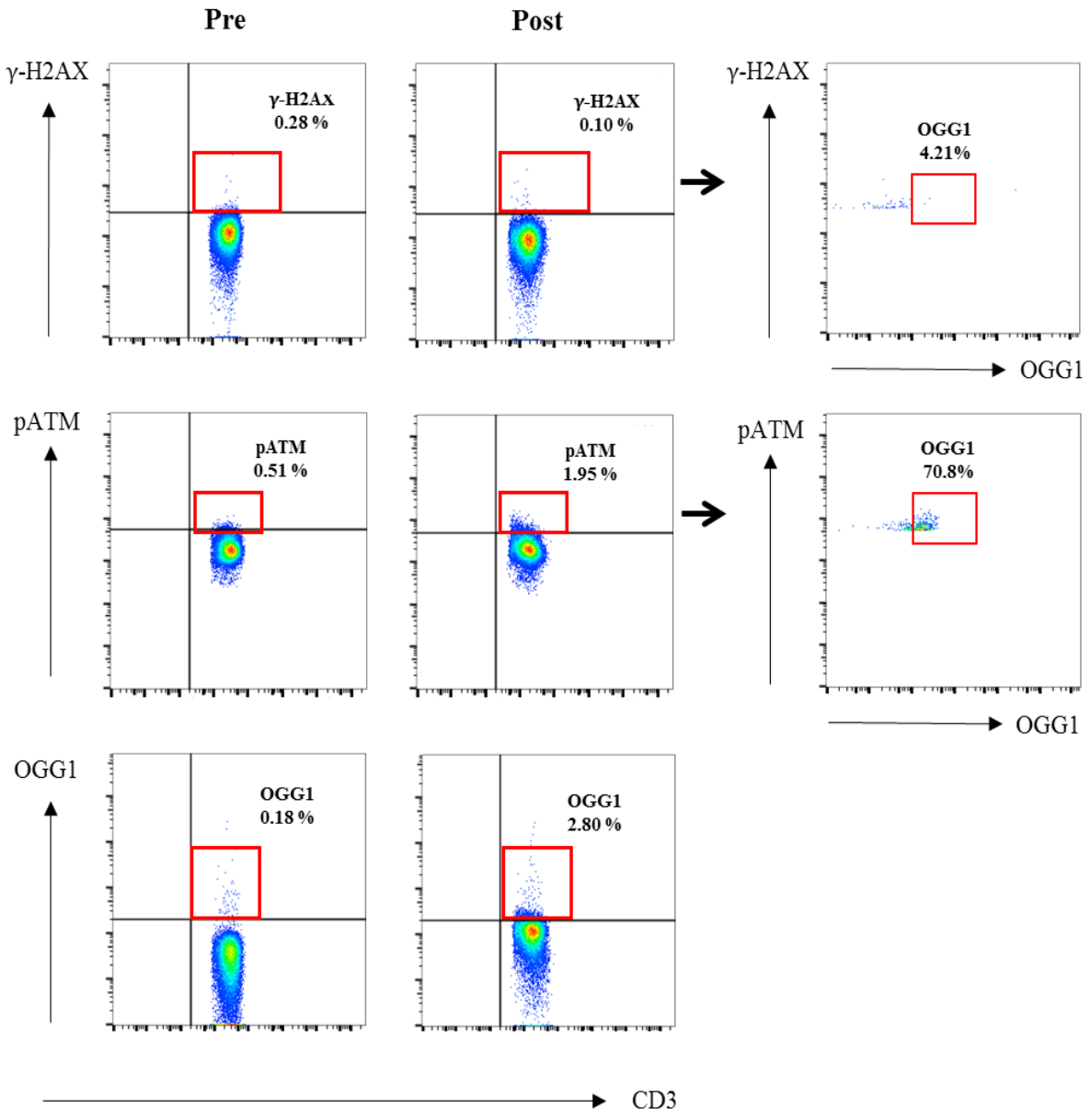

Figure 3.39 FACS analysis of radiation induced DNA base oxidation in lymphocytes
Flow cytometric dot blots showing both OGG1 and pATM *were upregulated in operator's CD3+ T lymphocytes when they performed IEVAR. pATM expression CD3+ lymphocytes also expressed high percentage of OGG1, in contrast to γ-H2AX expressing cells.*

3.4.8 Immunocytochemistry analysis of γ-H2AX in CD3+ T lymphocytes

3.4.8.1 Immunofluorescence staining of T lymphocytes

From a whole blood sample, CD3+ T lymphocytes were successfully stained with FITC-CD3 antibodies (Green) and identified using the previously explained immunohistochemistry technique.

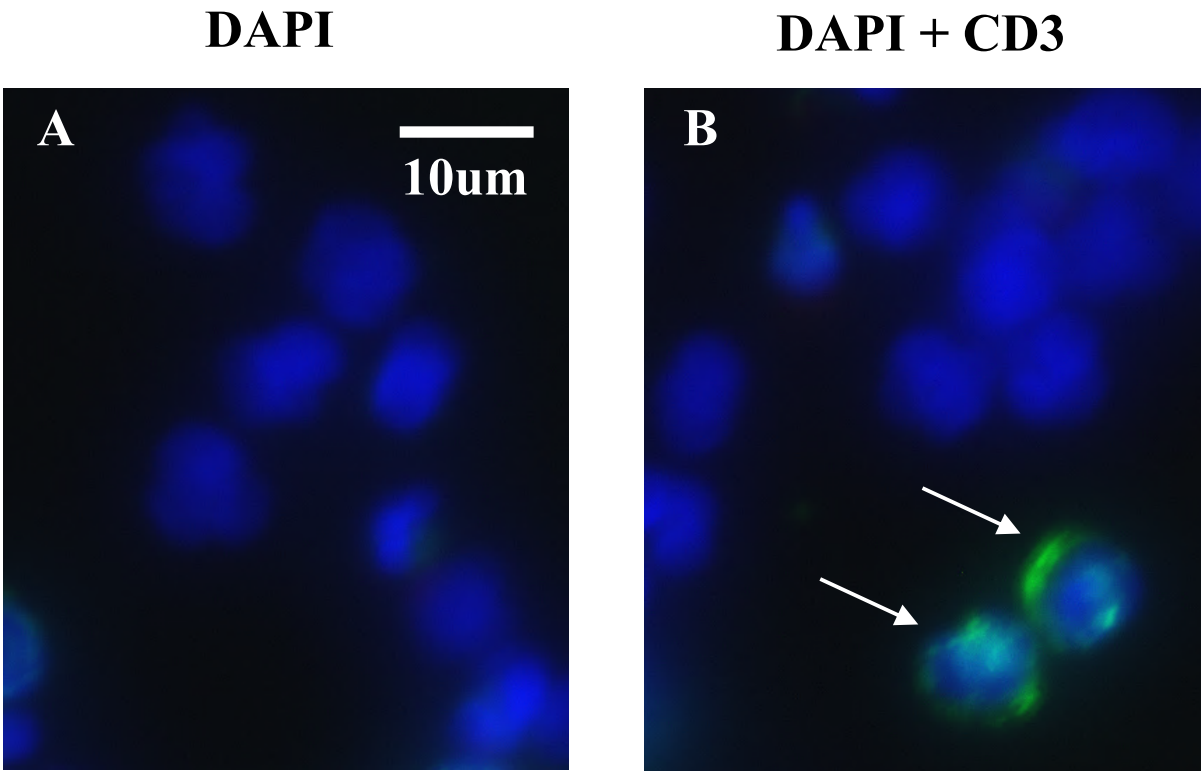

Figure 3.40 Immunofluorescence staining of T-lymphocytes from blood samples
(A) Blood cell nuclei stained with DAPI (blue), (B), T-lymphocytes, (white arrows), stained with both DAPI (blue) and CD3 fluorescent antibodies (green).

3.4.8.2 Immunohistochemistry of chemically induced γ-H2AX in T lymphocytes

From a whole blood sample, CD3+ T lymphocytes were successfully stained with CD3 (Green, Figure 3.41A and D) and expressed γ-H2AX (Red, Figure 3.41 B, E and F) when cells were chemically stimulated with Etoposide.

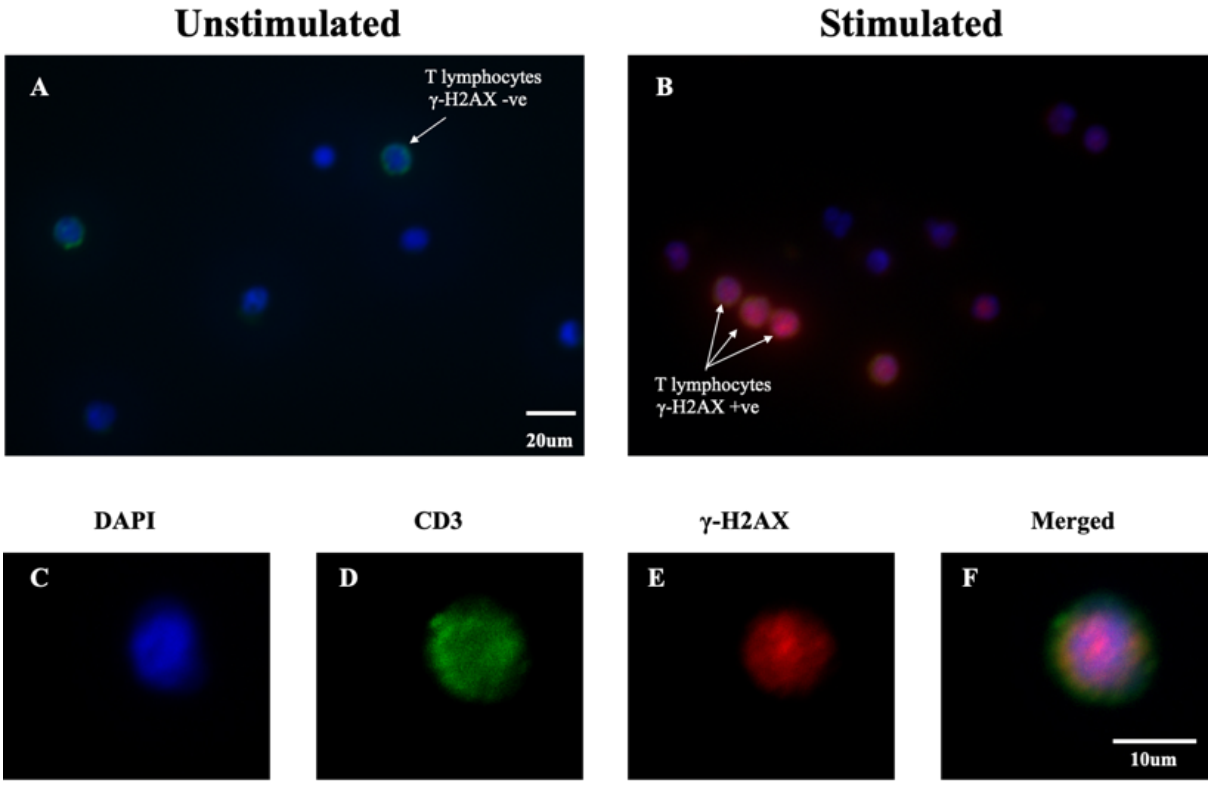

Figure 3.41 Etoposide induced γ-H2AX in T lymphocytes
(A) Unstimulated T lymphocytes cells stained with DAPI (blue) and CD3 (green). (B) Etoposide induced T lymphocytes are expressing γ-H2AX stained with DAPI (blue), CD3 (green) and γ-H2AX (pink). (C-E) an example of γ-H2AX expressing T lymphocyte stained by DAPI, CD3, γ-H2AX, and (F) DAPI, CD3 and γ-H2AX all merged.

3.4.8.3 Immunohistochemistry of radiation induced γ-H2AX in T lymphocytes

From an operator blood sample, the post-operative stimulated cells showed γ-H2AX (Red) was successfully identified in CD3 (Green) T lymphocytes compared to the pre-operative unstimulated cells.

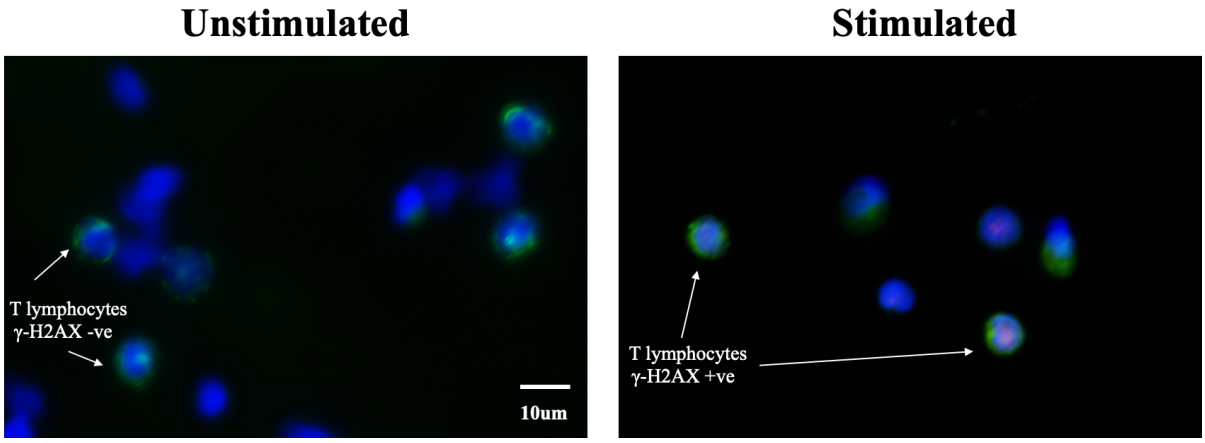

Figure 3.42 Immunofluorescence staining of radiation induced γ-H2AX in T lymphocytes
In the Unstimulated image, T lymphocytes cells stained with DAPI (blue) and CD3 (green). While in the Stimulated image, Etoposide induced T lymphocytes are expressing γ-H2AX stained with DAPI (blue), CD3 (green) and γ-H2AX (pink).

3.4.8.4 Immunocytochemistry analysis of γ-H2AX in isolated T lymphocytes

Isolated T lymphocytes from an operator, who performed EVAR procedure, showed upregulation of γ-H2AX (Figure 3.44) as a strong evidence of DNA damage that occurred as a consequence to radiation exposure that operator exposed to during the endovascular procedure. This upregulation was absent in the pre-operative isolated T lymphocytes (Figure 3.43).

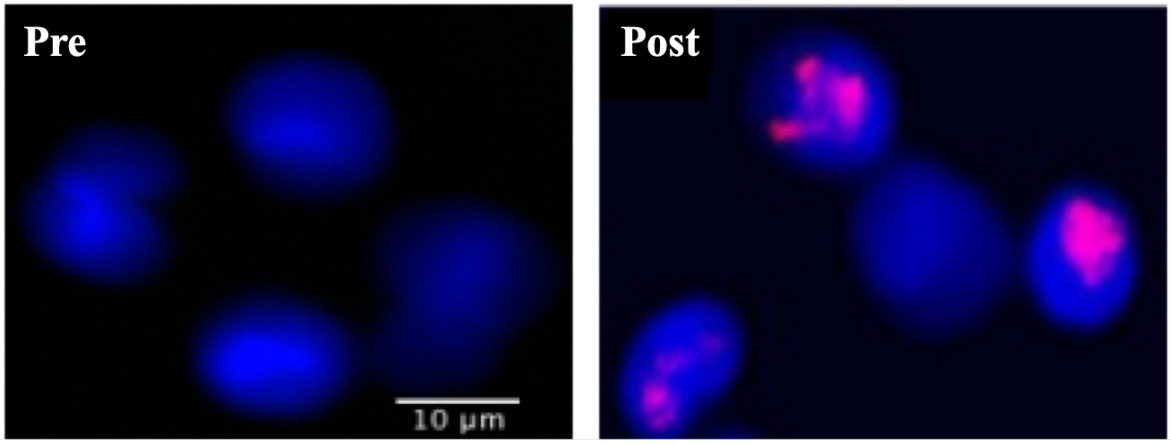

Figure 3.43 Immunofluorescence staining of radiation induced γ-H2AX in isolated T lymphocytes

In the Pre-operative image, isolated T lymphocytes cells stained with DAPI (blue) only, while in the Post-operative image, radiation induced T lymphocytes are expressing γ-H2AX stained with DAPI (blue), and γ-H2AX (pink).

3.5 Discussion

In this part of the study aimed to optimise a fully quantitative flow cytometric method to measure changes in peri-operative levels of γ-H2AX and pATM in the lymphocytes from blood samples from patients and operators. This technique among many advantages is able to detect extra and intra-cellular signals from hundred thousand of cells in few minutes.

An optimised flow cytometric method was validated using negative (pre-exposure/ non-exposed controls) and positive controls (chemically induced / radiation-induced) and compared with immunohistochemistry findings. Different reagents were used to optimise signals received from stimulated cells to measure γ-H2AX and pATM accurately. Flow cytometric analysis methodology was tested for reliability to ensure consistency and stability in measuring γ-H2AX and pATM levels. We also optimised a protocol to identify radiation-induced DNA base oxidation in operators performing endovascular interventions.

Further optimisation was extended to measure γ-H2AX and pATM upregulation levels in T lymphocytes subpopulations to identify which subsets expressing higher levels of these DNA damage biomarkers. A protocol to measure DNA damage biomarkers in haematopoietic and progenitor stem cells was optimised to understand the effect of radiation exposure on stem cells.

DNA damage/repair biomarkers, e.g., γ-H2AX and pATM, can be quantified either by immunofluorescence or flow cytometry.[328] Studies have suggested these markers could be used as useful biomarkers of DNA damage in low dose radiation exposure when measured by immunofluorescence as a valuable biomarker of human low-level radiation exposure.[329] In the immunofluorescence technique, numbers γ-H2AX foci, for example, are individually counted by microscopic evaluation. These foci were correlated with the flow cytometry assay signal after exposure to radiation (as low as 0.5Gy).[330, 331] Immunofluorescence techniques are mainly operator dependent which can lead to human errors and bias. They can only count few numbers of cells per examination which might miss out slight changes between different samples resulting in inaccurate results.

However, the flow cytometric method can quantify γ-H2AX and pATM upregulation in many cells (thousands or millions) in a short period (seconds to mins) by capturing fluorescence and accurately giving the count of γ-H2AX and pATM positive cells. This is facilitated by using fluorescence conjugated antibodies specific for γ-H2AX and pATM, and the positive cells are

automatically quantified. Flow cytometry offers a higher degree of precision of the duplicates due in no small number of cells analysed. This increased precision could allow the detection of an inter-individual variation in the DNA damage biomarkers signal at a given dose that was not detected using γ-H2AX foci counting. [330, 331]
The flow cytometric assay is fast, reliable, and it automatically calculates data minimises human interference. Even though flow cytometry has been used to quantify DNA damage, it is still not widely used to measure radiation-induced DNA damage biomarkers.[332, 333]

To optimise my methodology, I induced DNA damage in blood cells using chemical stimulants, e.g., Etoposide and Phorbol 12-myristate 13-acetate, to achieve intracellular DNA damage to test techniques such as cell fixation and permeabilisation. Optimising cell fixation and permeabilisation were challenging in the begging, and therefore different reagents were tested, e.g., Cytofix/Cytoperm and Cell Signalling Set A. Another challenge was identifying CD3+ T lymphocytes via CD3 antibodies that adhere to their extra-cellar antigen. This step was compromised by cell permeabilisation to facilitate intracellular staining of DNA damage biomarkers. After many trials and errors, I overcame this challenge by following the order of cell fixation, CD3 staining followed by cell permeabilisation, and intracellular staining using Cell Signalling Set A reagents. A technique that became successful in detecting DNA damage biomarkers, e.g., H2AX, pATM, and OGG1 in CD3+ T lymphocytes.

Using this optimised flow cytometric technique, I was able to study chemically and radiation-induced DNA damage/repair biomarkers γ-H2AX and pATM in individuals' blood samples at the cellular level. Flow cytometry enabled me to incorporate multiple cell surface antibodies to identify lymphocytes subsets, e.g., CD4 and CD8, and to study the aforementioned DNA damage biomarkers in these subsets.

I tried exploring the effect of radiation effect by measuring DNA damage biomarkers in haematopoietic stem/progenitor cells. However, these cell numbers were too low to draw any conclusions.

DNA base oxidation and the effect of reactive oxygen species were examined using the optimized method to understand further the effect of radiation-induced DNA damage in operators when they performed low-dose endovascular intervention. This finding has not been explored before, to my knowledge.

This will enable me to study the effect of radiation exposure during the endovascular intervention in patients and operators and detect subtle changes in their DNA biomarkers at the cellular level. Furthermore, I successfully managed to measure changes in DNA damage biomarkers against a range of radiation doses in-vitro, which will enable me to understand the correlation between radiation exposure and the acute phase of radiation-induced DNA damage in individuals. Also, it will enable me to compare the individual response to radiation exposure by measuring their DNA biomarkers levels in-vivo and in-vitro to shed some light on operators' susceptibility variation to ionising radiation. This will have a significant implication for a better understanding of the occupational hazards of radiation exposure and ways of mitigating this effect.

In this part of the study, a flow cytometric technique to measure γ-H2AX and pATM is optimised to study the immediate DNA damage in patients and operators exposed to radiation during endovascular aortic aneurysm repair.

3.6 Summary

A fully quantitative flow cytometric protocol was successfully optimised to measure changes of levels of γ-H2AX and pATM in blood samples. This will enable us to proceed with the next phase of the study to assess the biological effect of intraoperative radiation exposure in patients and operators during endovascular aortic repair.

CHAPTER 4

Radiation Induced DNA Damage During Endovascular Intervention

4.1 Introduction

In the United Kingdom, there are thought to be 700 cancers diagnoses and 100 deaths per year attributed to radiation exposure during diagnostic and therapeutic interventions, but this is likely to be an under estimation.[246, 334]

Endovascular aortic repair (EVAR), a fluoroscopically guided procedure, carries a significant burden of radiation exposure to both patient and operator. Fenestrated and branched endovascular aortic repair (FEVAR & BEVAR) are advanced forms of EVAR that require prolonged fluoroscopy guidance and multiple digital subtraction angiography acquisitions and therefore necessitate a higher radiation exposure to patients and medical staff. Previous studies reported that the amount of radiation exposure proportionally increased with the complexity of the EVAR procedure.[42, 43, 47]

DAP and fluoroscopy time are considered as standard methods of measuring radiation exposure during fluoroscopically guided endovascular procedures.[240] They are automatically generated by the fluoroscopy x-ray source, with minimal or no human interference, which makes them ideal tools for radiation exposure comparison between cases and institutions. Conventional dosimetry does not inform the biologically effects of radiation exposure for the individual after EVAR. Recent studies reported on biomarkers that showed promise on measuring this biological effect of radiation.[229 - 231]

DNA damage/repair biomarkers such as γ-H2AX and pATM are used for biodosimetry during the acute phase after radiation exposure. These biomarkers can be measured in the individual's circulating lymphocytes which are known to be cells that are highly sensitive to radiation. The aim of this part of the study is to measure these biomarkers in patients' and operators' circulating lymphocytes during the peri-operative period of EVAR e.g., pre, immediate and 24hrs. The 24hr measurement after intervention to check wether biomarkers returned to their

baseline 24hrs after procedures to focus on the acute DNA damage response, followed by a DNA repair process as previously described by Löbrich et al., 2005.[72]

4.2 Aims

(1) To measure the DNA damage/repair markers, γ-H2AX & pATM in patients and operators after EVAR and open AAA repair and compare this to operators preforming percutaneous coronary intervention.
(2) To study factors that impact γ-H2AX levels in operators

4.3 Radiation Induced DNA Damage in Patients

4.3.1 Methods:

4.3.1.1 Study participants

Blood samples were collected from patients who underwent endovascular and open aortic aneurysm repair at three different time points (prior to, immediately after and 24 hrs after procedure). This study was approved by the London–City & East Research Ethics Committee (16/LO/1111) following the principles of the Declaration of Helsinki, and written informed consent was obtained from each participant.

4.3.1.2 Procedural Details

All endovascular procedures were carried out in the same hybrid suite, equipped with the Philips Allura Xper FD20 fixed X-ray imaging system (Philips Healthcare). Default settings used were a pulse rate of 7.5 pulses per second for background fluoroscopy and 2 frames per second for digital subtraction angiography acquisitions. For both fluoroscopy and cineangiography, an x-ray beam filtration of 1.5 mm Al combined with 0.4 mm Cu was used. The equipment setup and operating staff positioning were similar for IEVAR and BEVAR/FEVAR procedures.

4.3.1.3. Peri-operative changes of peripheral blood cells in patients

The pre- and post-operative full blood counts were collated prospectively from the hospital electronic patient records. Peripheral leukocytes, monocytes and lymphocytes counts were

compared in patients after open aneurysm repair, infra-renal (IEVAR), and branched and fenestrated endovascular aneurysm repair (BEVAR/FEVAR), similar to section 2.3.1. Changes of cells among the 3 groups were analysed using Two-way analysis of variance (ANOVA) and Bonferroni post-hoc analysis.

4.3.1.4 Flow Cytometry

To study this biological effect of radiation during the acute phase, changes in levels of DNA damage biomarkers γ-H2AX & pATM were measured in patients' circulating lymphocytes during the perioperative period of EVAR. DNA damage biomarkers upregulation after EVAR was compared to similar cohort of patients who underwent open aortic aneurysm surgical repair. Venous blood samples were collected from patients, and red blood cells were lysed. Cells were then fixed followed by staining with CD3 antibody. This was followed by cell permeabilisation before staining for γ-H2AX and pATM antibodies. Samples were processed on a MACSQuant flow cytometer and analysed using FlowJo software. The detailed flow cytometric technique to study radiation induced γ-H2AX and pATM levels in peripheral blood cells are discussed in Chapter 3, "Optimisation of analysis of DNA damage/repair biomarkers".

4.3.1.5 Statistical Analysis

Data were analysed using GraphPad Prism 8.0 (GraphPad Software Inc) and SPSS-22 (SPSS Inc). Nonparametric Wilcoxon signed rank, Mann-Whitney U and 2-way analysis of variance tests were used. A *P* value <0.05 was considered to be statistically significant.

4.3.2 Results

4.3.2.1 Patient and procedure characteristics

A total of seventy-two patients were recruited to the study who underwent elective endovascular aortic repair, including 30 infra-renal EVAR and 42 complex BEVAR and FEVAR procedures. A cohort of controls included 14 patients who underwent open aortic aneurysm repair and were not exposed to radiation. Patients who underwent open repair were younger than the EVAR cohort. The sex, BMI and comorbidities did not, however, differ between the two groups. (Table 4.1, *P* value calculated using Fisher's exact tests).

Table 4.1 Patient and procedure characteristics

Characteristics	Open repair (n=14)	IEVAR (n=30)	BEVAR/FEVAR (n=42)	*p* value Open repair vs IEVAR	*p* value Open repair vs BEVAR
Age, years (median, range)	64.5 (48-79)	74 (63-88)	72 (58-86)	<0.0001	<0.0001
Gender %					
Male	100%	93.3%	90.5%		
BMI (kg/m^2)	27.45 (24.2 – 33.3)	26.2 (21- 37)	28 (17 – 39.3)	0.7	, 0.8
Comorbidities %					
HTN	9 (4.3)	16 (53.3)	20 (47.6)	0.5	0.3
Dyslipidemia	5 (35.7)	12 (40)	11 (26.2)	0.9	0.7
Smoking	7 (50)	8 (26.7)	10 (23.8)	0.1767	0.09
COPD	4 (28.6)	8 (26.7)	7 (16.7)	0.9	0.4
Coronary artery diseases	2 (14.3)	6 (20)	12 (28.6)	0.7	0.4
Diabetes Mellitus	1 (7.14)	2 (6.7)	6 (14.3)	0.9	0.6
Cancer	2 (14.3)	7 (23.3)	5 (11)	0.6	0.9
Chronic kidney disease	0	7 (23.3)	10 (23.8)	0.7	0.0998
Cerebral vascular disease	0	1 (3.3)	2 (4.8)	0.99	0.99
Peripheral vascular disease	1 (7.14)	4 (13.3)	3 (7.1)	0.6	0.99
				p value IEVAR vs BEVAR	
DAP (mGy.cm2)		60016 (2264-144257)	173564 (33382-421562)	<0.0001	
Personal dosimeter (µSv)		313 µSv [112-2155]	1440 µSv [229-9999]	< 0.0001	
Screening time (mins)		24.39 (8.01-73.42)	77.15 (24.39– 142.4)	<0.0001	

Open repair= open abdominal aortic aneurysm repair. IEVAR=infra-renal endovascular aortic repair. BEVAR=branched endovascular aortic repair. FEVAR=fenestrated endovascular aortic repair. BMI=body mass index. HTN=hypertension. COPD=chronic obstructive pulmonary disease. DAP=Dose area product.

4.3.2.2 Radiation exposure during EVAR

Complex, BEVAR/FEVAR procedures (n=22) were associated with 3-fold longer fluoroscopy time and higher DAP compared with infra-renal EVAR (n=14) (P<0.0001 for both, by Mann-Whitney U test, Figure 4.1).

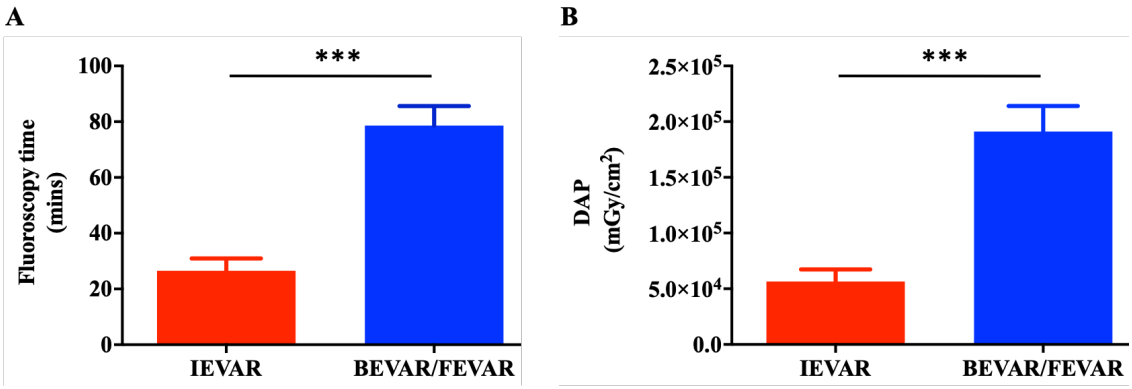

Figure 4.1 Radiation exposure during EVAR

Complex, BEVAR/FEVAR were associated with longer fluoroscopy time [P<0.0001, by Mann-Whitney Test, median 23.44mins (8.01-73.42) vs 82.17(22.12- 133.4) and higher DAP compared with IEVAR [P<0.0001, by Mann-Whitney Test, median 56196 mGy.cm² (2264-144257) vs 173564 (33382- 421526)]

4.3.2.3 Peri-operative changes of peripheral blood cells in patients during EVAR

Peripheral blood cells were prospectively studied in patients when they underwent open (n=14) and endovascular aortic repair (IEVAR, n=30 & BEVAR/FEVAR, n=42, Figure 4.2). Leukocytes and Monocytes increased on day one following all interventions to peak on day 2 then gradually returning to the baseline. No significant difference was associated with different interventions. However, Lymphocyte count dropped on day one after intervention and gradually recovered over the course of 7 days. There was a significant variation in these changes among open repair, IEVAR and BEVAR/FEVAR approaches (P<0.02, by Two Way ANOVA, Figure 4.2).

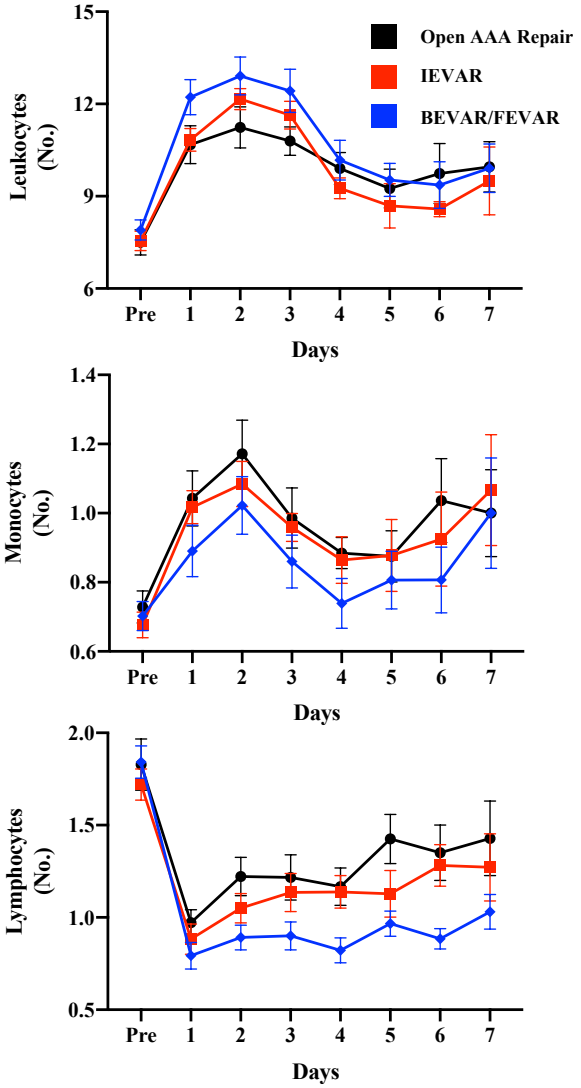

Figure 4.2 Perioperative blood cells changes in patients during aortic intervention
Graphs showing the changes of patient's peripheral blood cells when they underwent open AAA repair, IEVAR and BEVAR. Leukocytes and Monocytes increased on day one to reach peak on day 2 and then recovered gradually. Lymphocytes dropped after all interventions and recovered afterwards, with significant difference between different interventions (P<0.02, by Two Wany ANOVA test).

4.3.2.3 Peri-operative changes of DNA damage/repair biomarkers in patients

Expression of both γ-H2AX and pATM in circulating lymphocytes significantly increased immediately after EVAR (IEVAR and BEVAR/FEVAR grouped together (P<0.0001 for both by Wilcoxon matched pairs signed rank test, Figure 4.3). There was no change in γ-H2AX or pATM expression at any time point during the perioperative period in lymphocytes from patients who had open abdominal aortic aneurysm repair in contrast to EVAR group (P<0.0001, by Two Way ANOVA test, Figure 4.3). Results were not adjusted for patients' characteristics e.g., age, gender, or co-morbidities.

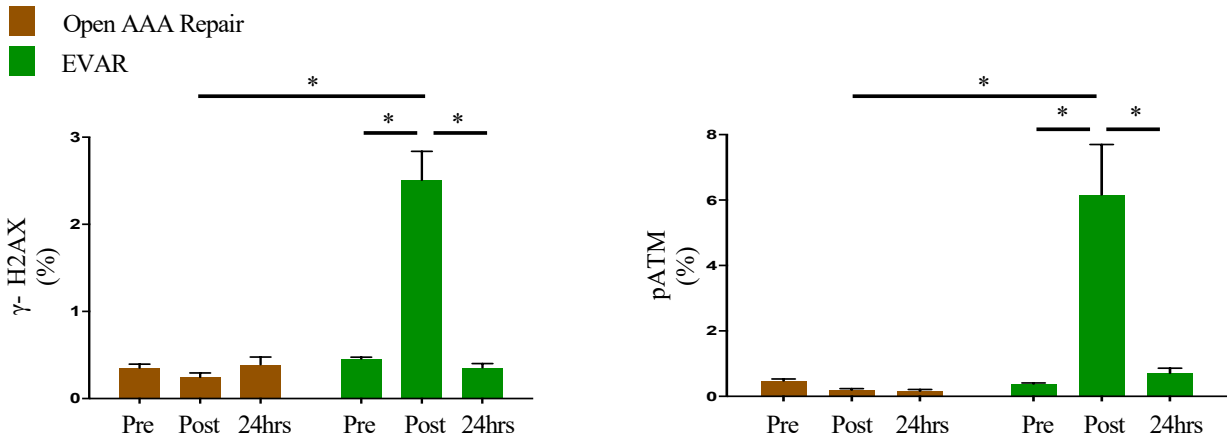

Figure 4.3 Perioperative changes of γ-H2AX & pATM in patients
Patient's CD3+ T lymphocytes expressing γ-H2AX and pATM increased immediately after EVAR (P<0.0001 for both by Wilcoxon matched pairs signed rank test) compared to open repair (P<0.0001, by Two Way ANOVA test). Both markers recovered after 24 hrs.

4.3.2.4 Biological effects of branched and fenestrated EVAR

Complex BEVARs and FEVARs (n=42) were associated with a greater increase in both γ-H2AX and pATM expression compared with IEVAR (n=30) (P=0.01 for both by Bonferroni's multiple comparisons test, Figure 4.4). Levels of both markers normalised 24 hrs after the procedure (P<0.0001 by Wilcoxon matched pairs signed rank test, Figure 4.4).

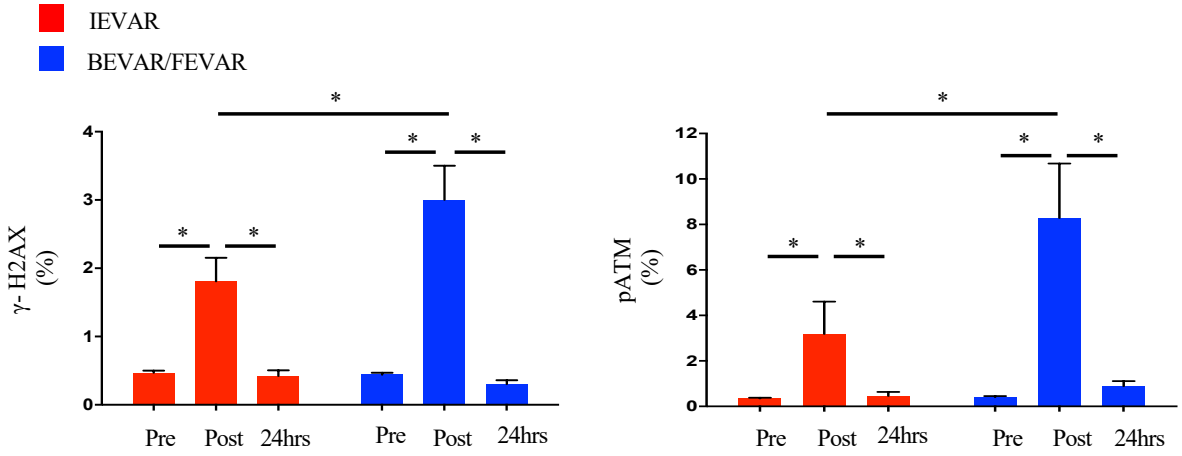

Figure 4.4 γ-H2AX & pATM in patients who underwent IEVAR and BEVAR/FEVAR
Patient's CD3+ T lymphocytes expressing γ-H2AX and pATM levels after complex were higher compared to IEVAR (P=0.01 for both by Two Way ANOVA test), and recovered after 24 hrs.

4.4 Radiation Induced DNA Damage in Operators

4.4.1 Radiation Induced DNA Damage in Vascular Operators During EVAR

4.4.1.1 Methods:

4.4.1.1.1 Study participants

Blood samples were collected from vascular surgeons and interventional radiologists before, immediately after, and 24 hrs after they performed endovascular (infrarenal EVAR and complex branched and fenestrated EVAR [BEVAR & FEVAR]) and open aortic repairs.

4.4.1.1.2 Procedural details

As mentioned above (section 4.3.1.2) all procedures were carried out in the same hybrid suite with the aforementioned settings. At the start of each case, the under-table lead shielding was specifically checked to ensure that it was in the optimal position. A ceiling- mounted lead shield was available and positioned at the operators' discretion for each procedure., Operators (n=15) wore standard protective lead garments which covered their trunks and upper thighs (0.35 mm thickness), leaded thyroid collars, and leaded goggles for all endovascular cases. Leg lead shields were not routinely worn. Studies were repeated on a cohort of 6 of the original 15 operators but this time they were asked to wear lower leg lead shielding (0.5 mm thickness, XENOLITE–TB, DuPont Technology, Lite Tech, Inc) as additional protection to study the effect of radiation exposure on operators when legs were protected.

4.4.1.1.3 Standard dosimetry

Electronic dosimeters (Hitachi-Aloka Medical PDM-127; Hitachi Aloka Medical Ltd) were used to measure direct radiation exposure for operators. These devices recorded cumulative measurements of the dose equivalence of absorbed radiation in micro-Sieverts for each case. Dosimeters were attached to three different areas on the operator: (1) left breast pocket under the protective lead garment, (2) left breast pocket over the protective lead garment, and (3) left mid-leg. The dose-area product (DAP) and fluoroscopy time were recorded for all procedures (Figure 4.4). Lead radiation attenuation rate is measured by comparing under lead and over lead doses for IEVAR and BEVAR/FEVAR.

4.4.1.1.4 Flow cytometry

To study this biological effect of radiation during the acute phase, changes in levels of DNA damage biomarkers γ-H2AX & pATM were measured in operators' lymphocytes during the perioperative period of EVAR. DNA damage biomarkers upregulation after EVAR is compared to similar cohort of operators who performed open aortic aneurysm surgical repair. The same optimised protocol to measure levels of γ-H2AX and pATM expression in circulating lymphocytes was used as mentioned in section 4.3.1.3.

Blood samples were collected from six operators after complex EVAR, and flow cytometric analysis was carried out, to study changes in γ-H2AX and pATM levels in CD3+ lymphocytes subsets, including CD8+ (cytotoxic) and CD4+ (helper) cells. These two cell subsets were further phenotyped into CD45RO-CCR7+ (Naïve), CD45RO+CCR7+ (Central Memory, TCM) and CD45RO+CCR7- (Effector Memory, TEM) cells.

The biological effect of ionising radiation was also evaluated on operators' circulating hematopoietic stem cells (HSCs, $CD45^{-}$ $CD34^{+}$ $CD38^{-}$ $CD90^{+}$) and haematopoietic stem/progenitor cells (HSPCs, $CD45^{-}$ $CD34^{+}$ $CD38^{+}$ $CD90^{-}$) during EVAR. As radiation induced damage in these progenitor blood cell lines might provide an idea about potential long-term biological hazards of occupational radiation exposure among medical staff.[232]

To study DNA damage caused by base oxidation, circulating lymphocytes from operators performing IEVAR were analysed for the expression of DNA base oxidation biomarker 8-oxoguanine DNA glycosylase-1 (OGG1).

4.4.1.1.5 Variation in operators' sensitivity to radiation exposure

To study operators' variation in their biological response to radiation exposure while performing EVAR, the amount of radiation was statically standardised by normalising the post-operative γ-H2AX in each case to dose area product of that particular case to identify intra-operative variation in operators' susceptibility.

Blood samples were then collected from six operators on three separate occasions and exposed in Polypropylene Eppendorf Safe-Lock tubes (1ml of blood in each tube) to radiation doses between 100 and 1000 mGy using a Darpac 2000 (Gulmay Medical) x-ray unit (energy: 80 kVp [half-value layer, 2.0mmAL], 6.9 mA, applicator: 8 cm diameter) positioned ≈25 cm from the x-ray source. Irradiated samples were then analysed using the previously described standard optimised flow cytometric analysis to measure levels of in γ-H2AX in T lymphocytes.

4.4.1.2 Results:

4.4.1.2.1 Operators and procedure characteristics

A total of fifteen operators (13 males, 40 years of age [34-49], Table 4.2) carried out 31endovascular (15 IEVAR and 16 BEVAR/FEVAR) and 14 open abdominal aortic aneurysm repair procedures.

Table 4.2 Operators demographics

Operator	Age (years)	Gender	Years of Interventional		Interventional sessions/month	Sampled For IEVAR/ BEVAR/FEVAR	Sampled for open AAA repair
			As Trainee	As Consultant			
1	42	M	3	6	3	Yes	No
2	36	M	7	0	4	Yes	Yes
3	43	M	5	7	1.5	Yes	Yes
4	39	M	2	2	4	Yes	Yes
5	48	M	4	10	24	Yes	No
6	40	M	4	3	3	Yes	No
7	34	M	4	0	12	Yes	Yes
8	45	M	10	8	6-8	Yes	No
9	39	F	13	1	2-4	Yes	Yes
10	37	M	6	4	4	Yes	Yes
11	36	M	7	0	6	Yes	Yes
12	49	M	5	14	20	Yes	No
13	41	M	7	6	5	Yes	Yes
14	40	F	10	0	5	Yes	No
15	42	M	7	0	12	Yes	Yes

4.4.1.2.2 Radiation exposure to operators during EVAR

BEVAR/FEVAR was associated with longer fluoroscopy time and higher DAP (P<0.0001 for both by Mann-Whitney U test, Figure 4.5 A&B) compared with IEVAR.

Operators' chests received higher doses when they carried out BEVAR/FEVAR compared with IEVAR ([27 mSv [4-150] vs [11 mSv [4-74], P=0.02 by Mann-Whitney U test Figure 4.5 C).

Wearing lead garments protected operators from the majority of amount radiation they exposed to while performing endovascular intervention measured by lead radiation attenuation rate (P<0.0001 for by Mann-Whitney U test, Figure 4.6A & B). There was no difference in lead radiation attenuation rate between standard and complex EVAR cases (Figure 4.6C). The unprotected lower leg region received a significant amount of radiation in both IEVAR and BEVAR/FEVAR procedures (Figure 4.4C)

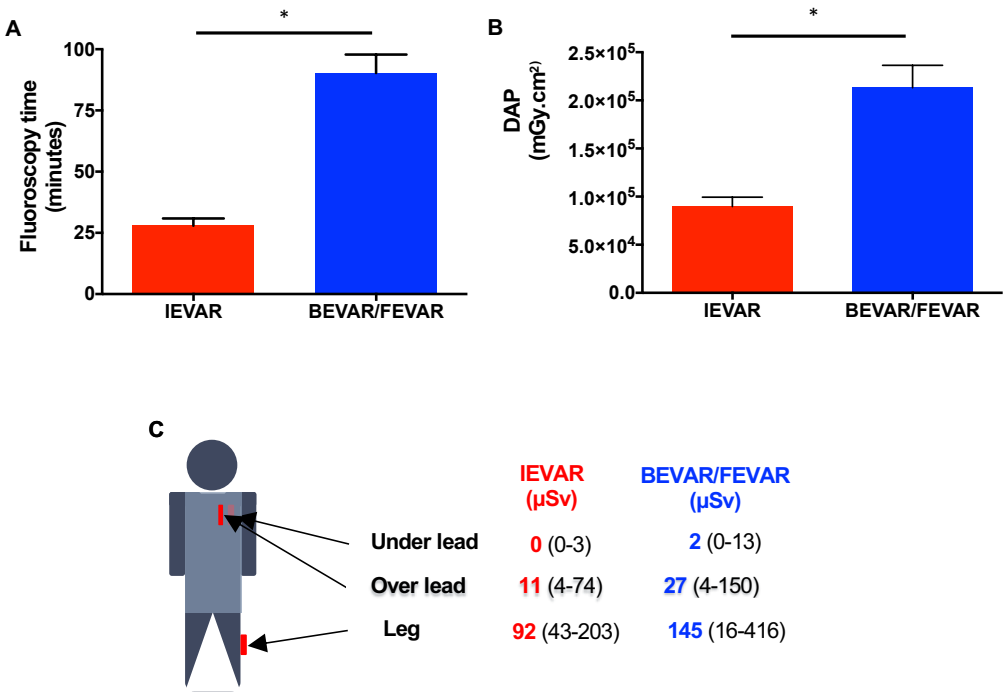

Figure 4.5 Radiation exposure to operators during EVAR

(A) Operators performed BEVAR/FEVAR exposed to longer fluoroscopy time [(P<0.0001 by Mann Whitney Test, median 24.78mins (14.06 - 49.39) vs 94.39 (40.32- 133.9)] and, (B) higher radiation doses measured by dose area product [P<0.0001 by Mann Whitney test, median 189927 mGy.cm^2 (108919-417006)], (C) Operators' leg dosimeters showed higher exposure during BEVAR/FEVAR particularly leg doses.

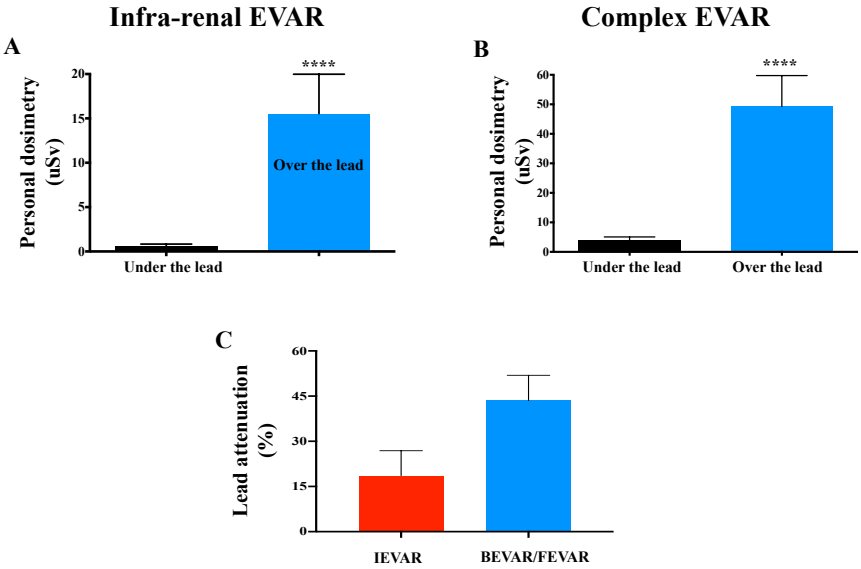

Figure 4.6 Operators' lead garment protection effect during EVAR

(A) Lead garments protected operators from majority of radiation doses when they performed IEVAR and, (B) during BEVAR/FEVAR (P<0.0001 by Mann Whitney Test for both). (C) However, no difference lead attenuation rate was observed between EIVAR and BEVAR/FEVAR.

4.4.1.2.3 Acute phase operators' response to radiation during EVAR

The expression of γ-H2AX and pATM in operators' circulating lymphocytes significantly increased immediately after EVAR (IEVAR and BEVAR/FEVAR grouped together) (P=0.0003 and P=0.0005, respectively by Wilcoxon matched pairs signed rank test, Figure 4.7). There were no changes in these DNA damage biomarkers in operators after open aortic aneurysm surgical repair (Figure 4.7).

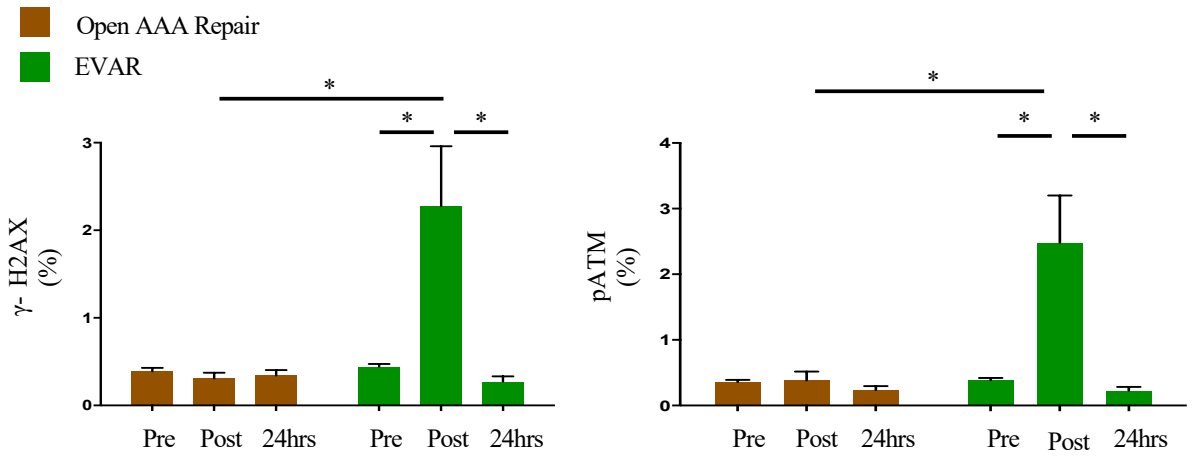

Figure 4.7 Perioperative changes of γ-H2AX & pATM in operators
Operators' T lymphocytes expressing γ-H2AX and pATM significantly increased immediately after they performed EVAR (P=0.0003 and P=0.0005, respectively by Wilcoxon matched pairs signed rank test) compared to after open repair (P<0.0001, by Two Way ANOVA test). Both markers recovered after 24 hrs.

4.4.1.2.4 Biological effects when operators performed complex EVAR

The post-operative expression of γ-H2AX and pATM was significantly higher in operators performing BEVAR/FEVAR, compared with IEVAR (P=0.0003, 0.007 respectively by Two Way ANOVA test). Only the level of pATM increased in the lymphocytes of operators who carried out IEVAR (P=0.04 by Wilcoxon matched pairs signed rank test). The expression of both markers recovered to baseline levels in all operators after 24 hrs (Figure 4.8).

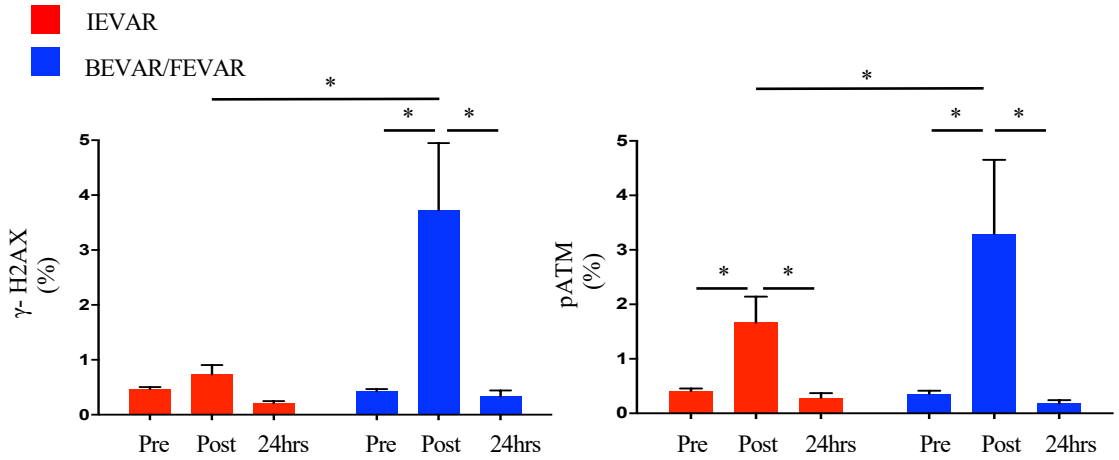

Figure 4.8 γ-H2AX & pATM in operators who performed IEVAR and BEVAR/FEVAR
γ-H2AX and pATM upregulation was higher in operators performing BEVAR/FEVAR compared with IEVAR (P=0.0003, 0.007, by Two Way ANOVA test). Only pATM was upregulated after IEVAR (P=0.04 by Wilcoxon matched pairs signed rank test).

4.4.1.2.5 Changes in γ-H2AX & pATM in operators' T lymphocyte subpopulations

γ-H2AX and pATM expression significantly increased in CD4+ T helper (P=0.02, P=0.04, respectively by Wilcoxon matched pairs signed rank test, Figure 4.9A) and CD8+ cytotoxic T (P=0.03, P=0.02, respectively by Wilcoxon matched pairs signed rank test, Figure 4.9B) cell subpopulations when operators performed complex EVAR.

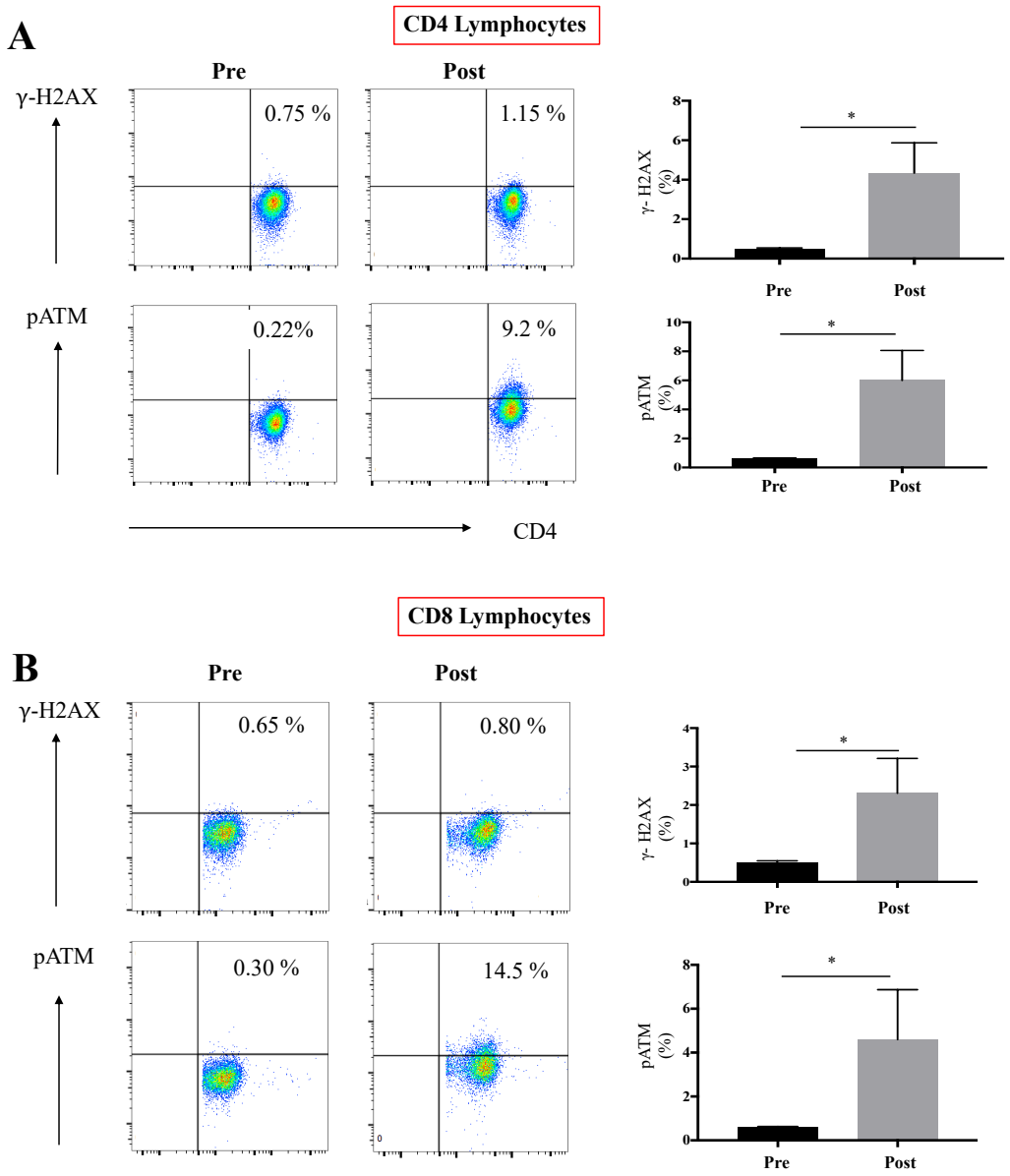

Figure 4.9 γ-H2AX & pATM expression in operators' CD4+ and CD8+ T lymphocytes
(A) BEVAR/FEVAR induced γ-H2AX and pATM upregulation operators' CD4+ T helper (P=0.02, P=0.04, respectively by Wilcoxon matched pairs signed rank test and (B) CD8+ cytotoxic T (P=0.03, P=0.02, respectively by Wilcoxon matched pairs signed rank test) cell subpopulations.

Post-operative γ-H2AX expression was relatively higher in T helper lymphocytes compared with cytotoxic T cells (P=0.04, by Bonferroni's multiple comparisons test, Figure 4.10).

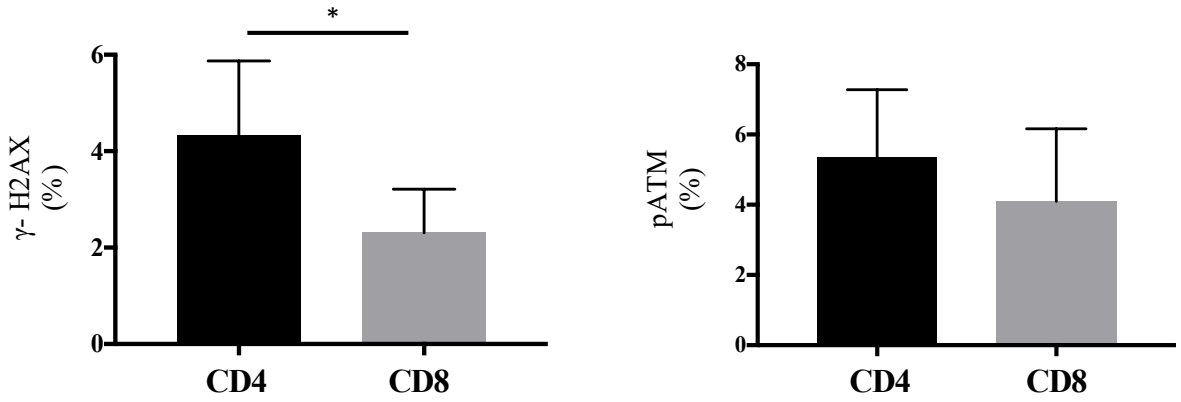

Figure 4.10 Comparison of γ-H2AX & pATM expression in operators' CD4+ and CD8+ T lymphocytes
Operators' T helper cells expressed higher γ-H2AX levels compared with cytotoxic T cells (P=0.04, by Bonferroni's multiple comparisons test), no difference in pATM expression level between two subpopulations.

Deeper phenotyping showed a significant increase in γ-H2AX levels in CD4+ naïve and central memory cells compared with other subpopulations (n=6, P<0.05 and P=0.2 respectively by Bonferroni's multiple comparisons test, Figure 4.10).

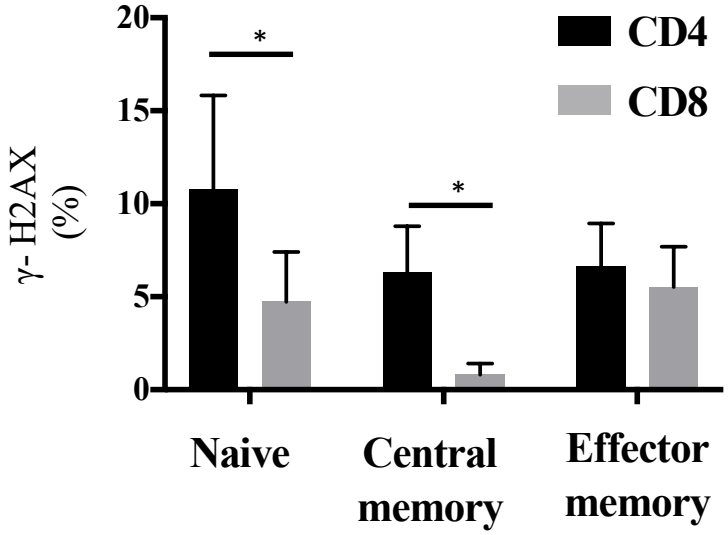

Figure 4.10 γ-H2AX & pATM expression in T lymphocytes subpopulations after EVAR

*Operators' CD4+ naïve and central memory cells expressed higher γ-H2AX levels compared with other subpopulations (*P<0.05 and P=0.2 respectively by Bonferroni's multiple comparisons test).

4.4.1.2.6 Changes in γ-H2AX & pATM in haematopoietic stem/progenitor cells

Both γ-H2AX and pATM expressions were studied in six operators' haematopoietic stem/progenitor cells. There were no observed significant changes in γ-H2AX or pATM in HSCs or HSPCs (n=6 operators, pre-operative means 0.96±0.19% vs post-operative 0.98±0.21%, and pre-operative 1.26±0.40% vs post-operative 0.9±0.42%) or HSPCs (n=6, pre-operative mean 1.81±0.46% vs post-operative 1.34±0.58%, and pre-operative 1.76±0.63% vs post-operative 1.21±0.62%). Nevertheless, the numbers of identifiable circulating HSCs/HPCs are very low (<200 cells compared with >20,000 lymphocytes, Figure 3.35 & 3.36).

4.4.1.2.6 EVAR is associated with DNA base oxidation in operators' lymphocytes

Upregulation of pATM, but not **γ-**H2AX, was found in operators' lymphocytes after IEVAR. Therefore, we studied the changes of OGG1 expression in their lymphocytes as a marker of DNA base oxidation. Similar to pATM, OGG1 expression increased after IEVAR (P=0.03 by Wilcoxon matched pairs signed rank test) and also OGG1 expression was upregulated in the lymphocytes expressing pATM following IEVAR (P<0.03 by Wilcoxon matched pairs signed rank test, Figure 4.11). This is in contrast to **γ-**H2AX that did not change in their lymphocytes.

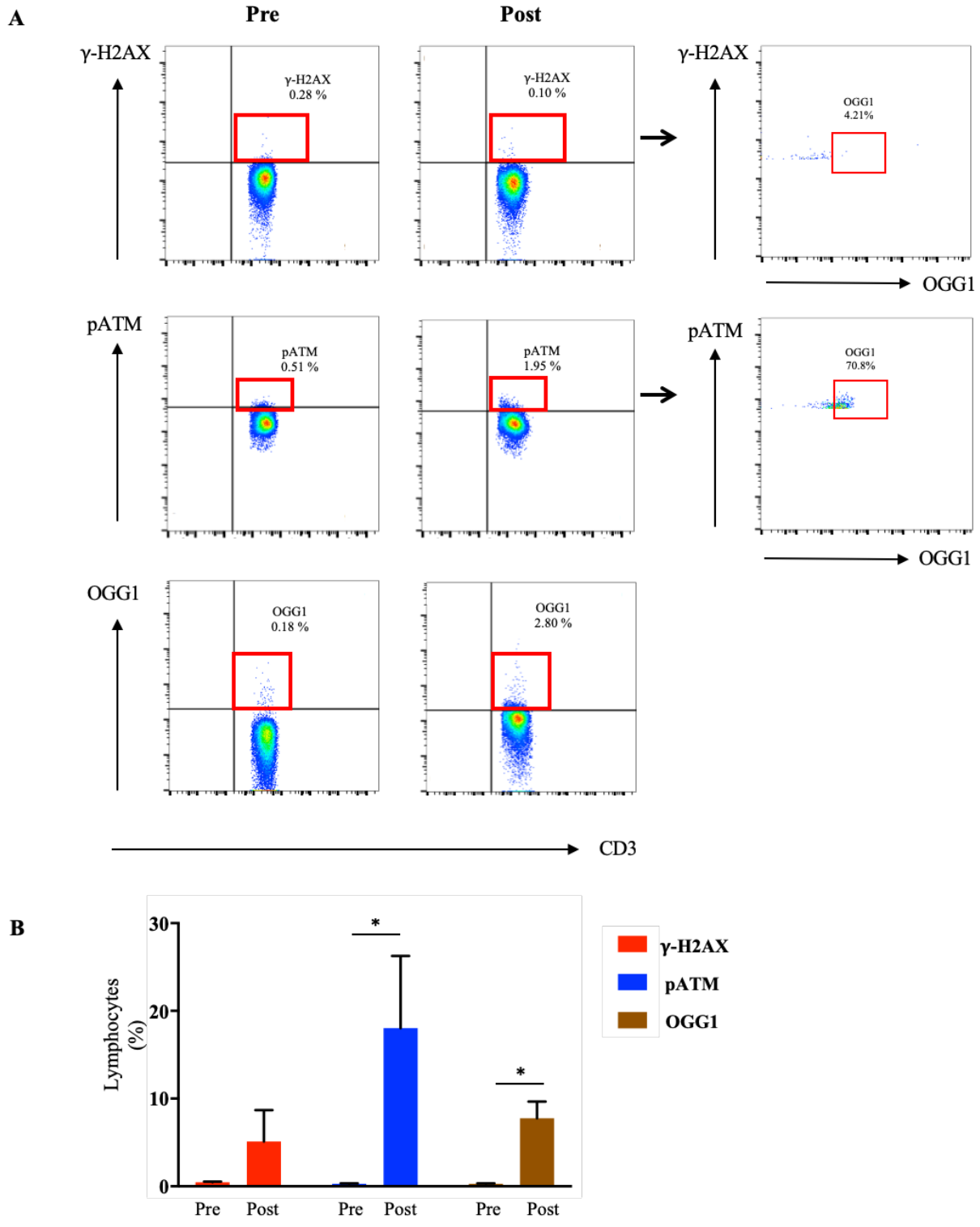

Figure 4.11 Operators' OGG1, pATM and γ-H2AX expression after IEVAR
(A) Flow cytometric dot blots showing operators' T lymphocytes following IEVAR, pATM and OGG1 expression increased (P<0.03 for both by Wilcoxon matched pairs signed rank test) in contrast to γ-H2AX. OGG1 expression increased in the lymphocytes expressing pATM following IEVAR (P<0.03 by Wilcoxon matched pairs signed rank test). (B) Comparison between pre and post γ-H2AX, pATM and OGG1 expressing operator's lymphocytes when they performed IEVAR.

4.4.1.2.7 Variation in operators' sensitivity to radiation exposure

4.4.1.2.7.1 Variation in operators' γ-H2AX expression after EVAR

In a further studying the biological effect of radiation exposure among operators, in a separate cohort of six operators (Table 4.3) who frequently perform endovascular interventions, γ-H2AX expression varied significantly between different operators (P<0.0001 by two-way ANOVA, Figure 4.12), despite similar baseline levels pre-operatively.

Table 4.3 Operators demographics

Operator	Age (years)	Gender	Years of Interventional		Interventional sessions/month
			As Trainee	As Consultant	
1	42	M	3	6	3
2	36	M	7	0	4
3	40	M	4	3	3
4	49	M	5	14	20
5	41	M	7	6	5
6	45	M	10	8	6-8

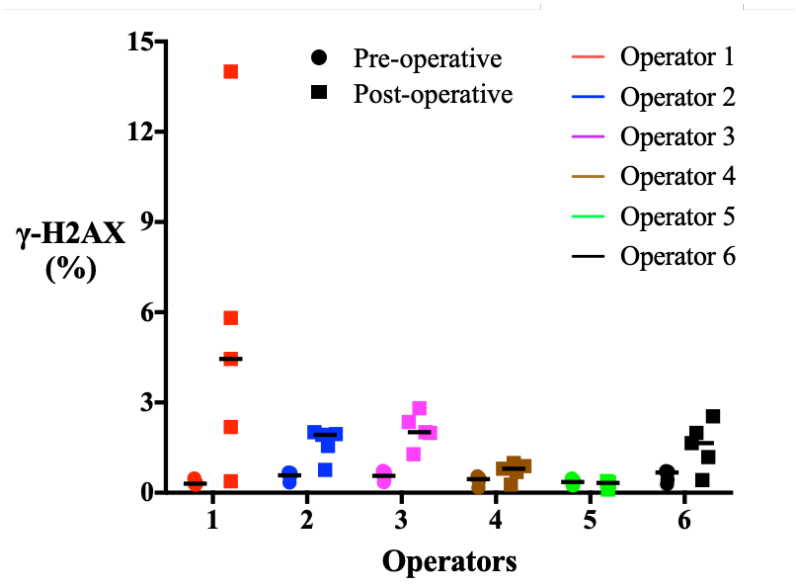

Figure 4.12 Peri-operative γ-H2AX changes in endovascular aortic repair operators
Pre and post-operative operators' γ-H2AX levels varied significantly when they performed 5 procedures for each operator (P<0.0001 by Two way ANOVA).

There was a significant variation in the changes in γ-H2AX expression even after standardising the level of this expression to the amount of radiation exposure in the different cases (P<0.003 by ANOVA, Figure 4.13).

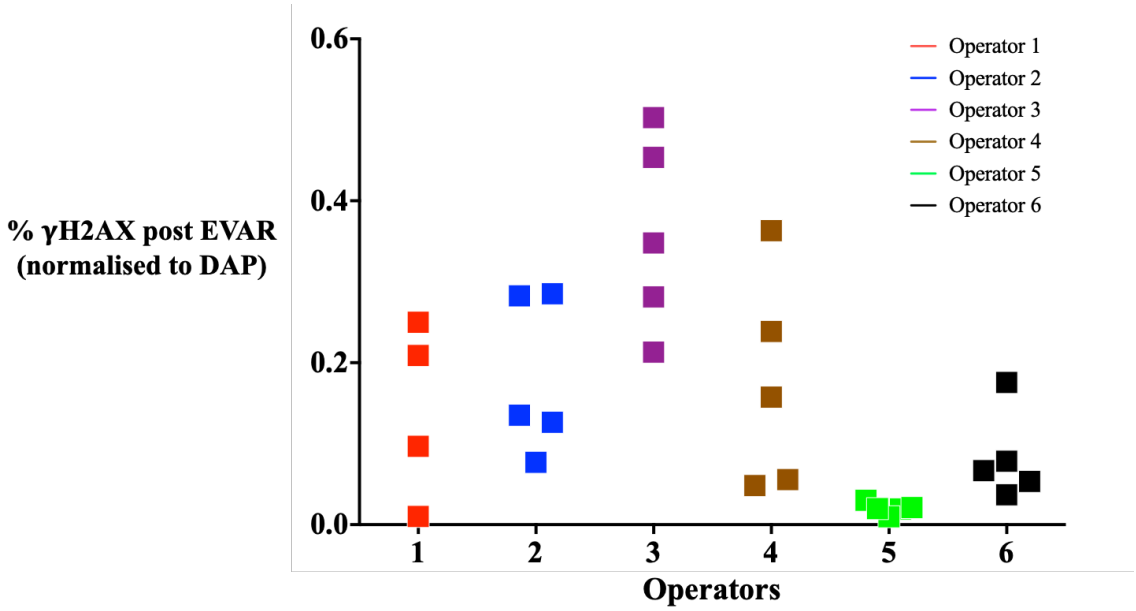

Figure 4.13 Variation in operators' γ-H2AX expression after EVAR
Post-operative levels of 6 operators' γ-H2AX varied significantly after 5 endovascular aortic repairs for each operator (P<0.0001 by Two Way ANOVA test) when they were exposed to standardised radiation doses.

4.4.1.2.7.1 Variation in operators' γ-H2AX in their CD3+ T lymphocytes in vitro

Following this finding of the variation in the 6 operators' response to radiation exposure, a further *in-vitro* analysis was carried out in a more controlled environment to eliminate any suggested variables such as intra-operative operators' behaviours during x-ray exposure.

There was a significant inter-individual variability in γ-H2AX on CD3+ T cells in response to a range of radiation doses (P<0.0001 by by Two-way analysis of variance test, Figure 4.14). The graph suggesting three different subgroups based on their response to radiation. For example, operator 3 showed the highest level of H2AX in-vitro and was among the high responders in-vivo too. Yet, operator 5 in vivo was a low responder despite being in the middle responders in-vitro. Therefore, it remains challenging to draw any conclusions from this part of the study considering low number of participants. Nevertheless, differences between in-vivo and in-vitro findings draw a great attention on multi-factors contribute to operators sensitivity to radiation exposure e.g., genetic, stress level, previous exposure, radiation protection strategies and intra-operative operators behaviours.

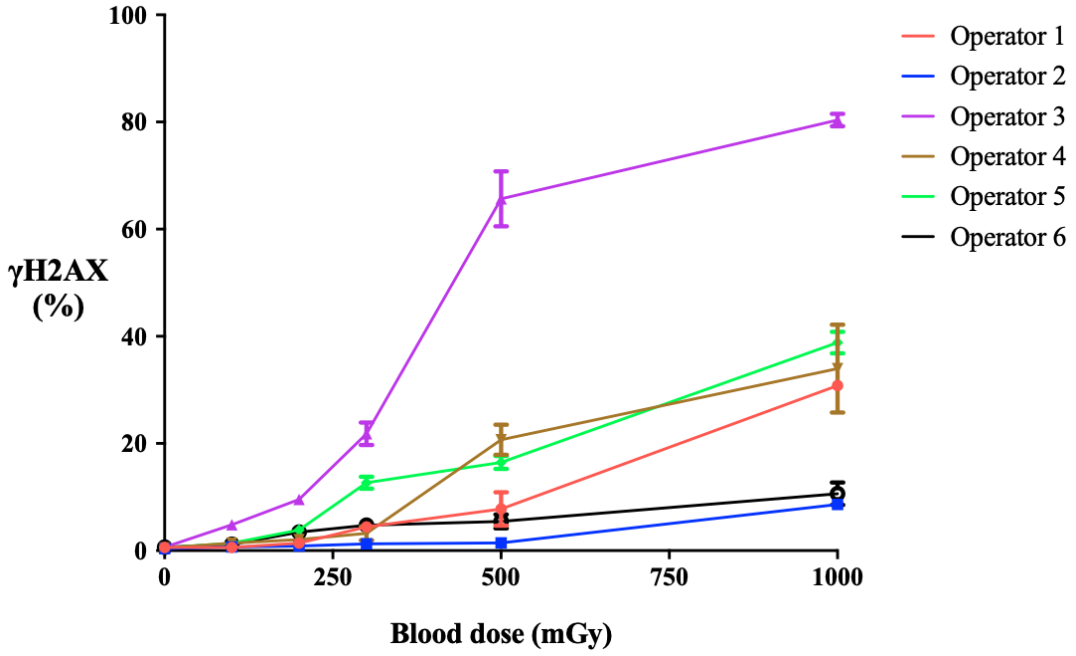

Figure 4.14 Variation in operators' γ-H2AX in vitro
In-vitro, levels of γ-H2AX in operators' CD3+ T lymphocytes irradiated in vitro were significantly different (P<0.0001, by Two Way ANOVA test) when their blood samples were irradiation to the same radiation doses.

4.4.1.2.8 Role of operators' leg protection in their response to radiation exposure

To identify the role of extra radiation protection using lower leg guards, another cohort of six operators performing BEVAR/FEVAR procedures were asked to wear lower leg shielding (Figure 4.15A). Blood samples were collected before and after they had performed each procedure, and then analysed using the previously described flow cytometric analysis to measure levels of in γ-H2AX and pATM in their T lymphocytes in section 4.4.1.4. However, there were similar over the leg exposure measurements, DAP and fluoroscopy times in both cohorts of complex EVAR cases, during which the operators wore leg lead shielding and those carried out without leg protection (Figure 4.15B).

A

Operators' Personal Dosimeters	
With Leg Shields	**Without Leg Shields**
28	16
40	23
69	40
73	94
74	145
112	149
129	153
130	171
153	416

B

	Without leg pads	With leg pads	*P value*
DAP (mGy.cm$^{2)}$	189927 (108919-417006)	165895 (149430-434251)	0.8
Screening time (mins)	94.39 (40.32-133.9)	97.70 (55.36-141.1)	0.5
Personal Dosimeter (µSv)	74 (28-153)	145 (16-416)	0.2

Figure 4.15 Comparison between radiation exposure with and without leg protection

(A) An operator is wearing leg lead guards (red arrows) with operators' personal dosimeter doses when they performed BEVAR/FEVAR with and without leg shields. (B) Comparable operators' radiation exposure when they performed BEVAR/FEVAR with and without leg protection.

Wearing lower leg lead protection (n=9 cases) abrogated the lymphocyte γ-H2AX and pATM response in operators after BEVAR/FEVAR, with no change in the expression of either markers immediately after the procedure (P=0.01 Bonferroni's multiple comparisons test, Figure 4.16).

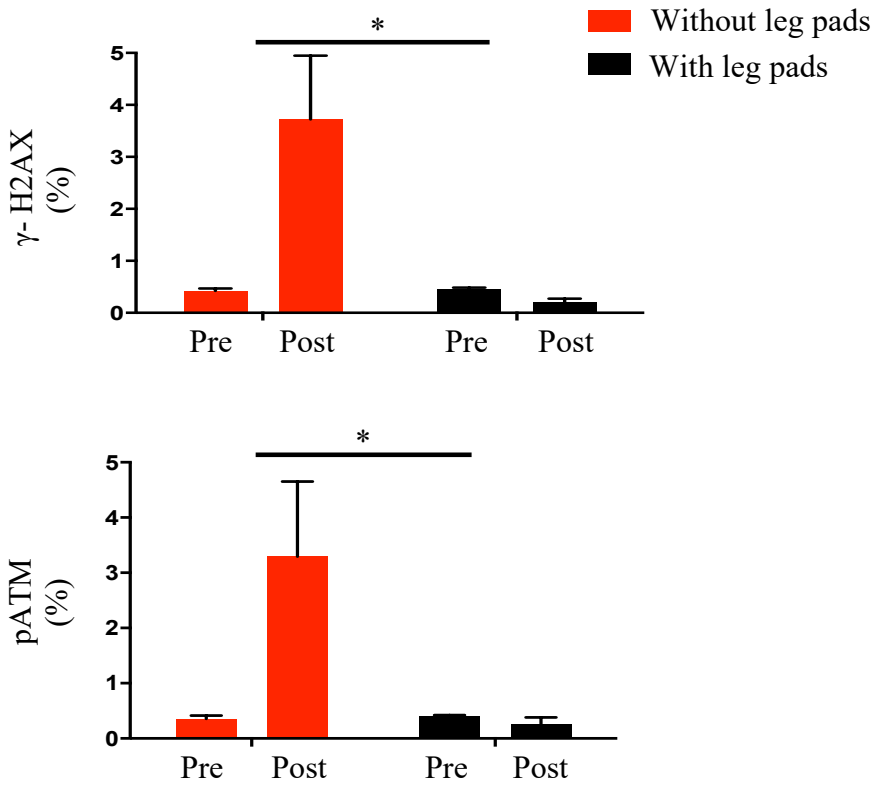

Figure 4.16 Effects of lower leg guards in operators' DNA damage biomarkers
Expression of γ-H2AX and pATM in operators after BEVAR/FEVAR did not change when they wore leg protection compared to without protection (P=0.01 by Bonferroni's multiple comparisons test).

4.4.2 Radiation Induced DNA Damage in Interventional Cardiologists During PCI

In this part of the study, we extended our evaluation of biological effect of radiation exposure during interventional procedures to include percutaneous coronary intervention (PCI) performed by interventional cardiologists.

This was to compare our findings of increased levels of DNA damage biomarkers among vascular surgeons and interventional radiologists when they carried out endovascular aortic repair to another cohort of interventionists such as interventional cardiologist who are also at risk of radiation exposure during performing interventional procedures such percutaneous coronary intervention and transcatheter aortic valve implantation.

4.4.2.1 Methods

4.5.1.1 Study participants

Interventional cardiologists were recruited to the study and blood samples were collected from them prior to and after they carried out elective percutaneous coronary interventions.

4.4.2.1.2 Procedural characteristics

All cardiac intervention procedures were carried out in the same cardiac catheter laboratory, equipped with the Philips Allura Xper FD20 fixed X-ray imaging system. Default settings were similar to EVAR procedures with a pulse rate of 7.5 pulses per second for background fluoroscopy and 2 frames per second for digital subtraction angiography acquisitions, and an x-ray beam filtration of 1.5 mm Al combined with 0.4 mm Cu was used.

4.4.2.1.3 Standard dosimetry

Electronic personal dosimeters were used to measure direct radiation exposure to record cumulative absorbed radiation dose for each case, as previously outlined in section 4.3.2.3. Dosimeters were attached to the recruited interventional cardiologists in the same positions as was used for the vascular surgeons recruited in section 4.4.1.3.

4.4.2.2.4 Flow cytometry

Changes in levels of DNA damage biomarkers (γ-H2AX & pATM) were measured in interventional cardiologist' lymphocytes during the peri-procedural period of percutaneous coronary intervention (PCI), using the same optimised protocol (as mentioned in section 4.3.1.3)

4.4.2.2 Results

4.5.2.1 Participants and procedure characteristics

A total of six senior interventional cardiologists were recruited to the study and performed nine elective percutaneous coronary interventions (Table 4.4).

Table 4.4 Interventional cardiologists' details and their workload

Operator	Age	Years of interventional		Interventional sessions/week	Interventional cases / session
		As Trainee	As Consultant		
1	46	8	9	3	3
2	62	8	22	2	4
3	53	5	18	4	4
4	36	6	1	3	5
5	52	5	16	2	3
6	42	8	5	1	3

4.4.2.2.3 Radiation exposure during PCI compared to EVAR

Interventional cardiologists radiation exposure during coronary intervention was measured with dose area product (DAP), screening/fluoroscopy time and operators'' personal dosimetry (Figure 4.17A). We found that interventional cardiologists were exposed to less radiation per case compared with vascular surgeons. This was evident as dose area product (DAP) and fluoroscopy times that were more than three and two folds, respectively, lower during PCI compared with infra-renal endovascular aortic repair (P=0.01, 0.007 respectively by Mann-Whitney U test, Figure 4.17B). Personal dosimetry similarly showed that the operator's leg dose was nearly 6 folds lower for PCI compared with IEVAR (P=0.003 by Mann-Whitney U test).

A

Radiation Exposure	Doses
DAP (mGy.cm²)	9940 (4440-170170)
Screening Time (mins)	11.2 (5.21-28.57)
Operator personal dosimetry (µSv)	
Under lead	0 (0-4)
Over lead	6 (2-11)
Leg	16 (2-48)

B

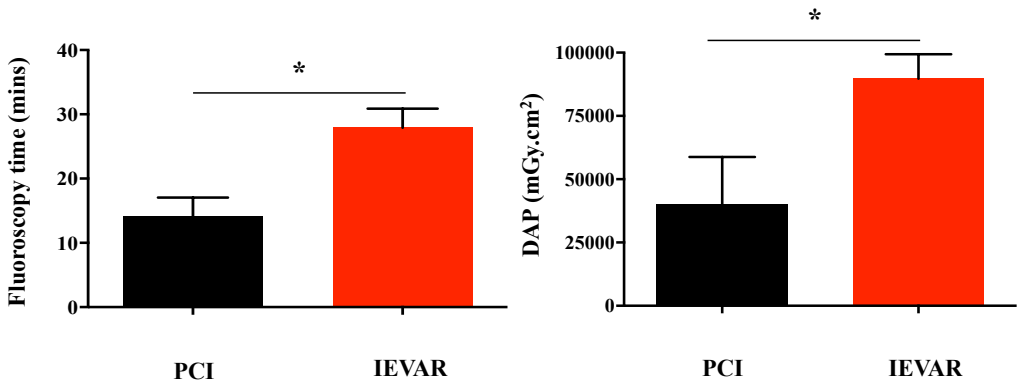

Figure 4.17 Radiation exposure during percutaneous coronary intervention
(A) Operators' radiation exposure measured by DAP, Screening time and personal dosimetry when they carried out coronary intervention. (B) IEVAR is associated with longer radiation exposure time and higher doses compared with PCI (P=0.01, 0.007 respectively by Mann Whitney test,).

4.4.2.2.4 γ-H2AX and pATM expression in interventional cardiologists after PCI

Immediately after percutaneous coronary intervention, both markers γ-H2AX and pATM increased significantly in interventional cardiologists' CD3+ T lymphocytes, and then returned to their base line after 24 hrs (P=0.004, 0.01 by Wilcoxon matched pairs signed rank test, Figure 4.18).

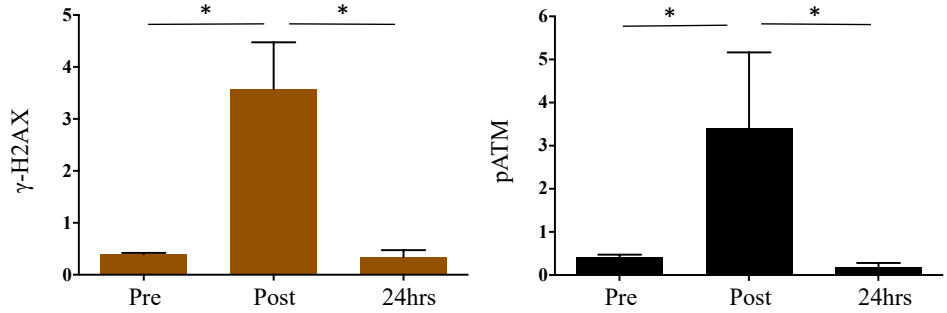

Figure 4.18 Peri-operative changes of γ-H2AX and pATM in interventional cardiologists
Both γ-H2AX and pATM expression was raised in interventional cardiologists immediately after they performed PCI and recovered after 24 hrs (P=0.004, 0.01 respectively by Wilcoxon matched pairs signed rank test).

4.4.2.2.4 Comparison between PCI and EVAR induced γ-H2AX and pATM upregulation

The magnitude of increase of γ-H2AX expression in cardiologists' lymphocytes was more than IEVAR (P<0.0001 by Mann-Whitney U test), and similar to complex BEVAR/FEVAR (Figure 4.19). pATM increased after PCI in interventional cardiologist similar to BEVAR/FEVAR levels however, there was no statically significant variation in the increased pATM between PCI and IEVAR.

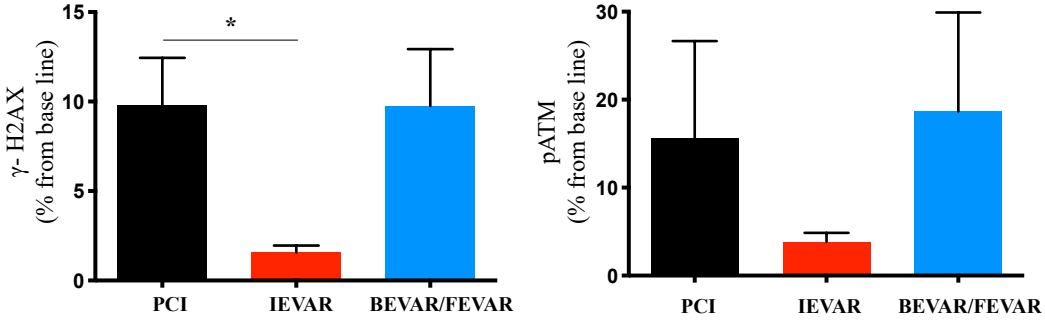

Figure 4.19 Changes of γ-H2AX and pATM expression after PCI and EVAR
A comparison between γ-H2AX and pATM expression in operators' when they performed PCI, IEVAR and BEVAR/FEVAR. Cardiologists performed PCI expressed higher levels of γ-H2AX in their CD3+ T lymphocytes compared to IEVAR operators (P<0.0001, by Mann Whitney test), and similar to BEVAR/FEVAR levels. pATM expression in cardiologists' lymphocytes was as high as BEVAR/FEVAR but not high enough to be significant compared to IEVAR.

4.5 Discussion

Humans experience cellular biological changes after exposure to ionising radiation, either accidental, while flying, during medical diagnostic/therapeutic procedures, or occupational exposure such as radiographers and nuclear workers. To accurately evaluate these radiation-induced neurobiological changes, biological dosimetry is required to assess the level of radiation exposure and its effects on individuals' cells and tissues. Ionising radiation directly deposits energy in nucleic acids in the cell. It indirectly generates reactive oxygen/nitrogen species, damaging the cellular DNA structure by causing base-pair alterations, nucleotide modifications, and single/double-strand DNA breaks.[75]

This study has shown a significant upregulation of DNA damage/repair biomarkers, γ-H2AX, and pATM, in both patients' and operators' circulating lymphocytes immediately after EVAR, particularly after complex EVAR. These changes were not seen during open aortic aneurysm surgical repair in either cohort, suggesting that our findings are related to radiation exposure rather than, for example, a stress response. This was more pronounced particularly in operators after performing complex EVAR procedures, which were associated with 3-fold longer fluoroscopy time and higher DAP compared with infra-renal EVAR, findings that match previous reports from our institution and others.[42, 43, 47, 48]

These expressions of γ-H2AX and pATM returned to their baseline 24 hrs after procedures suggesting that our observation was an acute response, followed by a DNA repair process as previously described by Löbrich et al., 2005.[72] γ-H2AX and pATM dephosphorylation has been demonstrated to be correlated with DSB repair, suggesting that the kinetics of H2AX and ATM foci loss of these protein biomarkers might also be used as an indicator of individual susceptibility to low-dose radiation exposure.[221, 329, 335] It is very important to point out that the kinetics of these biomarkers were not studied or measured and it is one of the limitation of this study.

Double-strand breaks are the most dangerous DNA damage patterns after ionising radiation. In response to these double-strand breaks, ATM activation and phosphorylation of several downstream DNA repair and checkpoint proteins, including H2AX. Histone H2AX is phosphorylated within seconds to form γ-H2AX, with levels peaking at 30 min. Both phosphorylated H2AX and ATM have been reported as useful biomarkers for low-dose radiation exposure in lymphocytes and fibroblasts, compared to cytogenetic biomarkers (e.g.,

dicentric chromosomes, micronuclei, and translocations), as H2AX and ATM foci formation can be detected as low as 1mGy.[72, 177, 222, 329, 335 - 338]

Myocardial perfusion CT imaging induced activation of the DNA damage response pathways demonstrated by an increase in H2AX and ATM phosphorylation and significant up-regulation of genes associated with DNA damage.[222] Low dose ionising radiation below one mGy during CT examinations resulted in a dose-dependent increase in γ-H2AX levels. These levels were also found to be negatively correlated with body size.[339, 340,341] These biomarkers can be used as a quantitative biomarker for low dose radiation exposure, as DNA damage measured by γ-H2AX levels in women exposed to chest-abdominal-pelvic CT was 8–10-fold higher than in patients had a chest CT only.[329] Levels of DNA damage biomarkers were affected by CT scan protocols, as γ-H2AX foci were significantly higher helical compared to sequential CT examinations demonstrating a significant correlation to radiation dose measured by dose length product.[342] Adjuvants to radiation for diagnostic or therapeutic purposes could worsen induced DNA damage. For example, iodine contrast was found to amplify DNA induced radiation damage in peripheral lymphocytes by approximately 30%, as patients who underwent contrast-enhanced CT had an increased amount of DNA radiation damage and γ-H2AX foci level compared to unenhanced CT examinations.[343 - 345]

18F-FDG PET/CT examination was found to increase levels of DNA damage biomarkers with peaks of radiation 18F-FDG PET/CT - induced DSBs were found 30 mins after FDG administration (radionuclide) and 5 mins after CT imaging. DSBs were strongly correlated with the dose length product.[346]

A randomised controlled study compares DNA damage resulting from diagnostic, interventional coronary angiography, and coronary CT scans. Patients who underwent coronary angiography showed γ-H2AX higher levels than patients exposed to coronary CT scans. H2AX foci in patients undergoing fluoroscopically guided cardiovascular procedures showed a linear correlation to dose area product for specific examination regions (e.g., pelvic and leg arteries).[335, 347]

T lymphocyte subsets' deeper phenotyping showed that both γ-H2AX and pATM were upregulated in T helper (CD4+) and cytotoxic cell (CD8+) subsets. γ-H2AX levels were significantly elevated in T helper cells and their CD4+ naïve and central memory cell subsets. Previous reports suggest that CD8+ cells are more sensitive to radiation-induced apoptosis in comparison with CD4+ cells.[348] Our finding of higher expression of γ-H2AX and pATM in CD4+ cells could, therefore, be explained by the fact that radiation-induced CD8+ apoptosis

might have prevented the detection of γ-H2AX- upregulation because the CD8+ cells had died. This inverse correlation between γ-H2AX-expression and radiation-induced apoptosis in lymphocytes subsets was suggested by Horn et al., 2013.[349]

No significant changes were observed in γ-H2AX and pATM expression in circulating hematopoietic stem cells (HSCs, CD45-/CD38-/CD34+/CD90+,) and haematopoietic stem/progenitor cells (HSPCs, CD45-/CD38+/CD34+/CD90-,). These cells circulate in very low numbers (<200). Therefore, it is very challenging to detect expression changes in these cells by flow cytometry.

The significant increase in 8-oxoguanine DNA glycosylase-1 (OGG1) expression in operators' lymphocytes after performing IEVAR suggests that radiation-induced DNA base oxidation most likely contributes to pATM upregulation rather than DNA double-stranded breaks. This was evident by the absence of γ-H2AX significant upregulation when operators performed IEVAR.[350]

Similar findings of an increase in both γ-H2AX and pATM in circulating lymphocytes were made in interventional cardiologists performing percutaneous coronary interventions. Even though PCIs are associated with lower radiation exposures than EVAR (roughly 6-fold lower than IEVAR), interventional cardiologists in the study perform more cases on each list (5-7 cases/day) compared with vascular surgeons. This may affect their sensitivity to radiation exposure or their DNA damage repair ability that might explain the upregulation of the two markers after low radiation dose PCI. This was also observed in studies from atomic bomb survivors, nuclear workers, and patients who received repeated low dose radiation showed an increased risk of radiation exposure's cumulative harmful effects.[351] Although interventional cardiologists recorded low dose radiation exposure below the international allowed limits the International Commission on Radiological Protection (ICRP), they demonstrated a significantly higher amount of DNA damage measured by the frequency of chromosomal aberrations and micronuclei compared with their unexposed colleagues. This was also observed when microarray analysis of a cohort of interventional cardiologists showed multiple miRNAs dysregulation, particularly brain-specific miR-134, associated with Alzheimer's disease and glioblastomas.[352 - 354]

Use of lower leg lead protection during complex BEVAR/FEVAR repairs that expose the operators to the most considerable amount of leg radiation completely abrogated the DNA damage/repair response previously detected without leg protection. This is even though radiation exposure during the procedures was similar to when their legs were not protected,

suggesting that operators' legs and their long bones received the most significant amount of scattered radiation that manifests as DNA damage in circulating lymphocytes.[355]

Our finding highlights the importance of operators ensuring that they wear lower leg lead protection and not rely solely on the lead skirt attached to the table for shielding the scatter radiation received from the x-ray source underneath the operating table.

Irradiating blood taken from our cohort of operators in vitro with fixed doses of radiation resulting in different amounts of upregulation of γ-H2AX and pATM, a proxy that may suggest operators have various sensitivities to the radiation exposure. Nevertheless, there was a difference between in-vivo and in-vitro findings which draw a great attention on multi-factors contribute to operators sensitivity to radiation exposure e.g., genetic, stress level, previous exposure, radiation protection strategies and intra-operative operators behaviours. Individual radiation sensitivity is a known phenomenon and means that perhaps screening operators decide who are at higher risk from radiation exposure and possibly should not perform lengthy procedures that are reliant on fluoroscopic guidance.[356] However, it remains challenging to draw any conclusions from this part of the study considering low number of participants.

Summary:

This study has shown that when patients and operators exposed to ionising radiation during endovascular aortic aneurysm repair, there circulating lymphocytes expressed a significant upregulation of DNA damage/repair biomarkers, γ-H2AX, and pATM. This acute response to radiation exposure was more pronounced after complex EVAR. Operators varied in their response to radiation exposure, which could be a tool to tailor individualised radiation protection strategies, taking in to account that lower leg shielding showed a significant role in mitigating the radiation induced DNA damage as per our study findings.

CHAPTER 5

General discussion and future studies

5.1 Discussion

The health effects of radiation exposure during diagnostic and interventional procedures are increasingly becoming of great concern. Minimally invasive endovascular procedures are associated with a risk of inevitable radiation exposure to both the patient and medical staff. The advent of complex aortic aneurysm repair such as fenestrated and branched endovascular repair has now resulted in an even higher risk of radiation exposure.[42, 45]

At a cellular level, ionising radiation can induce different forms of DNA damage, such as base damage, single-stranded, and double-strand breaks.[199, 200] As a response to these double-strand breaks, the DNA repair process is activated, causing phosphorylation of transcription factors and proteins such as ataxia-telangiectasia mutated (ATM) and histone protein H2AX resulting in pATM and γ-H2AX, respectively.

Both activated proteins (γ-H2AX and pATM) can be measured using flow cytometry or under immunofluorescence microscopy allowing detection of acute phase low radiation-induced DNA. Blood cells, in particular, circulating peripheral lymphocytes, are highly sensitive to radiation exposure.[228 - 233]

Branched and fenestrated endovascular aortic repair (BEVAR/FEVAR) are advanced procedures used to treat challenging aortic aneurysms with a custom-made device and are associated with a higher amount of radiation exposure to both patients and medical staff members. The aim of this study was to investigate the acute effect of radiation exposure to the patient and medical staff performing endovascular aortic aneurysm repair by measuring the changes in γ-H2AX and pATM expression in circulating lymphocytes during the peri-operative period.

5.1.1 Radiation induced H2AX and ATM phosphorylation in patient and operator

The initial aim of this study was to develop a flow cytometric assay for measuring the expression of DNA damage biomarkers, γ-H2AX, and pATM, on circulating lymphocytes.

This was particularly challenging as the half-life of γ-H2AX is between 30-60 mins from the time of exposure.[175]

In addition, there were no optimised protocols for the use of flow cytometry to measure these intracellular markers, and previous studies have utilised immunohistochemistry.[72, 177, 357]

The benefit of flow cytometry is the ability to quantify levels of expression in a higher-throughput way accurately. We optimised a flow cytometric method to measure γ-H2AX and pATM levels in circulating lymphocytes from blood samples. This method was validated using positive and negative controls, including samples from the open surgery group and pre-exposure blood samples. This flow cytometric technique also compared well with conventional immunohistochemistry.[72, 177, 357]

Following optimisation, γ-H2AX, and pATM levels in peripheral lymphocytes were measured during the peri-operative period of endovascular aortic intervention. Both DNA damage biomarkers (γ-H2AX and pATM) were studied in patients' mononuclear cells from after they exposed to radiation from computerised tomography (CT) scans,[72] and in children after cardiac catheterisation procedures.[177] Levels of both γ-H2AX and pATM expression were upregulated in operators and patients immediately after the endovascular aortic repair. Neither of these DNA damage markers γ-H2AX and pATM was increased in the control cohort of patients and operators after open aneurysm repair. Previous studies showed that open aortic aneurysm repair causes a higher degree of stress-related response measured by cortisol levels and incidence of systemic inflammatory response syndrome in patients compared with minimally invasive endovascular aortic aneurysm repair. However, this is clear that stress does not trigger the DNA damage/repair mechanism. Therefore, the findings of the present study suggest that DNA damage is directly related to radiation exposure during endovascular procedures.[358]

Neither γ-H2AX nor pATM has previously been studied in interventionists performing fluoroscopically guided aortic procedures. To our knowledge, the present study is the first to demonstrate elevated expression of these markers of DNA damage/repair in operators exposed to radiation.

5.1.2 Higher risk of DNA damage in complex EVAR

Compared to standard infra-renal EVAR, FEVAR and BEVAR are by large more challenging complex procedures that require prolonged screening time and higher use of radiation. These

procedures are, therefore, generally associated with greater radiation exposure to both the patient and the operator.[42, 47, 48, 50] The present study found that complex aortic procedures are associated with approximately a 3-fold longer fluoroscopy time, a 2-fold increase in dose area product (DAP), and 2-fold higher personal dosimetry readings for the operator at leg level compared to infra-renal endovascular aortic repair. This is similar to our previous and other centers' measurements of radiation during these procedures. [42, 47, 48, 50] These detected high levels of ionising radiation were reflected in the biological level as FEVAR & BEVAR were associated with a greater upregulation in both patient's and operators' DNA damage biomarkers in their circulating blood cells.

5.1.3 Variation in individual susceptibility to radiation

As part of this study, in order to identify variation between individuals' response to radiation exposure, operators' blood was collected and irradiated in vitro using a range of doses that exceeded usual occupational exposure to induce an amplified response with the purpose of revealing subtle differences in radiation sensitivity between individuals. This was carried out in a controlled environment and a standard manner on multiple occasions and γ-H2AX was measured using the same optimised flow cytometric method as used for the clinical part of our study.

Our analysis showed that there was an inter-individual variable in γ-H2AX response in the lymphocytes of operators when their blood samples were exposed to the same radiation doses. This observation suggests that interventionists' susceptibility to radiation-induced DNA damage may vary, and safe exposure limits may not apply universally.

Variation in individual radiosensitivity is a phenomenon that has been established in atomic bomb survivors, who showed a variable response to radiation exposure and differed in their propensity to develop radiation-induced malignancies.[310] Individual sensitivity to radiation is also thought to account for difference in response to radiotherapy in patients treated for malignancy.[276]

Some genetic mutations, such as ataxia telangiectasia and Nijmegen breakage syndromes, are known to predispose individuals to a higher risk of radiation induced malignancy.[279, 280] One wonders, however, how many more subtle, and perhaps as yet unknown, a genetic link to radio-susceptibility exist that dictate the individual's risk after exposure.

Identifying subtle variability in individuals' susceptibility to ionising radiation remains challenging, but some studies suggest that measuring the radiation-induced DNA damage/response after exposure could be a surrogate for radiosensitivity. This was observed when patients were exposed during computed tomography examinations as studied by counting the number of gamma-H2AX foci.[72]

When micronuclei assay was used to study in vivo and in vitro irradiated lymphocytes from different individuals, researchers found a significant variation in the amount of radiation-induced unrepaired DNA breaks at the time of cell division. It is also suggested that individuals' radiosensitivity depends on the variability of the efficiency of DNA damage repair and its' resulted cell apoptosis.[359] For example, DNA damage repair gene RAD51 was negatively correlated to the number of radiation-induced micronuclei and was suggested to be a marker for assessing individuals' radiosensitivity.[360]

However, a long-term follow-up study to connect interventionists' radiosensitivity to developing radiation-induced malignancies is required.[276]

This finding highlights the importance of future work in designing an individual risk profile in order to individually calculate the risk of radiation-induced cancer and to determine what radiation levels they can safely be exposed to.[177]

5.1.4 Effective DNA repair mechanism

Even though our finding of upregulation of γ-H2AX and pATM expression was detected immediately after the endovascular intervention, these levels returned to baseline 24 hrs after the procedure in patients and operators. This is secondary to the successful DNA repair process, which was previously reported in patients exposed to radiation.[72, 175] This observation could suggest that operators might need to avoid operating in two consecutive days in order to allow for adequate DNA repair. Further radiation exposure within 24 hrs might halt the repair process and result in mis-repaired genes that eventually might result in carcinogenesis.[361 – 362]

Further long-term follow-up studies are now required to identify if repeated low dose occupational exposure results in non or mis-repaired radiation-induced DNA damage and a consequently higher risk of mutagenesis and cancer development.

5.1.5 Biological assessment of cumulative low dose exposure

Calculations of cancer risk from ionising radiation exposure are mainly based on epidemiological studies such as from the atomic bomb survivors of Hiroshima and Nagasaki. These estimates of cancer risk are predominantly suitable for moderate to high radiation doses.[35, 363, 464] However, it is inappropriate to apply these risk estimates to occupational repeated exposures to low-dose radiation. Therefore, low dose induced cancer risk is calculated based on linear extrapolation using epidemiological data from high dose exposures. This calculated risk could be questionable as it does not take into account, for example, individual variation in response to radiation exposure, age, gender, and general health condition.[365 – 366] Biological markers, such as γ-H2AX and pATM, showed to be a very useful tool to study individual response during the acute phase. However, a long-term study in a larger cohort of medical staff is required using biological markers during endovascular interventions to lineate the direct relationship between exposure and its resulted cancer risk.

5.1.6 DNA damage in lymphocyte subpopulations

Further phenotyping of CD3+ T lymphocytes was carried out to determine which subset is particularly sensitive to radiation-induced DNA damage and whether this might predict long-term health consequences.

There was a postoperative rise in γ-H2AX and pATM in both T helper and cytotoxic cell populations (patients or operators), with a relatively higher expression of postoperative γ-H2AX in CD4+ T helper compared with CD8+ cytotoxic T cells. Other studies have also shown that CD8+ cells are more sensitive to radiation-induced apoptosis than CD4+ cells.[348] Radiation-induced apoptosis of CD8+ cells might even have under-estimated higher levels of γ-H2AX in lymphocytes.

Deeper T helper and cytotoxic T cell phenotyping showed postoperative γ-H2AX upregulation was significantly higher in CD4+ naïve and central memory cells compared with other subpopulations. Previous studies reported a significant drop in naïve and central memory cell levels in mice when they were exposed to ionising radiation, which is consistent with the findings of a decrease of naïve T cell numbers among atomic bomb survivors.[367, 368]

Radiation-induced DNA damage in these lymphocytes' subsets might contribute to chromosomal instability, which could be the first step towards lymphoid neoplasia such as lymphoma, multiple myeloma, and leukemia.[369]

5.1.7 Operators' DNA base damage during infra-renal EVAR

Operators performed infra-renal aortic repair (IEVAR) showed a significant increase in 8-oxoguanine DNA glycosylase-1 expression in their CD3+ lymphocytes. This reflects evidence of radiation-induced DNA base oxidation operators' circulating lymphocytes.[191] This also explains that the observed upregulation of pATM but not γ-H2AX in their lymphocytes after standard infra-renal EVAR, as pATM, is upregulated in response to both DNA base oxidation as well as double-strand breaks.

5.1.8 Advances in radiation protection strategies

Individuals, as well as institutions, have a great responsibility to tackle this imminent risk of radiation-induced health risks. Individual training, availability, and appropriate use of protective equipment and reliable radiation governing regulations are the way forward as fundamental radiation protection strategies.

5.1.8.1 Leg shields

Various occupational radiation protection tools that are available to the medical staff, such as lead aprons, thyroid collars, lead eye protection, and ceiling-suspended leaded shields.[370]

Operators do not routinely wear lower leg guards, although below table lead shielding is particularly crucial for minimising scatter radiation.[371] When our operators wore lower leg lead shielding during complex aneurysm repair, this mitigated the previously detected γ-H2AX and pATM radiation-induced upregulation in the same individuals.

This finding demonstrates that scatter radiation received at the operator lower part of the body was responsible for the majority of DNA damage occurs in lymphocytes. This observation matched our measurement of a 2-fold higher radiation level detected by operators' dosimetry at leg level when they performed BEVAR/FEVAR.

This result stresses the importance of using lower leg shielding as an essential occupational radiation protection strategy. One source of this high scatter radiation dose is the increase in using fixed-imaging systems to produce higher quality images contrasted to lower quality mobile c-arm. Nevertheless, that is associated with a significantly higher amount of scatter radiation.[372]

This observation, indeed, should encourage operators to use lower leg shielding as a routine method of protection rather than an optional method. Also, health care institutions should ensure the availability of these leg shields for their staff to use to minimise long term radiation occupational hazards.

5.1.8.2 Suspended Personal Radiation Protection Systems

One of the most recently used radiation protection equipment is the suspended radiation protection system (e.g., Zero-Gravity TM, Tidi products, Fenton, MI), which provides individual radiation protection. When using this system, operators do not have to suffer the burden of wearing heavy aprons throughout lengthy procedures.

Due to its suspended system, it allows the use of thicker lead protection (e.g., 1mm rather than 0.5mm), which covers a large surface area of the operator's body, down to the knees. Studies have shown that the suspended system provides greater protection to the chest, thyroid, and feet compared with conventional lead aprons.[373]

Its leaded-acrylic face-shield protects the front and sides of the head, which offered more than 80% protection compared with standard lead aprons with the ceiling and table-supported shields.[374] The zero-gravity system provides better eye protection than lead glasses, lead aprons, ceiling, and table-mounted shields; this is most probably due to coverage from all angles.[375, 376] Survey studies, amongst suspended protection system users, reported that the new system is more comfortable with less burden on the shoulder and lower back and less restrictive compared with conventional protection equipment. The main disadvantages are the cost of the system; particularly, as it only offers protection to the primary operator.

5.1.8.3 Real-time dosimetry

Medical facilities are responsible for medical staff dose monitoring to reduce the chances of exceeding the recommended dose limits published by the International Commission on Radiological Protection (ICRP).[35]

Monitoring these levels requires all staff to wear their dosimeter at all times while on duties that involve exposure to radiation. New methods of real-time monitoring of exposure have become available, and these might play an essential role in increasing operators' self-awareness to improve their intraoperative behaviours.

Greater awareness of exposures is required amongst medical staff, and they should be trained to appropriately follow radiation protection recommendations and minimise occupational radiation exposure and its long-term hazardous consequences.

Vascular surgeons are at higher risk of exposure to significant radiation doses compared with, for example, interventional cardiologists performing the percutaneous coronary intervention. From our observations, our vascular operators were exposed to approximately 6-fold higher amounts of radiation during IEVAR compared with percutaneous coronary interventions, accepting that interventional cardiologists operate more frequently.

5.1.8.4 Role of image fusion in radiation protection

Recent advances in x-ray guided EVAR procedures encouraged using 3D CT overlays, which is now started to be used in a few major vascular centres to carry out endovascular particularly complex procedures e.g., branched/fenestrated EVAR.

Image fusion uses a preoperative patient's CT scan, which is converted into a 3D model. This 3D model overlays the intra-operative real-time fluoroscopy images and automatically aligned to the patient's bony landmarks to produce a fused two-dimensionally and three-dimensional images. This new 3D overlaying technique provides a precise real-time intra-operative identification of target vessels and landmarks. 3D CT overlay reduces operative time, amount of radiation, contrast dose, complications, and improve patient outcome. In a comparison between 2D, 3D, and image fusion guided FEVAR/BEVAR, DAP was the lowest when image fusion guidance was used. 3D guided complex procedures, however, recorded the shortest fluoroscopy time.[377]

5.1.8.5 Alternative guidance to endovascular aneurysms repair

A small number of enthusiasts in the UK, Europe and USA are studying and optimising the role of endovascular robotic surgery for aortic aneurysm repair.[378] Although endovascular robot consoles provide an effective radiation protection method and avoid the burden of wearing lead aprons, these advanced robotic techniques remain unable to carry out complex endovascular tasks, particularly those that require haptic feedback

Few vascular centres worldwide are experimenting with the role of using magnetic resonance instead of conventional ionising radiation as a guide for endovascular aortic aneurysm repair. This technique will avoid the risk of radiation exposure. However, it remains in its infancy,

and a lot of modifications are required to achieve similar outcomes achieved by ionising radiation guided interventions.[379]

Other imaging modalities, such as intravascular ultrasound (IVUS) can provide operators with more intraoperative details. IVUS in an operator dependent technique and requires special training to interpret the data acquired. It can provide data that enable interventionists to identify atherosclerotic plaques sites and visceral vessels ostia. This can help in identifying target visceral vessels to facilitate stent-graft placements and visceral vessels cannulation, and consequently reduces the amount of radiation exposure during the procedure.[380]

5.1.8.6 Pharmacological/biological radioprotection

Studies suggest that antioxidants, such as thiol compounds, vitamin A, E, and C, showed promise as free radical scavengers, which can be an effective radiation protection strategy. These agents stabilise free radical molecules by either transferring hydrogen atoms or electrons to free radicals. This antioxidant effect is not specific to radiation-induced free radicals but can also be used to protect from any other oxidative stress-related activators.[381]

In a study, oral antioxidants such as ascorbate and N-acetylcysteine were found to be protective from radiation-induced-DNA damage, measured by gamma-H2AX foci. This was observed when antioxidants were given to patients before exposure to diagnostic imaging compared to the control group who did not take oral antioxidants. Therefore, antioxidants may provide an effective strategy to protect patients and interventionists from radiation-induced DNA damage. However, a long-term randomised control trials are required to study further their radiation-induced protective effect.

Gene and stem cell therapies might also provide a solution to mitigate hazardous radiation effects by tissue regeneration; however, these novel therapies remain in their primitive phase.[381- 383]

5.1.9 Occupational medical staff training and monitoring

Medical staff training on dose awareness and radiation protection is vital to minimise the effect of occupational radiation exposure. All interventional team members must receive standard training in radiation protection during fluoroscopically guided procedures, radiation safety, and how to use personal protection equipment. In some countries, a minimum of twenty hrs of initial training and periodic updates are required. Formal radiation safety training varies across

specialties. In the USA, for example, about than 2% of the interventional cardiology board exit exam content involves radiation-related issues to ensure a satisfactory level of radiation safety and awareness of its potential risks.[384]

In the UK, the new curriculum and training programme for vascular surgery trainees ensures trainees will receive regular training on policies of radiation protection and safety. Also, they are trained on principles and indications for vascular imaging, including dangers of ionising radiation, safe practice, monitoring of ionising radiation, and how to keep the radiation dose to a minimum by use of appropriate strategies. Trainees are also familiarised with regulations and requirements in the use of ionising radiation. All interventional team members are encouraged to attend Ionising Radiation (Medical Exposure) Regulations (IRMER) training courses.[385]

All operators engaged in procedures that involve radiation exposure should be very familiar with the "As Low as Reasonably Achievable (ALARA) principles" to minimise this exposure throughout interventions.[386] These principles include reducing the fluoroscopy rate where applicable, reducing the number of cinefluorography runs, and avoiding specific angulation such as left anterior oblique projection, which exposes the operating team to the highest amount of scatter radiation.[45]

All staff members are also encouraged to wear their dosimeters at all times, with cumulative doses monitored regularly by the internal medical physics department to avoid exceeding the internationally agreed limits of occupational exposure.

5.1.10 Implications of the study findings

This study was well received nationally and internationally since it was disseminated in a highly respected international journal and presented in multiple national and international meetings.

The study findings draw great attention to the acute effect of radiation-induced DNA damage, particularly among interventionists when they performed endovascular interventions. A novel finding raised concerns about the short and long term of occupational radiation exposure among vascular, radiology, and cardiology specialists. Therefore, as a response to my study's alarming results and the associated increasing concern of vascular intervention-related occupation hazards, the European Society of Endovascular Surgery has commissioned a committee to put in place European Society for Vascular Surgery (ESVS) radiation safety guidelines for endovascular aneurysm repair (EVAR) procedures to cover areas such as how

to set up the operating environment, considerations for patients, staff exposure, and best radiation safety practice.
Recovering the DNA damage biomarkers within 24 hours following radiation exposure could suggest avoiding operating in two consecutive days to allow the damaged DNA to be repaired prior to further exposure; a finding might be considered in the guidelines too.

The striking findings of the critical role of personal protection equipment, particularly lower leg shields, in mitigating radiation-induced DNA damage have encouraged many vascular centres to revise their risk assessments and standard operating procedures. More awareness and further work to reach a consensus are required to specify the minimal mandatory radiation protection personal equipment required in the health care settings.

Patients' reported DNA damage after endovascular intervention in this study urges more transparency about intra- and post-operative radiation risks associated with aortic intervention when discussing the benefits and risks of interventions with patients.

5.1.10 Limitations of the study

A few limitations of this study should be considered carefully when interpreting the study results and recommendations. One limitation was the retrospective analysis of peri-operative changes of peripheral blood cells in patients when they underwent aortic interventions due to the variability of the length of hospital stay and its associated variable availability of blood count results following major invasive open aortic repair compared to minimally invasive endovascular intervention.
The present study recruited operators in a single vascular/cardiology centre, resulting in a relatively low number of participants in particular subsections of the study, e.g., operators' sensitivity to radiation and the effect of radiation on interventional cardiologists.
Also, we did not study the relationship between the acute response (γ-H2AX and pATM levels) to radiation exposure and chronic low-dose radiation damage and the possibility of increased cancer risk. This would require longitudinal measurements in a larger cohort of operators with long-term prospective follow-up.

5.1.11 Future studies

A better understanding of radiation-induced DNA damage and repair is required. It is also essential to take into account factors such as age, sex, comorbidities, and chronicity of exposure and variation in individual susceptibility to radiation.

A study of the relationship between the acute response (γ-H2AX and pATM levels) and the residual damage that has accumulated over years of chronic exposure is important. Cytogenetic biomarkers can be used to demonstrate and quantify biological damage resulting from chronic exposure to low dose ionising radiation in vascular interventionists. Cytogenetic techniques, including solid staining and multiplex fluorescence in situ hybridization (mFISH) could be used to analyse patients and operators' blood samples for chromosome aberrations.[425] Quantitative polymerase chain reaction (qPCR) techniques could be used to analyse for aberrations in mitochondrial DNA.[426] Measurement of miRNAs, which are highly stable, could represent a useful tool in identifying the molecular connection between occupational chronic low dose radiation exposure and potential radiation induced health risks.[225, 226] Monte Carlo modelling is a method that can estimate the effective dose of radiation absorbed by the patient and operator during EVAR. Therefore, it would be beneficial for relating the effective radiation dose to the expression of DNA damage/repair markers over a longer period of time.[46] It would be beneficial to identify an individual risk profile and accurately calculate the risk of cancer to individuals. This will guide us to predict how much radiation each individual can be safely exposed to without increasing the risk of mutagenesis. Also, this risk profiling should be matched with operator intra-operative behaviour. This would provide us with a good plan of tailoring an individual radiation protection study taking in to account all previous factors in order to maximise the success rate of these strategies.

A longitudinal multi-centre study recruiting a larger number of interventionists is required to study their response to radiation exposure, variation in their response, and the effect of radiation protection strategies in mitigating radiation-induced adverse events. This includes studying multi-factors affecting operators' radiation susceptibility, such as wearing lower leg shields, zero gravity lead suits, and frequency of operating duties. It will be beneficial to study the radiation-induced biological effect across interventional specialties for better risk stratification per specialty rather. This would be better than the generalised risk assessment that was suggested not to be applicable considering our results among interventional cardiologists compared to vascular surgeons.

Appendix

6.1 Primary antibodies used for flow cytometric techniques to study DNA damage/repair biomarkers

Antibody	Conjugated fluorophore	Concentration µg/mL	Source
CD3	FITC	0.5	Miltenyi Biotec
CD4	Viogreen	0.5	BD Biosciences
CD8	APC/Cy7	0.5	BD Biosciences
CD45RO	PE/Cy7	0.5	BD Biosciences
CCR7	PerCP	0.5	BioLegend
CD14	Vioblue	0.25	BD Biosciences
CD45	Vioblue	0.5	BD Biosciences
CD34	PerCP	0.5	Miltenyi Biotec
CD38	Vioblue	0.5	Miltenyi Biotec
CD90	PE/Cy7	0.5	Miltenyi Biotec
CD34	PerCP/Cy7	0.5	Miltenyi Biotec
CD38	Vioblue	0.5	Miltenyi Biotec
CD56	Vioblue	0.5	Miltenyi Biotec
pATM	PE	0.1	BioLegend
γ-H2AX	APC	0.3	BD Biosciences
OGG1	PerCP	0.5	Novus Biologicals

6.2 Ethics Approval Documents

6.3 Publications, presentations, and published abstracts

Publications and presentations relate to this work include:

6.3.1 Publications

1. Patel, A. S., El-Sayed, T., Cho, J. S., Kelly, J. A., Ludwinski, F. E., Saha, P., Lyons, O. T., Smith, A., & Modarai, B. (2018). Response by Patel et al to Letter Regarding Article, "Radiation Induced DNA Damage in Operators Performing Endovascular Aortic Repair". Circulation, 137(24), 2680–2681. https://doi.org/10.1161/CIRCULATIONAHA.118.034639
2. El-Sayed, T., Patel, A. S., Cho, J. S., Kelly, J. A., Ludwinski, F. E., Saha, P., Lyons, O. T., Smith, A., Modarai, B., & Guy's and St Thomas' Cardiovascular Research Collaborative (2017). Radiation-Induced DNA Damage in Operators Performing Endovascular Aortic Repair. Circulation, 136(25), 2406–2416. https://doi.org/10.1161/CIRCULATIONAHA.117.029550

6.3.2 Published abstracts

1. El-Sayed, T., Patel A.S., Cho, J.S., Kelly J.A., Ludwinski, F.E., Saha, P. & Modarai B. (2018). Radiation Induced DNA Damage in Operators Performing Endovascular Aortic Repair. Journal of Vascular Surgery. 67(3),986.
2. El-Sayed, T., Patel A.S., Saha, P., Lyons, O., Ludwinski, F., Bell, R., Patel, S., Donati, T., Zayed, H., Sallam, M., Wilkins, J., Tyrrell, M., Dialynas, M., Sandford, B., Abisi, S., Gkoutzios, P., Black, S., Smith, A. & Modarai B. (2016). Radiation-Associated DNA Damage in Operators During Endovascular Aortic Repair. European Journal of Vascular and Endovascular Surgery. 52 (3), 279-422.
3. El-Sayed, T., Patel A.S., Saha, P., Lyons, O., Ludwinski, F., Bell, R., Patel, S., Donati, T., Zayed, H., Sallam, M., Wilkins, J., Tyrrell, M., Dialynas, M., Sandford, B., Abisi, S., Gkoutzios, P., Black, S., Smith, A. & Modarai B. (2016). Endovascular Aortic Repair Is Associated with Activation of Markers of Radiation Induced DNA Damage in Both Patients And Operators. European Journal of Vascular and Endovascular Surgery. 2016;52 (3), e55-e56.

6.3.3 Published Chapters

1. Patel, A.S., El-Sayed, T., Smith, A. & Modarai, A. (2017). Cellular markers of radiation damage during EVAR. Charing Cross International Symposium Update Book.

6.3.4 Oral presentations

1. El-Sayed, T., Patel A.S., Saha, P., Lyons, O., Ludwinski, F., Bell, R., Patel, S., Donati, T., Zayed, H., Sallam, M., Wilkins, J., Tyrrell, M., Dialynas, M., Sandford, B., Abisi, S., Gkoutzios, P., Black, S., Smith, A. & Modarai B. (2016). Radiation-Associated DNA Damage in Operators During Endovascular Aortic Repair. European Society of Vascular Surgery, Copenhagen, 2016
2. El-Sayed, T., Patel A.S., Saha, P., Lyons, O., Ludwinski, F., Bell, R., Patel, S., Donati, T., Zayed, H., Sallam, M., Wilkins, J., Tyrrell, M., Dialynas, M., Sandford, B., Abisi, S., Gkoutzios, P., Black, S., Smith, A. & Modarai B. (2016). Endovascular Aortic Repair Is Associated with Activation of Markers of Radiation Induced DNA Damage in Both Patients And Operators. British Society of Endovascular Therapy, Warwick, 2016

6.4 Prizes and awards

1. The Best Oral Presentation, European Society of Vascular Therapy (BSET) Annual Meeting, Copenhagen, Denmark, 2016

2. The Aortic Abstract Prize, British Society of Endovascular Surgery (ESVS) Annual Meeting, Warwick, UK, 2016

3. The Gold Medal, Yorkshire Vascular Forum, Leeds, UK, 2018

LIST OF REFERENCES

1. Patel, R., Sweeting, M. J., Powell, J. T., Greenhalgh, R. M., & EVAR trial investigators (2016). Endovascular versus open repair of abdominal aortic aneurysm in 15-years' follow-up of the UK endovascular aneurysm repair trial 1 (EVAR trial 1): a randomised controlled trial. Lancet (London, England), 388(10058), 2366–2374. https://doi.org/10.1016/S0140-6736(16)31135-7
2. Reeves, R. R., Ang, L., Bahadorani, J., Naghi, J., Dominguez, A., Palakodeti, V., Tsimikas, S., Patel, M. P., & Mahmud, E. (2015). Invasive Cardiologists Are Exposed to Greater Left Sided Cranial Radiation: The BRAIN Study (Brain Radiation Exposure and Attenuation During Invasive Cardiology Procedures). JACC. Cardiovascular interventions, 8(9), 1197–1206. https://doi.org/10.1016/j.jcin.2015.03.027
3. Roguin, A., Goldstein, J., Bar, O., & Goldstein, J. A. (2013). Brain and neck tumors among physicians performing interventional procedures. The American journal of cardiology, 111(9), 1368–1372. https://doi.org/10.1016/j.amjcard.2012.12.060
4. Linet, M. S., Kim, K. P., Miller, D. L., Kleinerman, R. A., Simon, S. L., & Berrington de Gonzalez, A. (2010). Historical review of occupational exposures and cancer risks in medical radiation workers. Radiation research, 174(6), 793–808. https://doi.org/10.1667/RR2014.1
5. Upchurch, G. R., Jr, & Schaub, T. A. (2006). Abdominal aortic aneurysm. American family physician, 73(7), 1198–1204.
6. Lucarotti, M., Shaw, E., Poskitt, K., & Heather, B. (1993). The Gloucestershire Aneurysm Screening Programme: the first 2 years' experience. European journal of vascular surgery, 7(4), 397–401. https://doi.org/10.1016/s0950-821x(05)80256-7
7. Norman, P. E., Jamrozik, K., Lawrence-Brown, M. M., Le, M. T., Spencer, C. A., Tuohy, R. J., Parsons, R. W., & Dickinson, J. A. (2004). Population based randomised controlled trial on impact of screening on mortality from abdominal aortic aneurysm. BMJ (Clinical research ed.), 329(7477), 1259. https://doi.org/10.1136/bmj.38272.478438.55
8. Vardulaki, K. A., Walker, N. M., Day, N. E., Duffy, S. W., Ashton, H. A., & Scott, R. A. (2000). Quantifying the risks of hypertension, age, sex and smoking in patients with abdominal aortic aneurysm. The British journal of surgery, 87(2), 195–200. https://doi.org/10.1046/j.1365-2168.2000.01353.x
9. Bengtsson, H., & Bergqvist, D. (1993). Ruptured abdominal aortic aneurysm: a population-based study. Journal of vascular surgery, 18(1), 74–80. https://doi.org/10.1067/mva.1993.42107
10. Office for National Statistics. Leading causes of Deaths in England and Wales, 2011. London: HMSO; 2012
11. Mortality results for randomised controlled trial of early elective surgery or ultrasonographic surveillance for small abdominal aortic aneurysms. The UK Small Aneurysm Trial Participants. (1998). Lancet (London, England), 352(9141), 1649–1655.
12. Metcalfe, D., Holt, P. J., & Thompson, M. M. (2011). The management of abdominal aortic aneurysms. BMJ (Clinical research ed.), 342, d1384. https://doi.org/10.1136/bmj.d1384
13. 13 - 21- Parodi, J. C., Palmaz, J. C., & Barone, H. D. (1991). Transfemoral intraluminal graft implantation for abdominal aortic aneurysms. Annals of vascular surgery, 5(6), 491–499. https://doi.org/10.1007/BF02015271

14. Dua, A., Kuy, S., Lee, C. J., Upchurch, G. R., Jr, & Desai, S. S. (2014). Epidemiology of aortic aneurysm repair in the United States from 2000 to 2010. Journal of vascular surgery, 59(6), 1512–1517. https://doi.org/10.1016/j.jvs.2014.01.007
15. Loftus, I., & Hinchliffe, R. (2018). Peripheral and abdominal aortic aneurysms. In Vascular and Endovascular Surgery: A Companion to Specialist Surgical Practice (6th ed., p. 207). Elsevier.
16. Naef A. P. (2004). The mid-century revolution in thoracic and cardiovascular surgery: Part 5. Interactive cardiovascular and thoracic surgery, 3(3), 415–422. https://doi.org/10.1016/j.icvts.2004.05.001
17. Nasim, A., Sayers, R. D., Thompson, M. M., Bell, P. R., & Bolia, A. (1994). Endovascular repair of abdominal aortic aneurysms. Lancet (London, England), 343(8907), 1230–1231. https://doi.org/10.1016/s0140-6736(94)92444-9
18. May, J., White, G., Waugh, R., Yu, W., & Harris, J. (1994). Treatment of complex abdominal aortic aneurysms by a combination of endoluminal and extraluminal aortofemoral grafts. Journal of vascular surgery, 19(5), 924–933. https://doi.org/10.1016/s0741-5214(94)70020-6
19. Chuter, T. A., Donayre, C., & Wendt, G. (1994). Bifurcated stent-grafts for endovascular repair of abdominal aortic aneurysm. Preliminary case reports. Surgical endoscopy, 8(7), 800–802. https://doi.org/10.1007/BF00593446
20. Coselli, J. S., Bozinovski, J., & LeMaire, S. A. (2007). Open surgical repair of 2286 thoracoabdominal aortic aneurysms. The Annals of thoracic surgery, 83(2), S862–S892. https://doi.org/10.1016/j.athoracsur.2006.10.088
21. Conrad, M. F., Crawford, R. S., Davison, J. K., & Cambria, R. P. (2007). Thoracoabdominal aneurysm repair: a 20-year perspective. The Annals of thoracic surgery, 83(2), S856–S892. https://doi.org/10.1016/j.athoracsur.2006.10.096
22. Rigberg, D. A., McGory, M. L., Zingmond, D. S., Maggard, M. A., Agustin, M., Lawrence, P. F., & Ko, C. Y. (2006). Thirty-day mortality statistics underestimate the risk of repair of thoracoabdominal aortic aneurysms: a state wide experience. Journal of vascular surgery, 43(2), 217–223. https://doi.org/10.1016/j.jvs.2005.10.070
23. Oderich, G. S. (2017). Historical Aspects and Evolution of Fenestrated and Branched Technology. In Endovascular Aortic Repair: Current Techniques with Fenestrated, Branched and Parallel Stent-Grafts (1st ed. 2017 ed., p. 3). New York, USA: Springer.
24. National Research Council. (2006). Health Risks from Exposure to Low Levels of Ionizing Radiation: BEIR VII Phase 2. Washington, DC: The National Academies Press. https://doi.org/10.17226/11340.
25. Ait-Ali, L., Andreassi, M. G., Foffa, I., Spadoni, I., Vano, E., & Picano, E. (2010). Cumulative patient effective dose and acute radiation-induced chromosomal DNA damage in children with congenital heart disease. Heart (British Cardiac Society), 96(4), 269–274. https://doi.org/10.1136/hrt.2008.160309.
26. Podgorsak, E. B. (2005). BASIC RADIATION PHYSICS. In Radiation Oncology Physics a Handbook for Teachers and Students: Handbook of Radiation Oncology (1st ed., Vol. 1, pp. 5–6). Vienna, Austria: Sales and Promotion Unit, Publishing Section, International Atomic Energy Agency.
27. Qi, C. (2016). Alpha decay as a probe for the structure of neutron-deficient nuclei. Reviews in Physics. (1), 77-89.
28. Welsh J. S. (2007). Beta decay in science and medicine. American journal of clinical oncology, 30(4), 437–439. https://doi.org/10.1097/01.coc.0000258753.09234.0c
29. Christillin, P. (1986). Nuclear Compton scattering. Journal of Physics G: Nuclear Physics. (12), 837–85. https://doi:10.1088/issn.0305-4616

30. Hill M. A. (2004). The variation in biological effectiveness of X-rays and gamma rays with energy. Radiation protection dosimetry, 112(4), 471–481. https://doi.org/10.1093/rpd/nch091
31. Donya, M., Radford, M., ElGuindy, A., Firmin, D., & Yacoub, M. H. (2014). Radiation in medicine: Origins, risks and aspirations. Global cardiology science & practice, 2014(4), 437–448. https://doi.org/10.5339/gcsp.2014.57
32. Straif, K., Benbrahim-Tallaa, L., Baan, R., Grosse, Y., Secretan, B., El Ghissassi, F., Bouvard, V., Guha, N., Freeman, C., Galichet, L., Cogliano, V., Grandjean, P., & WHO International Agency for Research on Cancer Monograph Working Group (2009). A review of human carcinogens - Part C: metals, arsenic, dusts, and fibres. Lancet Oncology, 10(5), 453-4.
33. International Commission on Radiation Units and Measurements. (1998). General Considerations. In Fundamental Quantities and Units for Ionising Radiation (Revised ed., Vol. 11, p. 12). Oxford, UK: International Commission on Radiation Units and Measurements.
34. Lomax, M. E., Folkes, L. K., & O'Neill, P. (2013). Biological consequences of radiation-induced DNA damage: relevance to radiotherapy. Clinical oncology (Royal College of Radiologists (Great Britain)), 25(10), 578–585. https://doi.org/10.1016/j.clon.2013.06.007
35. The 2007 Recommendations of the International Commission on Radiological Protection. ICRP publication 103. (2007). Annals of the ICRP, 37(2-4), 1–332. https://doi.org/10.1016/j.icrp.2007.10.003
36. Kim, S., Toncheva, G., Anderson-Evans, C., Huh, B. K., Gray, L., & Yoshizumi, T. (2009). Kerma area product method for effective dose estimation during lumbar epidural steroid injection procedures: phantom study. AJR. American journal of roentgenology, 192(6), 1726–1730. https://doi.org/10.2214/AJR.08.1713
37. University of California, S.C. (2000). Environmental Health & Safety, Radiation Safety Fundamentals Workbook. (4th ed., p. 55). University of California. Santa Cruz.
38. Devic, S., Tomic, N., & Lewis, D. (2016). Reference radiochromic film dosimetry: Review of technical aspects. Physica medica : PM : an international journal devoted to the applications of physics to medicine and biology : official journal of the Italian Association of Biomedical Physics (AIFB), 32(4), 541–556. https://doi.org/10.1016/j.ejmp.2016.02.008
39. Cember, H., & Johnson, T. E. (2008). HEALTH PHYSICS INSTRUMENTATION. In Introduction to Health Physics: Fourth Edition (4th ed., pp. 427–512). New York, USA: McGraw-Hill Education / Medical.
40. Oatway, WB., Holmes, A.L.J., Watson, S, S. & T Cabianca. (2016). *Ionising Radiation Exposure of the UK Population: 2010 Review. Public Health England*. Retrieved from https://assets.publishing.service.gov.uk/government/uploads/system/uploads/attachment_data/file/518487/PHE-CRCE-026_-_V1-1.pdf
41. Cuypers, P. W., Gardien, M., Buth, J., Peels, C. H., Charbon, J. A., & Hop, W. C. (2001). Randomized study comparing cardiac response in endovascular and open abdominal aortic aneurysm repair. The British journal of surgery, 88(8), 1059–1065. https://doi.org/10.1046/j.0007-1323.2001.01834.x
42. Howells, P., Eaton, R., Patel, A. S., Taylor, P., & Modarai, B. (2012). Risk of radiation exposure during endovascular aortic repair. European journal of vascular and endovascular surgery : the official journal of the European Society for Vascular Surgery, 43(4), 393–397. https://doi.org/10.1016/j.ejvs.2011.12.031
43. Hertault, A., Maurel, B., Sobocinski, J., Martin Gonzalez, T., Le Roux, M., Azzaoui, R., Midulla, M., & Haulon, S. (2014). Impact of hybrid rooms with image fusion on

radiation exposure during endovascular aortic repair. European journal of vascular and endovascular surgery : the official journal of the European Society for Vascular Surgery, 48(4), 382–390. https://doi.org/10.1016/j.ejvs.2014.05.026

44. Cusma, J. T., Bell, M. R., Wondrow, M. A., Taubel, J. P., & Holmes, D. R., Jr (1999). Real-time measurement of radiation exposure to patients during diagnostic coronary angiography and percutaneous interventional procedures. Journal of the American College of Cardiology, 33(2), 427–435. https://doi.org/10.1016/s0735-1097(98)00591-9
45. Sailer, A. M., Schurink, G. W., Bol, M. E., de Haan, M. W., van Zwam, W. H., Wildberger, J. E., & Jeukens, C. R. (2015). Occupational Radiation Exposure During Endovascular Aortic Repair. Cardiovascular and interventional radiology, 38(4), 827–832. https://doi.org/10.1007/s00270-014-1025-8
46. Blaszak, M. A., & Juszkat, R. (2014). Monte Carlo simulations for assessment of organ radiation doses and cancer risk in patients undergoing abdominal stent-graft implantation. European journal of vascular and endovascular surgery : the official journal of the European Society for Vascular Surgery, 48(1), 23–28. https://doi.org/10.1016/j.ejvs.2014.03.014
47. Maurel, B., Sobocinski, J., Perini, P., Guillou, M., Midulla, M., Azzaoui, R., & Haulon, S. (2012). Evaluation of radiation during EVAR performed on a mobile C-arm. European journal of vascular and endovascular surgery : the official journal of the European Society for Vascular Surgery, 43(1), 16–21. https://doi.org/10.1016/j.ejvs.2011.09.017
48. Albayati, M. A., Kelly, S., Gallagher, D., Dourado, R., Patel, A. S., Saha, P., Bajwa, A., El-Sayed, T., Salter, R., Gkoutzios, P., Carrell, T., Abisi, S., & Modarai, B. (2015). Editor's choice--Angulation of the C-arm during complex endovascular aortic procedures increases radiation exposure to the head. European journal of vascular and endovascular surgery : the official journal of the European Society for Vascular Surgery, 49(4), 396–402. https://doi.org/10.1016/j.ejvs.2014.12.032
49. Panuccio, G., Greenberg, R. K., Wunderle, K., Mastracci, T. M., Eagleton, M. G., & Davros, W. (2011). Comparison of indirect radiation dose estimates with directly measured radiation dose for patients and operators during complex endovascular procedures. Journal of vascular surgery, 53(4), 885–894. https://doi.org/10.1016/j.jvs.2010.10.106
50. Patel, A. P., Gallacher, D., Dourado, R., Lyons, O., Smith, A., Zayed, H., Waltham, M., Sabharwal, T., Bell, R., Carrell, T., Taylor, P., & Modarai, B. (2013). Occupational radiation exposure during endovascular aortic procedures. European journal of vascular and endovascular surgery : the official journal of the European Society for Vascular Surgery, 46(4), 424–430. https://doi.org/10.1016/j.ejvs.2013.05.023
51. Bordoli, S. J., Carsten, C. G., 3rd, Cull, D. L., Johnson, B. L., & Taylor, S. M. (2014). Radiation safety education in vascular surgery training. Journal of vascular surgery, 59(3), 860–864. https://doi.org/10.1016/j.jvs.2013.10.085
52. Charlton, D. E., Nikjoo, H., & Humm, J. L. (1989). Calculation of initial yields of single- and double-strand breaks in cell nuclei from electrons, protons and alpha particles. International journal of radiation biology, 56(1), 1–19. https://doi.org/10.1080/09553008914551141
53. Srinivas, U. S., Tan, B., Vellayappan, B. A., & Jeyasekharan, A. D. (2019). ROS and the DNA damage response in cancer. Redox biology, 25, 101084. https://doi.org/10.1016/j.redox.2018.101084

54. Scholes G. (1963). The Radiation Chemistry Of Aqueous Solutions Of Nucleic Acids And Nucleoproteins. Progress in biophysics and molecular biology, 13, 59–104. https://doi.org/10.1016/s0079-6107(63)80014-0
55. Dizdaroglu, M., & Jaruga, P. (2012). Mechanisms of free radical-induced damage to DNA. Free radical research, 46(4), 382–419. https://doi.org/10.3109/10715762.2011.653969
56. Roots, R., & Okada, S. (1972). Protection of DNA molecules of cultured mammalian cells from radiation-induced single-strand scissions by various alcohols and SH compounds. International journal of radiation biology and related studies in physics, chemistry, and medicine, 21(4), 329–342. https://doi.org/10.1080/09553007214550401
57. Lindahl,T. Instability and decay of the primary structure of DNA. Nature, 1993;362:709–715.
58. Bjelland, S., & Seeberg, E. (2003). Mutagenicity, toxicity and repair of DNA base damage induced by oxidation. Mutation research, 531(1-2), 37–80. https://doi.org/10.1016/j.mrfmmm.2003.07.002
59. Bauer, N. C., Corbett, A. H., & Doetsch, P. W. (2015). The current state of eukaryotic DNA base damage and repair. Nucleic acids research, 43(21), 10083–10101. https://doi.org/10.1093/nar/gkv1136
60. Dizdaroglu, M., & Jaruga, P. (2012). Mechanisms of free radical-induced damage to DNA. Free radical research, 46(4), 382–419. https://doi.org/10.3109/10715762.2011.653969.
61. Steenken, S. (1989). Purine bases, nucleosides, and nucleotides: aqueous solution redox chemistry and transformation reactions of their radical cations and e - and OH adducts. Chemical Reviews. 89 (3), 503-520. https://doi.org/10.1021/cr00093a003.
62. Steenken, S. & Jovanovic, S. (1997). How easily oxidizable is DNA? One-electron reduction potentials of adenosine and guanosine radicals in aqueous solution. Journal of the American Chemical Society. 119 (3), 617-618. https:doi.org/10.1021/ja962255b
63. Steenken, S., Telo, J.P., Novais, H.M. & Candeias, L.P. (1992). One-electron-reduction potentials of pyrimidine bases, nucleosides, and nucleotides in aqueous solution. Consequences for DNA redox chemistry. Journal of the American Chemical Society. 114 (12), 4701-4709. https://doi.org/10.1021/ja00038a037
64. Chatgilialoglu, C., D'Angelantonio, M., Guerra, M., Kaloudis, P., & Mulazzani, Q. G. (2009). A reevaluation of the ambident reactivity of the guanine moiety towards hydroxyl radicals. Angewandte Chemie (International ed. in English), 48(12), 2214–2217. https://doi.org/10.1002/anie.200805372
65. Chatgilialoglu, C., D'Angelantonio, M., Kciuk, G., & Bobrowski, K. (2011). New insights into the reaction paths of hydroxyl radicals with 2'-deoxyguanosine. Chemical research in toxicology, 24(12), 2200–2206. https://doi.org/10.1021/tx2003245
66. Mundy, C.J., Colvin & M.E., Quong, A.A. (2002). Irradiated guanine: a Car-Parrinello molecular dynamics study of dehydrogenation in the presence of an OH radical. The Journal of Physical Chemistry.106 (43), 10063-10071. https://doi.org/10.1021/jp0212904
67. Wu, Y., Mundy, C.J., Colvin, M.E. & Car, R. (2004). On the mechanisms of OH radical induced DNA-base damage: a comparative quantum chemical and Car-Parrinello molecular dynamics study. The Journal of Physical Chemistry. 108 (15), 2922-2929. https://doi.org/10.1021/jp0363592
68. Steenken, S. & Jovanovic, S.V. (1997). How easily oxidizable is DNA? One-electron reduction potentials of adenosine and guanosine radicals in aqueous solution. Journal of the American Chemical Society, 119(3), 617-618. https://doi.org/10.1021/ja962255b

69. Caldecott K. W. (2008). Single-strand break repair and genetic disease. Nature reviews. Genetics, 9(8), 619–631. https://doi.org/10.1038/nrg2380
70. Demple, B., & DeMott, M. S. (2002). Dynamics and diversions in base excision DNA repair of oxidized abasic lesions. Oncogene, 21(58), 8926–8934. https://doi.org/10.1038/sj.onc.1206178
71. Hegde, M. L., Hazra, T. K., & Mitra, S. (2008). Early steps in the DNA base excision/single-strand interruption repair pathway in mammalian cells. Cell research, 18(1), 27–47. https://doi.org/10.1038/cr.2008.8
72. Löbrich, M., Rief, N., Kühne, M., Heckmann, M., Fleckenstein, J., Rübe, C., & Uder, M. (2005). In vivo formation and repair of DNA double-strand breaks after computed tomography examinations. Proceedings of the National Academy of Sciences of the United States of America, 102(25), 8984–8989. https://doi.org/10.1073/pnas.0501895102
73. Vítor, A. C., Huertas, P., Legube, G., & de Almeida, S. F. (2020). Studying DNA Double-Strand Break Repair: An Ever-Growing Toolbox. Frontiers in molecular biosciences, 7, 24. https://doi.org/10.3389/fmolb.2020.00024
74. Rothkamm, K., Krüger, I., Thompson, L. H., & Löbrich, M. (2003). Pathways of DNA double-strand break repair during the mammalian cell cycle. Molecular and cellular biology, 23(16), 5706–5715. https://doi.org/10.1128/mcb.23.16.5706-5715.2003
75. Reisz, J. A., Bansal, N., Qian, J., Zhao, W., & Furdui, C. M. (2014). Effects of ionizing radiation on biological molecules--mechanisms of damage and emerging methods of detection. Antioxidants & redox signaling, 21(2), 260–292. https://doi.org/10.1089/ars.2013.5489
76. Hoeijmakers J. H. (2009). DNA damage, aging, and cancer. The New England journal of medicine, 361(15), 1475–1485. https://doi.org/10.1056/NEJMra0804615
77. Krokan, H. E., & Bjørås, M. (2013). Base excision repair. Cold Spring Harbor perspectives in biology, 5(4), a012583. https://doi.org/10.1101/cshperspect.a012583
78. Parikh, S. S., Mol, C. D., Slupphaug, G., Bharati, S., Krokan, H. E., & Tainer, J. A. (1998). Base excision repair initiation revealed by crystal structures and binding kinetics of human uracil-DNA glycosylase with DNA. The EMBO journal, 17(17), 5214–5226. https://doi.org/10.1093/emboj/17.17.5214
79. Krokan, H. E., & Bjørås, M. (2013). Base excision repair. Cold Spring Harbor perspectives in biology, 5(4), a012583. https://doi.org/10.1101/cshperspect.a012583
80. Burkovics, P., Szukacsov, V., Unk, I., & Haracska, L. (2006). Human Ape2 protein has a 3'-5' exonuclease activity that acts preferentially on mismatched base pairs. Nucleic acids research, 34(9), 2508–2515. https://doi.org/10.1093/nar/gkl259
81. Bennett, M.D. & Leitch, I.J. (1997). Nuclear Dna Amounts In Angiosperms - 583 new estimates, Annals of Botany. 80 (2),169–196. https://doi.org/10.1006/anbo.1997.0415.
82. Bollum F. J. (1960). Calf thymus polymerase. The Journal of biological chemistry, 235, 2399–2403.
83. Falaschi, A., & Kornberg, A. (1966). Biochemical studies of bacterial sporulation. II. Deoxy- ribonucleic acid polymerase in spores of Bacillus subtilis. The Journal of biological chemistry, 241(7), 1478–1482.
84. Lehman, I. R., Bessman, M. J., Simms, E. S., & Kornberg, A. (1958). Enzymatic synthesis of deoxyribonucleic acid. I. Preparation of substrates and partial purification of an enzyme from Escherichia coli. The Journal of biological chemistry, 233(1), 163–170.
85. Richardson, C. C., Schildkraut, C. L., Aposhian, H. V., & Kornberg, A. (1964). Enzymatic Synthesis Of Deoxyribonucleic Acid. Xiv. Further Purification And

Properties Of Deoxyribonucleic Acid Polymerase Of Escherichia Coli. The Journal Of Biological Chemistry, 239, 222–232.
86. Schachman, H. K., Adler, J., Radding, C. M., Lehman, I. R., & Kornberg, A. (1960). Enzymatic synthesis of deoxyribonucleic acid. VII. Synthesis of a polymer of deoxyadenylate and deoxythymidylate. The Journal of biological chemistry, 235, 3242–3249.
87. Zimmerman B. K. (1966). Purification and properties of deoxyribonucleic acid polymerase from Micrococcus lysodeikticus. The Journal of biological chemistry, 241(9), 2035–2041.
88. Whitehouse, C. J., Taylor, R. M., Thistlethwaite, A., Zhang, H., Karimi-Busheri, F., Lasko, D. D., Weinfeld, M., & Caldecott, K. W. (2001). XRCC1 stimulates human polynucleotide kinase activity at damaged DNA termini and accelerates DNA single-strand break repair. Cell, 104(1), 107–117. https://doi.org/10.1016/s0092-8674(01)00195-7
89. Kubota, Y., Nash, R. A., Klungland, A., Schär, P., Barnes, D. E., & Lindahl, T. (1996). Reconstitution of DNA base excision-repair with purified human proteins: interaction between DNA polymerase beta and the XRCC1 protein. The EMBO journal, 15(23), 6662–6670.
90. Marintchev, A., Mullen, M. A., Maciejewski, M. W., Pan, B., Gryk, M. R., & Mullen, G. P. (1999). Solution structure of the single-strand break repair protein XRCC1 N-terminal domain. Nature structural biology, 6(9), 884–893. https://doi.org/10.1038/12347
91. Braithwaite, E. K., Prasad, R., Shock, D. D., Hou, E. W., Beard, W. A., & Wilson, S. H. (2005). DNA polymerase lambda mediates a back-up base excision repair activity in extracts of mouse embryonic fibroblasts. The Journal of biological chemistry, 280(18), 18469–18475. https://doi.org/10.1074/jbc.M411864200
92. Beard, W. A., Prasad, R., & Wilson, S. H. (2006). Activities and mechanism of DNA polymerase beta. Methods in enzymology, 408, 91–107. https://doi.org/10.1016/S0076-6879(06)08007-4
93. Liu Y, Prasad R, Beard WA, Kedar PS, Hou EW, Shock DD, Wilson SH. Coordination of Steps in Single-nucleotide Base Excision Repair Mediated by Apurinic/Apyrimidinic Endonuclease 1 and DNA Polymerase β". Journal of Biological Chemistry. 2007;282:13532–13541.
94. Pascal, J. M., O'Brien, P. J., Tomkinson, A. E., & Ellenberger, T. (2004). Human DNA ligase I completely encircles and partially unwinds nicked DNA. Nature, 432(7016), 473–478. https://doi.org/10.1038/nature03082
95. Lehman I. R. (1974). DNA ligase: structure, mechanism, and function. Science (New York, N.Y.), 186(4166), 790–797. https://doi.org/10.1126/science.186.4166.790
96. Carroll, S.B.,Wessler, S.R., Griffiths, A.J.F.l. & Lewontin RC (2008). Introduction to genetic analysis. New York: W.H. Freeman and Co. p. 534.
97. Friedberg, E.C., Walker, G.C., Siede, W., Wood, R.D., Schultz, R.A. & Ellenberger, T. (2006) DNA Repair and Mutagenesis. 2nd Edition, ASM Press, Washington DC.
98. Park, C. J., & Choi, B. S. (2006). The protein shuffle. Sequential interactions among components of the human nucleotide excision repair pathway. The FEBS journal, 273(8), 1600–1608. https://doi.org/10.1111/j.1742-4658.2006.05189.x
99. Gillet, L. C., & Schärer, O. D. (2006). Molecular mechanisms of mammalian global genome nucleotide excision repair. Chemical reviews, 106(2), 253–276. https://doi.org/10.1021/cr040483f

100. Hanawalt, P. C., & Spivak, G. (2008). Transcription-coupled DNA repair: two decades of progress and surprises. Nature reviews. Molecular cell biology, 9(12), 958–970. https://doi.org/10.1038/nrm2549
101. Evans, E., Moggs, J. G., Hwang, J. R., Egly, J. M., & Wood, R. D. (1997). Mechanism of open complex and dual incision formation by human nucleotide excision repair factors. The EMBO journal, 16(21), 6559–6573. https://doi.org/10.1093/emboj/16.21.6559
102. Volker, M., Moné, M. J., Karmakar, P., van Hoffen, A., Schul, W., Vermeulen, W., Hoeijmakers, J. H., van Driel, R., van Zeeland, A. A., & Mullenders, L. H. (2001). Sequential assembly of the nucleotide excision repair factors in vivo. Molecular cell, 8(1), 213–224. https://doi.org/10.1016/s1097-2765(01)00281-7
103. Evans, E., Fellows, J., Coffer, A., & Wood, R. D. (1997). Open complex formation around a lesion during nucleotide excision repair provides a structure for cleavage by human XPG protein. The EMBO journal, 16(3), 625–638. https://doi.org/10.1093/emboj/16.3.625
104. Volker, M., Moné, M. J., Karmakar, P., van Hoffen, A., Schul, W., Vermeulen, W., Hoeijmakers, J. H., van Driel, R., van Zeeland, A. A., & Mullenders, L. H. (2001). Sequential assembly of the nucleotide excision repair factors in vivo. Molecular cell, 8(1), 213–224. https://doi.org/10.1016/s1097-2765(01)00281-7
105. Schärer O. D. (2013). Nucleotide excision repair in eukaryotes. Cold Spring Harbor perspectives in biology, 5(10), a012609. https://doi.org/10.1101/cshperspect.a012609
106. Peltomäki P. (2001). DNA mismatch repair and cancer. Mutation research, 488(1), 77–85. https://doi.org/10.1016/s1383-5742(00)00058-2
107. Kolodner, R. D., & Marsischky, G. T. (1999). Eukaryotic DNA mismatch repair. Current opinion in genetics & development, 9(1), 89–96. https://doi.org/10.1016/s0959-437x(99)80013-6
108. Buermeyer, A. B., Deschênes, S. M., Baker, S. M., & Liskay, R. M. (1999). Mammalian DNA mismatch repair. Annual review of genetics, 33, 533–564. https://doi.org/10.1146/annurev.genet.33.1.533
109. Jiricny, J., & Nyström-Lahti, M. (2000). Mismatch repair defects in cancer. Current opinion in genetics & development, 10(2), 157–161. https://doi.org/10.1016/s0959-437x(00)00066-6
110. Gradia, S., Subramanian, D., Wilson, T., Acharya, S., Makhov, A., Griffith, J., & Fishel, R. (1999). hMSH2-hMSH6 forms a hydrolysis-independent sliding clamp on mismatched DNA. Molecular cell, 3(2), 255–261. https://doi.org/10.1016/s1097-2765(00)80316-0
111. Blackwell, L. J., Bjornson, K. P., & Modrich, P. (1998). DNA-dependent activation of the hMutSalpha ATPase. The Journal of biological chemistry, 273(48), 32049–32054. https://doi.org/10.1074/jbc.273.48.32049
112. Buermeyer, A. B., Deschênes, S. M., Baker, S. M., & Liskay, R. M. (1999). Mammalian DNA mismatch repair. Annual review of genetics, 33, 533–564. https://doi.org/10.1146/annurev.genet.33.1.533
113. Umar, A., Buermeyer, A. B., Simon, J. A., Thomas, D. C., Clark, A. B., Liskay, R. M., & Kunkel, T. A. (1996). Requirement for PCNA in DNA mismatch repair at a step preceding DNA resynthesis. Cell, 87(1), 65–73. https://doi.org/10.1016/s0092-8674(00)81323-9
114. Lomax, M. E., Folkes, L. K., & O'Neill, P. (2013). Biological consequences of radiation-induced DNA damage: relevance to radiotherapy. Clinical oncology (Royal College of Radiologists (Great Britain)), 25(10), 578–585. https://doi.org/10.1016/j.clon.2013.06.007

115. Nikjoo, H., O'Neill, P., Goodhead, D. T., & Terrissol, M. (1997). Computational modelling of low-energy electron-induced DNA damage by early physical and chemical events. International journal of radiation biology, 71(5), 467–483. https://doi.org/10.1080/095530097143798
116. Nikjoo, H., O'Neill, P., Wilson, W. E., & Goodhead, D. T. (2001). Computational approach for determining the spectrum of DNA damage induced by ionizing radiation. Radiation research, 156(5 Pt 2), 577–583. https://doi.org/10.1667/0033-7587(2001)156[0577:cafdts]2.0.co;2
117. Schmid, T. E., Dollinger, G., Beisker, W., Hable, V., Greubel, C., Auer, S., Mittag, A., Tarnok, A., Friedl, A. A., Molls, M., & Röper, B. (2010). Differences in the kinetics of gamma-H2AX fluorescence decay after exposure to low and high LET radiation. International journal of radiation biology, 86(8), 682–691. https://doi.org/10.3109/09553001003734543
118. Reynolds, P., Anderson, J. A., Harper, J. V., Hill, M. A., Botchway, S. W., Parker, A. W., & O'Neill, P. (2012). The dynamics of Ku70/80 and DNA-PKcs at DSBs induced by ionizing radiation is dependent on the complexity of damage. Nucleic acids research, 40(21), 10821–10831. https://doi.org/10.1093/nar/gks879
119. Asaithamby, A., Uematsu, N., Chatterjee, A., Story, M. D., Burma, S., & Chen, D. J. (2008). Repair of HZE-particle-induced DNA double-strand breaks in normal human fibroblasts. Radiation research, 169(4), 437–446. https://doi.org/10.1667/RR1165.1
120. Botchway, S. W., Stevens, D. L., Hill, M. A., Jenner, T. J., & O'Neill, P. (1997). Induction and rejoining of DNA double-strand breaks in Chinese hamster V79-4 cells irradiated with characteristic aluminum K and copper L ultrasoft X rays. Radiation research, 148(4), 317–324.
121. Jeggo, P. A., & Löbrich, M. (2005). Artemis links ATM to double strand break rejoining. Cell cycle (Georgetown, Tex.), 4(3), 359–362. https://doi.org/10.4161/cc.4.3.1527
122. Jakob, B., Splinter, J., Conrad, S., Voss, K. O., Zink, D., Durante, M., Löbrich, M., & Taucher-Scholz, G. (2011). DNA double-strand breaks in heterochromatin elicit fast repair protein recruitment, histone H2AX phosphorylation and relocation to euchromatin. Nucleic acids research, 39(15), 6489–6499. https://doi.org/10.1093/nar/gkr230
123. Bakkenist, C. J., & Kastan, M. B. (2003). DNA damage activates ATM through intermolecular autophosphorylation and dimer dissociation. Nature, 421(6922), 499–506. https://doi.org/10.1038/nature01368
124. Petrini, J. H., & Stracker, T. H. (2003). The cellular response to DNA double-strand breaks: defining the sensors and mediators. Trends in cell biology, 13(9), 458–462. https://doi.org/10.1016/s0962-8924(03)00170-3
125. van den Bosch, M., Bree, R. T., & Lowndes, N. F. (2003). The MRN complex: coordinating and mediating the response to broken chromosomes. EMBO reports, 4(9), 844–849. https://doi.org/10.1038/sj.embor.embor925
126. Carson, C. T., Schwartz, R. A., Stracker, T. H., Lilley, C. E., Lee, D. V., & Weitzman, M. D. (2003). The Mre11 complex is required for ATM activation and the G2/M checkpoint. The EMBO journal, 22(24), 6610–6620. https://doi.org/10.1093/emboj/cdg630
127. Shiloh Y. (2003). ATM and related protein kinases: safeguarding genome integrity. Nature reviews. Cancer, 3(3), 155–168. https://doi.org/10.1038/nrc1011
128. Shiloh Y. (2003). ATM: ready, set, go. Cell cycle (Georgetown, Tex.), 2(2), 116–117. https://doi.org/10.4161/cc.2.2.342

129. Ditch, S., & Paull, T. T. (2012). The ATM protein kinase and cellular redox signaling: beyond the DNA damage response. Trends in biochemical sciences, 37(1), 15–22. https://doi.org/10.1016/j.tibs.2011.10.002
130. Shiloh Y. (2001). ATM and ATR: networking cellular responses to DNA damage. Current opinion in genetics & development, 11(1), 71–77. https://doi.org/10.1016/s0959-437x(00)00159-3
131. Shiloh, Y. (2004). Bridge over broken ends. The cellular response to DNA breaks in health and disease. DNA Repair. 3(8-9),779-1254.
132. Mladenov, E., & Iliakis, G. (2011). Induction and repair of DNA double strand breaks: the increasing spectrum of non-homologous end joining pathways. Mutation research, 711(1-2), 61–72. https://doi.org/10.1016/j.mrfmmm.2011.02.005
133. Baumann, P., & West, S. C. (1998). DNA end-joining catalyzed by human cell-free extracts. Proceedings of the National Academy of Sciences of the United States of America, 95(24), 14066–14070. https://doi.org/10.1073/pnas.95.24.14066
134. Critchlow, S. E., & Jackson, S. P. (1998). DNA end-joining: from yeast to man. Trends in biochemical sciences, 23(10), 394–398. https://doi.org/10.1016/s0968-0004(98)01284-5
135. Haber J. E. (1998). The many interfaces of Mre11. Cell, 95(5), 583–586. https://doi.org/10.1016/s0092-8674(00)81626-8
136. Petrini J. H. (1999). The mammalian Mre11-Rad50-nbs1 protein complex: integration of functions in the cellular DNA-damage response. American journal of human genetics, 64(5), 1264–1269. https://doi.org/10.1086/302391
137. Ward, J. F., Limoli, C. L., Calabro-Jones, P. M., & Aguilera, J. (1991). An examination of the repair saturation hypothesis for describing shouldered survival curves. Radiation research, 127(1), 90–96.
138. Peddi, P., Francisco, D. C., Cecil, A. M., Hair, J. M., Panayiotidis, M. I., & Georgakilas, A. G. (2008). Processing of clustered DNA damage in human breast cancer cells MCF-7 with partial DNA-PKcs deficiency. Cancer letters, 269(1), 174–183. https://doi.org/10.1016/j.canlet.2008.04.049
139. Wilson, T. E., Grawunder, U., & Lieber, M. R. (1997). Yeast DNA ligase IV mediates non-homologous DNA end joining. Nature, 388(6641), 495–498. https://doi.org/10.1038/41365
140. Sonoda, E., Sasaki, M. S., Buerstedde, J. M., Bezzubova, O., Shinohara, A., Ogawa, H., Takata, M., Yamaguchi-Iwai, Y., & Takeda, S. (1998). Rad51-deficient vertebrate cells accumulate chromosomal breaks prior to cell death. The EMBO journal, 17(2), 598–608. https://doi.org/10.1093/emboj/17.2.598
141. Thompson L. H. (1996). Evidence that mammalian cells possess homologous recombinational repair pathways. Mutation research, 363(2), 77–88. https://doi.org/10.1016/0921-8777(96)00008-0
142. Bianco, P. R., Tracy, R. B., & Kowalczykowski, S. C. (1998). DNA strand exchange proteins: a biochemical and physical comparison. Frontiers in bioscience : a journal and virtual library, 3, D570–D603. https://doi.org/10.2741/a304
143. Nickoloff, J. A., & Hoekstra, M. F. (1998). Chapter one. In DNA Damage and Repair: Volume I: DNA Repair in Prokaryotes and Lower Eukaryotes (Contemporary Cancer Research) (1998th ed., pp. 335–362). NJ, USA: Humana.
144. Buchhop, S., Gibson, M. K., Wang, X. W., Wagner, P., Stürzbecher, H. W., & Harris, C. C. (1997). Interaction of p53 with the human Rad51 protein. Nucleic acids research, 25(19), 3868–3874. https://doi.org/10.1093/nar/25.19.3868
145. Maity, A., McKenna, W. G., & Muschel, R. J. (1994). The molecular basis for cell cycle delays following ionizing radiation: a review. Radiotherapy and oncology :

journal of the European Society for Therapeutic Radiology and Oncology, 31(1), 1–13. https://doi.org/10.1016/0167-8140(94)90408-1
146. Bernhard, E. J., Maity, A., Muschel, R. J., & McKenna, W. G. (1995). Effects of ionizing radiation on cell cycle progression. A review. Radiation and environmental biophysics, 34(2), 79–83. https://doi.org/10.1007/BF01275210
147. Elledge S. J. (1996). Cell cycle checkpoints: preventing an identity crisis. Science (New York, N.Y.), 274(5293), 1664–1672. https://doi.org/10.1126/science.274.5293.1664
148. Nyberg, K. A., Michelson, R. J., Putnam, C. W., & Weinert, T. A. (2002). Toward maintaining the genome: DNA damage and replication checkpoints. Annual review of genetics, 36, 617–656. https://doi.org/10.1146/annurev.genet.36.060402.113540
149. Scully, R., & Livingston, D. M. (2000). In search of the tumour-suppressor functions of BRCA1 and BRCA2. Nature, 408(6811), 429–432. https://doi.org/10.1038/35044000
150. Venkitaraman A. R. (2001). Functions of BRCA1 and BRCA2 in the biological response to DNA damage. Journal of cell science, 114(Pt 20), 3591–3598.
151. Abraham R. T. (2001). Cell cycle checkpoint signaling through the ATM and ATR kinases. Genes & development, 15(17), 2177–2196. https://doi.org/10.1101/gad.914401
152. Giaccia, A. J., & Kastan, M. B. (1998). The complexity of p53 modulation: emerging patterns from divergent signals. Genes & development, 12(19), 2973–2983. https://doi.org/10.1101/gad.12.19.2973
153. Kastan, M. B., & Lim, D. S. (2000). The many substrates and functions of ATM. Nature reviews. Molecular cell biology, 1(3), 179–186. https://doi.org/10.1038/35043058
154. Sherr, C. J., & Roberts, J. M. (1995). Inhibitors of mammalian G1 cyclin-dependent kinases. Genes & development, 9(10), 1149–1163. https://doi.org/10.1101/gad.9.10.1149
155. Bartek, J., & Lukas, J. (2001). Mammalian G1- and S-phase checkpoints in response to DNA damage. Current opinion in cell biology, 13(6), 738–747. https://doi.org/10.1016/s0955-0674(00)00280-5
156. Mailand, N., Falck, J., Lukas, C., Syljuâsen, R. G., Welcker, M., Bartek, J., & Lukas, J. (2000). Rapid destruction of human Cdc25A in response to DNA damage. Science (New York, N.Y.), 288(5470), 1425–1429. https://doi.org/10.1126/science.288.5470.1425
157. Ekholm, S. V., & Reed, S. I. (2000). Regulation of G(1) cyclin-dependent kinases in the mammalian cell cycle. Current opinion in cell biology, 12(6), 676–684. https://doi.org/10.1016/s0955-0674(00)00151-4
158. Falck, J., Petrini, J. H., Williams, B. R., Lukas, J., & Bartek, J. (2002). The DNA damage-dependent intra-S phase checkpoint is regulated by parallel pathways. Nature genetics, 30(3), 290–294. https://doi.org/10.1038/ng845
159. Yazdi, P. T., Wang, Y., Zhao, S., Patel, N., Lee, E. Y., & Qin, J. (2002). SMC1 is a downstream effector in the ATM/NBS1 branch of the human S-phase checkpoint. Genes & development, 16(5), 571–582. https://doi.org/10.1101/gad.970702
160. Kim, S. T., Xu, B., & Kastan, M. B. (2002). Involvement of the cohesin protein, Smc1, in Atm-dependent and independent responses to DNA damage. Genes & development, 16(5), 560–570. https://doi.org/10.1101/gad.970602
161. Matsuoka, S., Rotman, G., Ogawa, A., Shiloh, Y., Tamai, K., & Elledge, S. J. (2000). Ataxia telangiectasia-mutated phosphorylates Chk2 in vivo and in vitro. Proceedings of the National Academy of Sciences of the United States of America, 97(19), 10389–10394. https://doi.org/10.1073/pnas.190030497

162. Falck, J., Mailand, N., Syljuåsen, R. G., Bartek, J., & Lukas, J. (2001). The ATM-Chk2-Cdc25A checkpoint pathway guards against radioresistant DNA synthesis. Nature, 410(6830), 842–847. https://doi.org/10.1038/35071124
163. Norbury, C., & Nurse, P. (1992). Animal cell cycles and their control. Annual review of biochemistry, 61, 441–470. https://doi.org/10.1146/annurev.bi.61.070192.002301
164. Crosby M. E. (2007). Cell Cycle: Principles of Control. The Yale Journal of Biology and Medicine, 80(3), 141–142.
165. Wang, Y., Ji, P., Liu, J., Broaddus, R. R., Xue, F., & Zhang, W. (2009). Centrosome-associated regulators of the G(2)/M checkpoint as targets for cancer therapy. Molecular cancer, 8, 8. https://doi.org/10.1186/1476-4598-8-8
166. Löbrich, M., & Jeggo, P. A. (2007). The impact of a negligent G2/M checkpoint on genomic instability and cancer induction. Nature reviews. Cancer, 7(11), 861–869. https://doi.org/10.1038/nrc2248
167. Smits, V. A., Klompmaker, R., Arnaud, L., Rijksen, G., Nigg, E. A., & Medema, R. H. (2000). Polo-like kinase-1 is a target of the DNA damage checkpoint. Nature cell biology, 2(9), 672–676. https://doi.org/10.1038/35023629
168. Xie, S., Wu, H., Wang, Q., Cogswell, J. P., Husain, I., Conn, C., Stambrook, P., Jhanwar-Uniyal, M., & Dai, W. (2001). Plk3 functionally links DNA damage to cell cycle arrest and apoptosis at least in part via the p53 pathway. The Journal of biological chemistry, 276(46), 43305–43312. https://doi.org/10.1074/jbc.M106050200
169. van Vugt, M. A., Smits, V. A., Klompmaker, R., & Medema, R. H. (2001). Inhibition of Polo-like kinase-1 by DNA damage occurs in an ATM- or ATR-dependent fashion. The Journal of biological chemistry, 276(45), 41656–41660. https://doi.org/10.1074/jbc.M101831200
170. Perry, J. A., & Kornbluth, S. (2007). Cdc25 and Wee1: analogous opposites?. Cell division, 2, 12. https://doi.org/10.1186/1747-1028-2-12
171. Little, M. P., Kwon, D., Doi, K., Simon, S. L., Preston, D. L., Doody, M. M., Lee, T., Miller, J. S., Kampa, D. M., Bhatti, P., Tucker, J. D., Linet, M. S., & Sigurdson, A. J. (2014). Association of chromosome translocation rate with low dose occupational radiation exposures in U.S. radiologic technologists. Radiation research, 182(1), 1–17. https://doi.org/10.1667/RR13413.1
172. Rothkamm, K., & Löbrich, M. (2003). Evidence for a lack of DNA double-strand break repair in human cells exposed to very low x-ray doses. Proceedings of the National Academy of Sciences of the United States of America, 100(9), 5057–5062. https://doi.org/10.1073/pnas.0830918100
173. Kuo, L. J., & Yang, L. X. (2008). Gamma-H2AX - a novel biomarker for DNA double-strand breaks. In vivo (Athens, Greece), 22(3), 305–309.
174. 174 – 183 Burma, S., Chen, B. P., Murphy, M., Kurimasa, A., & Chen, D. J. (2001). ATM phosphorylates histone H2AX in response to DNA double-strand breaks. The Journal of biological chemistry, 276(45), 42462–42467. https://doi.org/10.1074/jbc.C100466200
175. Rogakou, E. P., Pilch, D. R., Orr, A. H., Ivanova, V. S., & Bonner, W. M. (1998). DNA double-stranded breaks induce histone H2AX phosphorylation on serine 139. The Journal of biological chemistry, 273(10), 5858–5868. https://doi.org/10.1074/jbc.273.10.5858
176. Löbrich, M., Shibata, A., Beucher, A., Fisher, A., Ensminger, M., Goodarzi, A. A., Barton, O., & Jeggo, P. A. (2010). gammaH2AX foci analysis for monitoring DNA double-strand break repair: strengths, limitations and optimization. Cell cycle (Georgetown, Tex.), 9(4), 662–669. https://doi.org/10.4161/cc.9.4.10764

177. Beels, L., Bacher, K., De Wolf, D., Werbrouck, J., & Thierens, H. (2009). gamma-H2AX foci as a biomarker for patient X-ray exposure in pediatric cardiac catheterization: are we underestimating radiation risks?. Circulation, 120(19), 1903–1909. https://doi.org/10.1161/CIRCULATIONAHA.109.880385
178. Tang, X., Hui, Z. G., Cui, X. L., Garg, R., Kastan, M. B., & Xu, B. (2008). A novel ATM-dependent pathway regulates protein phosphatase 1 in response to DNA damage. Molecular and cellular biology, 28(8), 2559–2566. https://doi.org/10.1128/MCB.01711-07
179. Shiloh Y. (2006). The ATM-mediated DNA-damage response: taking shape. Trends in biochemical sciences, 31(7), 402–410. https://doi.org/10.1016/j.tibs.2006.05.004
180. Ditch, S., & Paull, T. T. (2012). The ATM protein kinase and cellular redox signaling: beyond the DNA damage response. Trends in biochemical sciences, 37(1), 15–22. https://doi.org/10.1016/j.tibs.2011.10.002
181. Pandita, T. K., & Hittelman, W. N. (1992). The contribution of DNA and chromosome repair deficiencies to the radiosensitivity of ataxia-telangiectasia. Radiation research, 131(2), 214–223.
182. Pandita, T. K., Lieberman, H. B., Lim, D. S., Dhar, S., Zheng, W., Taya, Y., & Kastan, M. B. (2000). Ionizing radiation activates the ATM kinase throughout the cell cycle. Oncogene, 19(11), 1386–1391. https://doi.org/10.1038/sj.onc.1203444
183. Burrows, C. J., & Muller, J. G. (1998). Oxidative Nucleobase Modifications Leading to Strand Scission. Chemical reviews, 98(3), 1109–1152. https://doi.org/10.1021/cr960421s
184. Ba, X., & Boldogh, I. (2018). 8-Oxoguanine DNA glycosylase 1: Beyond repair of the oxidatively modified base lesions. Redox biology, 14, 669–678. https://doi.org/10.1016/j.redox.2017.11.008
185. Ba, X., Aguilera-Aguirre, L., Rashid, Q. T., Bacsi, A., Radak, Z., Sur, S., Hosoki, K., Hegde, M. L., & Boldogh, I. (2014). The role of 8-oxoguanine DNA glycosylase-1 in inflammation. International journal of molecular sciences, 15(9), 16975–16997. https://doi.org/10.3390/ijms150916975
186. Lindahl, T., & Barnes, D. E. (2000). Repair of endogenous DNA damage. Cold Spring Harbor symposia on quantitative biology, 65, 127–133. https://doi.org/10.1101/sqb.2000.65.127
187. Dizdaroglu M. (1985). Formation of an 8-hydroxyguanine moiety in deoxyribonucleic acid on gamma-irradiation in aqueous solution. Biochemistry, 24(16), 4476–4481. https://doi.org/10.1021/bi00337a032
188. Radak, Z., & Boldogh, I. (2010). 8-Oxo-7,8-dihydroguanine: links to gene expression, aging, and defense against oxidative stress. Free radical biology & medicine, 49(4), 587–596. https://doi.org/10.1016/j.freeradbiomed.2010.05.008
189. Akiyama, M., Maki, H., Sekiguchi, M., & Horiuchi, T. (1989). A specific role of MutT protein: to prevent dG.dA mispairing in DNA replication. Proceedings of the National Academy of Sciences of the United States of America, 86(11), 3949–3952. https://doi.org/10.1073/pnas.86.11.3949
190. Shibutani, S., Takeshita, M., & Grollman, A. P. (1991). Insertion of specific bases during DNA synthesis past the oxidation-damaged base 8-oxodG. Nature, 349(6308), 431–434. https://doi.org/10.1038/349431a0
191. David, S. S., O'Shea, V. L., & Kundu, S. (2007). Base-excision repair of oxidative DNA damage. Nature, 447(7147), 941–950. https://doi.org/10.1038/nature05978
192. Dizdaroglu, M., Kirkali, G., & Jaruga, P. (2008). Formamidopyrimidines in DNA: mechanisms of formation, repair, and biological effects. Free radical biology & medicine, 45(12), 1610–1621. https://doi.org/10.1016/j.freeradbiomed.2008.07.004

193. Michaels, M. L., Pham, L., Cruz, C., & Miller, J. H. (1991). MutM, a protein that prevents G.C----T.A transversions, is formamidopyrimidine-DNA glycosylase. Nucleic acids research, 19(13), 3629–3632. https://doi.org/10.1093/nar/19.13.3629
194. Izumi, T., Wiederhold, L. R., Roy, G., Roy, R., Jaiswal, A., Bhakat, K. K., Mitra, S., & Hazra, T. K. (2003). Mammalian DNA base excision repair proteins: their interactions and role in repair of oxidative DNA damage. Toxicology, 193(1-2), 43–65. https://doi.org/10.1016/s0300-483x(03)00289-0
195. Mitra, S., Hazra, T. K., Roy, R., Ikeda, S., Biswas, T., Lock, J., Boldogh, I., & Izumi, T. (1997). Complexities of DNA base excision repair in mammalian cells. Molecules and cells, 7(3), 305–312.
196. Hazra, T. K., Das, A., Das, S., Choudhury, S., Kow, Y. W., & Roy, R. (2007). Oxidative DNA damage repair in mammalian cells: a new perspective. DNA repair, 6(4), 470–480. https://doi.org/10.1016/j.dnarep.2006.10.011
197. Tumurkhuu, G., Shimada, K., Dagvadorj, J., Crother, T. R., Zhang, W., Luthringer, D., Gottlieb, R. A., Chen, S., & Arditi, M. (2016). Ogg1-Dependent DNA Repair Regulates NLRP3 Inflammasome and Prevents Atherosclerosis. Circulation research, 119(6), e76–e90. https://doi.org/10.1161/CIRCRESAHA.116.308362
198. Nikitaki, Z., Nikolov, V., Mavragani, I. V., Mladenov, E., Mangelis, A., Laskaratou, D. A., Fragkoulis, G. I., Hellweg, C. E., Martin, O. A., Emfietzoglou, D., Hatzi, V. I., Terzoudi, G. I., Iliakis, G., & Georgakilas, A. G. (2016). Measurement of complex DNA damage induction and repair in human cellular systems after exposure to ionizing radiations of varying linear energy transfer (LET). Free radical research, 50(sup1), S64–S78. https://doi.org/10.1080/10715762.2016.1232484
199. Eccles, L. J., O'Neill, P., & Lomax, M. E. (2011). Delayed repair of radiation induced clustered DNA damage: friend or foe?. Mutation research, 711(1-2), 134–141. https://doi.org/10.1016/j.mrfmmm.2010.11.003
200. Schipler, A., & Iliakis, G. (2013). DNA double-strand-break complexity levels and their possible contributions to the probability for error-prone processing and repair pathway choice. Nucleic acids research, 41(16), 7589–7605. https://doi.org/10.1093/nar/gkt556
201. Tucker J. D. (2008). Low-dose ionizing radiation and chromosome translocations: a review of the major considerations for human biological dosimetry. Mutation research, 659(3), 211–220. https://doi.org/10.1016/j.mrrev.2008.04.001
202. Maffei, F., Angelini, S., Forti, G. C., Violante, F. S., Lodi, V., Mattioli, S., & Hrelia, P. (2004). Spectrum of chromosomal aberrations in peripheral lymphocytes of hospital workers occupationally exposed to low doses of ionizing radiation. Mutation research, 547(1-2), 91–99. https://doi.org/10.1016/j.mrfmmm.2003.12.003
203. Ait-Ali, L., Foffa, I., & Andreassi, M. G. (2007). Diagnostic and therapeutic radiation exposure in children: new evidence and perspectives from a biomarker approach. Pediatric radiology, 37(1), 109–111. https://doi.org/10.1007/s00247-006-0328-6
204. Hagmar, L., Strömberg, U., Tinnerberg, H., & Mikoczy, Z. (2004). Epidemiological evaluation of cytogenetic biomarkers as potential surrogate end-points for cancer. IARC scientific publications, (157), 207–215.
205. Vral, A., Decorte, V., Depuydt, J., Wambersie, A., & Thierens, H. (2016). A semi-automated FISH-based micronucleus-centromere assay for biomonitoring of hospital workers exposed to low doses of ionizing radiation. Molecular medicine reports, 14(1), 103–110. https://doi.org/10.3892/mmr.2016.5265
206. Andreassi, M. G., Cioppa, A., Botto, N., Joksic, G., Manfredi, S., Federici, C., Ostojic, M., Rubino, P., & Picano, E. (2005). Somatic DNA damage in interventional cardiologists: a case-control study. FASEB journal : official publication of the

Federation of American Societies for Experimental Biology, 19(8), 998–999. https://doi.org/10.1096/fj.04-3287fje

207. Chang, W. P., Hwang, B. F., Wang, D., & Wang, J. D. (1997). Cytogenetic effect of chronic low-dose, low-dose-rate gamma-radiation in residents of irradiated buildings. Lancet (London, England), 350(9074), 330–333. https://doi.org/10.1016/S0140-6736(97)11056-X
208. Bettega, D., Calzolari, P., Doneda, L., Belloni, F., Tallone, L., & Redpath, J. L. (2003). Differential effectiveness of solar UVB subcomponents in causing cell death, oncogenic transformation and micronucleus induction in human hybrid cells. International journal of radiation biology, 79(3), 211–216. https://doi.org/10.1080/0955300031000075345
209. Bonassi, S., Znaor, A., Ceppi, M., Lando, C., Chang, W. P., Holland, N., Kirsch-Volders, M., Zeiger, E., Ban, S., Barale, R., Bigatti, M. P., Bolognesi, C., Cebulska-Wasilewska, A., Fabianova, E., Fucic, A., Hagmar, L., Joksic, G., Martelli, A., Migliore, L., Mirkova, E., … Fenech, M. (2007). An increased micronucleus frequency in peripheral blood lymphocytes predicts the risk of cancer in humans. Carcinogenesis, 28(3), 625–631. https://doi.org/10.1093/carcin/bgl177
210. Andreassi, M. G., Foffa, I., Manfredi, S., Botto, N., Cioppa, A., & Picano, E. (2009). Genetic polymorphisms in XRCC1, OGG1, APE1 and XRCC3 DNA repair genes, ionizing radiation exposure and chromosomal DNA damage in interventional cardiologists. Mutation research, 666(1-2), 57–63. https://doi.org/10.1016/j.mrfmmm.2009.04.003
211. Matullo, G., Palli, D., Peluso, M., Guarrera, S., Carturan, S., Celentano, E., Krogh, V., Munnia, A., Tumino, R., Polidoro, S., Piazza, A., & Vineis, P. (2001). XRCC1, XRCC3, XPD gene polymorphisms, smoking and (32)P-DNA adducts in a sample of healthy subjects. Carcinogenesis, 22(9), 1437–1445. https://doi.org/10.1093/carcin/22.9.1437
212. Borghini, A., Mercuri, A., Turchi, S., Chiesa, M. R., Piccaluga, E., & Andreassi, M. G. (2015). Increased circulating cell-free DNA levels and mtDNA fragments in interventional cardiologists occupationally exposed to low levels of ionizing radiation. Environmental and molecular mutagenesis, 56(3), 293–300. https://doi.org/10.1002/em.21917
213. Nie, H., Shu, H., Vartak, R., Milstein, A. C., Mo, Y., Hu, X., Fang, H., Shen, L., Ding, Z., Lu, J., & Bai, Y. (2013). Mitochondrial common deletion, a potential biomarker for cancer occurrence, is selected against in cancer background: a meta-analysis of 38 studies. PloS one, 8(7), e67953. https://doi.org/10.1371/journal.pone.0067953
214. Meissner, C., Bruse, P., Mohamed, S. A., Schulz, A., Warnk, H., Storm, T., & Oehmichen, M. (2008). The 4977 bp deletion of mitochondrial DNA in human skeletal muscle, heart and different areas of the brain: a useful biomarker or more?. Experimental gerontology, 43(7), 645–652. https://doi.org/10.1016/j.exger.2008.03.004
215. Kawamura, K., Qi, F., & Kobayashi, J. (2018). Potential relationship between the biological effects of low-dose irradiation and mitochondrial ROS production. Journal of radiation research, 59(suppl_2), ii91–ii97. https://doi.org/10.1093/jrr/rrx091
216. Borghini, A., Vecoli, C., Piccaluga, E., Guagliumi, G., Picano, E., & Andreassi, M. G. (2019). Increased mitochondrial DNA4977-bp deletion in catheterization laboratory workers with long-term low-dose exposure to ionizing radiation. European journal of preventive cardiology, 26(9), 976–984. https://doi.org/10.1177/2047487319831495

217. Lu, J., Sharma, L. K., & Bai, Y. (2009). Implications of mitochondrial DNA mutations and mitochondrial dysfunction in tumorigenesis. Cell research, 19(7), 802–815. https://doi.org/10.1038/cr.2009.69
218. Kabacik, S., Manning, G., Raffy, C., Bouffler, S., & Badie, C. (2015). Time, dose and ataxia telangiectasia mutated (ATM) status dependency of coding and noncoding RNA expression after ionizing radiation exposure. Radiation research, 183(3), 325–337. https://doi.org/10.1667/RR13876.1
219. Amundson S. A. (2008). Functional genomics in radiation biology: a gateway to cellular systems-level studies. Radiation and environmental biophysics, 47(1), 25–31. https://doi.org/10.1007/s00411-007-0140-1
220. Amundson, S. A., Lee, R. A., Koch-Paiz, C. A., Bittner, M. L., Meltzer, P., Trent, J. M., & Fornace, A. J., Jr (2003). Differential responses of stress genes to low dose-rate gamma irradiation. Molecular cancer research : MCR, 1(6), 445–452.
221. Nguyen, P. K., Lee, W. H., Li, Y. F., Hong, W. X., Hu, S., Chan, C., Liang, G., Nguyen, I., Ong, S. G., Churko, J., Wang, J., Altman, R. B., Fleischmann, D., & Wu, J. C. (2015). Assessment of the Radiation Effects of Cardiac CT Angiography Using Protein and Genetic Biomarkers. JACC. Cardiovascular imaging, 8(8), 873–884. https://doi.org/10.1016/j.jcmg.2015.04.016.
222. Lee, W. H., Nguyen, P., Hu, S., Liang, G., Ong, S. G., Han, L., Sanchez-Freire, V., Lee, A. S., Vasanawala, M., Segall, G., & Wu, J. C. (2015). Variable activation of the DNA damage response pathways in patients undergoing single-photon emission computed tomography myocardial perfusion imaging. Circulation. Cardiovascular imaging, 8(2), e002851. https://doi.org/10.1161/CIRCIMAGING.114.002851
223. Cui, W., Ma, J., Wang, Y., & Biswal, S. (2011). Plasma miRNA as biomarkers for assessment of total-body radiation exposure dosimetry. PloS one, 6(8), e22988. https://doi.org/10.1371/journal.pone.0022988
224. He, L., He, X., Lim, L. P., de Stanchina, E., Xuan, Z., Liang, Y., Xue, W., Zender, L., Magnus, J., Ridzon, D., Jackson, A. L., Linsley, P. S., Chen, C., Lowe, S. W., Cleary, M. A., & Hannon, G. J. (2007). A microRNA component of the p53 tumour suppressor network. Nature, 447(7148), 1130–1134. https://doi.org/10.1038/nature05939
225. Pan, J. Y., Zhang, F., Sun, C. C., Li, S. J., Li, G., Gong, F. Y., Bo, T., He, J., Hua, R. X., Hu, W. D., Yuan, Z. P., Wang, X., He, Q. Q., & Li, D. J. (2017). miR-134: A Human Cancer Suppressor?. Molecular therapy. Nucleic acids, 6, 140–149. https://doi.org/10.1016/j.omtn.2016.11.003
226. Borghini, A., Vecoli, C., Mercuri, A., Carpeggiani, C., Piccaluga, E., Guagliumi, G., Picano, E., & Andreassi, M. G. (2017). Low-Dose Exposure to Ionizing Radiation Deregulates the Brain-Specific MicroRNA-134 in Interventional Cardiologists. Circulation, 136(25), 2516–2518. https://doi.org/10.1161/CIRCULATIONAHA.117.031251
227. La Motte-Mohs, R. N., Herer, E., & Zúñiga-Pflücker, J. C. (2005). Induction of T-cell development from human cord blood hematopoietic stem cells by Delta-like 1 in vitro. Blood, 105(4), 1431–1439. https://doi.org/10.1182/blood-2004-04-1293
228. Blomgren, H., Edsmyr, F., Näslund, I., Petrini, B., & Wasserman, J. (1983). Distribution of lymphocyte subsets following radiation therapy directed to different body regions. Clinical oncology, 9(4), 289–298.
229. Raben, M., Walach, N., Galili, U., & Schlesinger, M. (1976). The effect of radiation therapy on lymphocyte subpopulations in cancer patients. Cancer, 37(3), 1417–1421. https://doi.org/10.1002/1097-0142(197603)37:3<1417::aid-cncr2820370324>3.0.co;2-n

230. Rotstein, S., Blomgren, H., Petrini, B., Wasserman, J., & Baral, E. (1985). Long term effects on the immune system following local radiation therapy for breast cancer. I. Cellular composition of the peripheral blood lymphocyte population. International journal of radiation oncology, biology, physics, 11(5), 921–925. https://doi.org/10.1016/0360-3016(85)90114-2
231. Heier H. E. (1978). The influence of therapeutic irradiation of blood and peripheral lymph lymphocytes. Lymphology, 11(4), 238–242.
232. Gray, W. C., Chretien, P. B., Suter, C. M., Revie, D. R., Tomazic, V. T., Blanchard, C. L., Aygun, C., Amornmarn, R., & Ordonez, J. V. (1985). Effects of radiation therapy on T-lymphocyte subpopulations in patients with head and neck cancer. Otolaryngology--head and neck surgery : official journal of American Academy of Otolaryngology-Head and Neck Surgery, 93(5), 650–660. https://doi.org/10.1177/019459988509300515
233. Razzaghdoust, A., Mozdarani, H., Mofid, B., Aghamiri, S. M., & Heidari, A. H. (2014). Reduction in radiation-induced lymphocytopenia by famotidine in patients undergoing radiotherapy for prostate cancer. The Prostate, 74(1), 41–47. https://doi.org/10.1002/pros.22725
234. Stjernswärd, J., Jondal, M., Vánky, F., Wigzell, H., & Sealy, R. (1972). Lymphopenia and change in distribution of human B and T lymphocytes in peripheral blood induced by irradiation for mammary carcinoma. Lancet (London, England), 1(7765), 1352–1356. https://doi.org/10.1016/s0140-6736(72)91091-4
235. Stratton, J. A., Byfield, P. E., Byfield, J. E., Small, R. C., Benfield, J., & Pilch, Y. (1975). A comparison of the acute effects of radiation therapy, including or excluding the thymus, on the lymphocyte subpopulations of cancer patients. The Journal of clinical investigation, 56(1), 88–97. https://doi.org/10.1172/JCI108084
236. Brown, K. R., & Rzucidlo, E. (2011). Acute and chronic radiation injury. Journal of vascular surgery, 53(1 Suppl), 15S–21S. https://doi.org/10.1016/j.jvs.2010.06.175
237. Valentin J. (2000). Avoidance of radiation injuries from medical interventional procedures. Annals of the ICRP, 30(2), 7–67. https://doi.org/10.1016/S0146-6453(01)00004-5
238. Killewich, L. A., Falls, G., Mastracci, T. M., & Brown, K. R. (2011). Factors affecting radiation injury. Journal of vascular surgery, 53(1 Suppl), 9S–14S. https://doi.org/10.1016/j.jvs.2010.07.025
239. Neil, S., Padgham, C., & Martin, C. J. (2010). A study of the relationship between peak skin dose and cumulative air kerma in interventional neuroradiology and cardiology. Journal of radiological protection : official journal of the Society for Radiological Protection, 30(4), 659–672. https://doi.org/10.1088/0952-4746/30/4/002
240. Ketteler, E. R., & Brown, K. R. (2011). Radiation exposure in endovascular procedures. Journal of vascular surgery, 53(1 Suppl), 35S–38S. https://doi.org/10.1016/j.jvs.2010.05.141
241. Koenig, T. R., Wolff, D., Mettler, F. A., & Wagner, L. K. (2001). Skin injuries from fluoroscopically guided procedures: part 1, characteristics of radiation injury. AJR. American journal of roentgenology, 177(1), 3–11. https://doi.org/10.2214/ajr.177.1.1770003
242. Koenig, T. R., Mettler, F. A., & Wagner, L. K. (2001). Skin injuries from fluoroscopically guided procedures: part 2, review of 73 cases and recommendations for minimizing dose delivered to patient. AJR. American journal of roentgenology, 177(1), 13–20. https://doi.org/10.2214/ajr.177.1.1770013
243. Vlietstra, R. E., Wagner, L. K., Koenig, T., & Mettler, F. (2004). Radiation burns as a severe complication of fluoroscopically guided cardiological interventions. Journal of

interventional cardiology, 17(3), 131–142. https://doi.org/10.1111/j.1540-8183.2004.09885.
244. Kato, M., Chida, K., Sato, T., Oosaka, H., Tosa, T., Munehisa, M., & Kadowaki, K. (2012). The necessity of follow-up for radiation skin injuries in patients after percutaneous coronary interventions: radiation skin injuries will often be overlooked clinically. Acta radiologica (Stockholm, Sweden : 1987), 53(9), 1040–1044. https://doi.org/10.1258/ar.2012.120192
245. Weiss D, Pipinos I, Longo M, Lynch T, Rutar F, Johanning J, et al. Of patient radiation exposure during endovascular aortic aneurysm repair. Ann Vasc Surg 2008;6:723-9.
246. Walsh, S. R., Cousins, C., Tang, T. Y., Gaunt, M. E., & Boyle, J. R. (2008). Ionizing radiation in endovascular interventions. Journal of endovascular therapy : an official journal of the International Society of Endovascular Specialists, 15(6), 680–687. https://doi.org/10.1583/08-2495.1
247. Weerakkody, R. A., Walsh, S. R., Cousins, C., Goldstone, K. E., Tang, T. Y., & Gaunt, M. E. (2008). Radiation exposure during endovascular aneurysm repair. The British journal of surgery, 95(6), 699–702. https://doi.org/10.1002/bjs.6229
248. Lee, T., Sigurdson, A. J., Preston, D. L., Cahoon, E. K., Freedman, D. M., Simon, S. L., Nelson, K., Matanoski, G., Kitahara, C. M., Liu, J. J., Wang, T., Alexander, B. H., Doody, M. M., Linet, M. S., & Little, M. P. (2015). Occupational ionising radiation and risk of basal cell carcinoma in US radiologic technologists (1983-2005). Occupational and environmental medicine, 72(12), 862–869. https://doi.org/10.1136/oemed-2015-102880
249. Andreassi, M. G., Piccaluga, E., Guagliumi, G., Del Greco, M., Gaita, F., & Picano, E. (2016). Occupational Health Risks in Cardiac Catheterization Laboratory Workers. Circulation. Cardiovascular interventions, 9(4), e003273. https://doi.org/10.1161/CIRCINTERVENTIONS.115.003273
250. Jacob, S., Michel, M., Brézin, A.P., Laurier, D. & Bernier, M.O. (2012). Ionizing radiation as a risk factor for cataract: What about low-dose effects? Journal of Clinical & Experimental Ophthalmology. S1-005:1. http://dx.doi.org/10.4172/2155-9570.S1-005
251. Kleiman, N. J. (2012). Radiation cataract. Annals of the ICRP, 41(3–4), 80–97. https://doi.org/10.1016/j.icrp.2012.06.018.
252. Worgul, B. V., Kundiyev, Y. I., Sergiyenko, N. M., Chumak, V. V., Vitte, P. M., Medvedovsky, C., Bakhanova, E. V., Junk, A. K., Kyrychenko, O. Y., Musijachenko, N. V., Shylo, S. A., Vitte, O. P., Xu, S., Xue, X., & Shore, R. E. (2007). Cataracts among Chernobyl clean-up workers: implications regarding permissible eye exposures. Radiation research, 167(2), 233–243. https://doi.org/10.1667/rr0298.1
253. Klein, L. W., Miller, D. L., Balter, S., Laskey, W., Haines, D., Norbash, A., Mauro, M. A., Goldstein, J. A., & Joint Inter-Society Task Force on Occupational Hazards in the Interventional Laboratory (2009). Occupational health hazards in the interventional laboratory: time for a safer environment. Journal of vascular and interventional radiology : JVIR, 20(7 Suppl), S278–S283. https://doi.org/10.1016/j.jvir.2009.04.027
254. Chodick, G., Bekiroglu, N., Hauptmann, M., Alexander, B. H., Freedman, D. M., Doody, M. M., Cheung, L. C., Simon, S. L., Weinstock, R. M., Bouville, A., & Sigurdson, A. J. (2008). Risk of cataract after exposure to low doses of ionizing radiation: a 20-year prospective cohort study among US radiologic technologists. American journal of epidemiology, 168(6), 620–631. https://doi.org/10.1093/aje/kwn171

255. Nakashima, E., Neriishi, K., & Minamoto, A. (2006). A reanalysis of atomic-bomb cataract data, 2000-2002: a threshold analysis. Health physics, 90(2), 154–160. https://doi.org/10.1097/01.hp.0000175442.03596.63
256. Kuon, E., Birkel, J., Schmitt, M., & Dahm, J. B. (2003). Radiation exposure benefit of a lead cap in invasive cardiology. Heart (British Cardiac Society), 89(10), 1205–1210. https://doi.org/10.1136/heart.89.10.1205
257. Authors on behalf of ICRP, Stewart, F. A., Akleyev, A. V., Hauer-Jensen, M., Hendry, J. H., Kleiman, N. J., Macvittie, T. J., Aleman, B. M., Edgar, A. B., Mabuchi, K., Muirhead, C. R., Shore, R. E., & Wallace, W. H. (2012). ICRP publication 118: ICRP statement on tissue reactions and early and late effects of radiation in normal tissues and organs--threshold doses for tissue reactions in a radiation protection context. Annals of the ICRP, 41(1-2), 1–322. https://doi.org/10.1016/j.icrp.2012.02.001
258. Vano, E., Kleiman, N. J., Duran, A., Rehani, M. M., Echeverri, D., & Cabrera, M. (2010). Radiation cataract risk in interventional cardiology personnel. Radiation research, 174(4), 490–495. https://doi.org/10.1667/RR2207.1
259. Ciraj-Bjelac, O., Rehani, M., Minamoto, A., Sim, K. H., Liew, H. B., & Vano, E. (2012). Radiation-induced eye lens changes and risk for cataract in interventional cardiology. Cardiology, 123(3), 168–171. https://doi.org/10.1159/000342458
260. Ciraj-Bjelac, O., Rehani, M. M., Sim, K. H., Liew, H. B., Vano, E., & Kleiman, N. J. (2010). Risk for radiation-induced cataract for staff in interventional cardiology: is there reason for concern?. Catheterization and cardiovascular interventions : official journal of the Society for Cardiac Angiography & Interventions, 76(6), 826–834. https://doi.org/10.1002/ccd.22670
261. Kim, K. P., & Miller, D. L. (2009). Minimising radiation exposure to physicians performing fluoroscopically guided cardiac catheterisation procedures: a review. Radiation protection dosimetry, 133(4), 227–233. https://doi.org/10.1093/rpd/ncp052
262. Attigah, N., Oikonomou, K., Hinz, U., Knoch, T., Demirel, S., Verhoeven, E., & Böckler, D. (2016). Radiation exposure to eye lens and operator hands during endovascular procedures in hybrid operating rooms. Journal of vascular surgery, 63(1), 198–203. https://doi.org/10.1016/j.jvs.2015.08.051
263. Vanhavere, F., Carinou, E., Domienik, J., Donadille, L., Ginjaume, M., Gualdrini G, *et al.* (2011). Measurements of eye lens doses in interventional radiology and cardiology: final results of the ORAMED project. Radiation Measurement. 46 (11),1243-7. https://doi.org/10.1016/j.radmeas.2011.08.013
264. Lam, W. W., Leung, S. F., So, N. M., Wong, K. S., Liu, K. H., Ku, P. K., Yuen, H. Y., & Metreweli, C. (2001). Incidence of carotid stenosis in nasopharyngeal carcinoma patients after radiotherapy. Cancer, 92(9), 2357–2363. https://doi.org/10.1002/1097-0142(20011101)92:9<2357::aid-cncr1583>3.0.co;2-k
265. Huang, T. L., Hsu, H. C., Chen, H. C., Lin, H. C., Chien, C. Y., Fang, F. M., Huang, C. C., Chang, H. W., Chang, W. N., Huang, C. R., Tsai, N. W., Kung, C. T., Wang, H. C., Lin, W. C., Cheng, B. C., Su, Y. J., Chang, Y. T., Chang, C. R., Tan, T. Y., & Lu, C. H. (2013). Long-term effects on carotid intima-media thickness after radiotherapy in patients with nasopharyngeal carcinoma. Radiation oncology (London, England), 8, 261. https://doi.org/10.1186/1748-717X-8-261
266. Smith, G. L., Smith, B. D., Buchholz, T. A., Giordano, S. H., Garden, A. S., Woodward, W. A., Krumholz, H. M., Weber, R. S., Ang, K. K., & Rosenthal, D. I. (2008). Cerebrovascular disease risk in older head and neck cancer patients after radiotherapy. Journal of clinical oncology : official journal of the American Society of Clinical Oncology, 26(31), 5119–5125. https://doi.org/10.1200/JCO.2008.16.6546

267. Yonehara, S., Brenner, A. V., Kishikawa, M., Inskip, P. D., Preston, D. L., Ron, E., Mabuchi, K., & Tokuoka, S. (2004). Clinical and epidemiologic characteristics of first primary tumors of the central nervous system and related organs among atomic bomb survivors in Hiroshima and Nagasaki, 1958-1995. Cancer, 101(7), 1644–1654. https://doi.org/10.1002/cncr.20543
268. Preston, D. L., Ron, E., Yonehara, S., Kobuke, T., Fujii, H., Kishikawa, M., Tokunaga, M., Tokuoka, S., & Mabuchi, K. (2002). Tumors of the nervous system and pituitary gland associated with atomic bomb radiation exposure. Journal of the National Cancer Institute, 94(20), 1555–1563. https://doi.org/10.1093/jnci/94.20.1555
269. Preston, D. L., Ron, E., Tokuoka, S., Funamoto, S., Nishi, N., Soda, M., Mabuchi, K., & Kodama, K. (2007). Solid cancer incidence in atomic bomb survivors: 1958-1998. Radiation research, 168(1), 1–64. https://doi.org/10.1667/RR0763.1
270. Yoshinaga, S., Mabuchi, K., Sigurdson, A. J., Doody, M. M., & Ron, E. (2004). Cancer risks among radiologists and radiologic technologists: review of epidemiologic studies. Radiology, 233(2), 313–321. https://doi.org/10.1148/radiol.2332031119
271. Berrington, A., Darby, S. C., Weiss, H. A., & Doll, R. (2001). 100 years of observation on British radiologists: mortality from cancer and other causes 1897-1997. The British journal of radiology, 74(882), 507–519. https://doi.org/10.1259/bjr.74.882.740507
272. Wakeford R. (2009). Radiation in the workplace-a review of studies of the risks of occupational exposure to ionising radiation. Journal of radiological protection : official journal of the Society for Radiological Protection, 29(2A), A61–A79. https://doi.org/10.1088/0952-4746/29/2A/S05
273. Valentin J. (2005). Low-dose extrapolation of radiation-related cancer risk. Annals of the ICRP, 35(4), 1–140. https://doi.org/10.1016/j.icrp.2005.11.002
274. Wang, J. X., Zhang, L. A., Li, B. X., Zhao, Y. C., Wang, Z. Q., Zhang, J. Y., & Aoyama, T. (2002). Cancer incidence and risk estimation among medical x-ray workers in China, 1950-1995. Health physics, 82(4), 455–466. https://doi.org/10.1097/00004032-200204000-00004
275. Ozasa K. (2016). Epidemiological research on radiation-induced cancer in atomic bomb survivors. Journal of radiation research, 57 Suppl 1(Suppl 1), i112–i117. https://doi.org/10.1093/jrr/rrw005
276. Habash, M., Bohorquez, L. C., Kyriakou, E., Kron, T., Martin, O. A., & Blyth, B. J. (2017). Clinical and Functional Assays of Radiosensitivity and Radiation-Induced Second Cancer. Cancers, 9(11), 147. https://doi.org/10.3390/cancers9110147
277. Yock, T. I., & Caruso, P. A. (2012). Risk of second cancers after photon and proton radiotherapy: a review of the data. Health physics, 103(5), 577–585. https://doi.org/10.1097/HP.0b013e3182609ba4
278. Marcu L. G. (2017). Photons - Radiobiological issues related to the risk of second malignancies. Physica medica : PM : an international journal devoted to the applications of physics to medicine and biology : official journal of the Italian Association of Biomedical Physics (AIFB), 42, 213–220. https://doi.org/10.1016/j.ejmp.2017.02.013
279. Rothblum-Oviatt, C., Wright, J., Lefton-Greif, M. A., McGrath-Morrow, S. A., Crawford, T. O., & Lederman, H. M. (2016). Ataxia telangiectasia: a review. Orphanet journal of rare diseases, 11(1), 159. https://doi.org/10.1186/s13023-016-0543-7
280. The I. (2000). Nijmegen breakage syndrome. The International Nijmegen Breakage Syndrome Study Group. Archives of disease in childhood, 82(5), 400–406. https://doi.org/10.1136/adc.82.5.400
281. Distel, L. V., Neubauer, S., Keller, U., Sprung, C. N., Sauer, R., & Grabenbauer, G. G. (2006). Individual differences in chromosomal aberrations after in vitro irradiation of

cells from healthy individuals, cancer and cancer susceptibility syndrome patients. Radiotherapy and oncology : journal of the European Society for Therapeutic Radiology and Oncology, 81(3), 257–263. https://doi.org/10.1016/j.radonc.2006.10.012

282. Crompton, N. E., Miralbell, R., Rutz, H. P., Ersoy, F., Sanal, O., Wellmann, D., Bieri, S., Coucke, P. A., Emery, G. C., Shi, Y. Q., Blattmann, H., & Ozsahin, M. (1999). Altered apoptotic profiles in irradiated patients with increased toxicity. International journal of radiation oncology, biology, physics, 45(3), 707–714. https://doi.org/10.1016/s0360-3016(99)00256-4
283. 283 – 252 Shinozuka J, Guanmin L, Wijit K, Uetsuka K, Nakayama H, Doi K (1997) T-2 toxin-induced apoptosis in lymphoid organs of mice. Exp Toxicol Pathol 49:387–392.
284. 284 – 253 Nunn, J. F., Sharp, J. A., & Kimball, K. L. (1970). Reversible effect of an inhalational anaesthetic on lymphocyte motility. Nature, 226(5240), 85–86. https://doi.org/10.1038/226085a0
285. 285 – 254 Oka, M., Hirazawa, K., Yamamoto, K., Iizuka, N., Hazama, S., Suzuki, T., & Kobayashi, N. (1996). Induction of Fas-mediated apoptosis on circulating lymphocytes by surgical stress. Annals of surgery, 223(4), 434–440. https://doi.org/10.1097/00000658-199604000-00013
286. Yamada, R., Tsuchida, S., Hara, Y., Tagawa, M., & Ogawa, R. (2002). Apoptotic lymphocytes induced by surgical trauma in dogs. Journal of anesthesia, 16(2), 131–137. https://doi.org/10.1007/s005400200008
287. Mokart, D., Leone, M., Sannini, A., Brun, J. P., Tison, A., Delpero, J. R., Houvenaeghel, G., Blache, J. L., & Martin, C. (2005). Predictive perioperative factors for developing severe sepsis after major surgery. *British journal of anaesthesia*, *95*(6), 776–781. https://doi.org/10.1093/bja/aei257
288. Lee, Y. Y., Choi, C. H., Sung, C. O., Do, I. G., Hub, S. J., Kim, H. J., Kim, T. J., Lee, J. W., Bae, D. S., & Kim, B. G. (2012). Clinical significance of changes in peripheral lymphocyte count after surgery in early cervical cancer. Gynecologic oncology, 127(1), 107–113. https://doi.org/10.1016/j.ygyno.2012.05.039
289. Kobayashi, E., & Yamauchi, H. (1997). Interleukin-6 and a delay of neutrophil apoptosis after major surgery. Archives of surgery (Chicago, Ill. : 1960), 132(2), 209–210. https://doi.org/10.1001/archsurg.1997.01430260107023
290. Sasajima, K., Inokuchi, K., Onda, M., Miyashita, M., Okawa, K. I., Matsutani, T., & Takubo, K. (1999). Detection of T cell apoptosis after major operations. The European journal of surgery = Acta chirurgica, 165(11), 1020–1023. https://doi.org/10.1080/110241599750007829
291. Kono, K., Takahashi, A., Iizuka, H., Fujii, H., Sekikawa, T., & Matsumoto, Y. (2001). Effect of oesophagectomy on monocyte-induced apoptosis of peripheral blood T lymphocytes. The British journal of surgery, 88(8), 1110–1116. https://doi.org/10.1046/j.0007-1323.2001.01833
292. Leães, P. E., Neumann, J., Jung, L. A., Blacher, C., Lucchese, F., & Clausell, N. (2004). Lymphocyte's activation and apoptosis after coronary artery bypass graft: a comparative study of two membrane oxygenators--one with and another without a venous-arterial shunt. ASAIO journal (American Society for Artificial Internal Organs : 1992), 50(6), 611–618. https://doi.org/10.1097/01.mat.0000144590.98621.4f
293. Ihnken, K., Winkler, A., Schlensak, C., Sarai, K., Neidhart, G., Unkelbach, U., Mülsch, A., & Sewell, A. (1998). Normoxic cardiopulmonary bypass reduces oxidative myocardial damage and nitric oxide during cardiac operations in the adult. The Journal

of thoracic and cardiovascular surgery, 116(2), 327–334. https://doi.org/10.1016/s0022-5223(98)70134-5
294. de Vroege, R., Wagemakers, M., te Velthuis, H., Bulder, E., Paulus, R., Huybregts, R., Wildevuur, W., Eijsman, L., van Oeveren, W., & Wildevuur, C. (2001). Comparison of three commercially available hollow fiber oxygenators: gas transfer performance and biocompatibility. ASAIO journal (American Society for Artificial Internal Organs : 1992), 47(1), 37–44. https://doi.org/10.1097/00002480-200101000-00010
295. Loop, T., Dovi-Akue, D., Frick, M., Roesslein, M., Egger, L., Humar, M., Hoetzel, A., Schmidt, R., Borner, C., Pahl, H. L., Geiger, K. K., & Pannen, B. H. (2005). Volatile anesthetics induce caspase-dependent, mitochondria-mediated apoptosis in human T lymphocytes in vitro. Anesthesiology, 102(6), 1147–1157. https://doi.org/10.1097/00000542-200506000-00014
296. Guo, Y., Dickerson, C., Chrest, F. J., Adler, W. H., Munster, A. M., & Winchurch, R. A. (1990). Increased levels of circulating interleukin 6 in burn patients. Clinical immunology and immunopathology, 54(3), 361–371. https://doi.org/10.1016/0090-1229(90)90050-z
297. Zheng, L., Fisher, G., Miller, R. E., Peschon, J., Lynch, D. H., & Lenardo, M. J. (1995). Induction of apoptosis in mature T cells by tumour necrosis factor. Nature, 377(6547), 348–351. https://doi.org/10.1038/377348a0
298. Munford, R. S., & Pugin, J. (2001). Normal responses to injury prevent systemic inflammation and can be immunosuppressive. American journal of respiratory and critical care medicine, 163(2), 316–321. https://doi.org/10.1164/ajrccm.163.2.2007102
299. Bartal, I., Melamed, R., Greenfeld, K., Atzil, S., Glasner, A., Domankevich, V., Naor, R., Beilin, B., Yardeni, I. Z., & Ben-Eliyahu, S. (2010). Immune perturbations in patients along the perioperative period: alterations in cell surface markers and leukocyte subtypes before and after surgery. Brain, behavior, and immunity, 24(3), 376–386. https://doi.org/10.1016/j.bbi.2009.02.010
300. Hughes, S. F., Hendricks, B. D., Edwards, D. R., Maclean, K. M., Bastawrous, S. S., & Middleton, J. F. (2010). Total hip and knee replacement surgery results in changes in leukocyte and endothelial markers. Journal of inflammation (London, England), 7, 2. https://doi.org/10.1186/1476-9255-7-2
301. Swartbol, P., Truedsson, L., & Norgren, L. (2001). The inflammatory response and its consequence for the clinical outcome following aortic aneurysm repair. European journal of vascular and endovascular surgery : the official journal of the European Society for Vascular Surgery, 21(5), 393–400. https://doi.org/10.1053/ejvs.2001.1352
302. Bown, M. J., Nicholson, M. L., Bell, P. R., & Sayers, R. D. (2001). Cytokines and inflammatory pathways in the pathogenesis of multiple organ failure following abdominal aortic aneurysm repair. European journal of vascular and endovascular surgery : the official journal of the European Society for Vascular Surgery, 22(6), 485–495. https://doi.org/10.1053/ejvs.2001.1522
303. Holmberg, A., Bergqvist, D., Westman, B., & Siegbahn, A. (1999). Cytokine and fibrinogen response in patients undergoing open abdominal aortic aneurysm surgery. European journal of vascular and endovascular surgery : the official journal of the European Society for Vascular Surgery, 17(4), 294–300. https://doi.org/10.1053/ejvs.1998.0767
304. Roumen, R. M., Hendriks, T., van der Ven-Jongekrijg, J., Nieuwenhuijzen, G. A., Sauerwein, R. W., van der Meer, J. W., & Goris, R. J. (1993). Cytokine patterns in patients after major vascular surgery, hemorrhagic shock, and severe blunt trauma. Relation with subsequent adult respiratory distress syndrome and multiple organ

failure. *Annals of surgery*, *218*(6), 769–776. https://doi.org/10.1097/00000658-199312000-00011

305. Tsilimigras, D. I., Sigala, F., Karaolanis, G., Ntanasis-Stathopoulos, I., Spartalis, E., Spartalis, M., Patelis, N., Papalampros, A., Long, C., & Moris, D. (2018). Cytokines as biomarkers of inflammatory response after open versus endovascular repair of abdominal aortic aneurysms: a systematic review. Acta pharmacologica Sinica, 39(7), 1164–1175. https://doi.org/10.1038/aps.2017.212
306. Spark, J. I., & Scott, D. J. (2001). Role of the neutrophil in the development of systemic inflammatory response syndrome and sepsis following abdominal aortic surgery. The British journal of surgery, 88(12), 1583–1589. https://doi.org/10.1046/j.0007-1323.2001.01925.
307. Berge, C., Hagen, A. I., Myhre, H. O., & Dahl, T. (2017). Preoperative White Blood Cell Count in Patients with Abdominal Aortic Aneurysms and Its Relation to Survival following Surgery. Annals of vascular surgery, 41, 127–134. https://doi.org/10.1016/j.avsg.2016.08.028
308. Gwak, M. S., Choi, S. J., Kim, J. A., Ko, J. S., Kim, T. H., Lee, S. M., Park, J. A., & Kim, M. H. (2007). Effects of gender on white blood cell populations and neutrophil-lymphocyte ratio following gastrectomy in patients with stomach cancer. Journal of Korean medical science, 22 Suppl(Suppl), S104–S108. https://doi.org/10.3346/jkms.2007.22.S.S104
309. Franke, A., Lante, W., Kurig, E., Zöller, L. G., Weinhold, C., & Markewitz, A. (2006). Is interferon gamma suppression after cardiac surgery caused by a decreased interleukin-12 synthesis?. The Annals of thoracic surgery, 82(1), 103–109. https://doi.org/10.1016/j.athoracsur.2006.02.042
310. Tashiro, T., Yamamori, H., Takagi, K., Hayashi, N., Furukawa, K., Nitta, H., Toyoda, Y., Sano, W., Itabashi, T., Nishiya, K., Hirano, J., & Nakajima, N. (1999). Changes in immune function following surgery for esophageal carcinoma. Nutrition (Burbank, Los Angeles County, Calif.), 15(10), 760–766. https://doi.org/10.1016/s0899-9007(99)00151-3
311. Faist, E., Kupper, T. S., Baker, C. C., Chaudry, I. H., Dwyer, J., & Baue, A. E. (1986). Depression of cellular immunity after major injury. Its association with posttraumatic complications and its reversal with immunomodulation. Archives of surgery (Chicago, Ill. : 1960), 121(9), 1000–1005. https://doi.org/10.1001/archsurg.1986.01400090026004
312. O'Mahony, J. B., Palder, S. B., Wood, J. J., McIrvine, A., Rodrick, M. L., Demling, R. H., & Mannick, J. A. (1984). Depression of cellular immunity after multiple trauma in the absence of sepsis. The Journal of trauma, 24(10), 869–875. https://doi.org/10.1097/00005373-198410000-00001
313. McIrvine, A. J., O'Mahony, J. B., Saporoschetz, I., & Mannick, J. A. (1982). Depressed immune response in burn patients: use of monoclonal antibodies and functional assays to define the role of suppressor cells. *Annals of surgery*, *196*(3), 297–304. https://doi.org/10.1097/00000658-198209000-00008
314. Kimura, F., Shimizu, H., Yoshidome, H., Ohtsuka, M., & Miyazaki, M. (2010). Immunosuppression following surgical and traumatic injury. *Surgery today*, *40*(9), 793–808. https://doi.org/10.1007/s00595-010-4323-z
315. Delogu, G., Moretti, S., Antonucci, A., Marcellini, S., Masciangelo, R., Famularo, G., Signore, L., & De Simone, C. (2000). Apoptosis and surgical trauma: dysregulated expression of death and survival factors on peripheral lymphocytes. *Archives of surgery (Chicago, Ill. : 1960)*, *135*(10), 1141–1147. https://doi.org/10.1001/archsurg.135.10.1141

316. Christensen, D. M., Iddins, C. J., Parrillo, S. J., Glassman, E. S., & Goans, R. E. (2014). Management of ionizing radiation injuries and illnesses, part 4: acute radiation syndrome. The Journal of the American Osteopathic Association, 114(9), 702–711. https://doi.org/10.7556/jaoa.2014.138
317. Goans, R. E., Holloway, E. C., Berger, M. E., & Ricks, R. C. (2001). Early dose assessment in criticality accidents. Health physics, 81(4), 446–449. https://doi.org/10.1097/00004032-200110000-00009
318. Kanegasaki, S., Yamashita, T., & Tsuchiya, T. (2019). Reduced Number of Lymphocytes by X-ray Irradiation: A Problem in a Combination Therapy Trial that Elicits the Abscopal Effect in Preclinical Studies Using Electron Beam Irradiation. Cureus, 11(2), e4142. https://doi.org/10.7759/cureus.4142
319. Marieb, E., & Hoehn, K. (2018). *Human Anatomy & Physiology* (11th ed.). London, UK: Pearson.
320. Ellsworth S. G. (2018). Field size effects on the risk and severity of treatment-induced lymphopenia in patients undergoing radiation therapy for solid tumors. Advances in radiation oncology, 3(4), 512–519. https://doi.org/10.1016/j.adro.2018.08.014
321. Pike, L., Bang, A., Mahal, B. A., Taylor, A., Krishnan, M., Spektor, A., Cagney, D. N., Aizer, A. A., Alexander, B. M., Rahma, O., Balboni, T., Ott, P. A., Hodi, F. S., & Schoenfeld, J. D. (2019). The Impact of Radiation Therapy on Lymphocyte Count and Survival in Metastatic Cancer Patients Receiving PD-1 Immune Checkpoint Inhibitors. International journal of radiation oncology, biology, physics, 103(1), 142–151. https://doi.org/10.1016/j.ijrobp.2018.09.010
322. Redon, C. E., Dickey, J. S., Bonner, W. M., & Sedelnikova, O. A. (2009). γ-H2AX as a biomarker of DNA damage induced by ionizing radiation in human peripheral blood lymphocytes and artificial skin. *Advances in space research : the official journal of the Committee on Space Research (COSPAR)*, *43*(8), 1171–1178. https://doi.org/10.1016/j.asr.2008.10.011
323. Tanaka, T., Halicka, H. D., Traganos, F., Seiter, K., & Darzynkiewicz, Z. (2007). Induction of ATM activation, histone H2AX phosphorylation and apoptosis by etoposide: relation to cell cycle phase. *Cell cycle (Georgetown, Tex.)*, *6*(3), 371–376. https://doi.org/10.4161/cc.6.3.3835
324. Tarpey, M. M., Wink, D. A., & Grisham, M. B. (2004). Methods for detection of reactive metabolites of oxygen and nitrogen: in vitro and in vivo considerations. American journal of physiology. Regulatory, integrative and comparative physiology, 286(3), R431–R444. https://doi.org/10.1152/ajpregu.00361.2003
325. 325 – 354 Kalyanaraman, B., Darley-Usmar, V., Davies, K. J., Dennery, P. A., Forman, H. J., Grisham, M. B., Mann, G. E., Moore, K., Roberts, L. J., 2nd, & Ischiropoulos, H. (2012). Measuring reactive oxygen and nitrogen species with fluorescent probes: challenges and limitations. Free radical biology & medicine, 52(1), 1–6. https://doi.org/10.1016/j.freeradbiomed.2011.09.030
326. Rothe, G., & Valet, G. (1990). Flow cytometric analysis of respiratory burst activity in phagocytes with hydroethidine and 2',7'-dichlorofluorescin. Journal of leukocyte biology, 47(5), 440–448.
327. Wardman P. (2008). Methods to measure the reactivity of peroxynitrite-derived oxidants toward reduced fluoresceins and rhodamines. Methods in enzymology, 441, 261–282. https://doi.org/10.1016/S0076-6879(08)01214-7
328. Zhao, J., Guo, Z., Pei, S., Song, L., Wang, C., Ma, J., Jin, L., Ma, Y., He, R., Zhong, J., Ma, Y., & Zhang, H. (2017). pATM and γH2AX are effective radiation biomarkers in assessing the radiosensitivity of 12C6+ in human tumor cells. Cancer cell international, 17, 49. https://doi.org/10.1186/s12935-017-0419-5

329. Rothkamm, K., Balroop, S., Shekhdar, J., Fernie, P., & Goh, V. (2007). Leukocyte DNA damage after multi-detector row CT: a quantitative biomarker of low-level radiation exposure. Radiology, 242(1), 244–251. https://doi.org/10.1148/radiol.2421060171
330. Zein, N., Sinha, A. M., McGahren, W. J., & Ellestad, G. A. (1988). Calicheamicin gamma 1I: an antitumor antibiotic that cleaves double-stranded DNA site specifically. Science (New York, N.Y.), 240(4856), 1198–1201. https://doi.org/10.1126/science.3240341
331. Johansson, P., Fasth, A., Ek, T., & Hammarsten, O. (2017). Validation of a flow cytometry-based detection of γ-H2AX, to measure DNA damage for clinical applications. Cytometry. Part B, Clinical cytometry, 92(6), 534–540. https://doi.org/10.1002/cyto.b.21374.
332. Bourton, E. C., Plowman, P. N., Zahir, S. A., Senguloglu, G. U., Serrai, H., Bottley, G., & Parris, C. N. (2012). Multispectral imaging flow cytometry reveals distinct frequencies of γ-H2AX foci induction in DNA double strand break repair defective human cell lines. Cytometry. Part A : the journal of the International Society for Analytical Cytology, 81(2), 130–137. https://doi.org/10.1002/cyto.a.21171
333. Andrievski, A., & Wilkins, R. C. (2009). The response of gamma-H2AX in human lymphocytes and lymphocytes subsets measured in whole blood cultures. International journal of radiation biology, 85(4), 369–376. https://doi.org/10.1080/09553000902781147
334. Machado, R., Ferreira, V. M., Loureiro, L., Gonçalves, J., Oliveira, P., & Almeida, R. (2016). Radiation Exposure in Endovascular Infra-Renal Aortic Aneurysm Repair and Factors that Influence It. Brazilian journal of cardiovascular surgery, 31(6), 415–421. https://doi.org/10.5935/1678-9741.20160084
335. Kuefner, M. A., Grudzenski, S., Schwab, S. A., Wiederseiner, M., Heckmann, M., Bautz, W., Lobrich, M., & Uder, M. (2009). DNA double-strand breaks and their repair in blood lymphocytes of patients undergoing angiographic procedures. Investigative radiology, 44(8), 440–446. https://doi.org/10.1097/RLI.0b013e3181a654a5
336. Golfier, S., Jost, G., Pietsch, H., Lengsfeld, P., Eckardt-Schupp, F., Schmid, E., & Voth, M. (2009). Dicentric chromosomes and gamma-H2AX foci formation in lymphocytes of human blood samples exposed to a CT scanner: a direct comparison of dose response relationships. Radiation protection dosimetry, 134(1), 55–61. https://doi.org/10.1093/rpd/ncp061
337. Lassmann, M., Hänscheid, H., Gassen, D., Biko, J., Meineke, V., Reiners, C., & Scherthan, H. (2010). In vivo formation of gamma-H2AX and 53BP1 DNA repair foci in blood cells after radioiodine therapy of differentiated thyroid cancer. Journal of nuclear medicine : official publication, Society of Nuclear Medicine, 51(8), 1318–1325. https://doi.org/10.2967/jnumed.109.071357
338. Löbrich, M., Shibata, A., Beucher, A., Fisher, A., Ensminger, M., Goodarzi, A. A., Barton, O., & Jeggo, P. A. (2010). gammaH2AX foci analysis for monitoring DNA double-strand break repair: strengths, limitations and optimization. Cell cycle (Georgetown, Tex.), 9(4), 662–669. https://doi.org/10.4161/cc.9.4.10764
339. Halm, B. M., Franke, A. A., Lai, J. F., Turner, H. C., Brenner, D. J., Zohrabian, V. M., & DiMauro, R. (2014). γ-H2AX foci are increased in lymphocytes in vivo in young children 1 h after very low-dose X-irradiation: a pilot study. Pediatric radiology, 44(10), 1310–1317. https://doi.org/10.1007/s00247-014-2983-3
340. Fukumoto, W., Ishida, M., Sakai, C., Tashiro, S., Ishida, T., Nakano, Y., Tatsugami, F., & Awai, K. (2017). DNA damage in lymphocytes induced by cardiac CT and

comparison with physical exposure parameters. European radiology, 27(4), 1660–1666. https://doi.org/10.1007/s00330-016-4519-8

341. Osipov, A. N., Pustovalova, M., Grekhova, A., Eremin, P., Vorobyova, N., Pulin, A., Zhavoronkov, A., Roumiantsev, S., Klokov, D. Y., & Eremin, I. (2015). Low doses of X-rays induce prolonged and ATM-independent persistence of γH2AX foci in human gingival mesenchymal stem cells. Oncotarget, 6(29), 27275–27287. https://doi.org/10.18632/oncotarget.4739
342. Kuefner, M. A., Grudzenski, S., Hamann, J., Achenbach, S., Lell, M., Anders, K., Schwab, S. A., Häberle, L., Löbrich, M., & Uder, M. (2010). Effect of CT scan protocols on x-ray-induced DNA double-strand breaks in blood lymphocytes of patients undergoing coronary CT angiography. European radiology, 20(12), 2917–2924. https://doi.org/10.1007/s00330-010-1873-9
343. Piechowiak, E. I., Peter, J. F., Kleb, B., Klose, K. J., & Heverhagen, J. T. (2015). Intravenous Iodinated Contrast Agents Amplify DNA Radiation Damage at CT. Radiology, 275(3), 692–697. https://doi.org/10.1148/radiol.14132478
344. Wang, L., Li, Q., Wang, X. M., Hao, G. Y., Jie-Bao, Hu, S., & Hu, C. H. (2017). Enhanced radiation damage caused by iodinated contrast agents during CT examination. European journal of radiology, 92, 72–77. https://doi.org/10.1016/j.ejrad.2017.04.005
345. Grudzenski, S., Kuefner, M. A., Heckmann, M. B., Uder, M., & Löbrich, M. (2009). Contrast medium-enhanced radiation damage caused by CT examinations. Radiology, 253(3), 706–714. https://doi.org/10.1148/radiol.2533090468
346. May, M. S., Brand, M., Wuest, W., Anders, K., Kuwert, T., Prante, O., Schmidt, D., Maschauer, S., Semelka, R. C., Uder, M., & Kuefner, M. A. (2012). Induction and repair of DNA double-strand breaks in blood lymphocytes of patients undergoing ^{18}F-FDG PET/CT examinations. European journal of nuclear medicine and molecular imaging, 39(11), 1712–1719. https://doi.org/10.1007/s00259-012-2201-1
347. Geisel, D., Zimmermann, E., Rief, M., Greupner, J., Laule, M., Knebel, F., Hamm, B., & Dewey, M. (2012). DNA double-strand breaks as potential indicators for the biological effects of ionising radiation exposure from cardiac CT and conventional coronary angiography: a randomised, controlled study. European radiology, 22(8), 1641–1650. https://doi.org/10.1007/s00330-012-2426-1
348. Wilkins, R. C., Kutzner, B. C., Truong, M., & McLean, J. R. (2002). The effect of the ratio of CD4+ to CD8+ T-cells on radiation-induced apoptosis in human lymphocyte subpopulations. International journal of radiation biology, 78(8), 681–688. https://doi.org/10.1080/09553000210144475
349. Horn, S., Barnard, S., Brady, D., Prise, K. M., & Rothkamm, K. (2013). Combined analysis of gamma-H2AX/53BP1 foci and caspase activation in lymphocyte subsets detects recent and more remote radiation exposures. Radiation research, 180(6), 603–609. https://doi.org/10.1667/RR13342.1
350. Khoronenkova, S. V., & Dianov, G. L. (2015). ATM prevents DSB formation by coordinating SSB repair and cell cycle progression. Proceedings of the National Academy of Sciences of the United States of America, 112(13), 3997–4002. https://doi.org/10.1073/pnas.1416031112
351. Little, M. P., Wakeford, R., Tawn, E. J., Bouffler, S. D., & Berrington de Gonzalez, A. (2009). Risks associated with low doses and low dose rates of ionizing radiation: why linearity may be (almost) the best we can do. Radiology, 251(1), 6–12. https://doi.org/10.1148/radiol.2511081686

352. Zakeri, F., & Assaei, R. G. (2004). Cytogenetic monitoring of personnel working in angiocardiography laboratories in Iran hospitals. Mutation research, 562(1-2), 1–9. https://doi.org/10.1016/j.mrgentox.2004.04.005
353. Zakeri, F., & Hirobe, T. (2010). A cytogenetic approach to the effects of low levels of ionizing radiations on occupationally exposed individuals. European journal of radiology, 73(1), 191–195. https://doi.org/10.1016/j.ejrad.2008.10.015
354. Vellingiri, B., Shanmugam, S., Subramaniam, M. D., Balasubramanian, B., Meyyazhagan, A., Alagamuthu, K., Prakash, V., Shafiahammedkhan, M., Kathannan, S., Pappuswamy, M., Raviganesh, B., Anand, S., Shahnaz N, D., Cho, S. G., & Keshavarao, S. (2014). Cytogenetic endpoints and Xenobiotic gene polymorphism in lymphocytes of hospital workers chronically exposed to ionizing radiation in Cardiology, Radiology and Orthopedic Laboratories. Ecotoxicology and environmental safety, 100, 266–274. https://doi.org/10.1016/j.ecoenv.2013.09.036
355. Hertault, A., Maurel, B., Midulla, M., Bordier, C., Desponds, L., Saeed Kilani, M., Sobocinski, J., & Haulon, S. (2015). Editor's Choice - Minimizing Radiation Exposure During Endovascular Procedures: Basic Knowledge, Literature Review, and Reporting Standards. European journal of vascular and endovascular surgery : the official journal of the European Society for Vascular Surgery, 50(1), 21–36. https://doi.org/10.1016/j.ejvs.2015.01.014
356. Fukunaga, H., & Yokoya, A. (2016). Low-dose radiation risk and individual variation in radiation sensitivity in Fukushima. Journal of radiation research, 57(1), 98–100. https://doi.org/10.1093/jrr/rrv053
357. Muslimovic, A., Ismail, I. H., Gao, Y., & Hammarsten, O. (2008). An optimized method for measurement of gamma-H2AX in blood mononuclear and cultured cells. Nature protocols, 3(7), 1187–1193. https://doi.org/10.1038/nprot.2008.93
358. Pearson, S., Hassen, T., Spark, J. I., Cabot, J., Cowled, P., & Fitridge, R. (2005). Endovascular repair of abdominal aortic aneurysm reduces intraoperative cortisol and perioperative morbidity. Journal of vascular surgery, 41(6), 919–925. https://doi.org/10.1016/j.jvs.2005.02.040
359. Borràs-Fresneda, M., Barquinero, J. F., Gomolka, M., Hornhardt, S., Rössler, U., Armengol, G., & Barrios, L. (2016). Differences in DNA Repair Capacity, Cell Death and Transcriptional Response after Irradiation between a Radiosensitive and a Radioresistant Cell Line. Scientific reports, 6, 27043. https://doi.org/10.1038/srep27043
360. Bishay, K., Ory, K., Olivier, M. F., Lebeau, J., Levalois, C., & Chevillard, S. (2001). DNA damage-related RNA expression to assess individual sensitivity to ionizing radiation. Carcinogenesis, 22(8), 1179–1183. https://doi.org/10.1093/carcin/22.8.1179
361. Hasty, P., Campisi, J., Hoeijmakers, J., van Steeg, H., & Vijg, J. (2003). Aging and genome maintenance: lessons from the mouse?. Science (New York, N.Y.), 299(5611), 1355–1359. https://doi.org/10.1126/science.1079161
362. Broustas, C. G., & Lieberman, H. B. (2014). DNA damage response genes and the development of cancer metastasis. Radiation research, 181(2), 111–130. https://doi.org/10.1667/RR13515.1
363. United Nations Scientific Committee on the Effects of Atomic Radiation. Sources and effects of ionizing radiation: UNSCEAR 2000 report to the General Assembly of the United Nations. United Nations Publication. (1), 1– 654.
364. 1990 Recommendations of the International Commission on Radiological Protection. (1991). Annals of the ICRP, 21(1-3), 1–201.

365. 402 – 435 Land C. E. (1980). Estimating cancer risks from low doses of ionizing radiation. Science (New York, N.Y.), 209(4462), 1197–1203. https://doi.org/10.1126/science.7403879
366. Berrington de González, A., & Darby, S. (2004). Risk of cancer from diagnostic X-rays: estimates for the UK and 14 other countries. Lancet (London, England), 363(9406), 345–351. https://doi.org/10.1016/S0140-6736(04)15433-0
367. Li, H. H., Wang, Y. W., Chen, R., Zhou, B., Ashwell, J. D., & Fornace, A. J., Jr (2015). Ionizing Radiation Impairs T Cell Activation by Affecting Metabolic Reprogramming. International journal of biological sciences, 11(7), 726–736. https://doi.org/10.7150/ijbs.12009
368. Yamaoka, M., Kusunoki, Y., Kasagi, F., Hayashi, T., Nakachi, K., & Kyoizumi, S. (2004). Decreases in percentages of naïve CD4 and CD8 T cells and increases in percentages of memory CD8 T-cell subsets in the peripheral blood lymphocyte populations of A-bomb survivors. Radiation research, 161(3), 290–298. https://doi.org/10.1667/rr3143
369. Krem, M. M., Press, O. W., Horwitz, M. S., & Tidwell, T. (2015). Mechanisms and clinical applications of chromosomal instability in lymphoid malignancy. British journal of haematology, 171(1), 13–28. https://doi.org/10.1111/bjh.13507
370. Lynskey, G. E., 3rd, Powell, D. K., Dixon, R. G., & Silberzweig, J. E. (2013). Radiation protection in interventional radiology: survey results of attitudes and use. Journal of vascular and interventional radiology : JVIR, 24(10), 1547–51.e3. https://doi.org/10.1016/j.jvir.2013.05.039
371. Fetterly, K. A., Magnuson, D. J., Tannahill, G. M., Hindal, M. D., & Mathew, V. (2011). Effective use of radiation shields to minimize operator dose during invasive cardiology procedures. JACC. Cardiovascular interventions, 4(10), 1133–1139. https://doi.org/10.1016/j.jcin.2011.05.027
372. Kendrick, D. E., Miller, C. P., Moorehead, P. A., Kim, A. H., Baele, H. R., Wong, V. L., Jordan, D. W., & Kashyap, V. S. (2016). Comparative occupational radiation exposure between fixed and mobile imaging systems. Journal of vascular surgery, 63(1), 190–197. https://doi.org/10.1016/j.jvs.2015.08.062
373. Haussen, D. C., Van Der Bom, I. M., & Nogueira, R. G. (2016). A prospective case control comparison of the ZeroGravity system versus a standard lead apron as radiation protection strategy in neuroendovascular procedures. Journal of neurointerventional surgery, 8(10), 1052–1055. https://doi.org/10.1136/neurintsurg-2015-012038
374. Savage, C., Seale, T.M., Shaw, C.J., et al. (2013). Evaluation of a suspended personal radiation protection system vs. conventional apron shieldsin clinical interventional procedures. Open Journal of Radiology. 3(3),143-151
375. Marichal, D. A., Anwar, T., Kirsch, D., Clements, J., Carlson, L., Savage, C., & Rees, C. R. (2011). Comparison of a suspended radiation protection system versus standard lead apron for radiation exposure of a simulated interventionalist. Journal of vascular and interventional radiology : JVIR, 22(4), 437–442. https://doi.org/10.1016/j.jvir.2010.12.016
376. Cousin, A. J., Lawdahl, R. B., Chakraborty, D. P., & Koehler, R. E. (1987). The case for radioprotective eyewear/facewear. Practical implications and suggestions. Investigative radiology, 22(8), 688–692. https://doi.org/10.1097/00004424-198708000-00012
377. Tacher, V., Lin, M., Desgranges, P., Deux, J. F., Grünhagen, T., Becquemin, J. P., Luciani, A., Rahmouni, A., & Kobeiter, H. (2013). Image guidance for endovascular repair of complex aortic aneurysms: comparison of two-dimensional and three-

dimensional angiography and image fusion. Journal of vascular and interventional radiology : JVIR, 24(11), 1698–1706. https://doi.org/10.1016/j.jvir.2013.07.016
378. Antoniou, G. A., Riga, C. V., Mayer, E. K., Cheshire, N. J., & Bicknell, C. D. (2011). Clinical applications of robotic technology in vascular and endovascular surgery. Journal of vascular surgery, 53(2), 493–499. https://doi.org/10.1016/j.jvs.2010.06.154
379. Raman, V. K., Karmarkar, P. V., Guttman, M. A., Dick, A. J., Peters, D. C., Ozturk, C., Pessanha, B. S., Thompson, R. B., Raval, A. N., DeSilva, R., Aviles, R. J., Atalar, E., McVeigh, E. R., & Lederman, R. J. (2005). Real-time magnetic resonance-guided endovascular repair of experimental abdominal aortic aneurysm in swine. Journal of the American College of Cardiology, 45(12), 2069–2077. https://doi.org/10.1016/j.jacc.2005.03.029
380. von Segesser, L. K., Marty, B., Ruchat, P., Bogen, M., & Gallino, A. (2002). Routine use of intravascular ultrasound for endovascular aneurysm repair: angiography is not necessary. European journal of vascular and endovascular surgery : the official journal of the European Society for Vascular Surgery, 23(6), 537–542. https://doi.org/10.1053/ejvs.2002.1657
381. Mishra, K. N., Moftah, B. A., & Alsbeih, G. A. (2018). Appraisal of mechanisms of radioprotection and therapeutic approaches of radiation countermeasures. Biomedicine & pharmacotherapy = Biomedecine & pharmacotherapie, 106, 610–617. https://doi.org/10.1016/j.biopha.2018.06.150
382. Everett, W. H., & Curiel, D. T. (2015). Gene therapy for radioprotection. Cancer gene therapy, 22(4), 172–180. https://doi.org/10.1038/cgt.2015.8
383. Sémont, A., François, S., Mouiseddine, M., François, A., Saché, A., Frick, J., Thierry, D., & Chapel, A. (2006). Mesenchymal stem cells increase self-renewal of small intestinal epithelium and accelerate structural recovery after radiation injury. Advances in experimental medicine and biology, 585, 19–30. https://doi.org/10.1007/978-0-387-34133-0_2
384. Williams, J. P., Jackson, I.L., Shah, J.R., Czarniecki, C.W., Maidment, B.W., et al. (2012). Animal Models and Medical Countermeasures Development for Radiation-Induced Lung Damage:Report from an NIAID Workshop. Radiation Research. 177(5), e0025–e0039. https://doi.org/10.1667/RROL04.1
385. American board of Internal Medicine. (2020). Interventional Cardiology Maintenance of Certification (Moc) Examination Blueprint. Retrieved from https://www.abim.org/~/media/ABIM%20Public/Files/pdf/exam-blueprints/maintenance-of-certification/interventional-cardiology.pdf
386. British Institute of Radiology, Society and College of Radiographers and the Royal college of Radiologists. (2015). A guide to understanding the implications of the Ionising Radiation (Medical Exposure) Regulations in the diagnostic and interventional radiology. London. The Royal College of Radiologists. Retrieved from https://www.rcr.ac.uk/sites/default/files/bfcr152_irmer.pdf